2013 Volume 2

The Journal on Advanced Studies in Theoretical and Experimental Physics, including Related Themes from Mathematics

PROGRESS IN PHYSICS

"All scientists shall have the right to present their scientific research results, in whole or in part, at relevant scientific conferences, and to publish the same in printed scientific journals, electronic archives, and any other media."
— Declaration of Academic Freedom, Article 8

ISSN 1555-5534

The Journal on Advanced Studies in Theoretical and Experimental Physics, including Related Themes from Mathematics

PROGRESS IN PHYSICS

A quarterly issue scientific journal, registered with the Library of Congress (DC, USA). This journal is peer reviewed and included in the abstracting and indexing coverage of: Mathematical Reviews and MathSciNet (AMS, USA), DOAJ of Lund University (Sweden), Zentralblatt MATH (Germany), Scientific Commons of the University of St. Gallen (Switzerland), Open-J-Gate (India), Referativnyi Zhurnal VINITI (Russia), etc.

Electronic version of this journal:
http://www.ptep-online.com

Postal Address

Department of Mathematics and Science,
University of New Mexico,
705 Gurley Ave., Gallup, NM 87301, USA

ISSN: 1555-5534 (print)
ISSN: 1555-5615 (online)

Standard Address Number: 297-5092
Printed in the United States of America

APRIL 2013 **VOLUME 2**

CONTENTS

Information for Authors and Subscribers

Progress in Physics has been created for publications on advanced studies in theoretical and experimental physics, including related themes from mathematics and astronomy. All submitted papers should be professional, in good English, containing a brief review of a problem and obtained results.

All submissions should be designed in LaTeX format using *Progress in Physics* template. This template can be downloaded from *Progress in Physics* home page http://www.ptep-online.com. Abstract and the necessary information about author(s) should be included into the papers. To submit a paper, mail the file(s) to the Editor-in-Chief.

All submitted papers should be as brief as possible. We accept brief papers, no larger than 8 typeset journal pages. Short articles are preferable. Large papers can be considered in exceptional cases to the section *Special Reports* intended for such publications in the journal. Letters related to the publications in the journal or to the events among the science community can be applied to the section *Letters to Progress in Physics*.

All that has been accepted for the online issue of *Progress in Physics* is printed in the paper version of the journal. To order printed issues, contact the Editors.

This journal is non-commercial, academic edition. It is printed from private donations. (Look for the current author fee in the online version of the journal.)

Causal Version of Newtonian Theory by Time–Retardation of the Gravitational Field Explains the Flyby Anomalies

Joseph C. Hafele

Retired Physicist; Home Office: 618 S. 24th St., Laramie, WY, USA
E-mail: cahafele@bresnan.net

Classical Newtonian gravitational theory does not satisfy the causality principle because it is based on instantaneous action-at-a-distance. A causal version of Newtonian theory for a large rotating sphere is derived herein by time-retarding the distance between interior circulating point-mass sources and an exterior field-point. The resulting causal theory explains exactly the six flyby anomalies reported by Anderson et al. in 2008. It also explains exactly an anomalous decrease in the Moon's orbital speed. No other known theory has been shown to explain both the flyby anomalies and the lunar orbit anomaly.

1 Introduction

In 2008 Anderson *et al.* reported that anomalous orbital-energy changes have been observed during six spacecraft flybys of the Earth [1]. The reported speed-changes range from a maximum of +13.28 mm/s for the NEAR flyby to a minimum of −4.6 mm/s for the Galileo-II flyby. Anderson *et al.* also found an empirical prediction formula that gives calculated speed-changes that are close to the observed speed-changes. If the speed-change for the empirical prediction formula is designated by δv_{emp}, it can be expressed as follows

$$\delta v_{\text{emp}} = \frac{2v_{\text{eq}}}{c}\, v_{\text{in}}\, (\cos\lambda_{\text{in}} - \cos\lambda_{\text{out}}) = \\ = -\frac{2v_{\text{eq}}}{c}\, v_{\text{in}} \int_{t_{\text{in}}}^{t_{\text{out}}} \sin(\lambda(t))\, \frac{d\lambda}{dt}\, dt\,, \qquad (1)$$

where v_{eq} is the Earth's equatorial rotational surface speed, c is the vacuum speed of light, v_{in} is the initial asymptotic inbound speed, λ_{in} is the asymptotic inbound geocentric latitude, and λ_{out} is the asymptotic outbound geocentric latitude. If t is the observed coordinate time for the spacecraft in its trajectory, then $\lambda_{\text{in}} = \lambda(t_{\text{in}})$ and $\lambda_{\text{out}} = \lambda(t_{\text{out}})$. If $d\lambda/dt = 0$, then $\delta v_{\text{emp}} = 0$. An order of magnitude estimate for the maximum possible value for δv_{emp} is $2(5\times10^2/3\times10^8)\, v_{\text{in}} \sim 30$ mm/s.

The following is a direct quote from the conclusions of an article published in 2009 by M. M. Nieto and J. D. Anderson [2]:

> "Several physicists have proposed explanations of the Earth flyby anomalies. The least revolutionary invokes dark matter bound to Earth. Others include modifications of special relativity, of general relativity, or of the notion of inertia; a light speed anomaly; or anisotropy in the gravitational field —- all of those, of course, deny concepts that have been well tested. And none of them have made comprehensive, precise predictions of Earth flyby effects. For now the anomalous energy changes observed in Earth flybys remain a puzzle. Are they the result of imperfect understandings of conventional physics and experimental systems, or are they the harbingers of exciting new physics?"

It appears that a new and possibly unconventional theory is needed.

The empirical prediction formula found by Anderson *et al.* is not based on any mainstream theory (it was simply "picked out of the air"), but it is remarkably simple and does produce calculated speed-changes that are surprisingly close to the observed speed-changes. The formula for δv_{emp} (1) gives three clues for properties that need to be satisfied by any theory that is developed to explain the flyby anomaly: 1) the theory must produce a speed-change that is proportional to the ratio v_{eq}/c, 2) the anomalous force acting on the spacecraft must change the λ component of the spacecraft's speed, and 3) the speed-change must be proportional to v_{in}.

The objective of this article is threefold: 1) derive a new causal version of classical acausal Newtonian theory, 2) show that this new version is able to produce exact agreement with all six of the anomalous speed-changes reported by Anderson *et al.*, and 3) show that it is also able to explain exactly a "lunar orbit anomaly" that will be described below. The proposed new version for Newtonian theory requires only mainstream physics: 1) classical Newtonian theory and 2) the causality principle which requires time-retardation of the gravitational field. It also satisfies the three requirements of the empirical prediction formula.

The proposed theory is based on a simple correction that converts Newton's acausal theory into a causal theory. The resulting causal theory has a new, previously overlooked, time-retarded transverse component, designated $\boldsymbol{g}_{\text{trt}}$, which depends on $1/c_{\text{g}}$, where c_{g} is the speed of gravity, which approximately equals the speed of light. The new total gravitational field for a large spinning sphere, $\boldsymbol{g}$, has two components, the standard well-known classical acausal radial component, $\boldsymbol{g}_{\text{r}}$, and a new relatively small time-retarded transverse vortex component, $\boldsymbol{g}_{\text{trt}}$. The total vector field $\boldsymbol{g} = \boldsymbol{g}_{\text{r}} + \boldsymbol{g}_{\text{trt}}$. The zero-divergence vortex transverse vector field $\boldsymbol{g}_{\text{trt}}$ is orthogonal to the irrotational radial vector field $\boldsymbol{g}_{\text{r}}$.

The new total vector field is consistent with Helmholtz's theorem, which states that any physical vector field can be expressed as the sum of the gradient of a zero-rotational scalar potential and the curl of a zero-divergence vector potential [3]. This means that $\boldsymbol{g}_{\mathrm{r}}$ can be derived in the standard way from the gradient of a scalar potential, and $\boldsymbol{g}_{\mathrm{trt}}$ can be derived from the curl of a vector potential, but $\boldsymbol{g}_{\mathrm{trt}}$ cannot be derived from the gradient of a scalar potential.

The proposed causal version can be derived by using the slow-speed weak-field approximation for general relativity theory.

2 Summary of the derivation of the formulas for the time-retarded transverse gravitational field and the predicted flyby speed-changes

In the section entitled *The Linear Approximation to GR* in W. Rindler's popular textbook *Essential Relativity* [4], Rindler derives the formulas for the time-retarded scalar potential φ, the time-retarded "gravitoelectric" acceleration field $\boldsymbol{e}$, the time-retarded vector potential $\boldsymbol{a}$, and the time-retarded "gravitomagnetic" induction field $\boldsymbol{h}$. His formulas for φ, $\boldsymbol{e}$, $\boldsymbol{a}$, and $\boldsymbol{h}$ are derived from general relativity theory by using the slow-speed weak-field approximation. They are as follows

$$\left.\begin{aligned} &\varphi = G\iiint\left[\frac{\rho}{r''}\right]dV, \qquad \boldsymbol{a} = \frac{G}{c}\iiint\left[\frac{\rho\,\boldsymbol{u}}{r''}\right]dV \\ &\boldsymbol{e} = -\,\boldsymbol{\nabla}\varphi\,, \qquad\qquad\quad \boldsymbol{h} = \boldsymbol{\nabla}\times 4\,\boldsymbol{a} \end{aligned}\right\}, \quad (2)$$

where ρ is the mass-density of the central object, $\boldsymbol{u}$ is the inertial velocity (the velocity in an inertial frame) of a source-point-mass in the central object, $\boldsymbol{r}''$ is the vector distance from an inner source-point-mass to an outer field-point, and the square brackets [ ] mean that the enclosed function is to be evaluated at the retarded time, i.e., the time retarded by the light travel time from the source-point to the field-point.

Let the origin for an inertial (nonaccelerating and nonrotating) frame-of-reference coincide with the center-of-mass of a contiguous central object. Let $\boldsymbol{r}'$ be the radial vector from the origin to a source-point-mass in the central object, and let $\boldsymbol{r}$ be the radial vector from the origin to an external field-point, so that $\boldsymbol{r}'' = \boldsymbol{r} - \boldsymbol{r}'$. The square brackets in the triple integrals in (2) indicate that the integrands $[\rho/r'']$ and $[\rho\boldsymbol{u}/r'']$ are to be integrated over the volume of the central object at the retarded time.

Let m be the mass of a test-mass that occupies the field-point at $\boldsymbol{r}$, and let $\boldsymbol{v}$ be the inertial velocity of the test mass. The analogous Lorentz force law, i.e., the formula for the time-retarded gravitational force $\boldsymbol{F}$ acting on m at $\boldsymbol{r}$, is [4]

$$\boldsymbol{F} = -\,m\left(\boldsymbol{e} + \frac{1}{c}\,(\boldsymbol{v}\times\boldsymbol{h})\right) = -\,m\,\boldsymbol{\nabla}\left(G\iiint\left[\frac{\rho}{r''}\right]dV\right) - \\ -\,m\left(\boldsymbol{v}\times\left(\boldsymbol{\nabla}\times\left(\frac{4G}{c^2}\iiint\left[\frac{\rho\,\boldsymbol{u}}{r''}\right]dV\right)\right)\right). \quad (3)$$

Rindler's time-retarded version for the slow-speed weak-field approximation gives a complete stand-alone time-retarded solution. The time-retarded fields were derived from general relativity theory, but there is no need for further reference to the concepts and techniques of general relativity theory. Needed concepts and techniques are those of classical Newtonian theory.

Furthermore, Rindler's formulas satisfy the causality principle because the fields are time-retarded. Rindler's version gives a good first approximation only if

$$v^2 \ll c^2, \qquad u^2 \ll c^2, \qquad \frac{GM}{r} = |\varphi| \ll c^2, \quad (4)$$

where M is the total mass of the central object.

Notice in (3) that the acceleration caused by the gravitoelectric field $\boldsymbol{e}$ is independent of c, but the acceleration caused by the gravitomagnetic induction field $\boldsymbol{h}$ is reduced by the factor $1/c^2$. The numerical value for c is on the order of 3×10^8 m/s. If the magnitude for $\boldsymbol{e}$ is on the order of 10 m/s^2 (the Earth's field at the surface), and the magnitudes for $\boldsymbol{u}$ and $\boldsymbol{v}$ are on the order of 10^4 m/s, the relative magnitude for the acceleration caused by $\boldsymbol{h}$ would be on the order of $10\times4\,(10^4/3\times10^8)^2\mathrm{m/s}^2 \sim 10^{-8}\mathrm{m/s}^2$. This estimate shows that, for slow-speed weak-field practical applications in the real world, the acceleration caused by $\boldsymbol{h}$ is totally negligible compared to the acceleration caused by $\boldsymbol{e}$.

The empirical formula indicates that the flyby speed-change is reduced by $1/c$, not by $1/c^2$, which rules out the gravitomagnetic field as a possible cause for the flyby anomalies. The acceleration of $\boldsymbol{h}$ is simply too small to explain the flyby anomalies.

Consequently, the practicable version for Rindler's Lorentz force law becomes the same as a time-retarded version for Newton's well-known inverse-square law

$$\boldsymbol{F} = -\,Gm\,\boldsymbol{\nabla}\iiint\left[\frac{\rho}{r''}\right]dV, \quad (5)$$

where $\boldsymbol{F}$ is the time-retarded gravitational force acting on m.

Let $d^3\boldsymbol{F}$ be the time-retarded elemental force of an elemental point-mass source dm'. The time-retarded version for Newton's inverse-square law becomes

$$d^3\boldsymbol{F} = -\,Gm\,\frac{dm'}{r''^2}\,\frac{\boldsymbol{r}''}{r''}\,, \quad (6)$$

where $\boldsymbol{r}''/r''$ is a unit vector directed towards increasing $\boldsymbol{r}''$.

By definition, the gravitational field of a source at $\boldsymbol{r}'$ is the gravitational force of the source dm' that acts on a test-mass m at $\boldsymbol{r}$ per unit mass of the test-mass. The traditional symbol for the Newtonian gravitational field is $\boldsymbol{g}$. Therefore, the formula for the time-retarded elemental gravitational field $d^3\boldsymbol{g}$ of an elemental point-mass-source at $\boldsymbol{r}'$ for a field-point at $\boldsymbol{r}$ becomes

$$d^3\boldsymbol{g} = \frac{d^3\boldsymbol{F}}{m} = -\,G\,\frac{dm'}{r''^2}\,\frac{\boldsymbol{r}''}{r''}\,. \quad (7)$$

The negative sign indicates that the gravitational force is attractive.

Let t be the observed coordinate time at $\boldsymbol{r}$, let t' be the retarded time at $\boldsymbol{r}'$, and let $c_{\rm g}$ be the speed of propagation of the gravitational field. The connection between t and t' is

$$t = t' + \frac{r''}{c_{\rm g}}\,, \quad t' = t - \frac{r''}{c_{\rm g}}\,. \tag{8}$$

Obviously, $t(t')$ is a function of t', and *vice versa*, $t'(t)$ is a function of t. The Jacobian for the transformation from t to t' is given by

$$\text{Jacobian} = \frac{dt}{dt'} = 1 + \frac{1}{c_{\rm g}}\frac{dr''}{dt'}\,. \tag{9}$$

This Jacobian is needed to solve the triple integral over the volume of the central object. It leads to the necessary factor $1/c_{\rm g}$, where $c_{\rm g}$ is the speed of propagation of the Earth's gravitational field [5].

Let $\rho(\boldsymbol{r}')$ be the mass-density of the central object at $\boldsymbol{r}'$. Then

$$dm' = \rho(\boldsymbol{r}')\, dV. \tag{10}$$

The resulting formula for the elemental total gravitational field $d^3\boldsymbol{g}$, which consists of the radial component $d^3\boldsymbol{g}_{\rm r}$ and the transverse component $d^3\boldsymbol{g}_{\rm trt}$, becomes $d^3\boldsymbol{g} = d^3\boldsymbol{g}_{\rm r} + d^3\boldsymbol{g}_{\rm trt}$. The differential formulas for each component become

$$d^3\boldsymbol{g}_{\rm r} = -G\,\frac{dm'}{r''^2}\left(\frac{\boldsymbol{r}''}{r''}\right)_{\rm r}\,, \qquad d^3\boldsymbol{g}_{\rm trt} = -G\,\frac{dm'}{r''^2}\left(\frac{\boldsymbol{r}''}{r''}\right)_{\rm trt}\,, \tag{11}$$

where $(\boldsymbol{r}''/r'')_{\rm r}$ is the radial component of the unit vector and $(\boldsymbol{r}''/r'')_{\rm trt}$ is the transverse component of the unit vector. The total field is obtained by a triple integration over the volume of the central object at the retarded time.

Let (X, Y, Z) be the rectangular coordinates for the inertial frame-of-reference, and let the Z-axis coincide with the spin axis of the central object. Let RC be the relative radial component, and let TC_Z be the magnitude for the Z-axis component of the relative transverse component. As can be seen in Fig. 1, the formulas for RC and TC_Z are related to $\boldsymbol{r}$, $\boldsymbol{r}'$, and $\boldsymbol{r}''$ by

$$\left.\begin{aligned} RC &= \frac{\boldsymbol{r}\cdot\boldsymbol{r}''}{r''r} = \frac{\boldsymbol{r}\cdot\boldsymbol{r} - \boldsymbol{r}\cdot\boldsymbol{r}'}{r''r} \\ TC_Z &= \frac{(\boldsymbol{r}\times\boldsymbol{r}'')_Z}{r''r} = \frac{(\boldsymbol{r}'\times\boldsymbol{r})_Z}{r''r} = \frac{r'_X r_Y - r'_Y r_X}{r''r} \end{aligned}\right\}, \tag{12}$$

where r_X, r_Y are the X, Y components of $\boldsymbol{r}$, and r'_X, r'_Y are the X, Y components of $\boldsymbol{r}'$.

The formula for the magnitude of $\boldsymbol{g}_{\rm trt}$ becomes [5]

$$\boldsymbol{g}_{\rm trt} = \iiint\left(-G\,\frac{dm'}{r''^2}\right)(TC_Z)\,(\text{Jacobian})\,. \tag{13}$$

The triple integral is rather easy to solve by using numerical integration if the central object can be approximated by a large spinning isotropic sphere. To get a good first approximation, the Earth was simulated in [5] by a large spinning isotropic sphere.

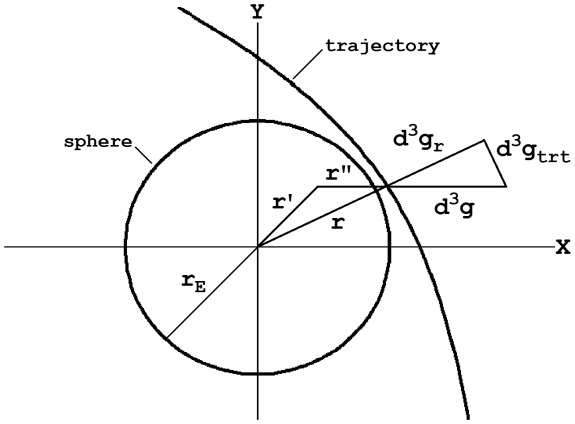

Fig. 1: Depiction of the vector distances $\boldsymbol{r}$, $\boldsymbol{r}'$, and $\boldsymbol{r}''$ and the components of the vector field $d^3\boldsymbol{g}$, $d^3\boldsymbol{g}_{\rm r}$, and $d^3\boldsymbol{g}_{\rm trt}$.

The formulas for the geocentric radial distance to the field-point and its derivative are

$$\left.\begin{aligned} r(\theta) &= \frac{r_{\rm p}\,(1+\varepsilon)}{1+\varepsilon\cos\theta} \\ \frac{dr}{d\theta} &= \frac{r(\theta)^2}{r_{\rm p}}\,\frac{\varepsilon}{1+\varepsilon}\,\sin\theta \end{aligned}\right\}, \tag{14}$$

where θ is the parametric polar coordinate angle for the spacecraft in the plane of the trajectory, $r_{\rm p}$ is the geocentric radial distance at perigee, and ε is the eccentricity of the trajectory.

It is shown in [5] that the formula for the Jacobian is

$$\begin{aligned} \text{Jacobian} &= 1 + \frac{1}{c_{\rm g}}\frac{dr''}{dt} = \\ &= 1 - \frac{r}{c_{\rm g}}\,\frac{r'}{r''}\left(\Omega_\phi - \Omega_{\rm E}\right)\cos\lambda'\,\sin\phi'. \end{aligned} \tag{15}$$

It is also shown in [5] that the only term for $d^3\boldsymbol{g}_{\rm trt}$ that will survive the triple integration is

$$d^3 g_{\rm trt} = -G\bar{\rho}\, r_{\rm E}\,\frac{\Omega_\phi - \Omega_{\rm E}}{\Omega_{\rm E}}\cos^2(\lambda)\, IG\,\frac{dr'}{r_{\rm E}}\, d\lambda'\, d\phi', \tag{16}$$

where $\bar{\rho}$ is the mean value for $\rho(r')$ and the formula for the integrand is

$$IG = \frac{r_{\rm E}^3}{r^3}\,\frac{\rho(r')}{\bar{\rho}}\,\frac{r'^4}{r_{\rm E}^4}\cos^3(\lambda')\frac{\sin^2\phi'}{(1+x)^2} \tag{17}$$

where the variable x is defined by

$$x \equiv \frac{r'^2}{r^2} - 2\,\frac{r'}{r}\cos\lambda'\,\cos\phi'. \tag{18}$$

It has been shown in [5] that the resulting formula for the magnitude of the transverse component is

$$g_{\rm trt}(\theta) = -G\,\frac{I_{\rm E}}{r_{\rm E}^4}\,\frac{v_{\rm eq}}{c_{\rm g}}\,\frac{\Omega_\phi(\theta) - \Omega_{\rm E}}{\Omega_{\rm E}}\,\cos^2(\lambda(\theta))\, PS\,(r(\theta))\,, \tag{19}$$

where G is the gravity constant, $I_{\rm E}$ is the Earth's spherical moment of inertia, $r_{\rm E}$ is the Earth's spherical radius, $\Omega_{\rm E}$ is the Earth's spin angular speed, $v_{\rm eq}$ is the Earth's equatorial surface speed, $c_{\rm g}$ is the speed of propagation of the Earth's gravitational field, θ is the spacecraft's parametric polar coordinate angle in the plane of the orbit or trajectory, $\Omega_\theta = d\theta/dt$ is the spacecraft's angular speed, Ω_ϕ is the azimuthal ϕ-component of Ω_θ, λ is the spacecraft's geocentric latitude, r is the spacecraft's geocentric radial distance, and $PS(r)$ is an inverse-cube power series representation for the triple integral over the Earth's volume. The formula for $PS(r)$ is [5]

$$PS(r) \equiv \left(\frac{r_{\rm E}}{r}\right)^3 \left(C_0 + C_2\left(\frac{r_{\rm E}}{r}\right)^2 + C_4\left(\frac{r_{\rm E}}{r}\right)^4 + C_6\left(\frac{r_{\rm E}}{r}\right)^6\right),$$

where the values for the coefficients are

$$C_0 = 0.50889, \quad C_2 = 0.13931,$$
$$C_4 = 0.01013, \quad C_6 = 0.14671.$$

If the magnitude is negative, i.e., if $\Omega_\phi > \Omega_{\rm E}$ (prograde), the vector field component $\boldsymbol{g}_{\rm trt}$ is directed towards the east. If $\Omega_\phi < 0$ (retrograde), it is directed towards the west.

The formula for the time-retarded transverse gravitational field, $g_{\rm trt}$, satisfies the first requirement of the empirical prediction formula. It is proportional to $v_{\rm eq}/c_{\rm g} \cong v_{\rm eq}/c$. But the empirical prediction formula also requires that the speed-change must be in the λ-component of the spacecraft's velocity, $\boldsymbol{v}_\lambda$. The magnitude for the λ-component is defined by

$$v_\lambda = r_\lambda \frac{d\lambda}{dt} = r_\lambda \frac{d\lambda}{d\theta}\frac{d\theta}{dt} = r_\lambda \Omega_\theta \frac{d\lambda}{d\theta}, \qquad (20)$$

where r_λ is the λ-component of r.

The velocity component, $\boldsymbol{v}_\lambda$, is orthogonal to $\boldsymbol{g}_{\rm trt}$. Consequently, $\boldsymbol{g}_{\rm trt}$ cannot directly change the magnitude of $\boldsymbol{v}_\lambda$ (it changes the direction).

However, a hypothesized induction-like field, designated $\boldsymbol{F}_\lambda$, can be directed perpendicularly to $\boldsymbol{g}_{\rm trt}$ in the $\boldsymbol{v}_\lambda$-direction. Assume that the ϕ-component of the curl of $\boldsymbol{F}_\lambda$ equals $-k\, d\boldsymbol{g}_{\rm trt}/dt$, where k is a constant. This induction-like field can cause a small change in the spacecraft's speed. The reciprocal of the constant k, $v_{\rm k} = 1/k$, called the "induction speed", becomes an adjustable parameter for each case. The average for all cases gives an overall constant for the causal theory.

The formula for the magnitude of $\boldsymbol{F}_\lambda$ has been shown in [5] to be

$$F_\lambda = \frac{v_{\rm eq}}{v_{\rm k}} \frac{r_{\rm E}}{r(\theta)} \int_0^\theta \frac{r(\theta)}{r_{\rm E}} \frac{\Omega_\theta(\theta)}{\Omega_{\rm E}} \frac{1}{r_{\rm E}} \frac{dr}{d\theta} \frac{dg_{\rm trt}}{d\theta}\, d\theta. \qquad (21)$$

The acceleration caused by $\boldsymbol{F}_\lambda$ satisfies the second requirement of the empirical prediction formula, the one that requires the anomalous force to change the λ-component of the spacecraft's velocity.

The anomalous time rate of change in the spacecraft's orbital energy is given by the dot product, $\boldsymbol{v} \cdot \boldsymbol{F}_\lambda$. It has been shown in [5] that the calculated asymptotic speed-change, $\delta v_{\rm trt}$, is given by

$$\delta v_{\rm trt} = \delta v_{\rm in} + \delta v_{\rm out}, \qquad (22)$$

where

$$\delta v_{\rm in} = \delta v(\theta_{\rm min}), \qquad \delta v_{\rm out} = \delta v(\theta_{\rm max}), \qquad (23)$$

and

$$\delta v(\theta) = \frac{v_{\rm in}}{2} \int_0^\theta \frac{r_\lambda(\theta)\, F_\lambda(\theta)}{v_{\rm in}^2} \frac{d\lambda}{d\theta}\, d\theta. \qquad (24)$$

The angles $\theta_{\rm min}$ and $\theta_{\rm max}$ are the minimum and maximum values for θ. The initial speed $v_{\rm in} = v(\theta_{\rm min})$. The speed-change $\delta v(\theta)$ is proportional to $v_{\rm in}$, which satisfies the third requirement of the empirical prediction formula.

3 Summary of the change in the Moon's orbital speed caused by the Earth's time-retarded transverse gravitational field

In 1995, F. R. Stephenson and L. V. Morrison published a remarkable study of records of eclipses from 700 BC to 1990 AD [6]. They conclude*: 1) the LOD has been increasing on average during the past 2700 years at the rate of $+1.70 \pm 0.05$ ms cy^{-1} (i.e. $(+17.0 \pm 0.5) \times 10^{-6}$ s per year), 2) tidal braking causes an increase in the LOD of $+2.3 \pm 0.1$ ms cy^{-1} (i.e. $(+23 \pm 1)\times 10^{-6}$ s per year), and 3) there is a non-tidal decrease in the LOD, numerically -0.6 ± 0.1 ms cy^{-1} (i.e. $(-6 \pm 1) \times 10^{-6}$ s per year).

Stephenson and Morrison state that the non-tidal decrease in the LOD probably is caused by post-glacial rebound. Post-glacial rebound decreases the Earth's moment of inertia, which increases the Earth's spin angular speed, and thereby decreases the LOD. But post-glacial rebound cannot change the Moon's orbital angular momentum.

According to Stephenson and Morrison, tidal braking causes an increase in the LOD of $(23 \pm 1) \times 10^{-6}$ seconds per year, which causes a decrease in the Earth's spin angular momentum, and by conservation of angular momentum causes an increase in the Moon's orbital angular momentum. It has been shown in [5] that tidal braking alone would cause an increase in the Moon's orbital speed of $(19 \pm 1) \times 10^{-9}$ m/s per year, which corresponds to an increase in the radius of the Moon's orbit of (14 ± 1) mm per year.

But lunar-laser-ranging experiments have shown that the radius of the Moon's orbit is actually increasing at the rate of (38 ± 1) mm per year [7]. This rate for increase in the radius corresponds to an increase in the orbital speed of $(52 \pm 2) \times 10^{-9}$ m/s per year. Clearly there is an unexplained or anomalous difference in the change in the radius of the orbit of (-24 ± 2) mm per year $(38 - 14 = 24)$, and a corresponding anomalous difference in the change in the orbital speed of

*LOD means length-of-solar-day and ms cy^{-1} means milliseconds per century.

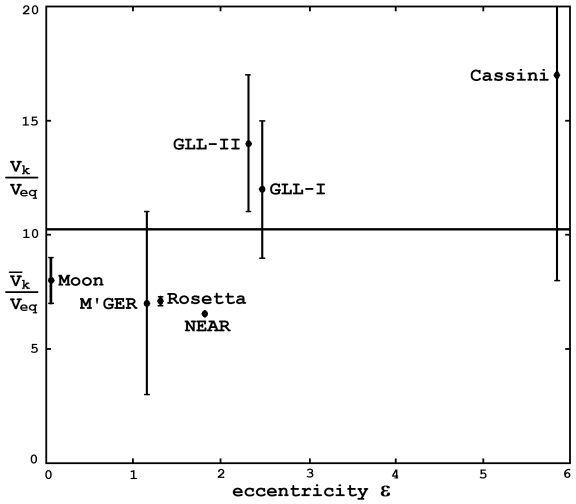

Fig. 2: Required induction speed ratio (designated by •), $v_k/v_{eq} \pm$ an estimate for the uncertainty, versus eccentricity ε. The mean value for all seven ratios is shown by the horizontal line.

$(-33 \pm 3) \times 10^{-9}$ m/s per year $(52 - 19 = 33)$. This "lunar orbit anomaly" cannot be caused by post-glacial rebound, but it can be caused by the proposed causal version of Newton's theory.

It has been shown in [5] that the causal version of Newton's theory produces a change in the Moon's orbital speed of $(-33 \pm 3) \times 10^{-9}$ m/s per year if the value for the induction speed $v_k = (8 \pm 1)\, v_{eq}$. Therefore, the causal theory explains exactly the lunar orbit anomaly. It gives a new closed orbit case for anomalous speed-changes.

4 Calculated speed-changes caused by the time-retarded version of Newton's theory

It has been shown in [5] that the causal version of Newton's theory explains exactly the six flyby anomalies reported by Anderson *et al.* [1]. The required values for v_k cluster between $6\, v_{eq}$ and $17\, v_{eq}$.

A graph of the required induction speed ratios, v_k/v_{eq}, versus eccentricity ε, Fig. 2, shows that the required value for v_k for the lunar orbit anomaly is consistent with the required values for v_k for the six Earth flyby anomalies. The average ± standard deviation is

$$\overline{v}_k = (10 \pm 4)\, v_{eq} = 5 \pm 2 \text{ km/s}. \qquad (25)$$

It will be interesting to compare this average, 5 ± 2 km/s, with parameter values for other flyby theories.

5 Predicted speed-changes for future high-precision Doppler-shift experiments

The speed-change caused by the causal version of Newton's theory depends on the speed of gravity c_g, the properties of the central sphere; mass M_E, radius r_E, angular speed Ω_E, moment of inertia I_E, and equatorial surface speed v_{eq}, on the orbital properties of the spacecraft; radius at perigee r_p, eccentricity ε, inclination to the equatorial plane α_{eq}, and latitude at perigee λ_p, and the induction speed v_k. If $\varepsilon = 0$ or if $\alpha_{eq} = 0$, the speed-change $\delta v_{trt} = 0$. Even if $\varepsilon \neq 0$ and $\alpha_{eq} \neq 0$, δv_{trt} is still equal to zero if perigee is over the equator $(\lambda_p = 0°)$ or one of the poles $(\lambda_p = \pm 90°)$. The maximum speed-change occurs for spacecrafts in highly eccentric and inclined near-Earth orbits.

r_p/r_E	P (hours)	δv_{yr} (mm/s per year)	$\delta v r_{yr}$ (mm/s per year)
2	11.2	+315	−517
3	20.7	+29.5	−76.8
4	31.8	+3.93	−21.0
5	44.4	+0.173	−7.97
6	58.4	−0.422	−3.69
7	73.6	−0.442	−1.95
8	89.9	−0.362	−1.14

Table 1: Calculated period P (in hours) and predicted speed-change for prograde orbits δv_{yr} (in mm/s per year), and the predicted speed-change for retrograde orbits $\delta v r_{yr}$ (in mm/s per year), for a spacecraft in a near-Earth orbit with $\varepsilon = 0.5$, $\alpha_{eq} = 45°$, $\lambda_p = 45°$, $v_k = 14\, v_{eq}$, and for r_p ranging from $2\, r_E$ to $8\, r_E$ [5].

Assume $c_g = c$ and the induction speed is its largest probable value, $v_k = 14\, v_{eq}$. Suppose the orbital properties for a spacecraft are $\varepsilon = 0.5$, $\alpha_{eq} = 45°$, and $\lambda_p = 45°$. Let r_p range from $2\, r_E$ to $8\, r_E$. The period P is given by Kepler's 3rd law, and the annual speed change for prograde $\delta v_{yr} = N_{rev}\, \delta v_{trt}$, and for retrograde $\delta v r_{yr} = N_{rev}\, \delta v_{trt}$, where N_{rev} is the number of revolutions per year. Calculated speed-changes are listed in Table 1 [5].

6 Other theories which explain the Earth flyby anomalies

There are at least two other published theories that explain the Earth flyby anomalies: 1) the 3-space flow theory of R. T. Cahill [8], and 2) the exponential radial field theory of H. J. Busack [9].

In [8] Cahill reviews numerous Michelson interferometer and one-way light-speed experiments which clearly show an anisotropy in the velocity of light. His calculated flyby speed-changes depend on the direction and magnitude for 3-space inflow at the spacecraft on the date and time of the flyby. Cahill found that the average speed for 3-space inflow is 12±5 km/s. Cahill's average, 12±5 km/s, essentially equals the average value for v_k (25), 5±2 km/s.

In [9] Busack applies a small exponential correction for the Earth's radial gravitational field. If $f(\boldsymbol{r}, \boldsymbol{v})$ is Busack's correction, the inverse-square law becomes

$$\boldsymbol{g}_r(\boldsymbol{r}, \boldsymbol{v}) = -\frac{GM_E}{r^2}\frac{\boldsymbol{r}}{r}(1 + f(\boldsymbol{r}, \boldsymbol{v}))\,,$$

where $f(\boldsymbol{r},\boldsymbol{v})$ is expressed as

$$f(\boldsymbol{r},\boldsymbol{v}) = A\exp\left(-\frac{r-r_{\mathrm{E}}}{B-C(\boldsymbol{r}\cdot\boldsymbol{v})/(\boldsymbol{r}\cdot\boldsymbol{v}_{\mathrm{Sun}})}\right).$$

The velocity $\boldsymbol{v}$ is the velocity of the field-point in the "gravitational rest frame in the cosmic microwave background", and $\boldsymbol{v}_{\mathrm{Sun}}$ is the Sun's velocity in the gravitational rest frame. Numerical values for the adjustable constants are approximately $A = 2.2\times10^{-4}$, $B = 2.9\times10^{5}$ m, and $C = 2.3\times10^{5}$ m. Busack found that these values produce rather good agreement with the observed values for the flyby speed-changes.

Both of these alternative theories require a preferred frame-of-reference. Neither has been tested for the lunar orbit anomaly, and neither satisfies the causality principle because neither depends on the speed of gravity.

7 Conclusions and recommendations

This article shows conclusively that the proposed causal version of Newton's theory agrees with the now-known facts-of-observation. It applies only for slow-speeds and weak-fields. Effects of time retardation appear at the relatively large first-order v/c_{g} level, but they have not been seen in the past because they decrease inversely with the cube of the closest distance. If perigee is very close, however, time retardation effects can be relatively large. It is recommended that various available methods be used to detect new observations of effects of the causality principle.

Acknowledgements

I thank Patrick L. Ivers for reviewing many manuscripts and suggesting improvements. I also thank Dr. Robert A. Nelson for bringing to my attention the study of eclipses by F. R. Stevenson and L. V. Morrison [6]. I am especially thankful to Dr. Dmitri Rabounski for encouragement and support for this research project.

A complete version for this research project, containing all necessary details and comprehensive proofs, has been accepted for publication in *The Abraham Zelmanov Journal* [5].

Submitted on: December 07, 2012 / Accepted on: December 08, 2012

References

1. Anderson J.D., Campbell J.K., Ekelund J.E., Ellis J., and Jordon J.F. Anomalous orbital-energy changes observed during spacecraft flybys of Earth. *Physical Review Letters*, 2008, v.100, 091102.
2. Nieto M.M. and Anderson J.D. Earth flyby anomalies. arXiv: gr-qc/0910.1321.
3. Morse P.M. and Feshbach H. Methods of Theoretical Physics. McGraw-Hill, New York, 1953.
4. Rindler W. Essential Relativity, Special, General, and Cosmological. Springer, New York, 1977.
5. Hafele J.C. Earth flyby anomalies explained by time-retarded causal version of Newtonian gravitational theory. *The Abraham Zelmanov Journal*, 2012, v.5 (*under press*).
6. Stephenson F.R. and Morrison L.V. Long-term fluctuations in the Earth's rotation: 700 BC to AD 1990. *Philosophical Transactions of the Royal Society of London A*, 1995, v.351, 165–202.
7. Measuring the Moon's Distance. *LPI Bulletin*, 1994, http://eclipse.gsfc.nasa.gov/SEhelp/ApolloLaser.html
8. Cahill R.T. Combining NASA/JPL one-way optical-fibre light-speed data with spacecraft Earth-flyby Doppler-shift data to characterise 3-space flow. *Progress in Physics*, 2009, v.4, 50–64.
9. Busack H.J. Simulation of the flyby anomaly by means of an empirical asymmetric gravitational field with definite spatial orientation. arXiv: gen-ph/0711.2781.

Dynamical 3-Space Gravitational Waves: Reverberation Effects

Reginald T. Cahill and Samuel T. Deane

School of Chemical and Physical Sciences, Flinders University, Adelaide 5001, Australia. E-mail: Reg.Cahill@flinders.edu.au

Gravity theory missed a key dynamical process that became apparent only when expressed in terms of a velocity field, instead of the Newtonian gravitational acceleration field. This dynamical process involves an additional self-interaction of the dynamical 3-space, and experimental data reveals that its strength is set by the fine structure constant, implying a fundamental link between gravity and quantum theory. The dynamical 3-space has been directly detected in numerous light-speed anisotropy experiments. Quantum matter has been shown to exhibit an acceleration caused by the time-dependence and inhomogeneity of the 3-space flow, giving the first derivation of gravity from a deeper theory, as a quantum wave refraction effect. EM radiation is also refracted in a similar manner. The anisotropy experiments have all shown 3-space wave/turbulence effects, with the latest revealing the fractal structure of 3-space. Here we report the prediction of a new effect, namely a reverberation effect, when the gravitational waves propagate in the 3-space inflow of a large mass. This effect arises from the non-linear dynamics of 3-space. These reverberations could offer an explanation for the Shnoll effect, in which cosmological factors influence stochastic processes, such as radioactive decay rates.

1 Introduction

Newton's inverse square law of gravity, when expressed in terms of an acceleration field $\mathbf{g}(\mathbf{r}, t)$, has the differential form:

$$\nabla \cdot \mathbf{g} = -4\pi G\rho, \quad \nabla \times \mathbf{g} = \mathbf{0} \tag{1}$$

where G is the gravitational constant and ρ is the real matter density. The $\mathbf{g}$ field was believed to exist within an actual Euclidean space. It has become increasingly evident through the observation of spiral galaxies, the expanding universe and gravitational anomalies, that Newton's inverse square law is an incomplete theory of gravity. However a unique generalisation of (1) has lead to a resolution of these anomalies, by writing the acceleration field $\mathbf{g}(\mathbf{r}, t)$ in terms of the Euler acceleration of a velocity field $\mathbf{v}(\mathbf{r}, t)$ [1, 2]:

$$\mathbf{g} = \frac{\partial \mathbf{v}}{\partial t} + (\mathbf{v} \cdot \nabla)\mathbf{v}, \tag{2}$$

$$\nabla \cdot \left(\frac{\partial \mathbf{v}}{\partial t} + (\mathbf{v} \cdot \nabla)\mathbf{v} \right) = -4\pi G\rho, \quad \nabla \times \mathbf{v} = \mathbf{0}. \tag{3}$$

This approach utilises the the well known Galilean covariant Euler acceleration for a fluidic flow of the substratum with velocity $\mathbf{v}(\mathbf{r}, t)$. The velocity field is defined relative to an observer. The time dependent nature of the flow means that Newtonian gravity, within this flow formalism, can support wave phenomena. But a unique term can be added to (3) that generalises the flow equation, but also preserves the Keplerian nature of the planetary motions that underlie Newton's gravity formalisation:

$$\begin{gathered} \nabla \cdot \left(\frac{\partial \mathbf{v}}{\partial t} + (\mathbf{v} \cdot \nabla)\mathbf{v} \right) + \frac{\alpha}{8} \left((trD)^2 - tr(D^2) \right) = -4\pi G\rho, \\ \nabla \times \mathbf{v} = \mathbf{0}, \quad D_{ij} = \frac{1}{2} \left(\frac{\partial v_i}{\partial x_j} + \frac{\partial v_j}{\partial x_i} \right). \end{gathered} \tag{4}$$

Analysis of Bore Hole $\mathbf{g}$ anomaly data revealed that α is the fine structure constant [1]. The additional dynamics explains the "dark matter" effects, and so may be referred to as the dark matter term:

$$\rho_{DM}(\mathbf{r}) = \frac{\alpha}{32\pi G} \left((trD)^2 - tr(D^2) \right) \tag{5}$$

whereby

$$\nabla \cdot \mathbf{g} = \nabla \cdot \left(\frac{\partial \mathbf{v}}{\partial t} + \nabla \left(\frac{\mathbf{v}^2}{2} \right) \right) = -4\pi G \left(\rho_M + \rho_{DM} \right) \tag{6}$$

Dynamical 3-Space is unlike the dualistic space and aether theories of the past, as herein only space exists, and there is no aether. This dynamical and structured space provides an observable and observed local frame of reference. The flow of the dynamical 3-space has been detected many times dating back to the Michelson and Morley 1887 experiment, which has always, until 2002, been mistakenly reported as a null experiment. Wave effects, essentially gravitational waves, are apparent in the data from various anisotropy experiments*. A large part of understanding gravitational waves lies in how they originate, and also in understanding how they propagate. This work herein investigated the propagation of these gravitational waves within the background in-flow of a large mass, such as the earth or the sun. In doing so it was discovered that the dynamics of the propagation resulted in a reverberation effect, caused by the non-linear nature of the flow dynamics, apparent in (3) and (4).

*Vacuum mode Michelson interferometers have zero sensitivity to these waves. So such devices have a fundamental design flaw when intended to detect such waves.

2 3-Space flow dynamics

First we establish the in-flow of space into a spherical mass, assuming for simplicity that the mass is asymptotically at rest, which means that the in-flow has spherical symmetry. In the case of the earth we know that the earth has a large velocity with respect to to the local 3-space frame of reference, some 486 km/s in the direction RA = 4.3^h, Dec = -75° [3]. Here we restrict the analysis to the case of a spherically symmetric inflow into a spherical mass, with density $\rho(r)$ and total mass M. Then (4) becomes ($v' \equiv \partial v(r,t)/\partial r$)

$$\frac{\partial v'}{\partial t} + vv'' + \frac{2vv'}{r} + (v')^2 + \frac{\alpha}{2}\left(\frac{v^2}{2r^2} + \frac{vv'}{r}\right) = -4\pi G\rho \qquad (7)$$

which for a static flow has the exact solution

$$v(r)^2 = \frac{2\beta}{r^{\frac{\alpha}{2}}} + \frac{2G}{(1-\frac{\alpha}{2})r}\int_0^r 4\pi s^2\rho(s)ds + \\ + \frac{2G}{(1-\frac{\alpha}{2})r^{\frac{\alpha}{2}}}\int_r^\infty 4\pi s^{1+\frac{\alpha}{2}}\rho(s)ds, \qquad (8)$$

Here M is the total matter mass, and β is a free parameter. The term $2\beta/r^{\alpha/2}$ describes an inflow singularity or "black hole" with arbitrary strength. This is unrelated to the putative black holes of General Relativity. This corresponds to a primordial black hole. As well the last term in (8) also has a $1/r^{\alpha/2}$ inflow-singularity, but whose strength is mandated by the matter density, and is absent when $\rho(r) = 0$ everywhere. This is a minimal "black hole", and is present in all matter systems. The $2\beta/r^{\alpha/2}$ term will produce a novel long range gravitational acceleration $g = \alpha\beta/2r^{1+\alpha/2}$, as observed in spiral galaxies. For the region outside the sun Keplerian orbits are known to well describe the motion of the planets within the solar system, apart from some small corrections, such as the Precession of the Perihelion of Mercury, which follow from relativistic effects in the more general form of (2) [1]. The case $\beta = 0$ applies to the sun and earth, having only induced "Minimal Attractor" black holes. These minimal black holes contribute to the external $g(r) = GM^*/r^2$ gravitational acceleration, through an effective mass

$$M^* \approx M + \frac{\alpha}{2}M \qquad (9)$$

Outside of a spherical mass, with only an induced black hole, (8) has a solution $v \propto 1/\sqrt{r}$, and then $\rho_{DM} = 0$ outside of the sphere, which explains why the $\alpha-$term in (4) went undiscovered until 2005.

3 Gravitational wave reverberations

We now demonstrate that gravitational waves incoming on, say, a star or planet develop reverberations, in which the wave generates following copies of itself. For numerical accuracy in solving for time dependent effects in (4), we assume a spherically symmetric incoming wave, which is clearly unrealistic, and so find numerical solutions to (7), by using the ansatz $v(r,t) = v(r) + w(r,t)$, where $v(r) \sim -1/\sqrt{r}$ is the static in-flow from (8), applicable outside of the star/planet, and so ignoring the galactic background flow, and where $w(r,t)$ is the wave effect, with the initial wave $w(r,0)$ having the form of a pulse, as shown in fig.1, where the time evolution of $w(r,t)$ is also shown. We see that the initial pulse develops following copies of itself. This is a direct consequence of the non-linearity of (4), or even (3).

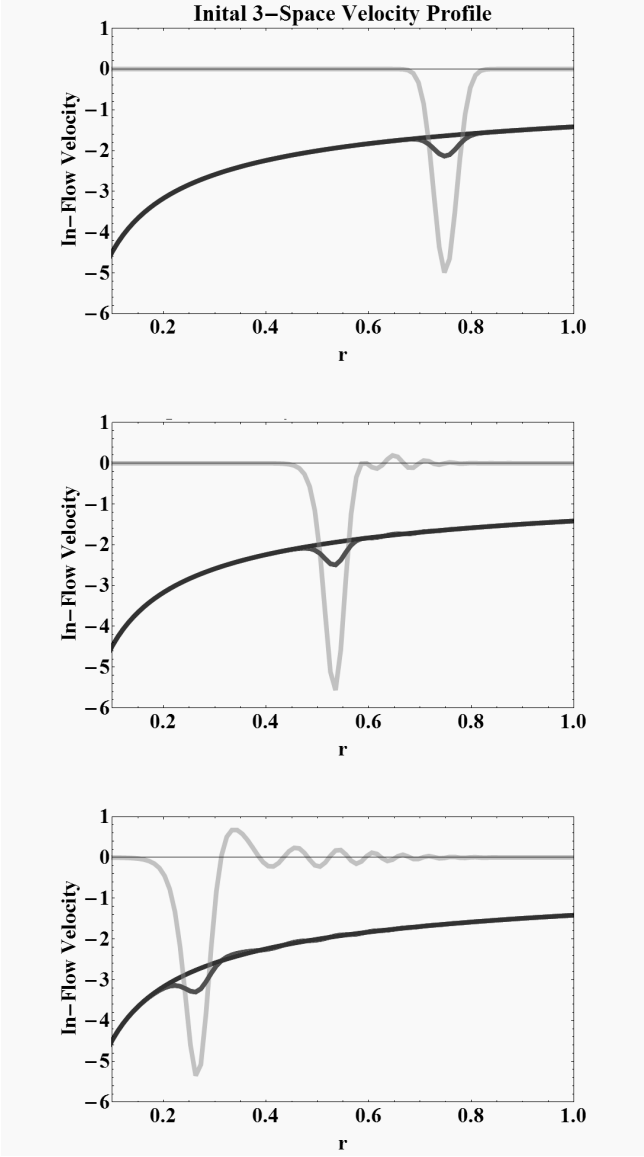

Fig. 1: Inflowing 3-space perturbation $w(r,t)$ (red) and un-perturbed inflow $v(r)$ (blue) velocity profiles outside a mass, with the waveform $w(r,t)$ also shown magnified (yellow).

These reverberations are expected to be detectable in EM speed anisotropy experiments. However because the 3-space

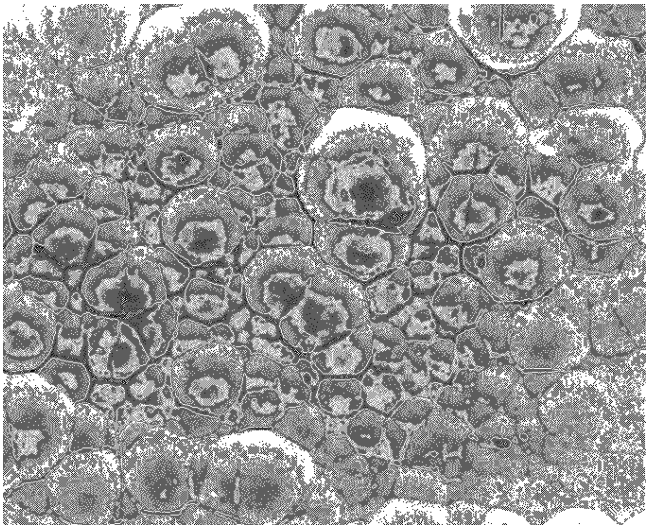

Fig. 2: Representation of the wave data revealing the fractal textured structure of the 3-space, with cells of space having slightly different velocities, and continually changing, and moving with respect to the earth with a speed of ∼500km/s, from [4].

is fractal, as illustrated in fig.2 [4], the reverberations are expected to be complex. As well all systems would generate reverberations, from planets, moons, sun and the galaxy. The timescale for such reverberations would vary considerably. As well as being directly observable in EM anisotropy and gravitational wave detectors, these reverberations would affect, for example, nuclear decay rates, as the magnitude of the 3-space fractal structure is modulated by the reverberations, and this fractal structure will stimulate nuclear processes. Patterns in the decay rates of nuclei have been observed by Shnoll *et al.*, with periodicities over many time scales [5].

The 3-space is detectable because the speed of EM waves, in vacuum is $c \approx 300,000$km/s with respect to that space itself, whereas an observer, in general, will observe anisotropy when the observer is in motion with respect to the space. This effect has been repeatedly observed for over 120 years. The anisotropy detections have always revealed wave/turbulence effects, including the original Michelson-Morley experiment. These wave effects are known as "gravitational waves", although a more appropriate description would be "space waves". In the limit $\alpha \to 0$, (4) and also (7) still have space wave effects, but these generate gravitational wave effects, namely fluctuations in the matter acceleration field $\mathbf{g}(r, t)$, only when $\alpha \neq 0$. So the α-dynamical term is not only responsible for the earth bore hole $\mathbf{g}$ anomaly, and for the so-called "dark matter" effects in spiral galaxies, but can also result in forces acting on matter resulting from the space wave phenomena, and will be large when significant wave effects occur, with large wave effects being essentially a galactic effect.

4 Acknowledgements

This report is from the Flinders University Gravitational Wave Detector Project, funded by an Australian Research Council Discovery Grant: *Development and Study of a New Theory of Gravity*. Special thanks to Dr David Brotherton-Ratcliffe and Professor Igor Bray for ongoing support.

Submitted on: December 7, 2012 / Accepted on December 10, 2012

References

1. Cahill R.T. Process Physics: From Information Theory to Quantum Space and Matter. Nova Science Pub., New York, 2005.
2. Cahill R.T. Dynamical 3-Space: A Review. *Ether Space-time and Cosmology: New Insights into a Key Physical Medium, Duffy M. and Lévy J., eds.*, Apeiron, Montreal, 2009, 135–200.
3. Cahill R.T. Combining NASA/JPL One-Way Optical-Fiber Light-Speed Data with Spacecraft Earth-Flyby Doppler-Shift Data to Characterise 3-Space Flow, *Progress in Physics*, 2009, v. 4, 50–64.
4. Cahill R.T. Characterisation of Low Frequency Gravitational Waves from Dual RF Coaxial-Cable Detector: Fractal Textured Dynamical 3-Space. *Progress in Physics*, 2012, v. 3, 3–10.
5. Shnoll S.E. Cosmophysical Factors in Stochastic Processes. American Research Press, Rehoboth, New Mexico, USA, 2012.

Derivation of Electromagnetism from the Elastodynamics of the Spacetime Continuum

Pierre A. Millette

University of Ottawa (alumnus), Ottawa, Canada. E-mail: PierreAMillette@alumni.uottawa.ca

We derive Electromagnetism from the Elastodynamics of the Spacetime Continuum based on the identification of the theory's antisymmetric rotation tensor with the electromagnetic field-strength tensor. The theory provides a physical explanation of the electromagnetic potential, which arises from transverse (shearing) displacements of the spacetime continuum, in contrast to mass which arises from longitudinal (dilatational) displacements. In addition, the theory provides a physical explanation of the current density four-vector, as the 4-gradient of the volume dilatation of the spacetime continuum. The Lorentz condition is obtained directly from the theory. In addition, we obtain a generalization of Electromagnetism for the situation where a volume force is present, in the general non-macroscopic case. Maxwell's equations are found to remain unchanged, but the current density has an additional term proportional to the volume force.

1 Introduction

Since Einstein first published his Theory of General Relativity in 1915, the problem of the unification of Gravitation and Electromagnetism has been and remains the subject of continuing investigation (see for example [1–9] for recent attempts). The Elastodynamics of the Spacetime Continuum [10, 11] is based on the application of a continuum mechanical approach to the spacetime continuum *(STC)*. Electromagnetism is found to come out naturally from the theory in a straightforward manner.

In this paper, we derive Electromagnetism from the Elastodynamics of the Spacetime Continuum (*STCED*). This theory thus provides a unified description of the spacetime deformation processes underlying general relativistic Gravitation [11] and Electromagnetism, in terms of spacetime continuum displacements resulting from the strains generated by the energy-momentum stress tensor.

1.1 A note on units and constants

In General Relativity and in Quantum Electrodynamics, it is customary to use "geometrized units" and "natural units" respectively, where the principal constants are set equal to 1. The use of these units facilitates calculations since cumbersome constants do not need to be carried throughout derivations. In this paper, all constants are retained in the derivations, to provide insight into the nature of the equations being developed.

In addition, we use rationalized MKSA units for Electromagnetism, as the traditionally used Gaussian units are gradually being replaced by rationalized MKSA units in more recent textbooks (see for example [12]). Note that the electromagnetic permittivity of free space ϵ_{em}, and the electromagnetic permeability of free space μ_{em} are written with "*em*" subscripts as the "0" subscripts are used in *STCED* constants. This allows us to differentiate between for example μ_{em}, the electromagnetic permeability of free space, and μ_0, the Lamé elastic constant for the shear modulus of the spacetime continuum.

2 Theory of Electromagnetism from *STCED*

2.1 Electromagnetic field strength

In the Elastodynamics of the Spacetime Continuum, the antisymmetric rotation tensor $\omega^{\mu\nu}$ is given by [11]

$$\omega^{\mu\nu} = \frac{1}{2}\left(u^{\mu;\nu} - u^{\nu;\mu}\right) \tag{1}$$

where u^μ is the displacement of an infinitesimal element of the spacetime continuum from its unstrained position x^μ. This tensor has the same structure as the electromagnetic field-strength tensor $F^{\mu\nu}$ defined as [13, see p. 550]:

$$F^{\mu\nu} = \partial^\mu A^\nu - \partial^\nu A^\mu \tag{2}$$

where A^μ is the electromagnetic potential four-vector $(\phi, \vec{A})$, ϕ is the scalar potential and $\vec{A}$ the vector potential.

Identifying the rotation tensor $\omega^{\mu\nu}$ with the electromagnetic field-strength tensor according to

$$F^{\mu\nu} = \varphi_0 \omega^{\mu\nu} \tag{3}$$

leads to the relation

$$A^\mu = -\frac{1}{2}\varphi_0 u^\mu_\perp \tag{4}$$

where the symbolic subscript $\perp$ of the displacement u^μ indicates that the relation holds for a transverse displacement (perpendicular to the direction of motion) [11].

Due to the difference in the definition of $\omega^{\mu\nu}$ and $F^{\mu\nu}$ with respect to their indices, a negative sign is introduced, and is attributed to (4). This relation provides a physical explanation

for the electromagnetic potential: it arises from transverse (shearing) displacements of the spacetime continuum, in contrast to mass which arises from longitudinal (dilatational) displacements of the spacetime continuum [11]. Sheared spacetime is manifested as electromagnetic potentials and fields.

2.2 Maxwell's equations and the current density four-vector

Taking the divergence of the rotation tensor of (1), gives

$$\omega^{\mu\nu}{}_{;\mu} = \frac{1}{2}\,(u^{\mu;\nu}{}_{\mu} - u^{\nu;\mu}{}_{\mu}). \tag{5}$$

Recalling (28) from Millette [11], viz.

$$\mu_0 u^{\nu;\mu}{}_{\mu} + (\mu_0 + \lambda_0) u^{\mu}{}_{;\mu}{}^{\nu} = -X^{\nu} \tag{6}$$

where X^{ν} is the volume force and λ_0 and μ_0 are the Lamé elastic constants of the spacetime continuum, substituting for $u^{\nu;\mu}{}_{\mu}$ from (6) into (5), interchanging the order of partial differentiation in $u^{\mu;\nu}{}_{\mu}$ in (5), and using the relation $u^{\mu}{}_{;\mu} = \varepsilon^{\mu}{}_{\mu} = \varepsilon$ from (19) of [11], we obtain

$$\omega^{\mu\nu}{}_{;\mu} = \frac{2\mu_0 + \lambda_0}{2\mu_0}\,\varepsilon^{;\nu} + \frac{1}{2\mu_0}\,X^{\nu}. \tag{7}$$

As seen in [11], in the macroscopic local case, the volume force X^{ν} is set equal to zero to obtain the macroscopic relation

$$\omega^{\mu\nu}{}_{;\mu} = \frac{2\mu_0 + \lambda_0}{2\mu_0}\,\varepsilon^{;\nu} \tag{8}$$

Using (3) and comparing with the covariant form of Maxwell's equations [14, see pp. 42–43]

$$F^{\mu\nu}{}_{;\mu} = \mu_{em} j^{\nu} \tag{9}$$

where j^{ν} is the current density four-vector $(c\varrho, \vec{j})$, ϱ is the charge density scalar, and $\vec{j}$ is the current density vector, we obtain the relation

$$j^{\nu} = \frac{\varphi_0}{\mu_{em}}\,\frac{2\mu_0 + \lambda_0}{2\mu_0}\,\varepsilon^{;\nu}. \tag{10}$$

This relation provides a physical explanation of the current density four-vector: it arises from the 4-gradient of the volume dilatation of the spacetime continuum. A corollary of this relation is that massless (transverse) waves cannot carry an electric charge or produce a current.

Substituting for j^{ν} from (10) in the relation [15, see p. 94]

$$j^{\nu} j_{\nu} = \varrho^2 c^2, \tag{11}$$

we obtain the expression for the charge density

$$\varrho = \frac{1}{2}\,\frac{\varphi_0}{\mu_{em} c}\,\frac{2\mu_0 + \lambda_0}{2\mu_0}\,\sqrt{\varepsilon^{;\nu}\varepsilon_{;\nu}} \tag{12}$$

or, using the relation $c = 1/\sqrt{\epsilon_{em}\mu_{em}}$,

$$\varrho = \frac{1}{2}\,\varphi_0 \epsilon_{em} c\,\frac{2\mu_0 + \lambda_0}{2\mu_0}\,\sqrt{\varepsilon^{;\nu}\varepsilon_{;\nu}}. \tag{13}$$

Up to now, our identification of the rotation tensor $\omega^{\mu\nu}$ of the Elastodynamics of the Spacetime Continuum with the electromagnetic field-strength tensor $F^{\mu\nu}$ has generated consistent results, with no contradictions.

2.3 The Lorentz condition

The Lorentz condition can be derived directly from the theory. Taking the divergence of (4), we obtain

$$A^{\mu}{}_{;\mu} = -\frac{1}{2}\,\varphi_0 u_{\perp}{}^{\mu}{}_{;\mu}. \tag{14}$$

From (23) of [11], viz.

$$\omega^{\mu}{}_{\mu} = u_{\perp}{}^{\mu}{}_{;\mu} = 0, \tag{15}$$

(14) simplifies to

$$A^{\mu}{}_{;\mu} = 0. \tag{16}$$

The Lorentz condition is thus obtained directly from the theory. The reason for the value of zero is that transverse displacements are massless because such displacements arise from a change of shape (distortion) of the spacetime continuum, not a change of volume (dilatation).

2.4 Four-vector potential

Substituting (4) into (5) and rearranging terms, we obtain the equation

$$\nabla^2 A^{\nu} - A^{\mu;\nu}{}_{\mu} = \varphi_0 \omega^{\mu\nu}{}_{;\mu} \tag{17}$$

and, using (3) and (9), this equation becomes

$$\nabla^2 A^{\nu} - A^{\mu;\nu}{}_{\mu} = \mu_{em} j^{\nu}. \tag{18}$$

Interchanging the order of partial differentiation in the term $A^{\mu;\nu}{}_{\mu}$ and using the Lorentz condition of (16), we obtain the well-known wave equation for the four-vector potential [14, see pp. 42–43]

$$\nabla^2 A^{\nu} = \mu_{em} j^{\nu}. \tag{19}$$

The results we obtain are thus consistent with the macroscopic theory of Electromagnetism, with no contradictions.

3 Electromagnetism and the volume force X^{ν}

We now investigate the impact of the volume force X^{ν} on the equations of Electromagnetism. Recalling (7), Maxwell's equation in terms of the rotation tensor is given by

$$\omega^{\mu\nu}{}_{;\mu} = \frac{2\mu_0 + \lambda_0}{2\mu_0}\,\varepsilon^{;\nu} + \frac{1}{2\mu_0}\,X^{\nu}. \tag{20}$$

Substituting for $\omega^{\mu\nu}$ from (3), this equation becomes

$$F^{\mu\nu}{}_{;\mu} = \varphi_0 \frac{2\mu_0 + \lambda_0}{2\mu_0}\,\varepsilon^{;\nu} + \frac{\varphi_0}{2\mu_0}\,X^{\nu}. \tag{21}$$

The additional X^{ν} term can be allocated in one of two ways:

1. either j^ν remains unchanged as given by (10) and the expression for $F^{\mu\nu}{}_{;\mu}$ has an additional term as developed in Section 3.1 below,
2. or $F^{\mu\nu}{}_{;\mu}$ remains unchanged as given by (9) and the expression for j^ν has an additional term as developed in Section 3.2 below.

Option 2 is shown in the following derivation to be the logically consistent approach.

3.1 j^ν unchanged (contradiction)

Using (10) (j^ν unchanged) into (21), Maxwell's equation becomes

$$F^{\mu\nu}{}_{;\mu} = \mu_{em} j^\nu + \frac{\varphi_0}{2\mu_0} X^\nu. \tag{22}$$

Using (20) into (17) and making use of the Lorentz condition, the wave equation for the four-vector potential becomes

$$\nabla^2 A^\nu - \frac{\varphi_0}{2\mu_0} X^\nu = \mu_{em} j^\nu. \tag{23}$$

In this case, the equations for $F^{\mu\nu}{}_{;\mu}$ and A^ν both contain an additional term proportional to X^ν.

We show that this option is not logically consistent as follows. Using (10) into the continuity condition for the current density [14]

$$\partial_\nu j^\nu = 0 \tag{24}$$

yields the expression

$$\nabla^2 \varepsilon = 0. \tag{25}$$

This equation is valid in the macroscopic case where $X^\nu = 0$, but disagrees with the general case (non-zero X^ν) given by (35) of [11], viz.

$$(2\mu_0 + \lambda_0)\nabla^2 \varepsilon = -X^\nu{}_{;\nu}. \tag{26}$$

This analysis leads to a contradiction and consequently is not valid.

3.2 $F^{\mu\nu}{}_{;\mu}$ unchanged (logically consistent)

Proper treatment of the general case requires that the current density four-vector be proportional to the RHS of (21) as follows ($F^{\mu\nu}{}_{;\mu}$ unchanged):

$$\mu_{em} j^\nu = \varphi_0 \frac{2\mu_0 + \lambda_0}{2\mu_0} \varepsilon^{;\nu} + \frac{\varphi_0}{2\mu_0} X^\nu. \tag{27}$$

This yields the following general form of the current density four-vector:

$$j^\nu = \frac{1}{2} \frac{\varphi_0}{\mu_{em}\mu_0} [(2\mu_0 + \lambda_0)\varepsilon^{;\nu} + X^\nu]. \tag{28}$$

Using this expression in the continuity condition for the current density given by (24) yields (26) as required.

Using (28) into (21) yields the same covariant form of the Maxwell equations as in the macroscopic case:

$$F^{\mu\nu}{}_{;\mu} = \mu_{em} j^\nu \tag{29}$$

and the same four-vector potential equation

$$\nabla^2 A^\nu = \mu_{em} j^\nu \tag{30}$$

in the Lorentz gauge.

3.3 Homogeneous Maxwell equation

The validity of this analysis can be further demonstrated from the homogeneous Maxwell equation [14]

$$\partial^\alpha F^{\beta\gamma} + \partial^\beta F^{\gamma\alpha} + \partial^\gamma F^{\alpha\beta} = 0. \tag{31}$$

Taking the divergence of this equation over α,

$$\partial_\alpha \partial^\alpha F^{\beta\gamma} + \partial_\alpha \partial^\beta F^{\gamma\alpha} + \partial_\alpha \partial^\gamma F^{\alpha\beta} = 0. \tag{32}$$

Interchanging the order of differentiation in the last two terms and making use of (29) and the antisymmetry of $F^{\mu\nu}$, we obtain

$$\nabla^2 F^{\beta\gamma} + \mu_{em}(j^{\beta;\gamma} - j^{\gamma;\beta}) = 0. \tag{33}$$

Substituting for j^ν from (28),

$$\nabla^2 F^{\beta\gamma} = -\frac{\varphi_0}{2\mu_0} [(2\mu_0 + \lambda_0)(\varepsilon^{;\beta\gamma} - \varepsilon^{;\gamma\beta}) + (X^{\beta;\gamma} - X^{\gamma;\beta})]. \tag{34}$$

(42) of [11], viz.

$$\mu_0 \nabla^2 \varepsilon^{\mu\nu} + (\mu_0 + \lambda_0)\varepsilon^{;\mu\nu} = -X^{(\mu;\nu)} \tag{35}$$

shows that $\varepsilon^{;\mu\nu}$ is a symmetrical tensor. Consequently the difference term $(\varepsilon^{;\beta\gamma} - \varepsilon^{;\gamma\beta})$ disappears and (34) becomes

$$\nabla^2 F^{\beta\gamma} = -\frac{\varphi_0}{2\mu_0} (X^{\beta;\gamma} - X^{\gamma;\beta}). \tag{36}$$

Expressing $F^{\mu\nu}$ in terms of $\omega^{\mu\nu}$ using (3), the resulting equation is identical to (39) of [11], viz.

$$\mu_0 \nabla^2 \omega^{\mu\nu} = -X^{[\mu;\nu]} \tag{37}$$

confirming the validity of this analysis of Electromagnetism including the volume force.

(28) to (30) are the self-consistent electromagnetic equations derived from the Elastodynamics of the Spacetime Continuum with the volume force. In conclusion, Maxwell's equations remain unchanged. The current density four-vector is the only quantity affected by the volume force, with the addition of a second term proportional to the volume force. It is interesting to note that the current density obtained from the quantum mechanical Klein-Gordon equation with an electromagnetic field also consists of the sum of two terms [16, see p. 35].

4 Discussion and conclusion

In this paper, we have derived Electromagnetism from the Elastodynamics of the Spacetime Continuum based on the identification of the theory's antisymmetric rotation tensor $\omega^{\mu\nu}$ with the electromagnetic field-strength tensor $F^{\mu\nu}$.

The theory provides a physical explanation of the electromagnetic potential: it arises from transverse (shearing) displacements of the spacetime continuum, in contrast to mass which arises from longitudinal (dilatational) displacements of the spacetime continuum. Hence sheared spacetime is manifested as electromagnetic potentials and fields.

In addition, the theory provides a physical explanation of the current density four-vector: it arises from the 4-gradient of the volume dilatation of the spacetime continuum. A corollary of this relation is that massless (transverse) waves cannot carry an electric charge or produce a current.

The transverse mode of propagation involves no volume dilatation and is thus massless. Transverse wave propagation is associated with the distortion of the spacetime continuum. Electromagnetic waves are transverse waves propagating in the *STC* itself, at the speed of light.

The Lorentz condition is obtained directly from the theory. The reason for the value of zero is that transverse displacements are massless because such displacements arise from a change of shape (distortion) of the spacetime continuum, not a change of volume (dilatation).

In addition, we have obtained a generalization of Electromagnetism for the situation where a volume force is present, in the general non-macroscopic case. Maxwell's equations are found to remain unchanged, but the current density has an additional term proportional to the volume force X^{ν}.

The Elastodynamics of the Spacetime Continuum thus provides a unified description of the spacetime deformation processes underlying general relativistic Gravitation and Electromagnetism, in terms of spacetime continuum displacements resulting from the strains generated by the energy-momentum stress tensor.

Submitted on December 9, 2012 / Accepted on December 10, 2012

References

1. Horie K. Geometric Interpretation of Electromagnetism in a Gravitational Theory with Space–Time Torsion. arXiv: hep-th/9409018v1.
2. Sidharth B.G. The Unification of Electromagnetism and Gravitation in the Context of Quantized Fractal Space Time. arXiv: gen-ph/0007021v1.
3. Wu N. Unification of Electromagnetic Interactions and Gravitational Interactions. arXiv: hep-th/0211155v1.
4. Rabounski D. A Theory of Gravity Like Electrodynamics. *Progress in Physics*, 2005, v. 2, 15–29.
5. Wanas M.I. and Ammar S.A. Space-Time Structure and Electromagnetism. arXiv: gr-qc/0505092v2.
6. Shahverdiyev S.S. Unification of Electromagnetism and Gravitation in the Framework of General Geometry. arXiv: gen-ph/0507034v1.
7. Chang Y.-F. Unification of Gravitational and Electromagnetic Fields in Riemannian Geometry. arXiv: gen-ph/0901.0201v1.
8. Borzou A. and Sepangi H.R. Unification of Gravity and Electromagnetism Revisited. arXiv: gr-qc/0904.1363v3.
9. Chernitskii A.A. On Unification of Gravitation and Electromagnetism in the Framework of a General-Relativistic Approach. arXiv: gr-qc/0907.2114v1.
10. Millette P.A. On the Decomposition of the Spacetime Metric Tensor and of Tensor Fields in Strained Spacetime. *Progress in Physics*, 2012, v. 4, 5–8.
11. Millette P.A. The Elastodynamics of the Spacetime Continuum as a Framework for Strained Spacetime. *Progress in Physics*, 2013, v. 1, 55–59.
12. Baylis W.E. Electrodynamics, A Modern Approach. Birkhäuser, Boston, 2002.
13. Jackson J.D. Classical Electrodynamics, 2nd ed. John Wiley & Sons, New York, 1975.
14. Charap J.M. Covariant Electrodynamics, A Concise Guide. The John Hopkins University Press, Baltimore, 2011.
15. Barut A.O. Electrodynamics and Classical Theory of Fields and Particles. Dover Publications, New York, 1980.
16. Greiner W. Relativistic Quantum Mechanics, Wave Equations. Springer-Verlag, New York, 1994.

Peculiar Relations in Cosmology

U. V. S. Seshavatharam* and S. Lakshminarayana†

*Honorary faculty, I-SERVE, Alakapuri, Hyderabad, AP, India. E-mail: seshavatharam.uvs@gmail.com
†Department of Nuclear Physics, Andhra University, Visakhapatnam-03, AP, India. E-mail: lnsrirama@yahoo.com

Within the expanding cosmic Hubble volume, the Hubble length can be considered as the gravitational or electromagnetic interaction range. The product of 'Hubble volume' and 'cosmic critical density' can be called the 'Hubble mass'. Based on this cosmic mass unit, the authors noticed three peculiar semi empirical applications. With these applications it is possible to say that in atomic and nuclear physics, there exists a cosmological physical variable. By observing its rate of change, the future cosmic acceleration can be verified, time to time Hubble's constant can be estimated and finally a unified model of the four cosmological interactions can be developed.

1 Introduction

If we write $R_0 \cong (c/H_0)$ as a characteristic cosmic Hubble radius then the characteristic cosmic Hubble volume is $V_0 \cong \frac{4\pi}{3}R_0^3$. With reference to the critical density $\rho_c \cong \frac{3H_0^2}{8\pi G}$ and the characteristic cosmic Hubble volume, the characteristic cosmic Hubble mass can be expressed as $M_0 \cong \rho_c \cdot V_0 \cong \frac{c^3}{2GH_0}$. If we do not yet know whether the universe is spatially closed or open, then the idea of Hubble volume [1–3] or Hubble mass can be used as a tool in cosmology and unification. This idea is very close to Mach's idea of distance cosmic background. It seems to be a quantitative description to Mach's principle. In understanding the basic concepts of unification of the four cosmological interactions, the cosmic radius (c/H_0) can be considered as the infinite range of the gravitational or electromagnetic interaction. Within the Hubble volume it is noticed that: 1) Each and every point in free space is influenced by the Hubble mass. 2) Hubble mass plays a vital role in understanding the properties of electromagnetic and nuclear interactions and 3) Hubble mass plays a key role in understanding the geometry of the universe.

2 Application 1

Note that large dimensionless constants and compound physical constants reflect an intrinsic property of nature [4,5]. If $\rho_c c^2$ is the present cosmic critical energy density and aT_0^4 is the present cosmic thermal energy density, with this M_0 it is noticed that $\ln\sqrt{\frac{aT_0^4}{\rho_c c^2}\cdot\frac{4\pi\epsilon_0 GM_0^2}{e^2}} \cong \frac{1}{\alpha}$ and at present if $T_0 \cong 2.725$ °K, obtained $H_0 \cong 71.415$ km/sec/Mpc [6,7]. It is also noticed that $\ln\left[\frac{\rho_m}{\rho_c}\sqrt{\frac{4\pi\epsilon_0 GM_0^2}{e^2}}\right] \cong \frac{1}{\alpha}$ where ρ_m is the present cosmic matter density. Obtained $\rho_m \cong 6.70\times10^{-29}$ kg/m^3 is matching with the matter density of spiral and elliptical galaxies. Please note that almost (60 to 70)% of the galaxies are in the form of elliptical and spiral galaxies.

3 Application 2

With this M_0 it is noticed that, $\frac{\hbar c}{Gm_p\sqrt{M_0 m_e}} \cong 1$ where m_p and m_e are the rest masses of proton and electron respectively. This is a very peculiar result. With this relation, obtained value of the present Hubble's constant is 70.75 km/sec/Mpc. From this relation it is clear that, in the presently believed atomic and nuclear "physical constants", there exists one cosmological variable! By observing its cosmological rate of change, the "future" cosmic acceleration can be verified.

4 Application 3

With reference to the Planck mass $M_p \cong \sqrt{\hbar c/G}$ and the elementary charge e, a new mass unit $M_C \cong \sqrt{e^2/4\pi\epsilon_0 G}$ can be constructed. With M_0 and M_C it can be assumed that cosmic thermal energy density, matter energy density and the critical energy density are in geometric series and the geometric ratio is $1+\ln\left(\frac{M_0}{M_C}\right)$. Thus, $\left(\frac{\rho_c c^2}{\rho_m c^2}\right)_0 \cong \left[1+\ln\left(\frac{M_0}{M_C}\right)\right]$ and $\left(\frac{\rho_c c^2}{aT^4}\right)_0 \cong \left[1+\ln\left(\frac{M_0}{M_C}\right)\right]^2$. It is another peculiar observation and the corresponding present CMBR temperature is $T_0 \cong 2.718$ °K. Independent of the cosmic redshift and CMBR observations, with these coincidences it is possible to understand and decide the cosmic geometry. The mystery can be resolved only with further research, analysis, discussions and encouragement.

Submitted on December 13, 2012 / Accepted on December 17, 2012.

References

1. Seshavatharam U. V. S. Physics of rotating and expanding black hole universe. *Progress in Physics*, 2010, v. 2, 7–14.
2. Seshavatharam U. V. S. and Lakshminarayana S. Hubble volume and the fundamental interactions. *International Journal of Applied and Natural Sciences (IJANS)*, 2012, v. 1 (2), 45–58.
3. Seshavatharam U. V. S. and S. Lakshminarayana S. Atom, universe and the fundamental interactions. *Global Journal of Science Frontier Research (A)*, 2012, v. 12 (5), 1.
4. Dirac P. A. M. The cosmological constants. *Nature*, 1937, v. 139, 323.
5. Dirac P. A. M. A new basis for cosmology. *Proc. Roy. Soc. A*, 1938, v. 165, 199.
6. Huchara J. Estimates of the Hubble Constant. *Harvard-Smithsonian Center for Astrophysics*, 2010, http://hubble.plot.dat.
7. Freedman W. L. et al. Final Results from the Hubble Space Telescope Key Project to Measure the Hubble Constant. *The Astrophysical Journal*, 2001, v. 553 (1) 47–72.

Change of Measure between Light Travel Time and Euclidean Distances

Yuri Heymann

3 rue Chandieu, 1202 Geneva, Switzerland. E-mail: y.heymann@yahoo.com

The problem of cosmological distances is approached using a method based on the propagation of light in an expanding Universe. From the change of measure between Light Travel Time and Euclidean Distances, a formula is derived to compute distances as a function of redshift. This formula is identical to Mattig's formula (with $q_0 = 1/2$) which is based on Friedmann's equations of general relativity.

1 Introduction

Euclidean Distances were introduced in [1], and it was suggested that Euclidean Distances need to be used in order to derive the galactic density profile which is the evolution of galactic density over time. The LTD (Light Travel Distance) is the distance traversed by a photon between the time it is emitted and the time it reaches the observer, which may be also referred to as the Light Travel Time. We define the Euclidean distance as the equivalent distance that would be traversed by a photon between the time it is emitted and the time it reaches the observer if there were no expansion of the Universe.

In the present study, a time-varying Hubble coefficient in the Euclidean framework is introduced assuming that the Hubble law observed in the LTD framework is still applicable in the Euclidean framework. The model provides a "kinematic age of the Universe" which is purely mathematical as it is a result of the change of measure between LTDs and Euclidean Distances. A proof is made that a flat Hubble constant in the LTD framework (i.e that does not vary with LTD) is equivalent to a second order forward time-varying Euclidean Hubble coefficient in the Euclidean framework.

2 Foundations of the theory

The observed Hubble constant that is commonly referred to in the literature is a measure of space expansion with respect to LTDs. The Euclidean Hubble coefficient is being defined as the space expansion with respect to Euclidean Distances. This is a change of measure considering that the Euclidean Hubble coefficient varies with time such that the Hubble law is still applicable in the Euclidean framework. This leads to the following equation

$$H_i(t) = \frac{\dot{a}}{a}, \tag{1}$$

where H_i is the instantaneous Euclidean Hubble coefficient, $\dot{a}$ is the Universe expansion velocity and a the scale factor

The main postulate of the present study is that the Euclidean Hubble coefficient needs to be used in order to compute the scale factor in metric distances and not on the basis of LTDs, see (1). If we did not compute the scale factor on the basis of metric distances, the equation would fail to work with cosmological redshifts, which are a homothetic transformation for describing the evolution of light wavelength.

The instantaneous Euclidean Hubble coefficient is defined as the rate of expansion in Euclidean metrics at any given point in time along the trajectory of a light ray reaching the observer.

As space between the photon and the observer expands, this expansion is added to the overall distance the photon has to travel in order to reach the observer; therefore, the Euclidean Distance between the photon and the observer is defined by the following differential equations, respectively in the temporal and metric form:

1) In the LTD framework (the temporal form)

$$\frac{dy}{dt} = -c + H_0\, c\, T, \tag{2}$$

where: y is the Euclidean Distance between the photon and the observer, T the LTD between the observer and the photon, c the celerity of light, and H_0 the Hubble constant as of today;

2) In the Euclidean framework (the metric form)

$$\frac{dy}{dt} = -c + H_i(t)\, y, \tag{3}$$

where y is the Euclidean Distance between the photon and the observer, c the celerity of light, and $H_i(t)$ the Euclidean time-varying Hubble coefficient.

For the purpose of convenience let us consider the following form for the Euclidean time-varying Hubble coefficient

$$H_i(t) = \frac{n}{t}, \tag{4}$$

where $H_i(t)$ is the Euclidean time-varying Hubble coefficient, n the order of the time-varying Euclidean Hubble, and t the time from the hypothetical big bang for which time was set to zero.

Note that in the present study both the Hubble constant and the Euclidean Hubble coefficient are expressed in units of $[time^{-1}]$ by converting all distances into Light Travel Time, and with the celerity $c = 1$.

3 Proof that a flat Hubble constant in the LTD framework is time varying of order two in the Euclidean framework

First, let us solve the differential equation for the propagation of light in the LTD framework assuming a flat Hubble constant (i.e. that does not vary with LTD). Let us consider a photon initially situated at a Euclidean Distance y_0 from the observer and moving at celerity c in the direction of the observer. Let us say T is the initial LTD between the photon and the observer, and define the Hubble constant function of LTDs.

The differential equation describing the propagation of light in the LTD framework is described by (2). By setting time zero at a reference T_b in the past, we have $t = T_b - T$; therefore, $dt = -dT$. Hence, (2) becomes

$$\frac{dy}{dT} = c - H_0\, c\, T\,, \tag{5}$$

with boundary conditions $y(T) = y_0$, and $y(0) = 0$.

By integration from 0 to T, the following relationship relating Euclidean Distances y to Light Travel Distances T is obtained

$$y = c\, T - \frac{c\, H_0\, T^2}{2}\,. \tag{6}$$

Now let us derive the differential equation for the propagation of light in the Euclidean framework assuming the time-varying Hubble coefficient from (4) (see Figure 1). From the differential equation describing the propagation of light in the Euclidean framework (3), we get

$$\frac{dy}{dt} = -c + \frac{n}{t}\, y\,. \tag{7}$$

By integrating this first order non-homogeneous differential equation between $T_b - T$ and T_b, the following solution is obtained which describes the relationship between Euclidean Distances and LTDs

$$y = \frac{c}{n-1}\left(Tb - T - Tb^{1-n}\,(Tb - T)^n\right). \tag{8}$$

By setting n equal to 2 in (8) for a second order time-varying Hubble coefficient, we get

$$y = c\left(T - \frac{T^2}{T_b}\right). \tag{9}$$

Based on the recession speed, the relationship between the Hubble constant defined function of LTDs, and the Euclidean Hubble, for T small is as follows

$$H_0\, c\, T = \frac{n}{(Tb - T)}\, y\,. \tag{10}$$

Hence, $\frac{n}{T_b}$ is obtained by computing the following limit

$$\frac{n}{T_b} = \lim_{T\to 0}\left(\frac{H_0\, c\, T}{y}\right). \tag{11}$$

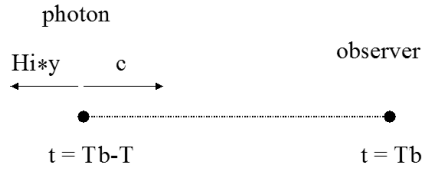

Fig. 1: Schema to represent the propagation of light in an expanding space in the Euclidean framework. Where T is the Light Travel Distance between the observer and the source of light, T_b is the kinematic age of the Universe, and n the order of the time-varying Hubble coefficient (time zero set at time T_b from today).

By substitution of y from (8), we get

$$\frac{n}{T_b} = \lim_{T\to 0}\left(\frac{(n-1)\, T\cdot H_0}{T_b - T - T_b^{1-n}\,(T_b - T)^n}\right) = H_0\,. \tag{12}$$

Therefore, the "kinematic age of the Universe" is

$$T_b = \frac{n}{H_0}, \tag{13}$$

with H_0 the Hubble constant as of today.

By substitution of $T_b = \frac{2}{H_0}$ into (9), we get

$$y = c\, T - \frac{c\, H_0\, T^2}{2}\,. \tag{14}$$

This solution is identical to (6) relating LTDs to Euclidean Distances for the flat Hubble constant in the LTD framework. This is the proof that a flat Hubble constant in the LTD framework is equivalent to a time-varying Hubble coefficient of order two in the Euclidean framework. The equation $H_i(t) = 2/t$ is the connection between (2) and (3).

We can easily show that the recession speed with the second order time-varying Hubble coefficient in the Euclidean framework is the same as the recession speed in the LTD framework. The calculations are as follow

$$H_i(t)\; y = \frac{2}{t}\, y = \frac{2\, c}{T_b - T}\left(T - \frac{H_0\, T^2}{2}\right). \tag{15}$$

By substitution of T_b from (13) (with a second order time-varying Hubble coefficient) into (15), we obtain

$$H_i(t)\, y = H_0\, c\, T\,, \tag{16}$$

where T is the LTD between the observer and the source of light, and y the Euclidean Distance.

4 Evolutionary model of the scale factor

The differential equation describing the evolution of the scale factor a is as follows, identical to (1),

$$\frac{da}{dt} = H_i(t)\, a\,. \tag{17}$$

As $H_i(t) = \frac{2}{t}$, we get

$$\int_{a_1}^{a_0} \frac{1}{a} da = \int_{T_b - T}^{T_b} \frac{2}{t} dt . \quad (18)$$

By integrating (18) , we obtain

$$\ln\left(\frac{a_0}{a_1}\right) = 2 \ln\left(\frac{T_b}{T_b - T}\right), \quad (19)$$

which is equivalent to

$$\frac{a_0}{a_1} = \left(\frac{T_b}{T_b - T}\right)^2 . \quad (20)$$

5 Expression of distances versus redshifts

From cosmological redshifts, we have

$$1 + z = \frac{a_0}{a_1} , \quad (21)$$

where a_0 is the present scale factor, a_1 the scale factor at redshift z.

Combining (20) and (21), we get

$$T = T_b \left(1 - \frac{1}{\sqrt{1+z}}\right). \quad (22)$$

By substitution of T_b from (13) for a second order time-varying Hubble coefficient, we get the following equation relating LTD to redshifts

$$T = \frac{2}{H_0} \left(1 - \frac{1}{\sqrt{1+z}}\right). \quad (23)$$

6 Comparison with the equation of Mattig

The equation of Mattig [2] is as follows

$$rR_0 = \frac{1}{H_0 q_0^2 (1+z)} \times \times \left(q_0 z + (q_0 - 1)(\sqrt{1 + 2q_0 z} - 1)\right), \quad (24)$$

where r is the distance, q_0 is the deceleration parameter, R_0 the present scale factor, z the redshift, H_0 the present scale factor.

For comparison purpose with the equation of the present study, we should set q_0 equal to 1/2 (flat matter dominated Universe), and R_0 to 1. Therefore, we obtain

$$r = \frac{2}{H_0} \left(1 - \frac{1}{\sqrt{1+z}}\right). \quad (25)$$

This formula is identical to (23). We have just shown that the solution to our problem is identical to Mattig formula for q_0 equal to 1/2.

7 Discussion

Based on the change of measure between LTD and Euclidean Distances, a formula that expresses distances versus redshifts is obtained. From the change of framework between LTD and Euclidean distances, it has been proved that a flat Hubble constant (that does not vary with LTD) is equivalent to a time-varying Euclidean Hubble coefficient of order two. Finally, the evolutionary model of the scale factor is derived and matched to the cosmological redshift equation in order to obtain the LTD versus redshift equation. This equation is identical to Mattig's formula (with $q_0 = 1/2$) which is based on Friedmann's equations of general relativity. The Euclidean Hubble coefficient was used in order to derive the evolution of the scale factor in metric distances; otherwise, the cosmological redshift equation would not be applicable to light wavelengths. This study proposes a new approach to compute cosmological distances which is based on the introduction of Euclidean Distances in addition to Light Travel Distances in an expanding Universe, and a change of measure. The calculations involved are quite simple and our definition of Euclidean Distances may be used as a source of inspiration to develop future cosmological models.

Acknowledgements

The author is deeply indebted to Edmund Wood for his support in correcting my English.

Submitted on December 4, 2012 / Accepted on December 15, 2012

References

1. Heymann Y. Building galactic density profiles. *Progress in Physics*, 2011, v. 4, 63–67.
2. Mattig W. Über den Zusammenhang zwischen Rotverschiebung und scheinbarer Helligkeit. *Astronomische Nachrichten*, 1958, v. 284, 109–111.

E(5) Characters to ^{100}Ru Isotope

Sohair M. Diab* and Salah A. Eid†
*College of Sciences (Women Section), Phys. Dept., Umm Al-Qura University, Saudi Arabia.
†Faculty of Engineering, Phys. Dept., Ain Shams University, Cairo, Egypt. E-mail: mppe2@yahoo.co.uk

The positive and negative parity states of ^{100}Ru isotope are studied within the frame work of the interacting boson approximation model ($IBA-1$). The calculated levels energy, potential energy surfaces, $V(\beta,\gamma)$, and the electromagnetic transition probabilities, $B(E1)$ and $B(E2)$, show that ^{100}Ru isotope has $E(5)$ Characters. Staggering effect, $\Delta I = 1$, has been observed between the positive and negative parity states. The electric monopole strength, $X(E0/E2)$, has been calculated. All calculated values are compared to the available experimental, theoretical data and reasonable agreement has been obtained.

1 Introduction

The mass region $A = 100$ has been of considerable interst for nuclear structure studies as it shows many interesting features. These nuclei show back bending at high spin and shape transitions from vibrational to γ-soft and rotational characters. Many attempts have made to explore these structural changes which is due mainly to the n-p interactions.

Experimentally, the nuclear reaction ^{100}Mo (α,xn) [1] has been used in studying levels energy of ^{100}Ru. Angular distribution, γ-γ coincidences were measured, half-life time has calculated and changes to the level scheme were proposed. Also, double beta decay rate of ^{100}Mo to the first excited 0^+ state of ^{100}Ru has been measured experimentally [2] using γ-γ coincidence technique.

Doppler-shift attenuation measurements following the ^{100}Ru (n, $n'\gamma$) reaction [3] has used to measure the life times of the excited states in ^{100}Ru. Absolute transition rates were extracted and compared with the interacting boson model description. The 2^+(2240.8 keV) state which decays dominantly to the 2^+ via 1701 keV transition which is almost pure $M1$ in nature considered as a mixed-symmetry state. Again ^{100}Ru has been studied [4] experimently and several levels were seen where some new ones are detected below 3.2 MeV.

Theoretically many models have been applied to ruthenium isotopes. Yukawa folded mean field [5] has applied to ^{100}Ru nucleus while the microscopic vibrational model has applied to ^{104}Ru and some other nuclei with their daughters [6]. The latter model was successful in describing the yrast 0^+ and 2^+ states of most of these nuclei and also some of their half-lives.

The very high-spin states of nuclei near A$\approx$100 are investigated by the Cranked Strutinsky method [7] and many very extended shape minima are found in this region. Interacting boson model has been used in studying *Ru* isotopes using a $U(5)$–$O(6)$ transitional Hamiltonian with fixed parameters [8-10] except for the boson number N. Hartree-Fock Bogoliubov [11] wave functions have been tested by comparing the theoretically calculated results for ^{100}Mo and ^{100}Ru nuclei with the available experimental data. The yrast spectra, reduced $B(E2, 0^+ \rightarrow 2^+)$ transition probabilities, quadrupole moments $Q(2^+)$ and g factors, g(2^+) are computed. A reasonable agreement between the calculated and observed values has been obtained.

The microscopic anharmonic vibrator approach (MAVA) [12] has been used in investigating the low-lying collective states in $^{98-108}$Ru. Analysis for the level energies and electric quadrupole decays of the two-phonon type of states indicated that ^{100}Ru can interpreted as being a transitional nucleus between the spherical anharmonic vibrator ^{98}Ru and the quasirotational $^{102-106}$Ru isotopes.

A new emprical approach has been proposed [13] which is based on the connection between transition energies and spin. It allows one to distinguish vibrational from rotational characters in atomic nuclei. The cranked interacting boson model [14] has been used in estimating critical frequencies for the rotation-induced spherical-to-deformed shape transition in $A = 100$ nuclei. The predictions show an agreement with the back bending frequencies deduced from experimental yrast sequences in these nuclei.

The aim of the present work is to use the $IBA-1$ [15, 16] for the following tasks:

1. Calculating the potential energy surfaces, $V(\beta,\gamma)$, to know the type of deformation existing for ^{100}Ru;
2. Calculating levels energy, electromagnetic transition rates $B(E1)$ and $B(E2)$;
3. Studying the relation between the angular momentum I and the rotational angular frequency $\hbar\omega$ for bending in ^{100}Ru;
4. Calculating staggering effect to see beat patterns and detect any interactions between the (+ve) and (−ve) parity states, and
5. Calculating the electric monopole strength $X(E0/E2)$.

2 (IBA-1) model

2.1 Level energies

IBA-1 model was applied to the positive and negative parity states of ^{100}Ru isotope. The Hamiltonian employed in the

nucleus	EPS	$PAIR$	ELL	QQ	OCT	HEX	$E2SD(eb)$	$E2DD(eb)$
^{100}Ru	0.5950	0.000	0.0085	−0.0200	0.0000	0.0000	0.1160	−0.3431

Table 1: Parameters used in IBA-1 Hamiltonian (all in MeV).

present calculation is:

$$\begin{aligned} H = \; & EPS \cdot n_d + PAIR \cdot (P \cdot P) \\ & + \tfrac{1}{2}\, ELL \cdot (L \cdot L) + \tfrac{1}{2}\, QQ \cdot (Q \cdot Q) \\ & + 5\, OCT \cdot (T_3 \cdot T_3) + 5 HEX \cdot (T_4 \cdot T_4) \end{aligned} \tag{1}$$

where

$$P \cdot p = \frac{1}{2} \left[\begin{array}{l} \left\{ (s^\dagger s^\dagger)^{(0)}_0 - \sqrt{5} (d^\dagger d^\dagger)^{(0)}_0 \right\} x \\ \left\{ (ss)^{(0)}_0 - \sqrt{5} (\tilde{d}\tilde{d})^{(0)}_0 \right\} \end{array} \right]^{(0)}_0 , \tag{2}$$

$$L \cdot L = -10 \sqrt{3} \left[(d^\dagger \tilde{d})^{(1)} x (d^\dagger \tilde{d})^{(1)} \right]^{(0)}_0 , \tag{3}$$

$$Q \cdot Q = \sqrt{5} \left[\begin{array}{l} \left\{ (S^\dagger \tilde{d} + d^\dagger s)^{(2)} - \dfrac{\sqrt{7}}{2} (d^\dagger \tilde{d})^{(2)} \right\} x \\ \left\{ (s^\dagger \tilde{d} + + \tilde{d} s)^{(2)} - \dfrac{\sqrt{7}}{2} (d^\dagger \tilde{d})^{(2)} \right\} \end{array} \right]^{(0)}_0 , \tag{4}$$

$$T_3 \cdot T_3 = - \sqrt{7} \left[(d^\dagger \tilde{d})^{(2)} x (d^\dagger \tilde{d})^{(2)} \right]^{(0)}_0 , \tag{5}$$

$$T_4 \cdot T_4 = 3 \left[(d^\dagger \tilde{d})^{(4)} x (d^\dagger \tilde{d})^{(4)} \right]^{(0)}_0 . \tag{6}$$

In the previous formulas, n_d is the number of boson; $P \cdot P$, $L \cdot L$, $Q \cdot Q$, $T_3 \cdot T_3$ and $T_4 \cdot T_4$ represent pairing, angular momentum, quadrupole, octupole and hexadecupole interactions between the bosons; EPS is the boson energy; and $PAIR$, ELL, QQ, OCT, HEX is the strengths of the pairing, angular momentum, quadrupole, octupole and hexadecupole interactions.

2.2 Transition rates

The electric quadrupole transition operator employed in this study is:

$$\begin{aligned} T^{(E2)} = \; & E2SD \cdot (s^\dagger \tilde{d} + d^\dagger s)^{(2)} + \\ & + \tfrac{1}{\sqrt{5}}\, E2DD \cdot (d^\dagger \tilde{d})^{(2)} . \end{aligned} \tag{7}$$

$E2SD$ and $E2DD$ are adjustable parameters.

The reduced electric quadrupole transition rates between $I_i \to I_f$ states are given by:

$$B(E_2, I_i - I_f) = \frac{[< I_f \parallel T^{(E_2)} \parallel I_i >]^2}{2 I_i + 1} . \tag{8}$$

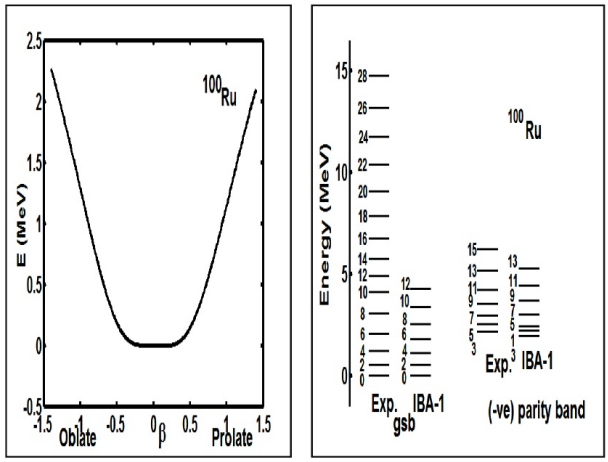

Fig. 1: A: Potential energy surfaces for ^{100}Ru. B: Comparison between exp. [19] and theoretical IBA-1 energy levels.

3 Results and discussion

3.1 The potential energy surfaces

The potential energy surfaces [17], $V(\beta, \gamma)$, as a function of the deformation parameters β and γ are calculated using:

$$\begin{aligned} & E_{N_\Pi N_\nu}(\beta, \gamma) = \; < N_\pi N_\nu; \beta\gamma \,|H_{\pi\nu}| N_\pi N_\nu; \beta\gamma > \; = \\ & = \zeta_d (N_\nu N_\pi) \beta^2 (1 + \beta^2) + \beta^2 (1 + \beta^2)^{-2} \times \\ & \times \left\{ k N_\nu N_\pi [4 - (\bar{X}_\pi \bar{X}_\nu) \beta \cos 3\gamma] \right\} + \\ & + \left\{ [\bar{X}_\pi \bar{X}_\nu \beta^2] + N_\nu (N_\nu - 1) \left(\frac{1}{10}\, c_0 + \frac{1}{7}\, c_2 \right) \beta^2 \right\} , \end{aligned} \tag{9}$$

where

$$\bar{X}_\rho = \left(\frac{2}{7} \right)^{0.5} X_\rho \qquad \rho = \pi \;\; \text{or} \;\; \upsilon . \tag{10}$$

The calculated potential energy surfaces, $V(\beta, \gamma)$, are presented in Fig. 1A. The flat potential in the critical symmetry point has supported quite well the $E(5)$ characters to ^{100}Ru nucleus. Also, the energy ratios presented in Table 4 as well as the existance of ^{100}Ru isotope between the spherical anharmonic vibrator ^{98}Ru and γ - soft ^{102}Ru nuclei [9] supported the $E(5)$ characters.

3.2 Energy spectra

The energy of the positive and negative parity states of ^{100}Ru isotope are calculated using computer code PHINT [18]. A

$I_i^+ I_f^+$	B(E2)	$I_i^+ I_f^+$	B(E1)
0_1 Exp*. 2_1	0.490(5)	$1_1\ 0_1$	0.0030
0_1 Theor. 2_1	0.4853	$1_1\ 0_2$	0.1280
$2_1\ 0_1$	0.0970	$3_1\ 2_1$	0.1211
$2_2\ 0_1$	0.0006	$3_1\ 2_2$	0.0415
$2_2\ 0_2$	0.0405	$3_1\ 2_3$	0.0002
$2_3\ 0_1$	0.0000	$3_2\ 2_1$	0.0024
$2_3\ 0_2$	0.0759	$3_2\ 2_2$	0.0197
$2_3\ 0_3$	0.0087	$3_2\ 2_3$	0.2126
$2_4\ 0_3$	0.0066	$5_1\ 4_1$	0.2533
$2_4\ 0_4$	0.0588	$5_1\ 4_2$	0.0480
$4_1\ 2_1$	0.1683	$5_1\ 4_3$	0.0006
$4_1\ 2_2$	0.0142	$7_1\ 6_1$	0.3950
$4_1\ 2_3$	0.0319	$7_1\ 6_2$	0.0446
$6_1\ 4_1$	0.2039	$9_1\ 8_1$	0.5439
$6_1\ 4_2$	0.0179	$9_1\ 8_2$	0.0342
$6_1\ 4_3$	0.0242	$11_1\ 10_1$	0.6983
$8_1\ 6_1$	0.2032		
$8_1\ 6_2$	0.0183		
$8_1\ 6_3$	0.0157		
$10_1\ 8_1$	0.1678		
$10_1\ 8_2$	0.0175		

Table 2: Calculated $B(E2)$ and $B(E1)$ in ^{100}Ru.

I_i^+	I_f^+	$I_{f'}^+$	$X_{if'f}\,(E0/E2)^{100}$Ru
0_2	0_1	2_1	0.027
0_3	0_1	2_1	0.347
0_3	0_1	2_2	0.009
0_3	0_1	2_3	0.042
0_3	0_2	2_1	0.086
0_3	0_2	2_2	0.002
0_3	0_2	2_3	0.010
0_4	0_1	2_2	0.010
0_4	0_1	2_3	0.010
0_4	0_1	2_4	0.113
0_4	0_2	2_2	0.030
0_4	0_2	2_3	0.034
0_4	0_2	2_4	0.340
0_4	0_3	2_1	0.454
0_4	0_3	2_2	0.010
0_4	0_3	2_3	0.011
0_4	0_3	2_4	0.113

Table 3: Calculated $X_{if'f}\,(E0/E2)$.

Energy Ratios	$E_{4_1^+}/E_{2_1^+}$	$E_{2_2^+}/E_{2_1^+}$
$E(5)$	2.19	2.20
Exp. [19]	2.27	2.52
$IBA-1$	2.12	2.11

Table 4: Energy ratios of $E(5)$ characters to ^{100}Ru.

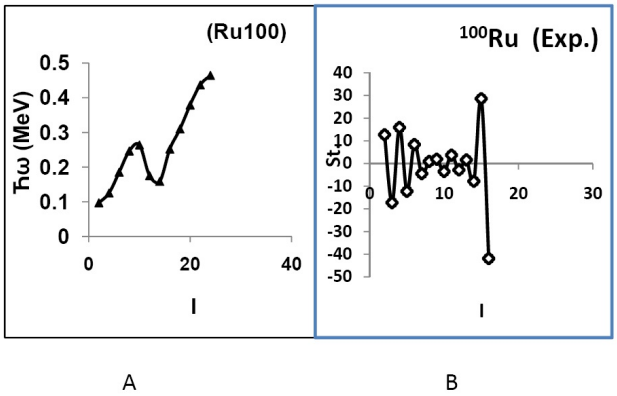

Fig. 2: A: Angular momentum I as a function of $(\hbar\omega)$. B: $(\Delta I = 1)$, staggering pattern for ^{100}Ru isotope.

comparison between the experimental spectra [19] and our calculations, using values of the model parameters given in Table 1 for the ground state band are illustrated in Fig. 1B. The agreement between the calculated levels energy and their correspondence experimental values are slightly higher especially for the higher excited states. We believe this is due to the change of the projection of the angular momentum which is due mainly to band crossing.

Unfortunately there is no enough measurements of electromagnetic transition rates $B(E1)$ or $B(E2)$ for ^{100}Ru nucleus. The only measured $B(E2, 0_1^+ \to 2_1^+)$ is presented, in Table 2 for comparison with the calculated values[20]. The parameters $E2SD$ and $E2DD$ displayed in Table 1 are used in the computer code NPBEM [18] for calculating the electromagnetic transition rates after normalized to the available experimental values. No new parameters are introduced for calculating electromagnetic transition rates $B(E1)$ and $B(E2)$ of intraband and interband.

The moment of inertia I and angular frequency $\hbar\omega$ are calculated using equations (11, 12):

$$\frac{2I}{\hbar^2} = \frac{4I-2}{\Delta E(I \to I-2)}\,, \tag{11}$$

$$(\hbar\omega)^2 = (I^2 - I + 1)\left[\frac{\Delta E(I \to I-2)}{(2I-1)}\right]^2\,. \tag{12}$$

The plot in Fig. 2A show back bending at angular momentum $I^+ = 10$. It means, there is a crossing between the $(+ve)$ and $(-ve)$ parity states in the ground state band which

was confirmed by calculating the staggering effect where a beat pattern has been observed, Fig. 2B.

3.3 Electric monopole transitions

The electric monopole transitions, $E0$, are normally occurring between two states of the same spin and parity by transferring energy and zero unit of angular momentum. The strength of the electric monopole transition, $X_{if'f}(E0/E2)$, [21] can be calculated using equations (13, 14); results are presented in Table 3

$$X_{if'f}(E0/E2) = \frac{B(E0, I_i - I_f)}{B(E2, I_i - I_{'f})}\,, \tag{13}$$

$$X_{if'f}(E0/E2) = (2.54\times 10^9)\,A^{3/4}\times \frac{E_\gamma^5(\mathrm{MeV})}{\Omega_{KL}}\,\alpha(E2)\,\frac{T_e(E0, I_i - I_f)}{T_e(E_2, I_i - I_{'f})}\,. \tag{14}$$

Here: A is mass number; I_i is spin of the initial state where E0 and E2 transitions are depopulating it; I_f is spin of the final state of E0 transition; $I_{'f}$ is spin of the final state of E2 transition; E_γ is gamma ray energy; Ω_{KL} is electronic factor for K,L shells [22]; $\alpha(E2)$ is conversion coefficient of the E2 transition; $T_e(E0, I_i - I_f)$ is absolute transition probability of the $E0$ transition between I_i and I_f states, and $T_e(E_2, I_i - I_{'f})$ is absolute transition probability of the $E2$ transition between I_i and $I_{'f}$ states.

3.4 The staggering

The presence of $(+ve)$ and $(-ve)$ parity states has encouraged us to study staggering effect [23–25] for ^{100}Ru isotope using staggering function equations (15, 16) with the help of the available experimental data [19].

$$St(I) = 6\Delta E(I) - 4\Delta E(I-1) - 4\Delta E(I+1) + \Delta E(I+2) + \Delta E(I-2)\,, \tag{15}$$

with

$$\Delta E(I) = E(I+1) - E(I)\,. \tag{16}$$

The calculated staggering patterns are illustrated in Fig. 2B and show an interaction between the $(+ve)$ and $(-ve)$ parity states for the ground state band of ^{100}Ru.

3.5 Conclusions

IBA-1 model has been applied successfully to ^{100}Ru isotope and:

1. The levels energy are successfully reproduced;
2. The potential energy surfaces are calculated and show $E(5)$ Characters to ^{100}Ru;
3. Electromagnetic transition rates $B(E1)$ and $B(E2)$ are calculated;
4. Bending for ^{100}Ru has been observed at angular momentum $I^+ = 10$;
5. Strength of the electric monopole transitions $X_{if'f}(E0/E2)$ are calculated; and
6. Staggering effect has been calculated and beat pattern has been obtained, showing an interaction between the $(-ve)$ and $(+ve)$ parity states.

Submitted on: December 12, 2012 / Accepted on: December 20, 2012

References

1. Maazek J., Honusek M., Spalek A., Bielcik J., Slivova J. and Pasternak A. A. Levels of ^{100,101}Ru excited in the reaction ^{100}Mo($\alpha\chi$n). *Acta Physica Polonica B*, 1998, v. 29, 433.
2. Braeckeleer L. L., Hornish M., Barabash A. and Umatov V. Measurement of the $\beta\beta$-decay rate of ^{100}Mo to the first excited 0^+ state of ^{100}Ru. *Physical Review*, 2001, v. 86, 3510.
3. Genilloud L., Brown T. B., Corminboeuf F., Garrett P. E., Hannant C. D., Jolie J., Warr N. and Yates S. W. Characterization of the three-phonon region of ^{100}Ru. *Nuclear Physics A*, 2001, v. 683, 287.
4. Horodynski-Matsushigue L. H., Rodrigues C. L., Sampaio F. C. and Lewin T. B. Particle spectroscopy of low-lying collective states in ^{100}Ru. *Nuclear Physics A*, 2002, v. 709, 73.
5. Nerlo-Pomorska B., Pomorski K. and Bartel J. Shell energy and the level- density parameter of hot nuclei. *Physical Review C*, 2006, v. 74, 034327.
6. Raina P. K. and Dhiman R. K. Systematics of $\beta\beta$ decay sensitive medium mass nuclei using quadrupole-quadrupole plus pairing interactions. *Physical Review C*, 2001, v. 64, 024310.
7. Chasman R. R. Very extended nuclear shapes near $A = 100$. *Physical Review C*, 2001, v. 64, 024311.
8. Frank A., Alonso C. E. and Arias J. M. Search for $E(5)$ symmetry in nuclei: the *Ru* isotopes. *Physical Review C*, 2001, v. 65, 014301.
9. Diab S. M. , Eid S. A. Nature of the excited states of the even-even $^{98\text{-}108}$Ru istopes. *Progress in Physics*, 2008, v. 4, 51.
10. Cejnar P., Jolie J. and Kern J. Universal anharmonicity anomly in nuclei. *Physical Review C*, 2001, v. 63, 047304.
11. Chaturvedi K., Dixit B. M. and Rath P. K. Two neutrino double β decay of ^{100}Mo to the 2^+ excited state of ^{100}Ru. *Physical Review C*, 2003, v. 67, 064317.
12. Kotila J., Suhonen J. and Delion D. S. Low-lying collective states in ^{98,106}Ru isotopes studied using a microscopic anharmonic vibrator approach. *Physical Review C*, 2003, v. 68, 054322.
13. Regan P. H., Beausang C. W., Zamfir N. V., Casten R. F., Zhang J., Meyer D. A. and Ressler J. J. Signature for vibrational to rotational evolution along the yrast line. *Physical Review Letters*, 2003, v. 90 , 152502.
14. Cejnar P. and Jolie J. Rotation-driven spherical-to-deformed shape transition in $A \approx 100$ nuclei and the cranked interacting boson model. *Physical Review C*, 2004, v. 69, 011301.
15. Arima A. and Iachello F. Interacting boson model of collective states: The vibrational limit. *Annals of Physics (N.Y.)*, 1976, v. 99, 253.
16. Arima A. and Iachello F. Interacting boson model of collective states: The rotational limit. *Annals of Physics (N.Y.)*, 1978, v. 111, 201.
17. Ginocchio J. N. and Kirson M. W. An intrinisic state for the interacting boson model and its relationship to the Bohr- Mottelson approximation. *Nuclear Physics A*, 1980, v. 350, 31.
18. Scholten O. *The programm package PHINT (1980) version, internal report KVI-63, Gronigen: Keryfysisch Versneller Institut.*
19. Balraj Singh. Adopted levels, gammas for ^{100}Ru. *Nuclear Data Sheets*, 1997, v. 81, 1997.

20. Raman S., Nestor JR.C.W., and Tikkanen P., Transition probability from the ground to the first-excited 2^+ state of even-even nuclides. *Atomic Data and Nuclear Data Tables*, 2001, v. 78, 1.

21. Rasmussen J. O. Theory of $E0$ transitions of spheroidal nuclei. *Nuclear Physics*, 1960, v. 19, 85.

22. Bell A. D ., Aveldo C. E., Davidson M. G. and Davidson J. P., Table of $E0$ conversion probability electronic factors. *Canadian Journal of Physics*, 1970, v. 48, 2542.

23. Minkov N., Yotov P., Drenska S. and Scheid W. Parity shift and beat staggering structure of octupolr bands in a collective model for quadrupole-octupole0deformed nuclei. *Journal of Physics G*, 2006, v. 32, 497.

24. Bonatsos D., Daskaloyannis C., Drenska S. B., Karoussos N., Minkov N., Raychev P. P. and Roussev R. P. $\Delta I = 1$ staggering in octupole bands of light actinides Beat patterns. *Physical Review C*, 2000, v. 62, 024301.

25. Minkov N., Drenska S. B., Raychev P. P., Roussev R. P. and Bonatsos D. Beat patterns for the odd-even staggering in octupole bands from quadrupole-octupole Hamiltonian. *Physical Review C*, 2001, v. 63, 044305.

A New Large Number Numerical Coincidences

Alexander Kritov
E-mail: alex@kritov.ru

In this article, the author gives a set of new hypothesis wherein he presents new, exact and simple relations between physical constants and numbers. The author briefly analyses the discovered coincidences in terms of their accuracy and confidence, while leaving himself aside any physical explanation of the presented formulas. Important: all the found relations have a common nature of the "power of two". The exact nature of this remains unknown for yet, so it requires further research. The presented material may also be viewed as a logical continuation and development of Dirac's and Eddington's Large Numbers Hypothesis (LNH). However, in contrast to Dirac's LNH, two of the presented ratios are not approximate but manifest exact equality. This allows a theoretical prediction of the Universe's radius as well as a calculation of the exact value of Newtonian gravitational constant G, which all fall within the range of the current measurement data and precision. The author formulates these Large Number Numerical (LNN) coincidences by realizing that further discovery of their meaning may lead to a significant change in our understanding of Nature. In this work, SI units are used.

Introduction

Many attempts of bringing together physics and numerology had been done before but a very important step was done in 1938 by Arthur Eddington. According to Eddington's proposal the number of protons in the entire Universe should be exactly equal to: $N_{Edd} = 136 \times 2^{256} \approx 10^{79}$ [1, 2, 17]. So, it was hypothesised that square root of N_{Edd} should be close to Dirac's Big number $N \approx \sqrt{136 \times 2^{256}} = \sqrt{136} \times 2^{128}$. Later on, Eddington changed 136 to 137 and insisted that the fine structure constant has to be precisely 1/137, and then his theory seemed to fail at this cornerstone. However, Eddington's statement also had the number $(2^{128})^2$ which has been left without proper attention. Actually, few years earlier, in 1929, it was German physicist R. Fürth who proposed to use 16^{32} (which is also 2^{128}) in order to connect gravitation to atomic constants [10]. However, all these coincidences have been left unexplained until present time. As G. Gamov said [16]: "Since the works of Sir Arthur Eddington, it has become customary to discuss from time to time the numerical relations between various fundamental constants of nature". For example, another interesting attempt to use "a log-base-2 relation" between electromagnetic and gravitational coupling constant was made by Saul-Paul Sirag, the researcher from San Francisco in 1979 [12]. Particularly, as noted, power of 2 should have significant role in numerical relations for physics constants according to the author's idea.

Suggested four Large Number Numerical (LNN) relations or coincidences are presented below. These coincidences are not dependent and related to each other, so prove or disprove of one of them does not mean the same for the others. They all have common number of 2^{128}. First two relations seem to be exact equations, and second two are valid with defined uncertainty. Because of that their nature is more hypothetical, so second two relations are also called "weak".

1 Cosmological coincidence

The relation is analogous to famous Dirac's ratio $R_U/r_e \sim 10^{40}$ which relates the Universe radius with classical electron radius. However, Dirac's ratio is actually valid only approximately (with precision of "the same order of magnitude"), in opposite, the suggested replacement is an exact equation given as follows:

$$\frac{R_U}{\lambda_e} = 2^{128}, \tag{1}$$

where R_U is value for the radius of the observable Universe and $\lambda_e = \hbar/m_e c \approx 3.86 \times 10^{-13}$ (m) is electron's reduced Compton wavelength (De Broglie wave). The relation (1) provides us with precise size and age of the observable Universe. So it leads to exact value for the Universe radius of $R_U = 1.314031 \times 10^{26}$ meters corresponding to the Universe age of 13.8896 billion years.

Recently F.M.Sanchez, V.Kotov, C.Bizouard discovered that the use of the reduced electron Compton wavelength is decisive for the compatibility of the Hubble-Lemaitre length with 2^{128} [13–15]. They use this length unit because of proposed holographic relation involving it. Here, the author independently developes this idea suggesting that (1) is an exact relation.

The age of the Universe, according to the Wilkinson Microwave Anisotropy Probe (WMAP) 7-year results, is 13.75 ± 0.13 billion years [9]. Latest NASA observation by Hubble gives the age of the Universe as 13.7 billion years [3]. It is very close to the obtained value and lies in the existing error range. So, the coincidence (1) seems to define the exact Universe elapsed life time as:

$$T_U = \frac{\lambda_e}{c} 2^{128}. \tag{1.1}$$

Important to note, that having (1.1), initial Dirac's relation may be expressed in the following form:

$$N_1 = \frac{R_U}{r_e} = \alpha^{-1}\, 2^{128}, \tag{1.2}$$

where $\alpha^{-1} = 137.036$ is inverted fine structure constant and $r_e = ke^2/(m_e c^2)$ — classical electron radius with eliminated numerical factor (i.e. equal to unity) and N_1 is exact value for the large number introduced by Dirac (4.66×10^{40}). As we know for sure that the Universe is expanding and $R_U(t)$ is dependent on time, so the equation (1) suggest that one or few of the fundamental constants (h, c, m_e) should also vary in time. However, current uncertainty in R_U measurement still leaves a room for other alternative ideas and possible coincidences. For example, noting that $m_p/m_e \sim 40/3 \times \alpha^{-1}$, relation (1) can have another form:

$$R_U = \frac{m_p}{m_e}\frac{1}{4}\left(\frac{3}{10}\frac{ke^2}{m_e c^2}\right) 2^{128} \tag{1.3}$$

which would correspond to 13.95809 Gyr. As this value is currently out of the present WMAP data frame, therefore it is not supported by the author here.

2 Electron-proton radius coincidence

Another interesting idea connects the classical proton radius and gravitational radius of the electron by an exact equation as follows:

$$\frac{r_p}{r_{ge}} = 2^{128}, \tag{2}$$

where $r_p = \frac{1}{2}\frac{3}{5}ke^2/(m_p c^2)$ — classical proton radius and $r_{gp} = 2Gm_e/c^2$ — gravitational electron radius (i.e. the Schwarzschild radius for the electron mass). Of course some comments are required regarding coefficients $\frac{1}{2}$ and $\frac{3}{5}$. Usually numerical factors are ignored or assumed to be close to unity when defining classical (electron) radius. However, suggested new definition has exact numerical factor $\frac{3}{10} = \frac{3}{5} \times \frac{1}{2}$, so it is obvious to have the following explanations for that one by one:

- Ratio $\frac{3}{5}$ is classical proton radius definition. The only important difference with modern representation of the classical radius is the coefficient $\frac{3}{5}$. It is well known from electrostatics that the energy required to assemble a sphere of constant charge density of radius r and charge r is $E = \frac{3}{5}ke^2/r$. Usually these factors like $\frac{3}{5}$ or $\frac{1}{2}$ are ignored while defining the classical electron radius. Surprisingly, the coincidence advices the use of $\frac{3}{5}$ which means that charge is equally spread within the sphere of the electron (or proton) radius.
- Ratio $\frac{1}{2}$ in classical proton radius definition. Usual definition of the classical radius does not require having $\frac{1}{2}$ because initially one relates total electrostatic energy (E_e) of the electron (or proton) to rest mass energy as following: $E_e = mc^2$. The factor $\frac{1}{2}$ appears if one postulates that electromagnetic energy (E_{em}) of the electron or proton is just a half of particle's rest mass energy as: $E_{em} = \frac{1}{2}mc^2$. There are two possible alternative explanations for this:
  1. The Virial Theorem that tells us that the potential energy inside a given volume is balanced by the kinetic energy of matter and equals to half of it. So if one considers electromagnetic energy as kinetic and rest mass as potential energy we would have: $E_{em} = \frac{1}{2}mc^2$;
  2. Simply assuming that half of total energy may be magnetic energy or of another nature. One may also propose that there could be no $\frac{1}{2}$ in classical proton radius definition, but there is 2^{129} instead of 2^{129} in formula (2). From the author's point of view this does not correspond to reality, and particularly the number 2^{128} should have strong presence in all numerical expressions of Nature.

It can be easily seen that $r_p = (m_e/m_p)r_e$, so another way to rewrite (2) is:

$$\frac{r_e}{r_{ge}} = \frac{m_p}{m_e}\, 2^{128}. \tag{2.1}$$

And this leads to another possible representation of the initial formula as:

$$\frac{r_e}{r_{gp}} = 2^{128}, \tag{2.2}$$

where r_e is classical electron radius, r_{gp} is gravitational (Schwarzschild) radius of the proton. The expression (2.2) is very similar to (2). So, we may actually combine them into another interesting equation:

$$r_p\, r_{gp} = r_e\, r_{ge}. \tag{2.2a}$$

The precision of the Electron-proton coincidence given by (2) is smaller than 0.02%. From the author's point of view this deviation originates from current uncertainty in gravitational constant (G) measurement. If we consider that the relative G uncertainty nowadays is around and not less than 0.02% then we must accept this amazing and unexplained coincidence that allows us to predict the exact value for the gravitational constant (G). So, this finding suggests that the following possible consequences are valid. Firstly, because of $\frac{3}{5}$ ratio proton or electron still may be considered as classical particle with uniform charge density inside its radius. And secondly, directly from (2) one can express the value of the Newtonian constant of gravitation (G) exactly as follows:

$$G = \frac{3}{20}\frac{ke^2}{m_p m_e}\, 2^{-128}. \tag{2.3}$$

It leads to exact value for $G = 6.674632 \times 10^{-11}$. This value is within the frame of 2010 CODATA-recommended

value with standard uncertainty given by: $6.67384 \pm 0.00080 \times 10^{-11}$ [6] (See also figure). One may compare this expression with the similar one obtained in 1929 by R. Fürth [10]:

$$G = \frac{hc}{\pi(m_p + m_e)^2} = 16^{32}$$

that is read in SI units for G as:

$$G = \frac{2\hbar c}{(m_p + m_e)^2}\, 16^{-32}.$$

It is interesting to compare it to (2.3) to note obvious similarity. However, one may see that the expression is not satisfactory because it leads to the value of ($G = 6.63466 \times 10^{-11}$) which has significant deviation (0.59%) and is far out of 2010 CODATA range. So, the expression 2.3 (which fits well to modern data) is quite challenging because it may be confirmed or disproved by future experimental data for G.

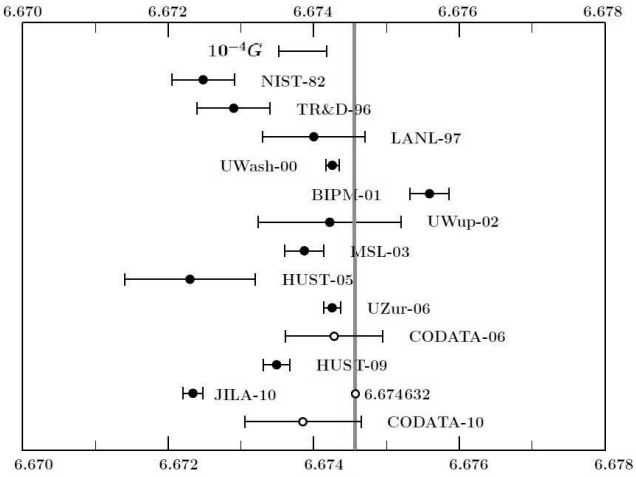

Fig. 1: The figure with recent experimental data for the Newtonian constant of gravitation G. The vertical line corresponds to the value obtained from (2.3).

Though the obtained value fits quite well into current experimental data, the author does not exclude some possible small deviations caused by vacuum polarisation and consequent slight deviation from the uniformity of the charge distribution (like Uehling Potential). So we will look at this in future works.

It is also important to stress that the use of classical proton radius here is very provisional and in principle could be avoided: so the same result for G may be obtained using only the electron's classical radius.

It is easy to note also that Dirac's Large Number N precisely equals to:

$$N = \frac{ke^2}{m_p m_e} = \frac{20}{3}\, 2^{128}. \tag{2.4}$$

This means that variation of Dirac's Large Number (N) in time is hardly possible, because 2^{128} represents simply the constant number. So the ratio of the electromagnetic force to the gravitational one remains always constant during the current epoch.

3 Weak cosmological coincidence

$$\frac{2c^3}{G} \approx \frac{m_p}{t_p}\, 2^{128}, \tag{3}$$

where c is speed of light, G is the gravitational constant, $t_p = \hbar/(m_p c^2)$-period of reduced Compton wave of the proton. This equation may be interpreted as relation of rate of mass growth or the expansion rate of the Universe [4, 5] to harmonic properties of the proton as wave. However the relative precision of (3) is 0.48% (or even 0.49% if we accept definition of G as in 2.3) which is unsatisfactory for modern measurements and it makes the expression valid only approximately. In order to become more precise the expression should have the following representation:

$$\frac{2c^3}{G} \approx \frac{m_p + 9m_e}{t_p}\, 2^{128}. \tag{3.1}$$

Or alternatively (to become exactly precise):

$$\frac{2c^3}{G} = \frac{m_p}{t_p}\frac{20}{3}\, \alpha^{-1}\, 2^{128}. \tag{3.2}$$

But further discussion of this topic will be explored in future works.

4 Weak electron-proton mass ratio

The attempts to explain large numbers by placing inverted fine structure constant in exponential function have been done many times before [11, 12]. Another interesting hypothesis could relate proton to electron mass ratio with fine structure constant and the number 2^{128} in the following manner:

$$\frac{m_p}{m_e} \simeq \frac{7}{2}\, 2^{(\alpha^{-1} - 128)}. \tag{4}$$

However the relative precision is comparably high (0.06%) and is out of the error frame of the current experimental data. However, using this relation as approximation, one can find similar connections of derived formulas to the similar ones in work [12].

Conclusion

The basic meaning of all these relations may be viewed in the form of exact equality for large Dirac's number N (see 2.4). However, all these proposals disprove one of the Dirac's hypothesis regarding the equality of the big numbers [2, see p. 200]. So, the author has shown that the number N, which is the ratio of the electromagnetic force to its gravitational force given by (2.4), is actually not equal to number N_1 which is

the ratio of Universe radius to classical electron radius (1.2). However these two differ only by the numerical factor of $20.55 = \alpha^{-1} \times (3/20)$. So, the main conclusions of this study are as follows:

- Current Universe age and radius can be calculated exactly (13.8896 Gyr);
- The value of Newtonian constant of gravitation (G) can be derived exactly (6.674632×10^{-11});
- The number 2^{128} should have a real significance in the constants of Nature.

Generally the concept of "power of two" could be regarded as having two properties in science. Firstly, it is digital (logical) math where power of two has common use. So this may support an idea of holographic concept of the Universe or some of the fractal theories. Secondly, it is used in wave mechanics, and it could be viewed in accordance with wave properties of the elementary particles in quantum physics. In terms of wave concept, the number of 2^{128} corresponds to the tone of 128-th octave or to some higher harmonic ("overtone") of the main tone. It is interesting to mention that a very close idea has been brought few years ago. The idea relates particles mass levels within two sequences that descend in geometric progression from the Plank Mass. Sub-levels are arranged in subsequence of common ratio which uses a power of 2 [7, 8]. The author is also very supportive to the point of view given in [13–15], however it is important to stress that physics should be free from approximate relations and should have only precise equalities and formulas. Some of the exact formulas which may help to support such general ideas have been presented in this work. If new suggested relations for Large Numbers are correct then it should probably lead to new search for its hidden meaning. As always, we must accept the fact that in often cases new findings lead to new questions instead of the answers and that might become a new challenge for new investigations and theories. Assuming that at least one of the discovered relations is correct in the future we may become a bit closer to the true view on physical reality.

Submitted on December 17, 2012 /Accepted on December 20, 2012

References

1. Eddington A.S. The Philosophy of Physical Science, Tarner Lectures, 1938, Cambridge At The University Press, 1939.
2. Barrow, J.D. The Constants of Nature From Alpha to Omega — The Numbers that Encode the Deepest Secrets of the Universe. Pantheon Books, 2002.
3. NASA website NASA's Hubble Finds Most Distant Galaxy Candidate Ever Seen in Universe, News release from NASA: Jan. 26, 2011, Release: 11-025.
4. Kostro L. Physical interpretation of the coefficients c/G, c^2/G, c^3/G, c^4/G, c^5/G that appear in the equations of general relativity.
5. Schiller C. General relativity and cosmology derived from principle of maximum power or force, 2008, arXiv: physics/0607090.
6. Peter J. Mohr, Barry N. Taylor, and David B. Newell CODATA Recommended Values of the Fundamental Physical Constants: 2010. March 15, 2012. arXiv: physics.atom-ph/1203.5425.
7. Riley B.F. Particle mass levels, 2009. viXra: 0909.0006.
8. Riley B.F. A unified model of particle mass. arXiv: physics/0306098.
9. Jarosik, N., et.al. Seven-Year Wilkinson Microwave Anisotropy Probe (WMAP) Observations: Sky Maps, Systematic Errors, and Basic Results, 2011, ApJS, 192, 14. arXiv: astro-ph.CO/1001.4744.
10. Fürth R. Versuch einer quantentheoretischen Berechnung der Massen von Proton und Elektron, Physikalische Zeitschrift, 1929, from Helge Kragh Magic Number: A Partial History of the Fine-Structure Constant, DOI 10.1007/s00407-002-0065-7, *Archive for History of Exact Sciences*, 2003, v. 57, 395–431.
11. Brandmüller J. and Rüchardt E. Die Sommerfeldsche Feinstrukturkonstante und das Problem der spektroskopischen Einheiten, *Die Naturwissenschaften*, 1950, v. 37, from R. Baggiolini On a remarkable relation between atomic and universal constants, *American Journal of Physics*, 1957, v. 25, 324.
12. Sirag, Saul-Paul Physical constants as cosmological constraints, *International Journal of Theoretical Physics*, 1983, v. 22(12), 1067–1089.
13. Sanchez F.M., Kotov V., Bizouard C. Evidence for a steady-state, holographic, tachyonic and super-symmetric cosmology, *Galilean Electrodynamics*, 2009, v. 20, Special Issues, no. 3, 43–53.
14. Sanchez F.M., Kotov V., Bizouard C. Towards a synthesis of two cosmologies, *Journal of Cosmology*, v.17, 2011.
15. Sanchez F.M., Kotov V., Bizouard C. Towards Coherent Cosmology, *Galilean Electrodynamics*, 2012.
16. Gamov G. Numerology fo the constants of nature. *Procedings of the National Academy of Science U.S.A.*, 1968, v. 59(2), 313–318.
17. Whitrow G.J. An Elementary Deviation of Eddington Number 10^{78}, *Nature*, 1952, no. 4302, 611–612.

Proper Space Kinematics

Sean Wade
P.O. Box 246, Highmount, NY, 12441. E-mail: seanwadePSK@verizon.net

It is desirable to understand the movement of both matter and energy in the universe based upon fundamental principles of space and time. Time dilation and length contraction are features of Special Relativity derived from the observed constancy of the speed of light. Quantum Mechanics asserts that motion in the universe is probabilistic and not deterministic. While the practicality of these dissimilar theories is well established through widespread application inconsistencies in their marriage persist, marring their utility, and preventing their full expression. After identifying an error in perspective the current theories are tested by modifying logical assumptions to eliminate paradoxical contradictions. Analysis of simultaneous frames of reference leads to a new formulation of space and time that predicts the motion of both kinds of particles. *Proper Space* is a real, three-dimensional space clocked by proper time that is undergoing a densification at the rate of c. Coordinate transformations to a familiar *object space* and a mathematical *stationary space* clarify the counterintuitive aspects of Special Relativity. These symmetries demonstrate that within the local universe stationary observers are a forbidden frame of reference; all is in motion. In lieu of Quantum Mechanics and Uncertainty the use of the imaginary number i is restricted for application to the labeling of mass as either material or immaterial. This material phase difference accounts for both the perceived constant velocity of light and its apparent statistical nature. The application of Proper Space Kinematics will advance more accurate representations of microscopic, macroscopic, and cosmological processes and serve as a foundation for further study and reflection thereafter leading to greater insight.

1 Introduction

The planets dancing in the heavens, an apple falling to earth each kindle curiosity about the dynamical universe. The mysteries of the unseen world and its apparent influences on daily life inspire wonder and imagination. Such observations drive the search for hidden constraints that govern the actions of atomic particles and molecules, ballistic objects, and celestial bodies. Guided by tools of logic, intuition, and creativity philosophers, scientists, and mathematicians strive to model laws that describe movement in each realm. Many years of disparate effort and the resulting accumulation of knowledge demonstrate that there are underlying commonalities that apply across all physical scales. This connectedness prompts the realization that searching for unifying first principles based upon fundamental aspects of space and time is an attainable goal. Understanding the foundation that the universe is built upon enables the continuing pursuit of deeper and more profound truths and further illuminates the miracle of human existence.

In 1905 Albert Einstein published his landmark work *Zur Elektrodynamik bewegter Körper* [1] (translated as *On the Electrodynamics of Moving Bodies* [2]). He stated that it was well known that under transformation to a moving reference frame Max-well's equations acquired asymmetries that were not present in nature. Einstein resolved these inconsistencies by introducing two fundamental principles [2]:

1. *The laws by which the states of physical systems undergo change are not affected, whether these changes of state be referred to the one or the other of two systems of co-ordinates in uniform translatory motion.*
2. *Any ray of light moves in the "stationary" system of co-ordinates with the determined velocity c, whether the ray be emitted by a stationary or by a moving body.*

The first postulate identified inertial frames of reference. The second postulate emphasized the constancy of the speed of light. From these followed the development of Special Relativity as a basis for motion.

Although the efficacy of Special Relativity cannot be denied it is a mathematical physics derived from the observations of light approaching any observer at the same speed regardless of the specific frame of reference. Any element of a theory that behaves identically under all applications must itself lie outside this theory and for this reason the action of discrete quanta requires a separate and distinctly different explanation.

This leads to the hard-fought and hard-won triumph of the Copenhagen interpretation of Quantum Mechanics culminating in its emergence as the preeminent theory of modern physics [3]. Owing to their experimental origins the composition of each theory contains mathematical elements that are not immediately obvious and consequently can act as obstacles to understanding and usage. If the basic realities of space and time are known then it is possible to properly explain the curious details of motion of all objects in the native environment and show that they proceed in a logical and intuitive way from this physical foundation.

This research is motivated by a personal failure of understanding attributable to the lack of a fundamental mechanics capable of explaining all rudimentary motion in the universe as derived from the basic condition of spacetime. Guided by instinct and curiosity the contemporary scientific theories and the corresponding philosophies are explored through a careful analysis of perspective; long-held premises are tested and discarded by virtue of the necessity to eliminate contradiction. The result of the methodology described in this paper addresses a kinematics which describes free motion without forces and interactions and with no regard for collisions and the associated quantities of energy, momentum and mass. A first principles theory is significant in that it can immeasurably improve physics on every level by serving as a foundation for the advancement of larger fields of research. The sluggish pace of grand unification, the overwrought complexity of string theory, the extremes of quantum gravity, the perplexity of dark matter, and the simplistic seeming three body problem are currently unresolved issues in physics [4]. These problems along with technological improvements to solar cell efficiency and medical scanning devices are among those that can potentially benefit from the application of Proper Space Kinematics.

2 Methodology

As a part of natural skepticism and scientific inquiry it is often useful to be able to replicate the research process both as a test of results and as a guide to understanding. In theoretical work much of the effort is introspective and it is impossible to retrace the labyrinthine mental pathways that lead to these results. In light of this difficulty it is practical to detail the initial impetus that motivated the author and to provide an overview of the techniques employed in the striving for enlightenment.

It is always more difficult to understand the fundamental principles that govern a system when the only perspectives available lie within the system itself. For this reason it is desirable to find a vantage point or frame of reference that lies outside the system so as not to be influenced by or subject to whatever constraints are imposed upon its occupants. In reviewing the basic elements of Special Relativity it is troubling that there are inconsistencies in the currently used theory between the common explanations and the mathematical model. While the equations purport to explain motion from an exterior viewpoint it is a theory of *relative* motion that performs as if a massive object occupies the choice of origin. This fallacy compounds the suspicion that an accurate picture of reality may not be known and necessitates the need for further exploration of this phenomena the source of which must thereafter be inferred from these confused aspects. In a similar mien the self-circular reasoning involved in using light itself as a mediator to measure lightspeed is also an obstacle to understanding and conceals basic mechanisms that are vital to accurately model the system mathematically.

Other concerns arise from a thoughtful analysis of the present philosophy. If the lightspeed barrier is a limiting condition then this implies that the velocity of an object is a more important kinematical consideration than position or acceleration. A cursory examination of the invariant interval suggests that its spatial and temporal components act in opposition to each other across varied reference frames although the use of hyperbolic functions would conversely imply a conjunction of underlying influences. The question of balance imparts an impression of rotation along a spectrum instead of a deviation from zero which is compounded by the inability to rotate a vector of zero length and might lead to the conclusion that nothing is static. The Quantum Mechanical proposition that the universe is unknowable at its most basic level and the ensuing enigma of wave-particle duality raise further reservations. Intuitively the structure of the universe should be based on the least number and simplest of principles although wisdom dictates that allowances be made for the possibility of deliberate design.

Logic is a weak tool for dissecting a system that is known to have defects in its application and for this reason a trial-by-solution is likely to be ineffective. Therefore the course of action must include an exploration using physical intuition and not only a mathematical manipulation of equations. This is accomplished through repeated testing of both implicit and explicit assumptions to find the origins of paradoxical situations and then to remove these faults. The movements of both energy and matter in spacetime are studied with careful consideration of perspective in an attempt to unravel the knot of relativity and to imagine an extrauniversal viewpoint. Producing an accurate answer to the dilemmas detailed here requires substantial time for trial calculations, for searching through potentially applicable literature, and for reevaluating conventional concepts through quiet reflection.

3 Results

The natural universe is undergoing a process of *densification* and is described here as being composed of three real spatial coordinates and one real monodirectional temporal counter. Densification is defined for this demesne as an increase in the density of space that occurs in the measure of distance between any two disparate points clocked by proper time and progressing at the rate of c. Previously referred to as lightspeed the particular value of the *characteristic velocity* as it has been measured serves as a label for the universe as well as all residents. It is further assumed that the inhabited universe is infinite though possibly bounded, is fixed relative to any preternatural background, if one exists, and is not undergoing additional physical alteration. The kinematics of finitesimal objects is derived for the movement of noninteracting rigid bodies traveling at constant speed. The premise of constant speed translates across all *spaces*. Initially this derivation is done without the qualification of particles as either matter or

energy. For the purposes of this paper it is practical and sufficient for understanding to consider equations of motion of only one dimension since any path traversed at constant speed can be parameterized as such and densifies at the same rate; extrapolation to all three dimensions is a straightforward task.

Length and time are measured with a ruler and a clock [5]. *Proper Space* is denoted by the variable z and experiences densification dependent on proper time which is denoted by the independent variable tau τ. In this case the clock is also embedded within the ruler and is not considered an additional physical dimension. In *object space* space and time are treated on equal footing as independent dimensions and are denoted by x and t, respectively. These variables have local values that manifest densification as contraction and dilation in mimicry of many of the details of Special Relativity and continue to suffer from dependence on frame-specific relative velocity.

Measurements of physical observables are made in object space and converted to values in proper space where the action originates. The coordinate transformation for length or displacement involves the scale change

$$dz = f\,dx. \tag{1}$$

The unitless scale factor f is defined for densification as a *density of points* which is represented by a ratio of infinities increasing from unity as

$$f = \left(\frac{dx + cdt}{dx}\right) = 1 + \left(\frac{cdt}{dx}\right). \tag{2}$$

Simple substitution of (2) into (1) yields the coordinate transformation between spaces

$$dz = dx + cdt. \tag{3}$$

This is the conversion for points in space with an explicit dependence on elapsed time. Contrary to expectation with densification a scale transformation from object space to proper space takes a form that is reminiscent of a Galilean boost [6].

The burgeoning density of proper space requires the use of additional notation for the proper *waxing velocity*, denoted by w, while in object space the concept of velocity is retained as it is traditionally used and remains denoted by v. The relationship between the two quantities is

$$w \triangleq \frac{dz}{d\tau} = \alpha\,(v + c)\,. \tag{4}$$

Values for the velocity in object space persist within the range of $(-c, c)$ while values for the waxing velocity are always positive within the range of $[c, 0)$. Open endpoints of each interval are forbidden for the same reason; denizens of the universe must always experience the advancement of proper time in some nonzero fraction. Accordingly values for the *temporal dilation coefficient*, marked by alpha α, vary as $[1, 0)$. Infinite dilation is taboo and is expressed by the avoidance of an asymptotic value of zero for α.

In a break from prior theories of motion it is important that velocities in all spaces are measured from a special class of perspectives hereinafter referred to as *proper frames*. The choice of axes may be made without particular regard for position but must be boosted to the specific velocity whereby t reaches the maximum expression of τ and experiences densification at its fullest flowering. Proper frames can be thought of as critical points and specific values associated with these perspectives are $w = c$, $v = 0$ and $\alpha = 1$.

For the sake of completeness it is worthwhile to also define a *stationary space*, denoted by y, which advances with the preceding variable of proper time τ. This nonphysical construct may be mathematically advantageous as it allows for the use of global variables that forgo dependence on relative perspective but carries the caveat that the space is not demonstrative of physical reality. The scale-densification — to — boost technique above is repeated to provide the transformation to proper space as

$$dz = dy + cd\tau. \tag{5}$$

Measurements of length or distance are converted from object space to corresponding values in stationary space through the transitive property with application of (3) and (5) to yield

$$dy + cd\tau = dx + cdt. \tag{6}$$

For stationary space a *pseudovelocity* is defined as u and takes on the values $(-c, c)$. Values of u are somewhat analogous to velocities v in object space e.g., adopting the value of zero in a proper frame where $dt = d\tau$. The relation for the two quantities is

$$u \triangleq \frac{dy}{d\tau} = \alpha\,(v + c) - c. \tag{7}$$

As proper space and stationary space both share the variable τ as proper time the relationship between velocities is more simple as

$$w = u + c. \tag{8}$$

The choice of alphabetically proximate variables is a mnemonic convenience that is intended to be familiar and resemble current definitions but not to imply any other mathematical relationship including equivalence with commonly used spatial unit vectors. The invariant variable s is reserved for possible future use.

4 Discussion

Change is the true nature of the universe and the densification of proper space depicts the most authentic representation of space and time. A static ruler of fixed length is a forbidden item; an absolutely stationary observer is a nonsensical frame of reference that does not exist. Although this picture of reality is not mathematically convenient it is the correct philosophy to accurately model basic kinematics. Object(-*ive*) space is the milieu where action is perceived and measurements are made. The coordinate transformation to proper

space takes the form of a boost centered on c which arises, not surprisingly, from the defining feature of the universe. This conversion yields the advantage to the waxing velocity which can always be rotated since it is never zero as objects must experience some positive slice of proper time. Objects moving at the same rate as densification do not experience the passage of proper time and therefore cannot inhabit this universe. It should not be overlooked that the transformation is originally a scale change whereby the size of massive objects is growing relative to the coordinate system with the densification. It is the growth of the span between the center of mass of an object and any other contained point within that same object that is seemingly retarded in entities not occupying a proper frame of motion. Consideration of the action of only infinitesimal points does not reveal this detail. It is helpful if the time-dependent metric tensor is visualized as the ruler growing shorter and shorter thus creating an illusion of inflation. The author supposes that the idea of densification within fixed boundaries is an option that Einstein either discarded or failed to consider and is the source of his self-critical vacillation regarding the Cosmological Constant [7].

In a brief departure from kinematics an examination of multiple perspectives clarifies the necessity for a preferred frame of interaction. Collisions cannot have different outcomes in different frames otherwise every incident can be transformed into a destructive event. Synchronization to a proper frame is a sufficient condition to preserve the integrity of any physical interaction; the regimentation also reemphasizes the significance of velocity. This interpretation of simultaneity provides the means to intellectually resolve the well-known gedanken paradox [8]: what are the ages of the traveling twins? There currently exists an abundance of experimental and observational data which can be used to determine the validity of proper frames. The incongruity of superluminal travel can be rectified by application of the results discussed here and the presence of tachyons is discarded.

Terminology relating to motion must be used cautiously since the concepts involved vary among the different spaces despite a similarity in formulation. Calculations done in stationary space remove some of the difficulties of perspective that are inherent to the other spaces but readers are warned to remember that this is not a physical reality. In object space it is time that slows and space that contracts as a function of speed to the detriment of the occupying objects. A sequence of snapshots in proper space shows that movement in any direction produces an apparent spatial *and* temporal dilation based upon the movement of a mass impinging on the budding densification. Part of the virtue of proper space is that the object itself is not actually altered and the perception of dilation occurs only in the direction of motion while densification continues unabated along all other axes. Along with the increase in movement this retardation of proper space and proper time is demonstrated as a decrease in the waxing velocity although the moving particle still perceives densification continuing at c. A reasonable choice for a functional definition of w is the hyperbolic secant as a function of the *angle of dilation*, represented by phi φ, and demonstrated in $w = \operatorname{csech}(\varphi)$ making it more akin to a speed than a velocity. The positive-definite, even function is a rotation of phi through the real interval $(-\infty, \infty)$ as measured from a proper frame and this run equates with the previously detailed bounds for w of $[c, 0)$. The choice of hyperbolic functions is preferred over the circular transcendental equations as the hyperbolics are independent of the imaginary number i.

Consideration of the relative velocity between bulk objects with determinate length requires the use of a proper frame. A measurement of relative velocity is inadequate to completely determine the true states of objects in the system; two measurements are required to establish the correct scalings for space and time. Take the example in object space of two masses *at rest* to a specific proper frame as well as to each other; the waxing velocity of each frame in proper space is c. While the relative velocity in object space between the centers of mass remains at zero in proper space the relative velocity is characteristic and not zero as might be anticipated. This discrepancy can be partly reconciled by acknowledging the supplemental velocity acquired in proper space which is imparted by the densification of the gap between the two masses. Accordingly the correct velocities between the center of mass frames are emphasized by primed coordinates and subscripts enumerate the frames of reference for separate and distinct objects as

$$u' \triangleq u_2 - u_1, \tag{9.1}$$

$$w' \triangleq u' + c, \tag{9.2}$$

$$\text{and } v' \triangleq \left(\frac{w'}{\alpha'}\right) - c. \tag{9.3}$$

The sense of relative motion is preserved by these transformations; the distinction of an *alias* versus an *alibi* transformation is highlighted [9]. To determine the relative velocity in object space measurements are made there first, converted to pseudovelocities and the relative velocity calculated then reverted to object space. All direct measurements are relative with v' equal to v from a proper frame. Although this computation avoids direct expression of quantities in proper space the kernel of the action lies there.

The primed alpha coefficient α' serves as both the relative temporal dilation between objects as well as the transformation between frames in proper space. It is defined as a ratio in the range of real positive numbers $(0, \infty)$ and is most easily understand as an exponential with argument given as the difference between two angles and shown here

$$\alpha' \triangleq \left(\frac{\alpha_2}{\alpha_1}\right) = e^{-(\varphi_2 - \varphi_1)}. \tag{10}$$

These definitions in combination with some computation restore the hyperbolic tangent in a composition of velocities in

object space and yield a result that is in correspondence with rapidity [10]. The assertion that values of α' can exceed 1 is a specific deficiency in the conventional measurement of relative velocity. Attend to these calculations with care as variables of the traditional theory are ill-defined by the muddled use of mixed perspective due to a misconception in the choice of laboratory frame.

The derivation is accomplished to this point without the need for i; further descriptions of the manifest complexity of nature require the use of imaginary numbers. The kinematics is extended to distinguish between the movements of the two types of mass by applying a label of *material* or *immaterial* (i-material) to all particles whether they are matter or energy; the two types are interchangeable provided the exchange is done en masse. Real and imaginary objects occupy overlapping worlds within the same universe because the phase dichotomy causes a perception of near invisibility between the two categories of mass in which the contrary object collapses to a dimensionless point. As seen before with dilation the flattening is perceptual and not actual. The alternately phased object appears to ignore densification and to therefore exist in a forbidden state. In that the object doesn't seem to experience scaling it performs as with a waxing velocity of zero and erroneously claims relative velocities as $w' = c \pm c$ and $v' = 0 \pm c$. The relative motion of the oppositely phased objects either approaches or recedes depending on the relative angle of dilation. The tipping point occurs when $\varphi_1 = \varphi_2$ and $\alpha' = 1$ and can serve as a test provided it is possible to produce a series of identical immaterial objects. The author defers the specific method for this production to the expertise of experimentalists.

The expression $E = mc^2$ acquires a new complexion after revisiting the outmoded concepts of the rest mass of matter and the mass equivalence of energy. The characteristic velocity measured between real and imaginary particles is superficial and acts as a screening value whereby information is hidden from the casual observer but still preserved. Relying only on light as a mediator to comprehend motion introduces inaccuracies that must be corrected. A single physical measurement of an immaterial object is underdetermined and wrongly constrains the associated parameters of velocity and imaginary mass. Consequently the sources of wave nature are found to originate from the complex quality of mass and not directly from the tableau of spacetime. The seeming lack of determinate states which is the hallmark of Quantum Mechanics illustrates its subservience to statistical models and elucidates its failure of completeness and its misappropriation of fundamental reality.

5 Conclusions

Maintaining an open-minded attitude of skepticism lies at the heart of the scientific method; challenging established ideas is not necessarily an effort towards rebellion and anarchy. Persistent testing is an important undertaking in the quest to further humanity's understanding of life, the universe and everything. The author is awakened to the fact that the peculiar consequences of Albert Einstein's Special Relativity and subsequent geometric interpretation of space and time originate from observation and the theory does not proceed directly from a foundational source. Relying on relative viewpoints to predict motion has an inherent handicap and in combination with the confused measurement of lightspeed initially serve as motivation for study. The approach to creating a kinematics involves keeping a critical eye on perspective and attempting to dispel paradoxes in order to see through to the metaphysical center. It is a mistake to rely totally on mathematical models of nature as they are ultimately flawed and physicists must constantly endeavor to look beyond constructed images of reality. If the basic realities of space and time are known then it is possible to properly explain the curious details of motion of all objects in the native environment and show that they proceed in a logical and intuitive way from this physical foundation. The success of such a hypothesis would be the pedestal on which the future of physics could be built and would have a far-reaching influence on science and greatly impact its application to technology in addition to answering important philosophical questions.

The elegance of Proper Space Kinematics is that it proceeds directly from the fundamental concept that the fabric of the universe densifies at the unique quantity and quality of the characteristic velocity c maturing with an inescapable duration of proper time. This insight into the inner workings of space and time solidifies realizations regarding the arrow of time and the spectre of irreversible entropy. It is not surprising that in a study of motion appearances are deceiving and this deception necessitates a transformation to positions in other spaces which are difficult to visualize since the use of a time-dependent metric is not a well-developed field of study with much pertinent literature. Spatial densification is understood by a study of the steadily mounting density of points (Mind the infinities!) whereby a scale change converts the growing size of objects to the form of a boost. Care at the beginning: reconceptions of velocity and movement lead to new definitions such as proper space's waxing velocity and the interrelated temporal dilation coefficient. Additionally boosting perspective to any proper frame provides the linkage that shows these points of view can be logically related and provides for surety over the use of four-vectors and four-velocities. Scrutiny of these results discerns that stationary space is a fictitious point of view that proves to be a useful tool.

Densification clarifies the observed nuances of motion more clearly than Special Relativity by eschewing stationary states and shedding new light on the evolution of the aging universe. Scale expansion of objects is found to be a new source of motion where movement hinders the passage of time and limits experience. Thought problems are revisited

and explained by the introduction of new concepts such as proper frames providing ample opportunity for testing the validity of these new ideas; experimental and mathematical verification have many available avenues to explore. This kinematics shows that the movement of objects does not cause a physical change but merely alters appearances. As particles always experience their own perspective as characteristic the presented composition of velocities accurately details the difference between spectators and participants. The duality of mass shows that the landscape of space is a perpendicular reality for matter and energy which can be tested by manufacturing an experimental watershed. The screening between imaginary material phase shifts creates a Quantum confusion due to underdetermined measurements that the author feels does finally vindicate Einstein's intuition. (No Dice!)

As a first principles theory which meets the onus of the stated hypothesis Proper Space Kinematics claims jurisdiction over all motion in the universe. Proper motion supplants the golden relics of relative and absolute motion; the dubious lessons of Quantum nature must be extracted and distilled for their essential truths. As seen with Isaac Newton in his 1687 *Philosophiae Naturalis Principia Mathematica* [11] in the continuing quest for deeper insight new ideas are a harbinger for chaos as fundamental changes in understanding prompt the reevaluation of physics on every level and in every niche. The potential impact on science and its application expands from the theoretical to the technological to hopefully improve the quality of human life and reinvigorate the search for profundity. The author proposes that the next step in this study is to complete a mechanics in full generality with metric-tensor formalism to include a derivation of canonical coordinates with energy and momentum and an examination of accelerating objects with interactions via both collisions and forces-at-a-distance. Delving further raises a rich multitude of questions: Is densification in the universe constant? What does this mean for cosmology and the birth and death of the universe? Are there other characteristic parallel universes that are unseen? Is there a greater realm? How do these results apply to the standard model? Was the creation of life and homo sapiens sapiens an accident? Why are we here? Physicists have always searched the universe for bedrock on which to stand but to live in harmony with our world we must instead navigate the rising tide of space and time and learn to walk on water.

Acknowledgements

Although this research has been a solitary exercise I wish to express my gratitude to those who have lifted me up and helped make me capable of achieving this goal. To my family and friends, first and foremost of which are my parents Paul A. Wade and Margaret Aracich Wade, thank you for your love and support in helping me to build a place within myself where I can always stand strong. Thank you Dr. Stephen J. Nettel for your role in awakening my love of physics. Thank you to all of those people who have cared about and for my well-being for without each of you this work would never have been realized.

Submitted on December 21, 2012 / Accepted on December 24, 2012

References

1. Einstein A. Zur Elektrodynamik bewegter Körper. *Annalen der Physik*, 1905, Bd. 17, 891–921.
2. Einstein A. On the electrodynamics of moving bodies. In: *The Principle of Relativity* (Methuen and Company, Ltd., London, 1923), translation by W. Perrett and G. B. Jeffery, from *Das Relativatsprinzip* (Tuebner, Germany, 1922), 4th ed.
3. Faye J. Copenhagen Interpretation of Quantum Mechanics. *The Stanford Encyclopedia of Philosophy*, 2008, http://plato.stanford.edu/archives/fall2008/entries/qm-copenhagen
4. List of unsolved problems in physics. http://en.wikipedia.org/wiki/List_of_unsolved_problems_in_physics
5. Schouten J. A. Tensor Analysis for Physicists. Dover Publications, Inc., Mineola, 1989, 2nd ed., p. 217.
6. Misner C. W., Thorne K. S., and Wheeler J. A. Gravitation. W. H. Freeman and Company, New York, 1973, p. 295.
7. Mook D. E. and Vargish T. Inside Relativity. Princeton University Press, Princeton, 1987, p. 191.
8. Hartle J. B. Gravity: An Introduction to Einstein's General Relativity. Addison Wesley, San Francisco, 2003, p. 63.
9. Weisstein E. W. Transformation. http://mathworld.wolfram.com/Transformation.html
10. Foster J. and Nightingale J. D. A Short Course in General Relativity. Springer Science & Business Media, Inc., New York, 2006, p. 216.
11. Newton I. Philosophiae Naturalis Principia Mathematica. Jussu Societatis Regiae ac Typis Josephi Streater, Londini, 1687.

Liquid Metallic Hydrogen II. A Critical Assessment of Current and Primordial Helium Levels in the Sun

Pierre-Marie Robitaille
Department of Radiology, The Ohio State University, 395 W. 12th Ave, Columbus, Ohio 43210, USA. E-mail: robitaille.1@osu.edu

Before a solar model becomes viable in astrophysics, one must consider how the elemental constitution of the Sun was ascertained, especially relative to its principle components: hydrogen and helium. Liquid metallic hydrogen has been proposed as a solar structural material for models based on condensed matter (e.g. Robitaille P.-M. Liquid Metallic Hydrogen: A Building Block for the Liquid Sun. *Progr. Phys.*, 2011, v. 3, 60–74). There can be little doubt that hydrogen plays a dominant role in the universe and in the stars; the massive abundance of hydrogen in the Sun was established long ago. Today, it can be demonstrated that the near isointense nature of the Sun's Balmer lines provides strong confirmatory evidence for a distinct solar surface. The situation relative to helium remains less conclusive. Still, helium occupies a prominent role in astronomy, both as an element associated with cosmology and as a byproduct of nuclear energy generation, though its abundances within the Sun cannot be reliably estimated using theoretical approaches. With respect to the determination of helium levels, the element remains spectroscopically silent at the level of the photosphere. While helium can be monitored with ease in the chromosphere and the prominences of the corona using spectroscopic methods, these measures are highly variable and responsive to elevated solar activity and nuclear fragmentation. Direct assays of the solar winds are currently viewed as incapable of providing definitive information regarding solar helium abundances. As a result, insight relative to helium remains strictly based on theoretical estimates which couple helioseismological approaches to metrics derived from solar models. Despite their "state of the art" nature, helium estimates based on solar models and helioseismology are suspect on several fronts, including their reliance on solar opacities. The best knowledge can only come from the solar winds which, though highly variable, provide a wealth of data. Evaluations of primordial helium levels based on 1) the spectroscopic study of H-II regions and 2) microwave anisotropy data, remain highly questionable. Current helium levels, both within the stars (Robitaille J. C. and Robitaille P.-M. Liquid Metallic Hydrogen III. Intercalation and Lattice Exclusion versus Gravitational Settling, and Their Consequences Relative to Internal Structure, Surface Activity, and Solar Winds in the Sun. *Progr. Phys.*, 2013, v. 2, in press) and the universe at large, appear to be overstated. A careful consideration of available observational data suggests that helium abundances are considerably lower than currently believed.

> At the age of five Cecilia [Payne] saw a meteor, and thereupon decided to become an Astronomer. She remarked that she must begin quickly, in case there should be no research left when she grew up.
>
> Betty Grierson Leaf, 1923 [1, p. 72–73]

1 Introduction

Knowledge that helium [2, 3] was first observed in the Sun by Pierre Jules César Janssen [4] and Joseph Norman Lockyer [5], before being discovered on Earth by William Ramsay [6], might prompt the belief that the element was abundant on the solar surface. In fact, helium has never been identified in the absorption spectra of the quiet Sun. Janssen and Lockyer's fortunate discovery was restricted to helium lines appearing within the prominences of the corona and within the disturbed chromosphere [4, 5]. While the element was easily detectable in these regions [7], helium has remained relatively spectroscopically silent on the Sun. Conversely, the stars and the Sun display signs of extreme hydrogen abundance, as first observed by Cecilia Payne [8], Albrecht Unsöld [9], and Henry Norris Russell [10]. Few would take issue with the conclusion that the visible universe is primarily comprised of hydrogen. Helium abundances present a more arduous question.

Despite all the difficulties, several lines of reasoning sustain the tremendous attention that solar helium levels have received in astronomy. First, helium is the end product of the nuclear reactions currently believed to fuel many of the stars, either in the pp process or the CNO cycle [11–15]. Second, solar helium levels are inherently linked to the gaseous models of the Sun [16–18] and the application of theoretical findings to the interpretation of helioseismic results [19–23]. Finally, helium is thought to be a key primordial element in

Big Bang cosmology [3, 24–30]. As a result, the evaluation of helium levels in the Sun brings a unified vision of astrophysics, wherein accepted solar values lend credence to our current concept of the formation of the universe. Still, questions remain relative to the accuracy of modern helium determinations.

A flurry of initial studies had suggested that helium abundances in the stars approached 27% by mass (see [3] for a review). The findings provided support for those who proposed primordial formation of helium prior to the existence of the objects which populate the main sequence [3, 24]. However, these ideas were challenged when it was discovered that certain B-type stars, which should have been rich in helium lines, were almost devoid of such features [3]. As a result, in certain stars, helium was said to be gravitationally settling towards the interior [3, 31]. The desire to link helium levels in the Sun with those anticipated from the primordial synthesis continues to dominate modern solar theory [18]. Nonetheless, it can be demonstrated that the methods used to estimate primordial helium levels in the universe [24] are either highly suspect or implausible. Given these complexities, it is appropriate to compose a critical review of how helium abundances have been historically obtained and how they are currently determined, both in the Sun and in the universe at large.

2 Assessing elemental abundances in stellar spectra

2.1 The Saha Equations

Reasoning, like Lindemann [32] and Eggert [33] before him, that the fragmentation of an atom into an ion and an electron was analogous to the dissociation of a molecule, Megh Nad Saha [34, 35] formulated the ionization equations [36, 37] in the early 1920s. In so doing, he called upon the Nernst equation [38] and suggested that the free electron could be viewed as an ideal gas. He also relied on thermal equilibrium and the ionization potentials of the elements. Since Saha's equation was inherently related to parameters associated with the ideal gas (i.e. [39, p. 29–36] and [40, p. 107–117]) he demonstrated that the level of ionization could be increased either with elevated temperature or decreased pressure. Saha hypothesized that the pressure of the reversing layer approached 0.1–1 atm [36, p. 481] and was the first to utilize this assumption to account for the appearance of spectral lines across stellar classes as simple functions of temperature [36, 37]. He was concerned with the marginal appearance of spectral lines [36, 37], that point at which these features first appeared on a photographic plate. Cecilia Payne [1, 41] would soon estimate the abundance of the elements in the universe using the same criterion [8].

In his initial work, Saha would comment on the impossibility of solar temperatures increasing as one moves from the photosphere to the upper chromosphere: "*Lockyer's theory... [that elements become more ionized as higher elevations are reached within the chromosphere] ... would lead us to the hypothesis that the outer chromosphere is at a substantially higher temperature than the photosphere, and the lower chromosphere; and that the temperature of the sun increases as we pass radially outwards. This hypothesis is, however, quite untenable and is in flagrant contradiction to all accepted theories of physics*" [36, p. 473]. Saha had not suspected that 20th century solar theorists would maintain such a position. Lockyer's analysis was correct: ionization increased with elevation in the chromosphere. This was an important lesson relative to thermal equilibrium. In any case, Saha did observe that hydrogen was not fully ionized in the chromosphere, since the lines from H_α and H_β were evident at this level. He also recognized that hydrogen should be essentially ionized in O class stars and that the lines coincident with the Balmer series in these stars had originated from ionized helium. At the same time, he outlined that the same spectral lines for classes later than B2A were completely due to hydrogen [37, p. 151].

Subrahmanyan Chandrasekhar's (Nobel Prize, 1983 [42]) thesis advisor, Sir Ralph H. Fowler [43], had provided significant insight and criticisms into Saha's second manuscript [37, p. 153] and the resulting text was masterful. In 1927, Megh Nad Saha was elected a Fellow of the Royal Society [34].

In the meantime, Fowler [43] and Edward Arthur Milne [44] would collaborate and construct a wonderful extension [45, 46] of Saha's seminal papers [36, 37]. They improved the treatment of ionization to consider not only principle lines arising from atoms in their lowest energy states, but also the subordinate lines produced by excited atoms and ions [45, 46]. For his part, Saha had concentrated on the excitation and ionization of the neutral atom [36, 37]. Fowler and Milne understood that the marginal appearance of a spectral line could be used in determining relative concentrations and provided some indication of the minimum number of atoms necessary for appearance [45, 46]. They emphasized the idea that: "*the intensity of a given absorption line in a stellar spectrum is proportional to the concentration of atoms in the stellar atmosphere capable of absorbing the line*" [45, p. 404]. Their first paper also highlighted the value of the maximum of a spectral line in assessing the temperature and pressure of the reversing layer and outlined that this problem was not affected by the relative abundance of the element studied [45]. Using stellar data from the lines of Ca, Mg, Sr, and Ba they determined that the electron pressure of the reversing layer was on the order of 10^{-4} atm [45]. Fowler and Milne understood that electron pressure, P_e, of the reversing layer was not determined by a single ionization process, but by the ionization of many elements: "*In thus regarding P_e as fundamental we are in effect assuming that, due to the presence of more easily ionised atoms, there are so many electrons present that the partial electron pressure is practically independent of the degree of ionization of the element under discussion*" [45, p. 409]. They expressed concern that their results led to the assumption that absorbing species had very large absorption

coefficients [45]. Milne had already determined that the absorption coefficients should be very large [47] and would later devote another theoretical paper to their determination [48]. In their work together, Fowler and Milne explicitly assumed that the reversing layer could be treated as existing under conditions of thermal equilibrium, as Saha's treatment required [36]. The validity of such assumptions is not simple to ascertain.

At Cambridge, Milne met Cecilia Payne [1, p. 121], a student at Newnham College [1, p. 112] and learned of her impending access to the vast collection of photographic plates used to generate the Henry Draper Catalogue at the Harvard Observatory [1, p. 144–153]. Prior to the advent of the modern MKK classification [49], the Henry Draper Catalogue was the largest stellar library collection, with over 200,000 classified stars [1, p. 144–153]. Milne suggested that "*if he had... [Payne's] ... opportunity, he would go after the observations that would test and verify the Saha theory*" [1, p. 155]. Cecila Payne soon left Cambridge and sailed to America.

2.2 Cecilia Payne: What is the universe made of?

> "I remember when, as a student at Cambridge, I decided I wanted to be an astronomer and asked the advice of Colonel Stratton, he replied, "You can't expect to be anything but an amateur". I should have been discouraged, but I wasn't, so I asked Eddington the same question. He (as was his way) thought it over a very long time and finally said: "I can see no insuperable obstacle" [50, xv].

Nineteenth century scientists had little on which to base their understanding of the composition of the universe. Their clues could only come from the Earth itself and from the meteorites which occasionally tumbled onto its surface. Consequently, it was not unreasonable to expect that the universe's composition matched the terrestrial setting. However, stellar spectra, already stored on photographic plates throughout Europe and especially in the vast Henry Draper Collection, were hiding a drastically altered viewpoint. With the arrival of yet another woman at the Harvard Observatory [51–60], the stars could not much longer conceal their story. Surrounded by Pickering's Harem [51–60], Cecilia Payne [1, 41] completed her classic report on the abundance of the elements [8] and became the first to underscore the importance of hydrogen as the constitutive atom of universe. Her thesis had been carefully prepared and presented supportive laboratory evidence, not only of ionization potentials, but of the validity of Saha's treatment [8, p. 105–115].

Stellar spectra signaled hydrogen [61] was so abundant that several scientists, including Henry Norris Russell, could not fully accept the conclusion. Payne had written an early manuscript detailing the tremendous presence of hydrogen [1, p. 19]. Her thesis advisor, Harlow Shapley, forwarded the work to Russell who commented: "*It is clearly impossible that hydrogen should be a million times more abundant than the metals*" [1, p. 19]. That early manuscript was never published and has since been lost [1, p. 20]. Tempered by Russell and Shapley, Cecilia Payne finally produced her famous PhD dissertation: *Stellar Atmospheres: A Contribution to the Observational Study of High Temperature in the Reversing Layers of Stars* [8]. She would comment on hydrogen in this manner: "*Although hydrogen and helium are manifestly very abundant in stellar atmospheres, the actual values derived from the estimates of marginal appearance are regarded as spurious*" [8, p. 186]. A little later she would add: "*The outstanding discrepancies between the astrophysical and terrestrial abundances are displayed for hydrogen and helium. The enormous abundance derived for these elements in the stellar atmospheres is almost certainly not real*" [8, p. 188] and "*The lines of both atoms appear to be far more persistent, at high and low temperatures, than those of any other element*" [8, p. 189].

For her part, Payne privately maintained that hydrogen was tremendously abundant in the stars: "*When I returned to visit Cambridge after I finished this first essay in astrophysics, I went to see Eddington. In a burst of youthful enthusiasm, I told him that I believed that there was far more hydrogen in the stars than any other atom. 'You don't mean in the stars, you mean on the stars', was his comment. In this case, indeed, I was in the right, and in later years he was to recognize it too*" [1, p. 165].

Payne's work also highlighted the importance of helium in the O and B class stars [8]. For the first time, hydrogen and helium became the focus of scrutiny for their role as potential building blocks of the stars and the cosmos [8]. She emphasized that: "*there is no reason to assume a sensible departure from uniform composition for members of the normal sequence*" [8, p. 179] and "*The uniformity of composition of stellar atmospheres is an established fact*" [8, p. 189]. She also held, as Eddington and Zeipel had advanced, that given their gaseous nature: "*an effect of rotation of a star will be to keep the constituents well mixed, so that the outer portions of the sun or of a star are probably fairly representative of the interior*" [8, p. 185]. Still, Payne was cautious relative to extending her results as reflecting the internal composition of the stars: "*The observations on abundances refer merely to the stellar atmosphere, and it is not possible to arrive in this way at conclusions as to internal composition. But marked differences of internal composition from star to star might be expected to affect the atmosphere to a noticeable extent, and it is therefore somewhat unlikely that such differences do occur*" [8, p. 189].

Payne would conclude her thesis with a wonderful exposition of the Henry Draper Classification system [8, p. 190–198]. Otto Struve would come to regard the study as "*the most brilliant Ph.D. thesis ever written in astronomy*" [41]. Edwin Hubble would comment relative to Payne: "*She's the best man at Harvard*" [1, p. 184]. As Milne suggested, the first dissertation of the Harvard College Observatory was founded

upon the application of the ionization equations [36,37,45,46] to the detailed analysis of spectral lines across stellar classes. It did not specifically address elemental abundances in the Sun. Nonetheless, Payne's 1925 dissertation heralded the application of quantitative spectral analysis in astronomy [8].

2.3 Albrecht Unsöld, hydrogen abundance, and evidence for a solar surface

Albrecht Unsöld extended Payne's studies with a focus on the solar spectra [9]. Following in her footsteps [8], in 1928 [9], he applied the ionization formula [36, 37] to the chromosphere and estimated the levels of sodium, aluminum, calcium, strontium, and barium. In addition, Unsöld determined that the electron gas pressure in the chromosphere stood at $\sim 10^{-6}$ atm [9]. He also concluded that hydrogen must be about one million times more abundant than any other element in the Sun [9, 62]. William McCrea was soon to echo Unsöld, finding that hydrogen was a million times more abundant than Ca^{+} within the chromosphere [62, 63].

Importantly, Unsöld also documented that the absorbance of the hydrogen β, γ, and δ lines did not decrease across the Balmer series ($H_\alpha = 1$; $H_\beta = 0.73$; $H_\gamma = 0.91$; $H_\delta = 1.0$) as expected from quantum mechanical considerations ($H_\alpha = 1$; $H_\beta = 0.19$; $H_\gamma = 0.07$; $H_\delta = 0.03$) [9]. This was an important finding relative to the nature of the Sun. Recently, the behavior of hydrogen emission lines has been analyzed with non-LTE methods [64]. It has been concluded that the "*$n = 3$ and higher levels are in detailed balance deep in the photosphere, but they develop a non-LTE underpopulation further out. However, the levels with higher n-values stay in detailed balance relative to each other at these atmospheric depths, and they also collisionally couple tightly to the continuum*" [64]. Yet, in the gaseous models of the Sun, the continuum is not composed of condensed matter [65]. It represents an area of profoundly increased solar opacity [65]. Nevertheless, the behavior of the Balmer series in the solar atmosphere strongly supports the idea that the Sun is comprised of condensed matter. Only a physical entity of sufficient density, such as a surface, can permit tight collisional coupling to the continuum, as it is impossible to couple to the opacity changes which characterize the continuum in gaseous models [65]. These findings comprise the sixteenth and seventeenth lines of evidence that the Sun is comprised of condensed matter. The others are outlined by the author in recent publications (e.g. [66]).

2.4 Henry Norris Russell: Inability to estimate Helium from spectral lines

Soon Henry Norris Russell [67] surpassed Unsöld in his analysis of solar spectral lines and provided a detailed compositional analysis of the Sun. Relative to the occupied energy levels within atoms on the Sun, Russell affirmed that: "*It must further be born in mind that even at solar temperatures the great majority of the atoms of any given kind, whether ionized or neutral, will be in the state of lowest energy*" [10, p. 21]. At the same time, Russell realized that this rule was not observed by hydrogen, leading him to the conclusion that the element was extremely abundant in the Sun: "*One non-metal, however, presents a real and glaring exception to the general rule. The hydrogen lines of the Balmer series, and, as Babcock has recently shown, of the Paschen series as well, are very strong in the Sun, though the energy required to put an atom into condition to absorb these series is, respectively, 10.16 and 12.04 volts - higher than for any other solar absorption lines. The obvious explanation — that hydrogen is far more abundant than the other elements — appears to be the only one*" [10, p. 22]. In fact, even the hydrogen Brackett lines can be visualized in the infrared spectrum of the Sun [68]. Russell also highlighted Unsöld's observation [9] that the hydrogen β, γ, and δ lines did not decrease as expected. That the hydrogen lines were extremely broad in the Sun had already been well established. Russell echoed some of his contemporaries and suggested that this might result from a Stark effect [10, p. 50].

Finally, Russell accepted Payne's findings relative to hydrogen and reported her numbers for the elements without comment in his table XVI [10, p. 65]. He stated that: "*The most important previous determination of the abundance of the elements by astrophysical means is that by Miss Payne. . .*" [10, p. 64]. Russell found the correlation between their works to display "*a very gratifying agreement*" [10, p. 65]

Like Payne, Russell had relied on the work of Fowler and Milne [45, 46] to set the composition of the Sun. He implemented their suggestion that electron pressures, P_e, could be gathered by considering the spectra and the ionization potential for elements like Ca, Sc, Ti, Sr and Yt. From these, he deduced a P_e of 3.1×10^{-6} atm, in close agreement with Milne (2.5×10^{-5} atm), and Payne and Hogg (2.54×10^{-6} atm) in class G0 stars [10, p. 54–55]. Along with John Quincy Stewart, Russell had previously considered various means of determining the pressures at the Sun's surface and had determined that the pressure of the reversion layer could not be more than 10^{-4} atm [69]. But Russell reported a factor of at least 10 in discordance in calculating electron pressures based on either the ionization formula or the numbers of metallic atoms and ions [10, p. 70–71]. He would resolve the difficulty at the end of his treatise when setting the final elemental composition for the Sun [10, p. 72].

At the same time, while Payne had understood the importance of local thermal equilibrium (LTE) for the proper application of Saha's equation [8, p. 92–101], she did not attempt to make an explicit correction for the lack of equilibrium. Conversely, Russell placed a correction factor in his work for departure from LTE: "*We have finally to take into consideration the fact that the atmosphere may not be in thermodynamic equilibrium. The comparison of solar and stellar spectra affords evidence that this is the case*" [10, p. 52]. Relative

to his final abundances he commented: "*The main source of uncertainty which affects them is the magnitude of the correction for departure from thermodynamic equilibrium*" [10, p. 58] and "*If the correction for departure from thermodynamic equilibrium should be wholly disregarded, the calculated abundance of hydrogen — already very great — would be increased thirty fold*" [10, p. 62]. In the 1920s, of course, there was hesitancy concerning the tremendous levels of hydrogen observed in the solar atmosphere.

For Russell, oxygen appeared as abundant as all other metals combined. He also argued against, although did not fully dismiss, gravitational settling in the Sun for the heaviest metals: "*It does not appear necessary, therefore, to assume that downward diffusion depletes the sun's atmosphere of the heavier elements, though the possibility of such an influence remains*" [10, p. 59]. Importantly, he noted: "*The statement that enhanced lines are found in the sun for those elements which have lines of low excitation potential in the accessible region has therefore few exceptions*" [10, p. 35]. At the same time, he advanced that for those elements "*which fail to show enhancement lines in the sun, the excitation potentials for the accessible lines are high in every case for which they have been determined*" [10, p. 35]. Furthermore Russell hypothesized that: "*It appears, therefore, that the principle factor which is unfavourable to the appearance of a spectral line in the sun is a high excitation potential*" [10, p. 35]. This was precisely the case relative to helium.

With respect to the second element, Russell wrote: "*There is but one element known to exist in the sun for which no estimate of abundance has now been made - and this is He. The intensity of its lines in the chromosphere shows that it must be present in considerable amount, but no quantitative estimate seems possible*" [10, p. 62]. Here was an explicit admission that solar helium abundances could not be ascertained using spectral data.

Helium was abundantly visible in early type stars, as Cecilia Payne had already discovered [8] and Paul Rudnick [70] and Anne Underhill continued to confirm [71–73]. Estimates of the number of hydrogen to helium atoms in O and B type stars varied from values as low as 3.2 to more than 27 [73, p. 156]. A factor of nearly 10 in relative abundances from spectral lines in such stars was hardly reassuring. Nonetheless, Underhill still surmised that the number of helium atoms was at the 4–5% level [73]. Yet for the Sun, data about helium abundance remained wanting.

2.5 Local Thermal Equilibrium

Milne was perhaps the greatest authority relative to local thermal equilibrium (LTE) in astronomy [74–77] and many of the most salient aspects of his arguments have been reviewed [78]. Milne advocated that LTE existed in the center of a star and that his treatment permitted "*us to see in a general way why the state of local thermodynamic equilibrium in the interior of a star breaks down as we approach the surface*" [77, p. 81–83]. In 1928, Milne would express concern relative to the appropriateness of the inferred thermal equilibrium in the reversing layer, as required by the Saha equations [36, 37], although he believed that studies based on the validity of the ionization equations should be pursued: "*The recent work of Adams and Russell brings forward evidence that the reversing layers of stars are not in thermodynamic equilibrium. This suggests a degree of caution in applying the fundamental method and formulae of Saha to stellar spectra. Nevertheless, departure from thermodynamic equilibrium can only be found by pushing to as great a refinement as possible the theory which assumes thermodynamic equilibrium*" [48]. Gerasimovic had already advanced corrections for small deviations from thermal equilibrium [79] and Russell applied corrections directly in his work [10]. By 1925, the Saha equations had been generally confirmed under experimental conditions (e.g. [8, p. 111–112] and [80]), but only in the broadest sense. Over time, the ionization equations continued to be widely studied and the problems considered were extended to include two-temperature plasmas (e.g. [81]), high pressures (e.g. [82]), varying opacities (e.g. [83]), and non-LTE (e.g. [84–88]). The Saha equations eventually became a useful staple in the treatment of plasma physics [89, p. 164] and stellar atmospheres [90–92].

As Auer highlighted relative to solar models [88], under non-LTE, a set of rate equations enters into the problem of determining the abundance of any given electronic state. Furthermore, the radiation field is introduced directly into the equations [88] utilized to calculate both opacities and populations. The problem therefore becomes dependent on "*simultaneous knowledge of the radiation field at all frequencies and all depths*" [88, p. 576].

While ionization appeared tractable given modern computing, the solution became linked to the knowledge of stellar opacities, an area of theory whose weaknesses have already been outlined [78]. Nonetheless, non-LTE approaches have been successful in addressing the spectra of early type stars [93–95]. Today, such methods also account for electronic, atomic, and ionic collision processes [64]. Non-LTE approaches have provided considerable insight into the Balmer and Paschen series associated with the hydrogen spectrum of the Sun [64].

Finally, it appears that the treatment adopted by Cecilia Payne might not have been too far afield [8]. For many of the cooler stars, simple LTE seems sufficient to address ionization problems [94]. Non-LTE methods become most important for the O and A class stars [93–95]. In any case, helium cannot be assessed on the Sun using the ionization equations due to the lack of appropriate spectral lines. As a result, while the LTE and non-LTE settings may be fundamental to the proper treatment of spectral lines, the methods have little bearing on the proper evaluation of helium levels in the Sun.

3 Helium from solar theory

3.1 Henry Norris Russell

Since Russell was not able to extract helium abundances directly from spectral lines, he did so, without further scientific justification, by assuming that the Sun had an mean molecular weight of ∼ 2 [10, p. 72–73]. Such a value had also been suggested by Saha [36, p. 476], who had in turn adopted it from Eddington [96, p. 596]. As for Eddington, he had previously examined the radiation equilibrium of the stars using a mean molecular weight of 54 [97]. In 1916, this value had been selected based on the belief that the stars were principally composed of elements such as oxygen, silicon, and iron prior to full ionization [1, viii]. Eddington lowered the mean molecular weight to a value of 2 in 1917 [96, p. 596], based on the idea that the elements would be fully ionized in the stars. In the fully ionized state, hydrogen has a mean molecular weight of 0.5, helium of ∼ 1.3, and iron of ∼ 2 (see [40, p. 102–104] for a full discussion of mean molecular weights in astrophysics). It was this value which Russell was to adopt in his calculations.

Using a mean molecular weight corresponding to a metal rich star, Russell concluded that helium was 13% as abundant as hydrogen by weight [10, p. 73]. He then computed that the Sun had equal percentages of oxygen and other metals (∼ 24% each) and that hydrogen comprised just under half of the constitution (∼ 45%) by weight (see table XX in [10, p. 73]. If Russell had selected a mean atomic weight of ∼ 0.5, there would be dramatic changes in the calculated helium levels.

3.2 Early abundance calculations

In arbitrarily selecting mean molecular weights [96, 97], Eddington determined the mean central stellar temperatures and pressures along with the acceleration due to gravity at the surface (e.g. [97, p. 22]). In turn, these parameters altered the calculated absorption coefficient, and hence opacity, of stellar interiors [97, p. 22]. Consequently, the setting of mean atomic weight had a profound implication on nearly every aspect of stellar modeling, but opacity would always remain paramount. In 1922, Eddington had derived a relationship between opacity and temperature [98] which would become known as Kramer's law [99].

Soon, Strömgren introduced an interesting twist to Eddington's approach [100, 101]. Rather than assuming a mean atomic weight, Strömgren began his calculations by computing opacity values, and from there, estimating the fractional composition of hydrogen within several stars [100], relying in part on Russell's elemental composition [10]. He concluded that the fractional abundance of hydrogen was ∼ 0.3 and maintained that the presence of helium would have little effect on these calculations since "*hydrogen and helium do not contribute to the opacity directly*" [100, p. 139]. Strömgren would write: "*we have neglected the influence of helium. The helium proportion is rather uncertain and the error introduced by neglecting helium altogether small* [100, p. 142]. Modern stellar theory would come to rely greatly on the opacity contributions of the negative hydrogen ion (H^-) [102]. Strömgren's assumptions were premature. Still, he championed the idea of initially computing opacity, and from these values obtaining both solar parameters and elemental abundances [100, 101].

Following the publication of a key modeling paper by Cowling [103], Martin Schwarzschild was to take the next theoretical step [104]. First, he made use of the mass-luminosity relation while expressing mean molecular weight and opacity as a function of elemental composition (X = hydrogen, Y = helium) [104]. Then, reasoning that the energy output in the Sun from the CNO cycle [13] was directly related to elemental composition, he derived a fractional elemental composition for hydrogen, helium, and the metals equal to 0.47, 0.41, and 0.12, respectively [104]. The results were once again critically dependent on estimated opacities, which Schwartzchild, like Strömgren before him [100, 101], assumed to display Eddington's [98] −3.5 power dependence on temperature (see Eq. 9 in [104]). In fact, Schwarzschild utilized an even greater dependence on temperature for energy production, allowing a 17th power in the exponential (see Eq. 11 in [104]). Yugo Iinuma then advanced a broader approach to the stellar composition problem [105]. He was concerned with ranges of reasonable starting points, both for hydrogen concentration and average molecular weight. His treatment remained dependent on opacity computations, though less rigid in its conclusions [105]. Schwarzschild et al. [106] then introduced the effects of inhomogeneity in the solar interior and convective envelopes along with solar age into the abundance problem. They reached the conclusion that the temperatures at the core of the Sun were such that the carbon cycle should start to contribute to the problem. Hydrogen abundances were assumed in order to arrive both at a convection parameter and at helium values [106]. The critical link to opacity remained [106]. Weymann, who like Schwarzschild, was also at the Institute for Advanced Study, built on his findings [107]. Taking account of the carbon cycle, Weymann found that the core of the Sun was not convective [107]. Powers of 4 and 20 for temperature were assumed in the energy generation laws associated with the pp and CNO cycles [107]. The hydrogen fractional composition of the Sun was assumed and ranged from 0.60 to 0.80 (see Table 3 in [107]). This resulted in helium and metallic fractional compositions of 0.19–0.32 and 0.01–0.08, respectively (see Table 3 in [107]).

In 1961, Osterbrock and Rogerson would elegantly summarize the situation relative to estimating helium abundances in the Sun: "*Though helium is observed in the upper chromosphere and in prominences, the physical conditions in these regions are too complicated and imperfectly understood for the abundance ratio to be determined from measurements of*

these emission lines. Hence the only reliable way to find the helium abundance in the Sun is by analysis of its internal structure" [108]. Yet, given the progress to date, the determination of elemental compositions within the Sun had been a complex adventure involving either assumed values of average molecular weights, hydrogen abundances, energy generation reactions, and opacity. The latter would eventually present the greatest difficulties [78]. Osterbrock and Rogerson would utilize Weymann's calculation, along with making an assumption by setting the Z/X ratio at 6.4×10^{-2} [108], to estimate interior solar fractional abundances at $X = 0.67$, $Y = 0.29$, and $Z = 0.04$. They were guided in this estimation by the belief that: "*the solar, planetary nebula, and interstellar abundances are all essentially the same*" [108, p. 132]. For the planetary nebula NGC 7027 they set the fractional abundances at $X = 0.64$, $Y = 0.32$, and $Z = 0.04$ [108]. Solar elemental composition became decidedly linked to estimates from remote objects. The stage was set for conclusively linking solar elemental composition to stellar evolution and primordial nucleosynthesis.

3.3 Modern abundance calculation

Eventually, the solar neutrino problem entered theoretical modeling [16, 109]. In his simulations, John Bahcall would utilize fractional abundances of relatively narrow range ($X = 0.715 - 0.80$, $Y = 0.19 - 0.258$ and $Z = 0.01 - 0.027$), setting the central densities and temperatures near 150 g/cm^3 and 15 million Kelvin, respectively [16]. The results, as before, were reliant on the use of solar opacity estimates [78]. By the beginning of the 1970s, fractional abundances for helium and the metals were settling on values near 0.28 and 0.02 [25]. Solar models became increasingly complex, relying on stellar opacity tables [110–118], energy generation equations, neutrino flux, and solar age to arrive at internally consistent results [17, 18]. Complexity was also introduced by considering helium and heavy element diffusion throughout the solar body [17, 18, 119, 120]. It became important to establish not only modern helium content, but also the initial helium abundance in the Sun [17,21,121]. Gough had already suggested that helioseismology could be used to help establish fractional abundances: "*Thus one might anticipate inferring the hydrogen-helium abundance ratio by comparing the measured values with a sequence of model solar envelopes*" [19, p. 21]. Helioseismological results became strongly incorporated into solar modeling [20–23] and "*helioseismic techniques ... [became] ... the most accurate way to determine the solar helium abundance*" [20, p. 235]. The techniques remained linked to the equations of state which contained six unknowns including: elemental composition, density, temperature, and pressure [20, p. 224]. Moreover, the problems required an explicit knowledge of opacity [20, p. 224] from its associated tables [110–118].

Relative to solar models, the central problem remains linked to the determination of internal solar opacity. The questions are complex and have been addressed in detail already by the author [78]. In the end, opacity tables [110–118] have no place in the treatment of stellar problems, precisely because they are incapable of reproducing the thermal emission spectrum required [78]. They simply mask ignorance of a fundamental problem in astronomy: the mechanism for the production of a thermal spectrum. Their inability to account for the production of a single photon by graphite on Earth [78], establishes that stellar opacity derived from isolated atoms and ions can play no role in the proper understanding of thermal emissivity in the stars. As a result, helium levels can never be established using theoretical modeling based on the gaseous equations of state and their inherent association with stellar opacity tables [78].

4 Primordial helium abundances

The quest to understand helium levels in the stars has been further complicated by the inferred association of this element with primordial nucleosynthesis in Big Bang cosmology [24–30]. Early on, Alpher, Bethe, and Gamow postulated that the elements had been synthesized in a primordial fireball [122]. This nucleosynthesis was proposed to include the entire periodic table and even unstable elements, with short lifetimes, of greater atomic number [122]. Soon, the idea that the composition of the stars was largely related to primordial conditions was born, especially relative to hydrogen and helium [24, 123]. No other scheme appeared likely to explain the tremendous He levels in stellar atmospheres, which approached 27% by weight [3, 24]: "*It is the purpose of this article to suggest that mild 'cooking' [such as found in stars] is not enough and that most, if not all, of the material of our everyday world, of the Sun, of the stars in our Galaxy and probably of the whole local group of galaxies, if not the whole Universe, has been 'cooked' to a temperature in excess of* $10^{10}K$" [123, p. 1108]. By then, the astrophysical community had already accepted that the heavy elements, which constituted trivial amounts of matter compared to hydrogen and helium, had largely been synthesized in the stars [14]. Only ^{1}H, ^{2}H, ^{3}He, ^{4}He, and ^{7}Li became candidates for synthesis through a primordial process [124, 125].

The postulate that "*helium abundance is universal and was generated in a Big Bang*" [125] eventually came to wide acceptance. The entire theory was hinged on elevated helium abundances: "*We can now say that if the Universe originated in a singular way the He/H ratio cannot be less than about 0.14. This value is of the same order of magnitude as the observed ratios although it is somewhat larger than most of them. However, if it can be established empirically that the ratio is appreciably less than this in any astronomical object in which diffussive seperation is out of the question, we can assert that the Universe did not have a singular origin*" [123, p. 1109]. Elevated helium levels, along with the discovery

of the microwave background [126] and the red-shifts of distant galaxies [127, 128] became one of the three great pillars of Big Bang cosmology [24, 129, 130]. This explained why gravitational settling had become critical in discounting low helium abundances of certain B type stars [3, 30, 31]. If empirical helium levels fell into question and a mechanism existed to accept the tremendously decreased helium levels in these special B type stars [3, 31] by preventing gravitational settling [131], Big Bang cosmology could not survive. Stellar and solar helium abundances cannot be allowed to drop in modern cosmology.

Today, the quest to link helium abundances and primordial nucleosynthesis has continued [26–30] using two lines of reasoning: 1) the analysis of anisotropy in the microwave background [132, 133] and 2) the observation of helium and hydrogen lines from low-metallicity extragalactic HII regions [26, 134–137].

Unfortunately, the use of anisotropy data [132, 133] to analyze primordial helium abundances are highly suspect. First, insurmountable problems exist with the WMAP data sets, as already highlighted by the author [138]. WMAP suffers from significant galactic foreground contamination which cannot be properly removed [138]. In addition, the WMAP team cannot distinguish between signal arising from a hypothetically primordial origin from those produced throughout the universe as a result of normal stellar activity [138]. While evident 'point sources' are taken into account, it remains impossible to determine, on a pixel by pixel basis, whether the signal has a primordial origin, or originates from an unidentified non-cosmological object [138]. Furthermore, WMAP raw data has proven to be unstable from year to year in a manner inconsistent with the hypothesized cosmological origins of these signals [138]. The data suffers from poor signal to noise and the ILC coefficients used for generating the final anisotropy maps do not remain constant between data releases [138]. Most troubling, the data sets cannot be combined using a unique combination of spectral channels [138]. As a result, since no unique anisotropy data set can be extracted [138], the data has no scientific value in analyzing helium abundances. Similar problems will occur when data from the Planck satellite finally becomes available [139]. As a result, all helium abundances derived from microwave anisotropy data sets must be viewed with a high degree of suspicion.

On the surface, the extraction of primordial helium abundances from H II regions appears more feasible [26, 134–137]. H II regions are rich in both hydrogen and helium but have low heavy element abundances (~ 1/40 solar) [140]. Unlike H I regions (~ 60K), H II regions exist at temperatures between 7,500 and 13,000 K [141]. In H II regions "*the* ^{4}He *abundance is derived from the recombination lines of singly and doubly ionized* ^{4}He*; neutral* ^{4}He *is unobserved*" [140, p. 50]. Unfortunately, experiments which utilized H II regions to assess primordial helium cannot easily ascertain that the sample has a uniform elemental composition. Furthermore, the use of H II regions for this purpose discounts the idea that helium has been synthesized locally. Such a suggestion should not be easily dismissed, as the temperatures of observation [141] are well above those in equilibrium with the hypothesized residual temperature of the Big Bang (~ 3K) [130]. Only low metallicity supports the idea that these helium concentrations are primordial. Nothing should prevent stellar systems from creating regions of low metallicity outside of a cosmological context. In this regard, the elevated temperatures of H II regions suggest that a process well beyond primordial considerations is now influencing elemental abundances in these regions. As such, it is imprudent to derive primordial helium abundances from H II regions.

We do not know, and will probably never be able to ascertain, primordial helium abundances. In order to observe helium in astronomy, elevated temperatures are required. These immediately imply that the processes observed are no longer in thermal equilibrium with those of interest in cosmology [130].

5 Solar winds: The key to understanding helium

Helium abundances can also be monitored in the solar wind [143–152]. Presumably, the results are so dynamic that they cannot be utilized to establish helium levels in the Sun itself. However, solar winds [143–152] have presented astronomy with a wealth of scientific information, which could be used to profoundly alter our understanding of the Sun [131].

Already in 1971, it was recognized that solar wind helium abundance measurements gave values which were lower than those ascertained from theoretical experiments [143, p. 369]. The study of solar winds became linked to models of the corona. Although the relative abundance and velocities of hydrogen to helium were advanced as profoundly dependent on location [143], it remained evident that solar winds harbored a great deal of reliable information. Early on, it was known that helium to hydrogen density ratios in the solar wind could experience dramatic fluctuations [144], especially in slow winds [147], though values appeared more stable at high solar wind speeds [145]. Extremely low ratios of 0.01, rising to 0.08, with an average of 0.037, were reported [144]. Clearly, such values were in direct conflict with the elevated helium levels expected in the Sun from primordial arguments [123]. As such, solar wind measurements became viewed as unreliable relative to estimating helium abundances in the Sun [148].

Nonetheless, something truly fascinating was present in solar wind data. The Sun appeared to be expelling helium (J. C. Robitaille, personal communication [131]) with increased activity. The helium to hydrogen ratio was observed to increase in association with the onset of geomagnetic storms [144] and was highly responsive to the solar cycle [146, 149, 151]. The helium abundance could rise from average values of less than 2% at the solar minimum to around 4.5% at maximum [149]. After the early 1970s, the vari-

ation in solar wind helium abundance became increasingly pronounced. By 1982, helium abundances in the solar wind came to vary from values as low as 0.001 to as elevated as 0.35 [147]. A single value as high as 0.40 was reported [147]. At least half of all elevated helium abundance events were related to a transient interplanetary shock wave disturbance [147], though a significant portion were not associated with such events. Each of these extremes highlighted something phenomenal relative to solar winds. To explain the variability, theoretical models turned to the large scale structure of plasma. It was assumed that elevated helium abundance originated in regions of high magnetic field activity in the corona [131]. It was found that helium abundance "*enhancements often have unusually high ionization temperatures, indicative of an origin in active solar processes... Collectively, these observations suggest that... [helium abundance] ... enhancements in the solar wind signal the arrival of plasma ejected from low in the corona during a disturbance such as a large solar flare or an eruptive prominence*" [147]. While solar winds had a close link to the "*composition of the source material*" it could then "*be modified by the processes which operate in the transition zone and in the inner corona*" [148]. Primordial helium abundances within the Sun could be saved by discounting that solar wind helium abundances had any meaning whatsoever relative to the composition of the Sun itself. The idea that solar activity reflected the expulsion of helium from the Sun (J. C. Robitaille, personal communication [131]) was never advanced. While the scientific community maintained that helium abundances were not reliable, they claimed that it was possible to ascertain the fractional isotopic composition of the elements in the solar wind and relate them directly to the solar convective zone: "*The variability of the elemental abundances in the solar wind on all time scales and the FIP... [first ionization potential] ... effect, and its variability, will make it difficult to derive accurate solar abundances from solar wind measurements, with the exception of isotopic determinations*" [150]. Of course, isotope analysis could never constitute a challenge to the existence of large amounts of primordial helium in the Sun [123]. Solar wind helium abundances had to be simply correlated to the coronal magnetic field, although the correlation coefficient was not powerful ($\sigma \sim 0.3$) [152]. Nonetheless, helium abundance depressions could not be explained under such a scenario [152]. At the same time, it is currently believed that "*solar wind abundances are not a genuine, unbiased sample of solar abundances, but they are fractionated. One such fractionation depends on the first ionization potential (FIP): When comparing solar wind to solar abundances, elements with low FIP (<10 eV) are enriched by a significant factor, the FIP bias, over those with a high FIP ... Another fractionation process affects mainly helium, causing its abundance in the SW to be only about half of the solar abundance... It is most likely due to insufficient Coulomb drag between protons and alpha particles in the accelerating solar wind*" [154, p. 16]. Herein was an explicit admission that the cause of extremely low helium levels in the solar wind could not be adequately understood. Conversely, fractionation models continued to insist that elevated helium abundances were linked to the fractionation of large atoms by collisions with protons [152, 153]. Nothing could be gathered about solar helium abundances from solar winds precisely because theoretical constructs forbade such conclusions.

6 Conclusions

Modern day reports of elemental abundances in the Sun [154–156] maintain that the Sun has a relatively large proportion of helium with Y values typically near 0.248 and primordial values of 0.275. These values come from theoretical modeling, as helium remains spectroscopically silent in the photosphere and solar winds are viewed as unreliable [155, p. 166]. Therefore, claims that helium has "*very high abundance*" [155, p. 166] in the Sun are not supported by observational fact. In the end, mankind understands much less about this central element than a cursory review of the literature might suggest. Careful consideration of solar modeling establishes that all theoretical estimates of helium levels in the Sun cannot be relied upon, given their dependence of solar opacity tables [78]. This also applies to theoretical results which attempt to extract helium levels from helioseismology [156]. For this reason, it is simply not possible to establish elevated helium levels in the Sun from theory. As helium levels cannot be established spectroscopically, we are left with the solar winds for guidance.

Currently, solar winds are viewed as too complex to yield information relative to solar abundances. In large measure, this is because scientists are trying to understand this data in the context of an object whose helium abundance has been largely set in primordial times [24, 123, 155]. The idea that the Sun and the stars are actively working to control their helium levels has never been previously considered [131]. Nevertheless, the association of solar activity and elevated helium levels [146, 149, 151] strongly suggests that the active Sun is expelling helium and excluding it from its hydrogen based lattice (J. C. Robitaille, personal communication [131]). Herein can be found the cause of extremely low helium abundance often obtained in the slow solar wind: the Sun works to keep its helium levels low and solar activity represent a direct manisfestation of this fact. In the quiet Sun the slow solar winds can report fractional abundances of less than 2% and these should be viewed as steady state helium removal from the convective zone of the Sun. Such an idea strongly supports the contention that the Sun and the stars are primarily comprised of hydrogen in the liquid metallic state [131, 157].

In advancing that the universe is largely composed of hydrogen and that helium is being excluded from the stars (J. C. Robitaille, personal communication [131]), perhaps it is appropriate to turn once again to Cecilia Payne, as the first as-

tronomer to highlight the tremendous abundance of hydrogen in the universe [8]. As a child, she had been eager to become an astronomer "*in case there should be no research left when she grew up*" [1, p. 72–73]. Yet, her position changed dramatically with age: "*Looking back on my years of research, I don't like to dwell only on my mistakes; I am inclined to count my blessings, and two seem to me to be very especially valuable. The first blessing is that the process of discovery is gradual — if we were confronted with all the facts at once we should be so bewildered that we should not know how to interpret them. The second blessing is that we are not immortal. I say this because, after all, the human mind is not pliable enough to adapt to the continual changes in scientific ideas and techniques. I suspect there are still many astronomers who are working on problems, and with equipment, that are many years out of date. Now that I am old, I see that it is dangerous to be in too much of a hurry, to be too anxious to see the final result oneself. Our research does not belong to us, to our institution, or to our country. It belongs to mankind. And so I say to you, the young generation of astronomers: more power to you. May you continue to expand the picture of the universe, and may you never lose the thrill it gave you when it first broke on you in all its glory*" [Cecilia Payne-Gaposchkin, April 10, 1968 [50, p. xv]].

Dedication

This work is dedicated to my oldest son, Jacob.

Submitted on: December 25, 2012 / Accepted on: December 31, 2012
First published in online on: January 6, 2012

References

1. Haramundanis K. Cecilia Payne-Gaposchkin: An autobiography and other recollections (2nd Edition). Cambridge University Press, Cambridge, U.K., 1996.
2. Kragh H. The solar element: A reconsideration of helium's early history. *Ann. Science*, 2009, v. 66(2), 157–182.
3. Taylor R.J. The helium problem. *Quart. J. Roy. Astron. Soc.*, 1967, v. 8, 313–333.
4. Janssen J. Indications de quelques-uns des résultats obténus à Guntoor, pendant l'éclipse du mois d'août dernier. *Comptes Rendus*, 1868, v. 67, 838–39.
5. Lockyer J.N. Notice of an observation of the spectrum of a solar prominence. *Proc. Roy. Soc. London*, 1868, v. 17, 91–92.
6. Ramsey W. On a gas showing the spectrum of helium, the reputed cause of D3, one of the lines in the coronal spectrum. Preliminary note. *Proc. Roy. Soc. London*, 1895, v. 58, 347–352.
7. Hirayama T. The abundance of helium in the prominences and in the chromosphere. *Solar Physics*, 1971, v. 19, 384–400.
8. Payne C.H. The relative abundances of the elements. Stellar Atmospheres. Harvard Observatory Monograph no. 1 (Harlow Shapley, Editor), Harvard University Press, Cambridge, MA, 1925 (reprinted in part in Lang K.R. and Gingerich O. A source book in astronomy and astrophysics, 1900–1975, Harvard University Press, Cambridge, MA, 1979, p.245–248).
9. Unsöld A. Über die Struktur der Fraunhofersehen Linien und die quantitative Spektralanalyse der Sonnenatmosphäre. *Zeitschrift für Physik*, 1928, v.46(11–12), 765–781.
10. Russell H.N. On the composition of the Sun's atmosphere. *Astrophys. J.*, 1929, v.70, 11–82.
11. Bethe H.A. and Critchfield C.L. The formation of deuterons by proton combination. *Phys. Rev.*, 1938, v. 54, 248–254.
12. Bethe H.A. Energy production in stars. *Phys. Rev.*, 1939, v. 55(1), 103.
13. Bethe H.A. Energy production in stars. *Phys. Rev.*, 1939, v. 55(1), 434–456.
14. Burbidge E.M., Burbidge G.R., Fowler W.A. and Hoyle F. Synthesis of the elements in the stars. *Rev. Modern Phys.*, 1957, v. 29(4), 547–650.
15. Wallerstein G., Icko I., Parker P., Boesgaard A.M., Hale G.M., Champagne A.E., Barnes C.A., Käppeler F., Smith V.V., Hoffman R.D., Timmes F.X., Sneden C., Boyd R.N., Meyer B.S. and Lambert D.L. Synthesis of the elements in stars: forty years of progress. *Rev. Modern Phys.*, 1997, v. 69(4), 995–1084.
16. Bahcall J.N., Bahcall N.A. and Shaviv G. Present status of the theoretical predictions for the 37Cl solar-neutrino experiment. *Phys. Rev. Lett.*, 1968, v. 20(21), 1209–1212.
17. Bahcall J.N. and Pinsonneault M.H. Standard solar models, with and without helium diffusion, and the solar neutrino problem. *Rev. Mod. Phys.*, 1992, v. 64(4), 885–926.
18. Bachall J.N., Pinsonneault M.H. and Wasserburg G.J. Solar models with helium and heavy-element diffusion. *Rev. Mod. Phys.*, 1995, 67(4), 781–808.
19. Gough D.O. Towards a solar model. *Mem. Soc. Astron. Ital.*, 1984, v. 1–2, 13–35.
20. Basu S. and Antia H.M. Helioseismology and solar abundances. *Phys. Rep.*, 2008, v. 457, 217–283.
21. Serenelli A.M. and Basu S. Determining the initial helium abundance of the Sun. *Astrophys. J.*, 2010, v. 719(1), 865–872.
22. Delahaye F. and Pinsonneault M.H. The solar heavy-element abundances. I. Constraints from stellar interiors. *Astrophys. J.*, 2006, v. 649, 529–540.
23. van Saders J.L. and Pinsonneault M.H. The sensitivity of convection zone depth to stellar abundances: An absolute stellar abundance scale from asteroseismology. *Astrophys. J.*, 2012, v. 746, 16 (16 pages).
24. Peebles P.J.E. Primordial helium abundance and the primordial fireball. II. *Astrophys. J.*, 1966, v. 146, 542–552.
25. Danzinger I.J. The cosmic abundance of helium. *Ann. Rev. Astron. Astrophys.*, 1970, v. 8, 161–178.
26. Izotov Y.I. and Thuan T.X. The primordial abundance of 4He revisited. *Astrophys. J.*, 1998, v. 500, 188–216.
27. Olive K.A., Steigman G. and Walker T.P. Primordial nucleosynthesis: Theory and observations. *Phys. Rep.*, 2000, v. 333–334, 389–407.
28. Pagel B.E.J. Helium and Big Bang Nucleosynthesis. *Phys. Rep.*, 2000, v. 333–334, 433–447.
29. Steigman G. Primordial nucleosynthesis: Successes and challenges. *Int. J. Mod. Phys. E*, 2006, v. 15, 1–36.
30. Peimbert M. The primordial helium abundance. *Curr. Sci.*, 2008, v. 95, 1165–1176; arXiv: astro-ph/0811.2980.
31. Greenstein G.S., Truran J.W. and Cameron A.G.W. Helium deficiency in old halo B type stars. *Nature*, 1967, v. 213, 871.
32. Lindemann F.A. LXX. Note on the theory of magnetic storms. *Phil. Mag.*, 1919, v. 38(228), 669–684.
33. Eggert. J. Über den Dissoziationszustand der Fixsterngase. *Physikalische Zeitschrift*, 1919, v. 20, 570–574.
34. Kothari D.S. Meghnad Saha. 1893–1956. *Biogr. Mems. Fell. R. Soc.*, 1960, v. 5, 216–236.
35. Chatterjee S. Meghnad Saha — The scientist and the institution builder. *Ind. J. Hist. Sci.*, 1994, v. 29(1), 99–110; http://www.new.dli.ernet.in/rawdataupload/upload/insa/INSA_1/20005b68_99.pdf

36. Saha M.H. LIII. Ionization in the solar chromosphere. *Phil. Mag. Series 6*, 1920, v. 40, 472–488.
37. Saha M.H. On the physical theory of stellar spectra. *Proc. Roy. Soc. London A*, 1921, v. 99, 135–153.
38. Nernst W. Die theoretische un experimentellen Grundlagen des neuen Wärmesatzes. Verlag von Wilhelm Knapp, Halle, 1918, p.154.
39. Clayton D.D. Principles of stellar evolution and nucleosynthesis. Mcgraw-Hill, New York, N.Y., 1968.
40. Kippenhahn R. and Weigert A. Stellar structure and evolution. Springer-Verlag, Berlin, 1990.
41. Gingerich O. Obituary — Payne-Gaposchkin Cecilia. *Quart. J. Roy. Astron. Soc.*, 1982, v. 23, 450–451.
42. McCrea W. Obituary: Subramanyan Chandrasekhar. *The Observatory*, 1996, v. 116, 121–124.
43. Chandrasekhar S. Ralph Howard Fowler. *Astrophys. J.*, 1945, v.101(1), 1–5.
44. Taylor R.J. E.A. Milne(1896-1950) and the structure of stellar atmospheres and stellar interiors. *Quart. J. Roy. Astron. Soc.*, 1996, v. 37, 355–363.
45. Fowler R.H. and Milne E.A. The intensities of absorption lines in stellar spectra, and the temperature and pressures in the reversing layers of stars. *Mon. Not. Roy. Astron. Soc.*, 1923, v. 83, 403–424.
46. Fowler R.H. and Milne E.A. The maxima of absorption lines in stellar spectra (Second Paper). *Mon. Not. Roy. Astron. Soc.*, 1923, v. 83, 403–424.
47. Milne E.A. XVIII. Statistical equilibrium in relation to the photo-electric effect, and its application the determination of the absorption coefficients. *Phil. Mag. Ser. 6*, 1924, v. 47, 209–241.
48. Milne E.A. Ionization in stellar atmospheres. Part 1. Generalised Saha formulae, maximum intensities, and the determination of the coefficient of opacity. *Mon. Not. Roy. Astron. Soc.*, 1928, v. 89, 17–49.
49. Morgan W.W., Keenan P.C. and Kellman E. An atlas of stellar spectra. University of Chicago Press, Chicago, Il, 1943.
50. Gingerich O. Theory and observation of normal stellar atmospheres: Proceedings of the third Harvard-Smithsonian conference on stellar atmospheres. The M.I.T. Press, Cambridge, M.A., 1969.
51. Mitchell H.B. Henrietta Leavitt and the Cepheid variables. *The Physics Teacher*, 1976, v. 14(3), 162–167.
52. Bok P.F. Annie Jump Cannon 1863–1941. *Publ. Astron. Soc. Pac.*, 1941, v. 53, 168–170.
53. Merrill P. Annie Jump Cannon. *Mon. Not. Roy. Astron. Soc.*, 1942, v. 102(2), 74–76.
54. Gaposchkin C.P. Annie Jump Cannon. *Science*, 1941, v. 93(2419), 443–444.
55. Hoffleit D. Antonia C. Maury. *Sky & Telescope*, 1952, v. 11(5), 106.
56. Cannon A.J. Williamina Paton Fleming. *Science*, 1911, v. 33(861), 987–988.
57. Cannon A.J. Williamina Paton Fleming. *Astrophys. J.*, 1911, v. 34, 314–317.
58. Spradley J.L. The Industrious Mrs. Fleming. *Astronomy*, 1990, v. 18(7), 48–51.
59. Spradley J.L. Two centennials of star catalogs compiled by women. *Astron. Quart.*, 1990, v. 7(3), 177–184.
60. Lankford J. and Slavings R.L. Gender and Science: Women in American Astronomy, 1859–1940. *Phys. Today*, 1990, v. 43(3), 58–65.
61. Merton T.R. and Barratt S. Bakerian Lecture: On the spectrum of hydrogen. *Phil. Trans. Roy. Soc. London*, 1922, v. 222, 369–400.
62. Lang K.R. and Gingerich O. A source book in astronomy and astrophysics, 1900–1975. Harvard University Press, Cambridge, MA, 1979, Chap. 39, p.244.
63. McCrea W.H. The hydrogen chromosphere. *Mon. Not. Roy. Astron. Soc.*, 1929, v. 89, 483–497.
64. Przybilla N. and Butler K. The solar hydrogen spectrum in non-local thermodynamic equilibrium. *Astrophys. J.*, 2004, v. 610, L61–L24.
65. Robitaille P.-M. On the Presence of a Distinct Solar Surface: A Reply to Hervé Faye. *Prog. Phys.*, 2011, v. 3, 75–78.
66. Robitaille P.-M. Magnetic Fields and Directional Spectral Emissivity in Sunspots and Faculae: Complimentary Evidence of Metallic Behavior on the Surface of the Sun. *Prog. Phys.*, 2013, v. 1, 19–24.
67. Moore C.E. Henry Norris Russell. *The Observatory*, 1957, v. 77, 67–68.
68. de Jager C., Migeotte M., and Neven L. The profile of the Brackett alpha line in the solar spectrum. *Ann. Astrophys.*, 1956, v. 19, 9–18.
69. Russell H.N. and Stewart J.Q. Pressures at the Sun's surface. *Astrophys. J.*, 1924, v. 59, 197–209.
70. Rudnick P. A quantitative investigation of spectral line intensities in O- and B-type stars. *Astrophys. J.*, 1936, v. 83, 439–475.
71. Underhill A.B. and Petrie W. The stark effect of helium in some B type stars. *J. Roy. Astron. Soc. Canada*, 1944, v. 38, 385–394.
72. Underhill A.B. The relative abundance of hydrogen to helium in stars. *J. Roy. Astron. Soc. Canada*, 1953, v. 47, 153–159.
73. Underhill A.B. On the strength of the helium line in O-type stars. Les Processus Nucléaires dans les Astres. Communications présentées au cinquième *Colloque International d'Astrophysique* tenu à Liège les 10-12 Septembre, 1953, 374–386.
74. Milne E.A. Selective radiation-pressure and the structure of a stellar atmosphere. *Mon. Not. Roy. Astron. Soc.*, 1927, v. 87, 697–708.
75. Milne E.A. The effect of collisions on monochromatic radiative equilibrium. *Mon. Not. Roy. Astron. Soc.*, 1928, v. 88, 493–502.
76. Milne E.A. Bakerian Lecture: The structure and opacity of a stellar atmosphere. *Phil. Trans. Roy. Soc. London*, 1929, v. 228, 421–461.
77. Milne E.A. Thermodynamics of the stars. Handbuch der Astrophysik, 1930, v.3, Part 1, 65–255 (also in Menzel D.H. Selected Papers on the Transfer of Radiation: 6 papers by Arthur Schuster, K. Schwarzschild, A.S. Eddington, S. Rosseland, E.A. Milne. Dover Publications, Inc., New York, 1966, 77–269).
78. Robitaille P.M. Stellar opacity: The Achilles' heel of the gaseous Sun. *Progr. Phys.*, 2011, v. 3, 93–99.
79. Gerasimovic B.P. On the correction to Saha's formula for small deviations from thermodynamic equilibrium. *Proc. Nat. Acad. Sci. USA*, 1927, v. 13(4), 180–185.
80. Noyes A.A. and Wilson H.A. The thermal ionization of gaseous elements at high temperatures: a confirmation of Saha theory. *Astrophys. J.*, 1923, v. 57, 20–32.
81. van der Mullen J.A.M., Benoy D.A., Fey F.H.A.G. and van der Sijde B. Saha equation for two-temperature plasmas: Theories, experimental evidence, and interpretation. *Phys. Rev. B*, 1994, v. 50(5), 3925–3934.
82. Sweeney M.A. Thermodynamic inconsistency of the modified Saha equation at high pressures. *Astrophys. J.*, 1978, v. 220, 335–338.
83. Pottasch S.R. and Thomas R.N. Departures from the Saha equation under varying conditions of Lyman continuous opacity. *Astrophys. J.*, 1959, v. 130, 941–953.
84. Krawec R. Steady-state composition of low-density nonequilibrium hydrogen plasma. NASA Technical Note D-3457, Washington, D.C., October 1966.
85. Kurochka L.N. Saha's equation under deviation from thermodynamic equilibrium. *Bull. Astron. Inst. Czechoslovakia*, 1973, v. 24(4), 210–212.
86. Avrett E.H. Solution of non-LTE transfer problems. *J. Quant. Spectrosc. Radiat. Trans.*, 1971, v. 11(6), 511–529.

87. Canal G.P., Luna H., Galvão R.M.O. and Castell R. An approach to a non-LTE Saha equation based on Druyvesteyn energy distribution function: A comparison between electron temperature obtained from OES and the Langmuir probe analysis. *J. Phys. D*: *Appl. Phys.*, 2009, v. 42, 135202 (6 pages).
88. Auer L.H. The stellar atmosphere problem. *J. Quant. Spectrosc. Radiat. Transfer*, 1971, v. 11, 573–587.
89. Fridman A.A. and Kennedy L.A. Plasma physics and engineering. Taylor & Francis, New York, N.Y., 2004.
90. Mihalas D. Stellar atmospheres (2nd Edition). W.H. Freeman and Company, San Francisco, CA, 1978
91. Hubeny I. Theory and modeling of stellar atmospheres. *AIP Conf. Proc.*, 2010, v. 1268, 73–115.
92. Werner K. and Dreizler S. The classical stellar atmosphere problem. *J. Comp. Appl. Math.*, 1999, v. 109(1–2), 65-93.
93. Lecar M. Departures from local thermodynamic equilibrium in an A0 stellar atmosphere. NASA Technical Note, D 2110, 1964.
94. Przybilla N., Nieva M.-F. and Butler K. Testing common classical LTE and NLTE model atmosphere and line-formation codes for quantitative spectroscopy of early-type stars. *J. Phys. Conf. Ser.*, 2011, v. 328, 012015 (12 pages).
95. Nieva M.F. and Przybilla N. Hydrogen and helium line formation in OB dwarfs and giants: A hybrid non-LTE approach. *Astron. Astrophys.*, 2007, v. 467, 295–309.
96. Eddington A.S. Further notes on the radiative equilibrium of the stars. *Mon. Not. Roy. Astron. Soc.*, 1917, v. 77, 596–612.
97. Eddington A.S. On the radiative equilibrium of the stars. *Mon. Not. Roy. Astron. Soc.*, 1916, v. 77, 16–35.
98. Eddington A.S. On the absorption of radiation inside a star. *Mon. Not. Roy. Astron. Soc.*, 1922, v. 83, 32–46.
99. Kramers H.A. XCIII. On the theory of x-ray absorption and of the continuous x-ray spectrum. *Phil. Mag.*, 1923, 46(275), 836–871.
100. Strömgren B. The opacity of stellar matter and the hydrogen content of the stars. *Zeitschrift für Astrophysik*, 1932, v. 4, 118–152.
101. Strömgren B. On the interpretation of the Hertzaprung-Russell-Diagram. *Zeitschrift für Astrophysik*, 1933, v. 7, 222–248.
102. Wildt R. Electron affnity in astrophysics. *Astrophys. J.*, 1939, v. 89, 295–301.
103. Cowling T.G. The stability of gaseous stars. *Mon. Not. Roy. Astron. Soc.*, 1935, v. 96, 42–60.
104. Schwarzschild M. On the helium content of the Sun. *Astrophys. J.*, 1946, v. 104, 203–207.
105. Iinuma Y. On the determination of chemical composition of stars. *Publ. Astron. Soc. Japan*, 1949, v. 1(1–2), 18–23.
106. Schwarzschild M., Howard R. and Härm R. Inhomogeneous stellar models. V. A solar model with convective envelope and inhomogeneous interior. *Astrophys. J.*, 1957, v. 125, 233–241.
107. Weymann R. Inhomogeneous stellar models. VI. An improved solar model with the carbon cycle included. *Astrophys. J.*, 1957, v. 126, 208–212.
108. Osterbrock D.E. and Rogerson J.B. The helium and heavy-element content of gaseous nebulae and the Sun. *Publ. Astron. Soc. Pac.*, 1961, v. 73, 129–134.
109. Bahcall J.N., Fowler W.A., Iben I. and Sears R.L. Solar neutrino flux. *Astrophys. J.*, 1963, v. 137, 344–346.
110. Carson T.R. Stellar opacity. *Ann. Rev. Astron. Astrophys.*, 1976, v. 14, 95–117.
111. Rozsnyai B.F. Solar opacities. *J. Quant. Spec. Rad. Trans.*, 2001, v. 71, 655–663.
112. The Opacity Project Team. The Opacity Project. Institute of Physics Publishing, Bristol, UK, 1995, v.1.
113. The Opacity Project Team. The Opacity Project. Institute of Physics Publishing, Bristol, UK, 1996, v.2.
114. Rogers F.J. and Iglesias C.A. Stellar opacity. Lawrence Livermore National Laboratory, Preprint UCLRL-JC-137066.
115. Iglesias C.A. and Rogers F.J. Opacities for the solar radiative interior. *Astrophys. J.*, 1991, v. 371, 408–417.
116. Iglesias C.A. and Rogers F.J. Radiative opacities for carbon- and oxygen-rich mixtures. *Astrophys. J.*, 1993, v. 412, 752–760.
117. Rogers F.J. and Iglesias C.A. Rosseland mean opacities for variable compositions. *Astrophys. J.*, 1992, v. 401, 361–366.
118. Iglesias C.A. and Rogers F.J. Updated OPAL opacities. *Astrophys. J.*, 1996, v. 464, 943–953.
119. Aller L.H. and Chapman S. Diffusion in the Sun. *Astrophys. J.*, 1960, v. 132, 461–472.
120. Noerdlinger P.D. Diffusion of helium in the Sun. *Astron. Astrophys.*, 1977, v. 57, 407–415.
121. Aldo M. Serenelli A.M. and Basu S. Determining the initial helium abundance of the Sun. *Astrophys. J.*, 2010, v. 719(1), 865–872.
122. Alpher R.A., Bethe H., and Gamow G. The origin of chemical elements. *Phys. Rev.*, 1948, v. 73(7), 803–804.
123. Hoyle F. and Taylor R.J. The Mystery of the Cosmic Helium Abundance. *Nature*, 1964, v. 203(4950), 1108–1110.
124. Wagoner R.V., Fowler W.A. and Hoyle F. On the synthesis of elements at very high temperatures. *Astrophys. J.*, 1967, v. 148, 3–49.
125. Burbidge G. Cosmic helium. *Comm. Astrophys. Space Phys.*, 1969, v. 1, 101–106.
126. Penzias A. A. and Wilson R.W. A measurement of excess antenna temperature at 4080 Mc/s. *Astrophys. J.*, 1965, v. 1, 419–421.
127. Hubble E. A relation between distance and radial velocity among extragalactic nebulae. *PNAS*, 1929, v. 15(3), 168–173.
128. Rabounski D. On the Exact Solution Explaining the Accelerate Expanding Universe According to General Relativity. *Progr. Phys.*, 2012, v. 2, L1–L6.
129. Lemaître G. Un Univers homogène de masse constante et de rayon croissant rendant compte de la vitesse radiale des nébuleuses extragalactiques. *Annales de la Societé Scientifique de Bruxelles*, ser.A, 1927, v. 47, 49–59.
130. Dicke R.H., Peebles P.J.E., Roll P.G., and Wilkinson D.T. Cosmic black-body radiation. *Astrophys. J.*, 1965, v. 1, 414–419.
131. Robitaille J.C. and Robitaille P.M. Liquid metallic hydrogen III. Intercalation and lattice exclusion versus gravitational settling, and their consequences relative to internal structure, surface activity, and solar winds in the Sun. *Progr. Phys.*, 2013, v. 2, in press.
132. Komatsu E., Smith K.M, Dunkley J., Bennett C.L., Gold B., Hinshaw G., Jarosik N., Larson D., Nolta M.R., Page L., Spergel D.N., Halpern M., Hill R.S., Kogut A., Limon M., Meyer S.S., Odegard N., Tucker G.S., Weiland J.L., Wollack W. and Wright E.L. Seven-year wilkinson microwave anisotropy probe (WMAP*) observations: Cosmological interpretation. *Astrophys. J. Suppl. Ser.*, 2011, v. 192, 18 (47 pp).
133. Hinshaw G., Larson D., Komatsu E., Spergel D.N., Bennett C.L., Dunkley J., Nolta M.R., Halpern M., Hill R.S., Odegard N., Page L., Smith K.M., Weiland J.L., Gold B., Jarosik N., Kogut A., Limon M., Meyer S.S., Tucker G.S., Wollack E. and Wright E.L. Nine-year wilkinson microwave anisotropy probe (WMAP) observations: Cosmological parameter results. arXiv: astro-ph.CO/1212.5226.
134. Pagel B.E.J, Simonson E.A., Terlevich R.J. and Edmunds M.J. The primordial helium abundance from observations of extragalactic H II regions. *Mon. Not. Roy. Astron. Soc.*, 1992, v. 255, 325–345.
135. Peimbert M., Peimbert A. and Ruiz M.T. The chemical composition of the Small Magellanic Cloud H II region NGC 346 and the primordial helium abundance. *Astrophys. J.*, 2000, v. 541, 688–700.

136. Luridiana V., Peimbert A., Peimbert M. and Cerviño M. The effect of collisional enhancement of Balmer lines on the determination of the primordial helium abundance. *Astrophys. J.*, 2003, v. 592, 846–865.

137. Izotov Y.I. and Thuan T.X. Systematic effects and a new determination of the primordial abundance of 4He and dY/dZ from observations of blue compact galaxies. *Astrophys. J.*, 2004, v. 602, 200–230.

138. Robitaille P.M. WMAP: A radiological analysis. *Progr. Phys.*, 2006, v. 1, 3–18.

139. Planck Satellite website: http://www.rssd.esa.int/index.php?project=planck

140. Olive K.A. and Steigman G. On the abundance of primordial helium. *Astrophys. J. Suppl. Ser.*, 1995, v. 97, 49–58.

141. Spitzer L. and Savedoff M.P. The temperature of interstellar matter III. *Astrophys. J.*, 1950, v. 111, 593–608.

142. Dicke R.H., Peebles P.J.E., Roll P.G., and Wilkinson D.T. Cosmic black-body radiation. *Astrophys. J.*, 1965, v. 1, 414–419.

143. Formisano V. and Moreno G. Helium and heavy ions in the solar winds. *Revista del Nuovo Cimento*, 1971, v. 1(3), 365–422.

144. Robbins D.E., Hundhausen A.J. and Bame S.J. Helium in the solar wind. *J. Geophys. Res.*, 1970, v. 75(7), 1178–1187.

145. Ogilvie K.W. and Hirshberg J. The solar cycle variation of the solar wind helium abundance. *J. Geophys. Res.*, 1974, v. 79(31), 4595–4602.

146. Bame S.J., Asbridge J.R., Feldman W.C. and Gosling J.T. Evidence for a structure-free state at high solar wind speeds. *J. Geophys. Res.*, 1977, v. 82(10), 1487–1492.

147. Borrini G., Gosling J.T., Bame S.J., and Feldman W.C. Helium abundance enhancements in the solar wind. *J. Geophys. Res.*, 1982, v. 87(A9), 7370–7378.

148. Bochsler P. Structure of the solar wind and compositional variations. *Space Sci. Rev.*, 1998, v. 85, 291–302.

149. Aellig M.R., Lazarus A.J. and Steinberg J.T. The solar wind helium abundance: Variations with wind speed and solar cycle. *Geophys. Res. Let.*, 2001, v. 28(14), 2767–2770.

150. Wurz P. Solar Wind Composition. In: *The Dynamic Sun: Challenges for Theory and Observations*, ESA SP-600, 2005, v. 5.2, 1–9.

151. Kasper J.C., Stevens M.L., Lazarus A.J. and Ogilvie K.W. Solar wind and helium abundance as a function of speed and heliographic latitude: Variation through a solar cycle. *Astrophys. J.*, 2007, v. 660, 901–910.

152. Wang Y.M. Relating the solar wind helium abundance to the coronal magnetic field. *Astrophys. J.*, 2008, v. 683, 499–509.

153. Geiss J. and Bochsler P. Long time variations in solar wind properties: possible causes versus observations. In: *The Sun in Time* (Sonett C.P., Giampapa M.S., Matthews M.S., eds.), The University of Arizona Press, Tucson, AZ, 1991, p.98-117.

154. von Steiger R., Vial J.C., Bochsler P., Chaussidon M., Cohen C.M.S., Fleck B., Heber V.S., Holweger H., Issautier K., Lazarus A.J., Ogilvie K.W., Paquette J.A., Reisenfeld D.B, Teriaca L., Wilhelm K., Yusainee S., Laming J.M., and Wiens R.C. Measuring solar abundances. *AIP Conf. Proc.*, 2001, v. 598, 13–22.

155. Grevesse N. and Sauval A.J. Standard solar composition. *Space Science Reviews*, 1998, v. 85, 161–174.

156. Asplund M., Grevesse N., Sauval A.J. and Scott P. The chemical composition of the Sun. *Ann. Rev. Astron. Astrophys.*, 2009, v. 47, 481–522.

157. Robitaille P.M. Liquid Metallic Hydrogen: A Building Block for the Liquid Sun. *Progr. Phys.*, 2011, v. 3, 60–74.

New Constraints on Quantum Theories

Eliahu Comay

Charactell Ltd., PO Box 39019, Tel-Aviv, 61390, Israel. E-mail: elicomay@post.tau.ac.il

Hierarchical relationships between physical theories are discussed. It is explained how a lower rank theory imposes constraints on an acceptable structure of its higher rank theory. This principle is applied to the case of quantum mechanics and quantum field theory of massive particles. It is proved that the Dirac equation is consistent with these constraints whereas the Klein-Gordon equation, as well as all other second order quantum equations are inconsistent with the Schrödinger equation. This series of arguments undermines the theoretical structure of the Standard Model.

1 Introduction

The equations of motion are regarded as the basis of a physical theory. A mathematical analysis of these equations yields the complete form of a given theory and of its details. The validity of a mathematically correct physical theory should be consistent with two kinds of tests. Thus, it must agree with relevant experimental data and it must also be consistent with well established physical principles. (Evidently, the latter represent many experimental data in a concise form.) The following simple example illustrates the latter point. A new theory is unacceptable if its final results are inconsistent with the law of energy conservation. This point shows the significance of physical constraints that restrict the number of acceptable physical theories and guide theoretical and experimental efforts to take promising directions.

The definition of a domain of validity is an important element of a theory. For example, mechanics is the science used for predicting the motion of bodies. It is very successful in the case of the motion of planets moving around the sun. On the other hand, it cannot predict the motion of an eagle flying in the sky. This example does not mean that mechanics is incorrect. It means that mechanics is a very satisfactory science for a set of experiments. For example, Newtonian mechanics is acceptable for cases where the following conditions hold: the velocity is much smaller than the speed of light, the classical limit of quantum mechanics holds, and the force can be calculated in terms of position, time and velocity. The set of experiments where a given theory is successful is called the theory's domain of validity. This issue is used in the rest of this work.

The definition of the domain of validity illustrates an important aspect of the correctness of a physical theory. Indeed, this notion should be regarded in a relative sense. Thus, many measurements are given together with experimental error. For this reason, even if we know that a given theory is not perfect, it still can be regarded as a correct theory for cases where the theory's errors are smaller than the experimental errors.

In this work units where $\hbar = c = 1$ are used. In this system of units one kind of dimension applies and here it is the length $[L]$. Thus, the dimension of every physical quantity takes an appropriate power of $[L]$. For example, mass, energy and momentum take the dimension $[L^{-1}]$. The metric is diagonal and its entries are $(1, -1, -1, -1)$. Greek indices run from 0 to 3. The subscript symbol $_{,\mu}$ denotes the partial differentiation with respect to x^{μ}.

2 The dimensions of quantum fields

Consider the two sets of experiments S_A and S_B defining the domains of validity of the physical theories A and B, respectively.

Fig. 1 illustrates the hierarchical relationships between theories A and B. Here the sets S_A and S_B consist of all experiments that are described correctly by theory A and B, respectively. The set S_A is a subset of S_B. This relationship means that all experiments that are described successfully by theory A are also described successfully by theory B, but not vice versa. For this reason it can be stated that theory B has a more profound meaning because it is also valid for cases where theory A is useless. However, this fact does not mean that theory A is wrong, simply because this theory can be used successfully for all cases that belong to its domain of validity S_A.

This kind of relationships between theories has been recognized a long time ago. For example, A. Einstein mentions special relativity and general relativity and explains why special relativity should not be regarded as a wrong theory. The reason is that special relativity holds in cases where a flat space-time can be regarded as a good description of the

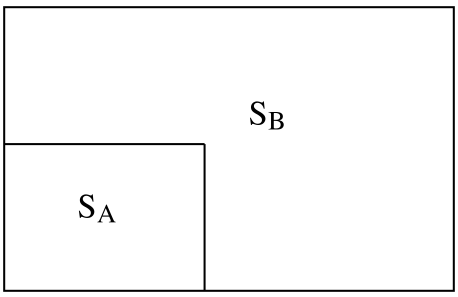

Fig. 1: Domains of validity of two theories (see text).

physical conditions. Similarly, considering electrostatics and Maxwellian electrodynamics, he explains why electrostatics is a good theory for cases where the charge carriers can be regarded as motionless objects (see [1], pp. 85, 86).

The issue of hierarchical relationships between theories is also discussed in Rohrlich's book (see [2], pp. 1–6). Here one can find explanation showing the hierarchical relationships between several pairs of theories. This discussion provides the reader with a broader overview of the structure of existing physical theories and of their hierarchical relationships.

As pointed out above, a physical theory that takes a higher hierarchical position has a more profound meaning. The rest of this work relies on another result obtained from these relationships. Thus, *a well established physical theory imposes constraints on appropriate limits of a higher rank theory.* For example, this requirement is satisfied by relativistic mechanics, whose low velocity limit agrees with Newtonian mechanics (see [3], pp. 26–30). Similarly, the classical limit of quantum mechanics agrees with classical physics (see [4], pp. 19–21 and [5], pp. 133–141). Below, this principle is called *constraints imposed by a lower rank theory.* It is shown in this work that this principle provides powerful constraints on the acceptability of physical theories.

3 Hierarchical Relationships Between Quantum Theories

Let us discuss the hierarchical relationships between three quantum theories of massive particles: non-relativistic quantum mechanics (QM), relativistic quantum mechanics (RQM) and quantum field theory (QFT) (see fig. 2). Thus, QM takes the lowest hierarchical rank because it is valid for cases where the absolute value of the momentum's expectation value is much smaller than the particle's self-mass. RQM is valid for cases where the number of particles can be regarded as a constant of the motion. QFT is a more general theory and RQM is its appropriate limit. The inherent relationships between these theories are well documented in the literature. Thus, S. Weinberg makes the following statement. "First, some good news: quantum field theory is based on the same quantum mechanics that was invented by Schrödinger, Heisenberg, Pauli, Born, and others in 1925-1926, and has been used ever since in atomic, molecular, nuclear and condense matter physics" (see [6], p. 49).

The Schrödinger equation takes the following form

$$i\frac{\partial\psi}{\partial t} = -\frac{1}{2m}\Delta\psi + U\psi. \tag{1}$$

An analysis of this equation yields an expression for a conserved current whose density is (see e.g. [4], pp. 53–55)

$$\rho = \psi^*\psi. \tag{2}$$

Relation (2) proves that the dimension of the Schrödinger function is

$$[\psi] = [L^{-3/2}]. \tag{3}$$

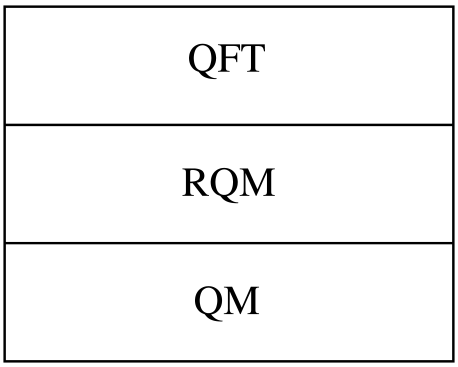

Fig. 2: Hierarchical relationships between three quantum theories (see text).

Here the expression for density depends only on the wave function and contains no derivatives. The form of the density (2) is an important element of the theory because it enables a construction of a Hilbert space of the time-independent functions which belong to the Heisenberg picture.

Let us examine the structure of QFT. The vital role of the Lagrangian density in QFT can be briefly described as follows. The phase is an indispensable element of quantum theories. Being an argument of an exponent which can be expanded in a power series, the phase must be a dimensionless Lorentz scalar. Thus, the phase is defined as a Lorentz scalar action (divided by $\hbar$). The following expression shows how the action is obtained from a given Lagrangian density $\mathcal{L}$

$$S = \int \mathcal{L}\, d^4x. \tag{4}$$

This expression proves that a dimensionless Lorentz scalar action is obtained from a Lagrangian density that is a Lorentz scalar whose dimension is $[L^{-4}]$.

This property of the Lagrangian density is used in an examination of two kinds of QFT theories. Let us begin with the first order Lagrangian density of a free Dirac field ψ_D (see [7], p. 54)

$$\mathcal{L}_D = \bar{\psi}_D[\gamma^\mu i\partial_\mu - m]\psi_D. \tag{5}$$

Now, the dimension $[L^{-4}]$ of the Lagrangian density and the dimension $[L^{-1}]$ of the operators ∂_μ and m prove that the dimension of the Dirac field ψ_D is $[L^{-3/2}]$. This value agrees with that of the Schrödinger function (3). It means that the Dirac field theory satisfies the dimension constraints imposed by the lower rank theory of QM.

A different result is obtained from the second order complex Klein-Gordon (KG) equation. The Lagrangian density of this equation is (see [7], p. 38)

$$\mathcal{L}_{KG} = g^{\mu\nu}\phi^*_{,\mu}\phi_{,\nu} - m^2\phi^*\phi. \tag{6}$$

Here the dimension of the operators is $[L^{-2}]$. Using the dimension $[L^{-4}]$ of the Lagrangian density, one infers that the

dimension of the KG function ϕ is $[L^{-1}]$. On the other hand, it is shown in (3) that the dimension of the Schrödinger wave function is $[L^{-3/2}]$. This outcome means that the complex KG function ϕ violates a constraint imposed by a lower rank theory.

It turns out that this inconsistency holds for other quantum equations where the dimension of their field function is $[L^{-1}]$. Thus, a dimension $[L^{-1}]$ is a property of the following field: the Yukawa particle (see [8], p. 211), the electroweak $W^{\pm}, Z$ bosons (see [9], p. 307) and the Higgs boson (see [10], p. 715). For this reason, quantum theories of all these particles are inconsistent with the dimensional constraint imposed by the Schrödinger equation.

One can also see immediately that the Yukawa and the Z fields introduce to the Lagrangian density an interaction term with a fermion ψ which takes the form

$$\mathcal{L}_{Int} = g\bar{\psi}\phi\psi. \tag{7}$$

This kind of interaction means that the field ϕ of each of these particles is a *real* field (in a mathematical sense). This conclusion stems from the facts that the action and the integration factor d^4x are real. These properties mean that all terms of a Lagrangian density must be real. Now, since g and the product $\bar{\psi}\psi$ are real, one finds that ϕ is real. Evidently, a theory of a real field is inconsistent with another constraint of QM. Indeed, QM uses a *complex* wave function and for this reason the non-relativistic limits of the *real* field of Yukawa and of Z particles also violate a second kind of constraint.

4 Concluding Remarks

It is explained in this work how hierarchical relationships between physical theories can be used for deriving necessary conditions that an acceptable higher rank theory must satisfy. This issue is applied to QFT theories and the non-relativistic limit of their field function is compared with properties of non-relativistic quantum mechanics. It is explained how such a comparison provides a powerful criterion for the acceptability of physical theories. The discussion examines the dimension of quantum functions of several specific theories and compares the dimension of QFT theories with that of the lower rank non-relativistic Schrödinger theory. It turns out that the Dirac field satisfies this criterion whereas the Klein-Gordon and the Yukawa theories as well as those of the $W^{\pm}, Z$ and the Higgs boson fail to satisfy this criterion.

An important evaluation of a theoretical idea is a comparison of its outcome with experimental results. Referring to this issue, one should note that a field function $\psi(x^{\mu})$ which is used in QM, RQM and QFT depends on a *single* set of four space-time coordinates x^{μ}. For this reason, $\psi(x^{\mu})$ describes an elementary point-like particle. The following example illustrates this matter. A pion consists of a quark-antiquark pair of the u, d flavor and each quark is described by a function that depends on its own 4-coordinates x^{μ}. Hence, a pion cannot be described by a function $\psi(x^{\mu})$, simply because this function has a smaller number of independent coordinates. It turns out that experimental data of all spin-1/2 Dirac particles, namely, leptons and quarks, are consistent with their pointlike attribute. On the other hand the pion, which was the original KG candidate is not pointlike and the $\pi^{\pm}$ mesons have a charge radius which is not much smaller than that of the proton [11]. There is still no experimental data concerning pointlike properties of the $W^{\pm}, Z$ and the Higgs boson.

As is well known, the $W^{\pm}, Z$ and the Higgs bosons are cornerstones of the Standard Model. It means that the series of arguments presented in this work undermines the theoretical structure of the Standard Model. Evidently, a physical theory that has an inconsistent structure is unacceptable. Hence, people who still adhere to the Standard Model must show why the arguments presented above are incorrect. It is also interesting to note that the results of this work are consistent with Dirac's lifelong objection to the second order KG equation of a spin-0 boson (see [12], pp. 3, 4).

Submitted on December 21, 2012 / Accepted on January 4, 2013

References

1. Einstein A. Albert Einstein in His Own Words. Portland House, New York, 2000.
2. Rohrlich F. Classical Charged Particle. World Scientific, New Jersey, 2007.
3. Landau L.D. and Lifshitz E.M. The Classical Theory of Fields. Elsevier, Amsterdam, 2005.
4. Landau L.D. and Lifshitz E.M. Quantum Mechanics. Pergamon, London, 1959.
5. Schiff L.I. Quantum Mechanics. McGraw-Hill, New York, 1955.
6. Weinberg S. The Quantum Theory of Fields, Vol. I, Cambridge University Press, Cambridge, 1995.
7. Bjorken J.D. and Drell S.D. Relativistic Quantum Fields. McGraw-Hill, New York, 1965.
8. Bjorken J.D. and Drell S.D. Relativistic Quantum Mechanics. McGraw-Hill, New York, 1964.
9. Weinberg S. The Quantum Theory of Fields, Vol. II, Cambridge University Press, Cambridge, 1996.
10. Peskin M.E. and Schroeder D.V. An Introduction to Quantum Field Theory. Addison-Wesley, Reading (Mass), 1995.
11. Beringer J. et al. REVIEW OF PARTICLE PHYSICS Particle Data Group. *Physical Review D*, 2012, v. 86, 010001.
12. Dirac P.A.M. In: Mathematical Foundations of Quantum Theory, Editor A.R. Marlow, Academic, New York, 1978.

The Nuclear Shape Phase Transitions Studied within the Geometric Collective Model

Khalaf A.M.* and Ismail A.M.†

*Physics Department, Faculty of Science, Al-Azhar University, Cairo, Egypt. E-mail: ali_khalaf43@hotmail.com
†Hot Laboratories Center, Atomic Energy Authority, Egypt, P.No. 13759, Cairo, Egypt. E-mail: ahmedismailph@yahoo.com

In the framework of the Geometric Collective Model (GCM), quantum phase transition between spherical and deformed shapes of doubly even nuclei are investigated. The validity of the model is examined for the case of lanthanide chains Nd/Sm and actinide chains Th/U. The parameters of the model were obtained by performing a computer simulated search program in order to obtain minimum root mean square deviations between the calculated and the experimental excitation energies. Calculated potential energy surfaces (PES's) describing all deformation effects of each nucleus are extracted. Our systematic studies on lanthanide and actinide chains have revealed a shape transition from spherical vibrator to axially deformed rotor when moving from the lighter to the heavier isotopes.

1 Introduction

The nuclear shape transitions were studied within the nuclear interacting boson model (IBM) [1–3]. The IBM-1 describes a system of a fixed number N of spin zero and two bosons (s and d bosons) subject to one- and two-body interactions. The IBM-1 reveals a transparent algebraic structure with U(6) as the dynamical group. Varying six free parameters of the model, one can reach three standard dynamical symmetries U(5), SU(3) and O(6) and two additional ones SU(3)* and O(6)* [2]. It turns out that these dynamical symmetries provide an appropriate framework for the description of low-energy collective motions of real nuclei with certain shape symmetries: The U(5) limit corresponds to spherical nuclei, the SU(3) and SU(3)* limits to axially symmetric nuclei with quadruple deformation (prolate and oblate shapes) and the O(6) and O(6)* limits to quadruply deformed nuclei that are unstable against the axial symmetry breaking. This is represented in the so called Casten triangle [2,4] with vertices corresponding to the standard dynamical symmetries and the other points to various transitional cases. Phase transitions between these shapes were studied, and it is known that the phase transition from U(5) to O(6) is second order, while any other transition within the Casten triangle from a spherical to a deformed shape is first order [5–15].

Alternative descriptions of nuclei at the critical point of phase transitions from spherical vibrator to deformed γ soft E(5) [16], and from spherical vibrator to deformed axially symmetric rotor X(5) [17], were proposed. These analytic solutions are obtained by introducing a square well potential in the Bohr Hamiltonian and yield parameter free predictions for both energies and electromagnetic transition probabilities. Empirical examples were suggested for both the proposed symmetries [18]. It was found [19, 20] that the X(5) predictions cannot be exactly reproduced by any point in the two parameter space of the IBM, whereas best agreement is obtained for parameters corresponding to a point close to, but outside, the shape phase transition region of the IBM. Since the IBM was formulated from the beginning in terms of creation and annihilation boson operators, its geometric interpretation in terms of shape variables is usually done by introducing a boson condensate with two shape parameters β and γ through the intrinsic state formalism (coherent state) [21]. The parameter β is related to the axial deformation of the system, while γ measures the deviation from axial symmetry. The equilibrium shape of the system is obtained by minimizing the intrinsic state. It is well know that the dynamical symmetry associated with U(5) corresponds to a spherical shape $\beta = 0$, the dynamical symmetry SU(3) is associated with an axially deformed shape $\beta \neq 0$ and $\gamma = 0, \pi/3$ and the dynamical symmetry O(6) is related to a γ-unstable deformed shape $\beta \neq 0$ and γ-independent.

A very flexible and powerful approach to describe nuclear collective excitations which is an extension of the Bohr-Mottelson vibrational Hamiltonian [22] is the GCM essentially based on the quadruple degrees of freedom [23,24]. The problem of nuclear collective motion is formulated by Bohr and Mottelson from the beginning in terms of the intrinsic parameters β, γ and the three Euler angels ω_i that characterize the orientation of a deformed nucleus.

The GCM is a macroscopic nuclear structure model in the sense that it considers the nucleus as a charged liquid drop with a definite surface, rather than a many-body system of constituent particles.

Neodymium isotopes are the members of the chain of nuclei which represent an ideal case for studying the influence of the shape transition from spherical to deformed nuclei. Therefore, in the chart of nuclei there is a very important lanthanide Nd/Sm transition region which exhibit a rapid structural change from spherical to well deformed when moving from the lighter to the heavier isotopes. Although this tran-

sitional region has been studied extensively in the framework of the IBM, the discussion of phase transitions has not always been treated in a proper way.

In the present paper, we have analyzed systematically the transitional region and phase transition in lanthanide and actinide chains of isotopes in the framework of GCM. For each isotope chain a fitting procedure is performed to get the model parameters. We have generated the PES to classify phase transitions and to decide if a nucleus is close to criticality. In these chains, nuclei evolve from spherical to deformed shapes.

2 The GCM Hamiltonian and the PES's

The Hamiltonian of the GCM [23] represents a concrete realization of the general Bohr Hamiltonian [22] describing the quadruple oscillations of the nuclear surface. The collective Hamiltonian restricted to quadruple deformations can be written in the notation of Rajah for tensor products of irreducible tensor operators. The α's are the well known collective coordinates, which are defined by the usual expansion of the nuclear radius in terms of spherical harmonics. The $\hat{\pi}$ is the covariant tensor of the canonically conjugate momenta. We start by writing the GCM Hamiltonian as:

$$\hat{H} = \hat{T} + \hat{V}. \tag{1}$$

The kinetic energy $\hat{T}$ up to second order is given by [2].

$$\hat{T} = \frac{1}{B_2}[\pi \times \pi]^0 + \frac{P_3}{3}\left[[\pi \times \alpha]^{(2)} \times \hat{\pi}\right]^{(0)} \tag{2}$$

where B_2 is the common mass parameter and P_3 is an enharmonic kinetic term which for simplicity, we set to zero here. A transformation to the intrinsic body fixed system leads to a formal separation of the rotational and vibrational variables expressed by the Euler angles and the shape parameters β and γ respectively. The potential energy V is given by

$$\begin{aligned} V &= C_2[\alpha \times \alpha]^{(2)} + C_3\left[[\alpha \times \alpha]^{(2)} \times \alpha\right]^{(0)} + \\ &+ C_4[\alpha \times \alpha]^{(0)}[\alpha \times \alpha]^{(0)} + \\ &+ C_5[\alpha \times \alpha]^{(0)}\left[[\alpha \times \alpha]^{(2)} \times \alpha\right]^{(0)} + \\ &+ C_6\left[[\alpha \times \alpha]^{(2)} \times \alpha\right]^{(0)}\left[[\alpha \times \alpha]^{(2)} \times \alpha\right]^{(0)} + \\ &+ D_6[\alpha \times \alpha]^{(0)}[\alpha \times \alpha]^{(0)}[\alpha \times \alpha]^{(0)}. \end{aligned} \tag{3}$$

The six stiffness parameters C_2, C_3, C_4, C_5, C_6 and D_6 occurring in the collective potential energy are constants for each nucleus. They are treated as adjustable parameters which have to be determined from the best fit to the experimental data, level energies, B(E2) transition strengths and quadruple moments. They depend however on the proton and neutron numbers due to shell structure. The potential energy, expressed in terms of the intrinsic variables β and γ, is

$$\begin{aligned} V(\beta,\gamma) &= C_2\tfrac{1}{\sqrt{5}}\beta^2 - C_3 rub\sqrt{\tfrac{2}{35}}\beta^3\cos(3\gamma) + \\ &+ C_4\tfrac{1}{5}\beta^4 - C_5\sqrt{\tfrac{2}{175}}\beta^3\cos(3\gamma) + \\ &+ C_6\tfrac{2}{35}\beta^6\cos^2(3\gamma) + D_6\tfrac{1}{5\sqrt{5}}\beta^6 \\ &= V_s(\beta) + V_{Po}(\beta,\gamma) + V_{na}(\beta,\gamma). \end{aligned} \tag{4}$$

Roughly speaking the C_2, C_4 and D_6 terms describe the γ-independent features of the PES. They form the contribution $V_s(\beta)$. The C_3 and C_5 terms are responsible for the prolate-oblate energy differences in the PES and are represented by $V_{po}(\beta,\gamma)$. The C_6 term is symmetric about the $\gamma = \pi/6$ axis and therefore can be used for the generation of non axial shape $V_{na}(\beta,\gamma)$. The selection of the eight parameters of the GCM Hamiltonian is impractical and difficult, because the available observation data are usually not sufficient to establish the qualitative nature of the GCM potential. It is therefore, often desirable to use a more tractable form of the model. In practice simplification for the GCM is to use a maximum of three parameters to describe all limits of nuclear structure: vibrator, rotor and γ-soft nuclei and transition regions in between. Then the potential energy up to the fourth power of β is simplified to be:

$$V(\beta,\gamma) = C_2\frac{1}{\sqrt{5}}\beta^2 - C_3\sqrt{\frac{2}{35}}\beta^3\cos(3\gamma) + C_4\frac{1}{5}\beta^4 \tag{5}$$

where $\beta \in [0,\infty]$ and $\gamma \in [0, 2\pi/3]$.

3 Critical Point Symmetries

The equilibrium shape associated with the GCM Hamiltonian can be obtained by determining the minimum of the energy surface with respect to the geometric variables β and γ, *i.e.* where the first derivative vanish.

Since the parameter C_3 controls the steepness of the potential, and therefore, the dynamical fluctuations in γ, it strongly affects the energies of excited intrinsic states. The parameter $C_3 = 0$ gives a γ-flat potential and an increase of C_3 introduces a γ-dependence in the potential with a minimum at $\gamma = 0$. Changing C_3 will indeed induce a γ-unstable to the symmetric rotor transition; it is best to simultaneously vary C_2 and C_4 as well.

The shape transition from vibrator to rotors is achieved by starting from the vibrator limit, lowering C_2 from positive to negative value, increasing C_4 to large positive value, with gradually increasing C_3 (lowering C_2 from positive to negative value, introducing a large positive C_4 and a positive C_3).

4 Numerical Results Applied to Lanthanide and Actinide chains

The first nucleus to be identified as exhibiting transition from spherical to axially deformed shapes was ^{152}Sm [18], followed by ^{150}Nd [24]. Further work on ^{152}Sm [25] and ^{150}Nd

[25, 26] reinforced this conclusion. In our calculation we will examine and systematically study the lanthanide $^{144-154}$Nd and $^{146-156}$Sm, isotopes and actinide $^{224-234}$Th and $^{230-238}$U isotopes because of the richness of available experimental data indicating a transition of nuclear shapes from spherical to deformed form. The optimized model parameters for each

Table 1: The GCM parameters by (MeV) as derived in fitting procedure used in the calculation.

Nucleus	C_2	C_3	C_4
^{144}Nd	12.46084	1.06407	−26.29034
^{146}Nd	7.98904	8.46249	−5.34827
^{148}Nd	−19.84450	41.41216	105.62500
^{150}Nd	−56.19267	83.37305	248.96600
^{152}Nd	−73.70551	104.57310	319.48270
^{154}Nd	−84.13947	118.02790	362.71460
^{146}Sm	14.49576	1.27688	−30.52593
^{148}Sm	8.89235	9.87290	−5.28215
^{150}Sm	−23.19850	47.32818	121.87500
^{152}Sm	−63.80397	93.79468	281.39990
^{154}Sm	−82.44842	116.19230	356.21830
^{156}Sm	−93.05583	129.83070	400.10950
^{224}Th	0.55766	4.96951	6.10300
^{226}Th	−0.11521	6.38937	9.70762
^{228}Th	−0.83906	7.98671	13.68875
^{230}Th	−1.63871	9.76153	18.10188
^{232}Th	−2.59264	11.71384	23.12250
^{230}U	−1.67560	9.76153	18.18437
^{232}U	−2.63289	11.71384	23.21250
^{234}U	−3.77666	13.84363	28.92012
^{236}U	−4.90299	16.15090	34.85125
^{238}U	−6.23928	18.63565	41.51437

nucleus was adjusted by fitting procedure using a computer simulated search program in order to describe the gradual change in the structure as neutron number varied and to reproduce the properties of the selected reliable state of positive parity excitation ($2_1^+, 4_1^+, 6_1^+, 8_1^+, 0_2^+, 2_3^+, 4_3^+, 2_2^+, 3_1^+$, and 4_2^+) and the two neutron separation energies of all isotopes in each isotopic chain. The resulting parameters are listed explicitly in Table 1. For the isotopic chains investigated here, the collective properties are illustrated by representing the calculated PES describing all deformation effects of the nucleus. We investigated the change of nuclear structure within these chains as illustrated in Figures 1-4. The PES's versus the deformation parameter β for lanthanide and actinide isotopic chains of nuclei evolving from spherical to axially symmetric well deformed nuclei. We remark that for all mentioned nuclei, the PES is not flat, exhibiting a deeper minimum in the prolate ($\beta > 0$) region and a shallower minimum in the oblate ($\beta < 0$) region. Relatively flat PES occur for the N = 86 nuclei ^{146}Nd and ^{148}Sm. A first order shape phase transition with change in number of neutrons when moving from the lighter to heavier isotopes, *i.e* U(5) - SU(3) transitional region are observed.

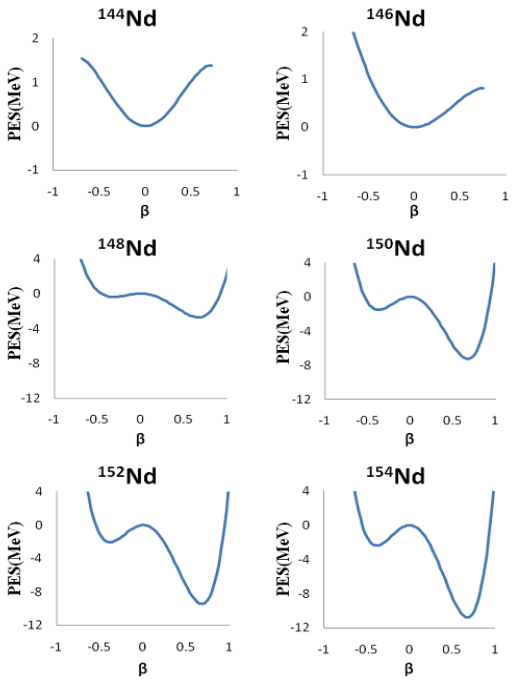

Fig. 1: PES calculated with GCM as a function of the shape parameter β for shape phase transition from spherical to prolate deformed for Neodymium isotope chain $^{144-154}$Nd.

The present results for $^{146-156}$Sm is in good agreement with Nilsson-Strutinsky (BCS)-calculations [26]. However, the existence of a bump in the PES is related to the success of the confined β-soft (BCS) rotor model, employing an infinite square well potential displaced from zero, as well as to the relevance of Davidson potentials [27, 28]. It also is related to the significant five-dimensional centrifugal effect [28, 29]. The actinide $^{228-234}$Th and $^{234-238}$U are all well-deformed rotors with energy ratio $E(4_1^+)/E(2_1^+)$ close to (3.3).

5 Conclusion

A simple approach of the GCM is discussed which reproduces the basic features of the three limits of the nuclear structure: spherical vibrator, axially symmetric rotor and γ-soft rotor, as well as the three phase shape transition regions linking them. The Hamiltonian is expressed as a series expansion in terms of surface deformation coordinates and a conjugate momentum. We considered only the lowest kinetic energy terms, so that the eigen problem for our Hamiltonian reduces to Schrodinger equation in five dimensional spaces. All calculations are performed for reference value of the common mass parameter, only a maximum of three parameters of the truncated form of GCM potential instead of the six are

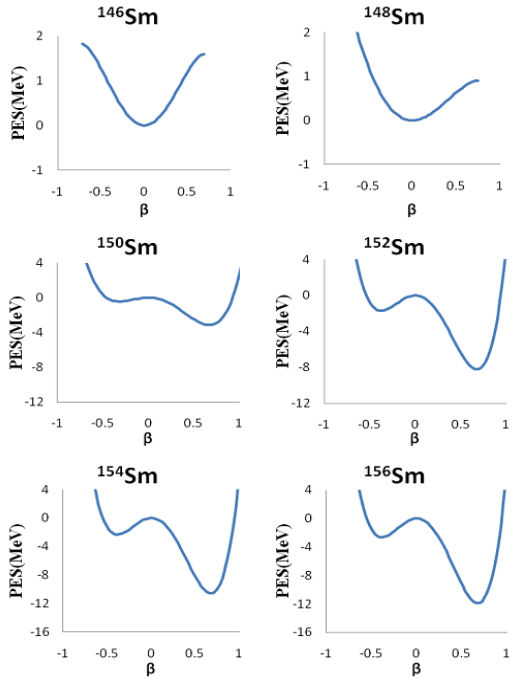

Fig. 2: PES calculated with GCM as a function of the shape parameter β for shape phase transition from spherical to prolate deformed for Samarium isotope chain $^{146-156}$Sm.

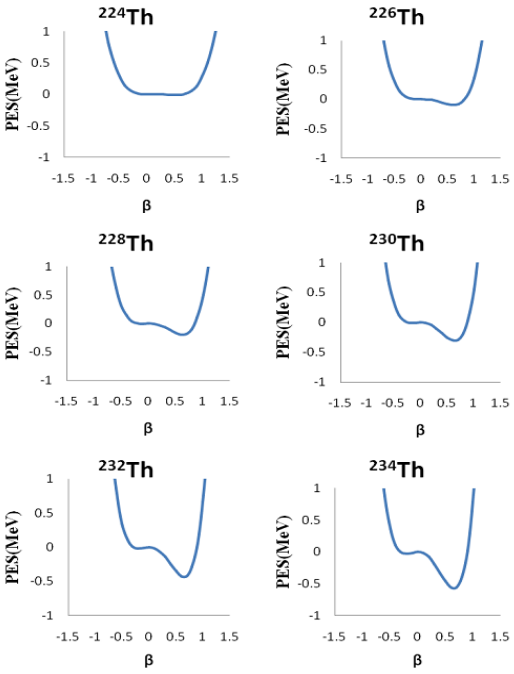

Fig. 3: PES calculated with GCM as a function of the shape parameter β for shape phase transition from spherical to prolate deformed for Thorium isotope chain $^{224-234}$Th.

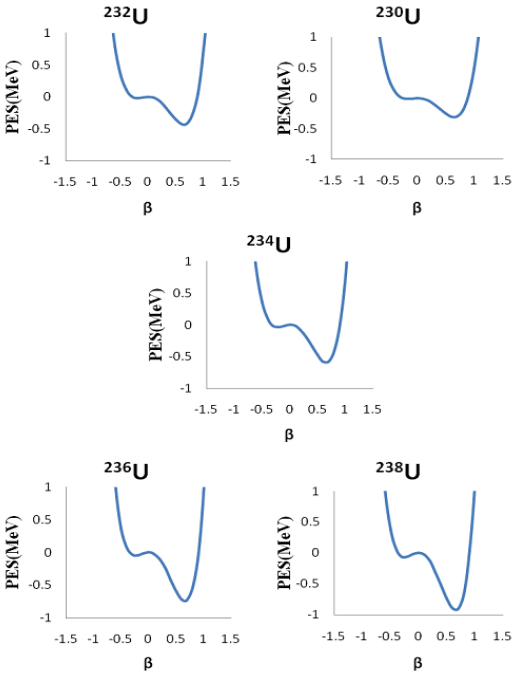

Fig. 4: PES calculated with GCM as a function of the shape parameter β for shape phase transition from spherical to prolate deformed for Uranium isotope chain $^{230-238}$U.

used. The parameter values for the description of a particular nucleus have been found through automated fitting of the nuclear energy levels.

The systematics of shape transitions versus neutron number is studied by the GCM. The capabilities of the model and the illustrative way of representing the collective properties by potential energy surfaces are demonstrated. For neutron number N = 90, the nucleus has a substantial static deformation, but for N = 80 the nucleus is soft or transitional and cannot be described as deformed.

Submitted on December 13, 2012 / Accepted on January 7, 2013

References

1. Khalaf A.M. and Awwad T.M. A Theoretical Description of U(5)-SU(3) Nuclear Shape Transitions in the Interacting Boson Model. *Progress in Physics*, 2013, v. 1, 7–11.
2. Iachello F. and Arima A. The Interacting Boson Model. Cambridge University Press, Cambridge, England, 1987.
3. Frank A. and VanIsacker P. Algebraic Methods in Molecular and Nuclear Structure Physics. Wiley, New York, 1994.
4. Casten R.F. Nuclear Structure from a Simple Prespective. Oxford University, Oxford, 1990.
5. José M.A. et al. Two-Level Interacting Boson Models Beyond the Mean Field. *Physical Review*, 2007, v. C75, 014301–014310.
6. Iachello F. and Zamfir N.V. Quantum Phase Transitions in Mesoscopic Systems. *Physical Review Letters*, 2004, v. 92 (3), 212501–212505.
7. Cejnar P., Heinze S. and Dobes J. Thermodynamic Analogy for Quantum Phase Transitions at Zero Temperature. *Physical Review*, 2005, v. C71, 011304R–011309R.

8. Rowe D.J., Turner P.S. and Rosensteel G. Scaling Properties and Asymptotic Spectra of Finite Models of Phase Transitions as They Approach Macroscopic Limits. *Physical Review Letters*, 2004, v. 93, 232502–232505.
9. Rowe D.J. Quasi Dynamical Symmetry in an Interacting Boson Model Phase Transition. *Physical Review Letters*, 2004, v. 93, 122502–122505.
10. Liu Y.X., Mu L.Z. and Wei H. Approach to The Rotation Driven Vibrational to Axially Rotational Shape Phase Transition Along The Yrast Line of a Nucleus. *Physics Letters*, 2006, v. B633, 49–53.
11. Zhang Y., Hau Z. and Liu Y.X. Distinguishing a First Order From a Second Order Nuclear Shape Phase Transition in The Interacting Boson Model. *Physical Review*, 2007, v. C76, 011305R–011308R.
12. Arios J.M., Dukelsky J. and Garcia-Ramos J.E. Quantum Phase Transitions in the Interacting Boson Model: Integrability, Level Repulsion and Level Crossing. *Physical Review Letters*, 2003, v. 91, 162502–162504.
13. Garcia-Ramos J.E. et al. Two-Neutron Separation Energies, Binding Energies and Phase Transitions in The Interacting Boson Model. *Nuclear Physics*, 2001, v. A688, 735–754.
14. Liu M.L. Nuclear Shape-Phase Diagrams. *Physical Review*, 2007, v. C76, 054304–054307.
15. Heyde K. et al. Phase Transitions Versus Shape Coexistence. *Physical Review*, 2004, v. C69, 054304–054309.
16. Iachello F. Dynamic Symmetries at The Critical Point. *Physical Review Letters*, 2000, v. 85, 3580–3583.
17. Iachello F. Analytic Prescription of Critical Point Nuclei in a Spherical Axially Deformed Shape Phase Transtion. *Physical Review Letters*, 2001, v. 87, 052502–052506.
18. Casten R.F. and Zamfir N.V. Evidence for a Possible E(5) Symmetry in ^{134}Ba. *Physical Review Letters*, 2000, v. 85, 3584–3586. Casten R.F. and Zamfir N.V. Empirical Realization of a Critical Point Description in Atomic Nuclei. *Physical Review Letters*, 2001, v. 87, 052503–052507.
19. McCutchan E.A., Zamfir N.V. and Casten R.F. Mapping The Interacting Boson Approximation Symmetry Triangle: New trajectories of Structural Evolution of Rare-Earth Nuclei. *Physical Review*, 2004, v. C69, 064306–064314. Bridging The Gap Between X(5) and The Interacting Boson Model. *Physical Review*, 2005, v. C71, 034309–034314.
20. McCutchan E.M., Bonatsos D. and Zamfir N.V. Connecting The X(5)-?2, X(5)-?4, and X(3) Models to the Shape/Phase-Transition Region of The Interacting Boson Model. *Physical Review*, 2006, v. C74, 034306–034316.
21. Dieperink A.E.L., Scholten O. On Shapes and Shape Phase Transitions in The Interacting Boson Model. *Nuclear Physics*, 1980, v. A346, 125–138.
22. Bohr A. and Mottelson. Nuclear Structure v. II. Benjamin, New York, 1975.
23. Troltenier D., Hess P.O. and Maruhn J. Computational Nuclear Physics, Vol. I, Nuclear Structure, Langanke eds.K., Maruhn J. and Koonin S.E. Springer, Berlin, Heidelberg, New York, 1991.
24. Krücken R. et al. B(E2) Values in ^{150}Nd and The Critical Point Symmetry X(5). *Physical Reviw Letters*, 2002, v. 88, 232501–232501.
25. Bijker R. et al. Test of X(5) for the γ Degree of Freedom. *Physical Reviw*, 2003, v. C68, 064304–064307 and Erratum: Test of X(5) for the γ Degree of Freedom. *Physical Review*, 2004, v. C69, 059901–059905.
26. Zhang D.L. and Zhao H.Y.C. Lifetime measurements in the γ band of ^{160}Er nuclei. *Physical Letters*, 2002, v. 19, 779–782.
27. Bonatsos D. et al. E(5) and X(5) Critical Point Symmetries Obtained From Davidson Potentials Through a Variational Procedure. *Physical Review*, 2004, v. C70, 024305–024314.
28. Caprio M.A. Effects of $\beta - \gamma$ coupling in transitional nuclei and the validity of the approximate separation of variables. *Physical Review*, 2005, v. C72, 054323–054333.
29. Rowe D.J. and Turner P.S. The Algebraic Collective Model. *Nuclear Physics*, 2005, v. A753, 94–105.

Quantum Uncertainty and Fundamental Interactions

Sebastiano Tosto
Italy. Email: stosto@inwind.it, stosto44@gmail.com

The paper proposes a simplified theoretical approach to infer some essential concepts on the fundamental interactions between charged particles and their relative strengths at comparable energies by exploiting the quantum uncertainty only. The worth of the present approach relies on the way of obtaining the results, rather than on the results themselves: concepts today acknowledged as fingerprints of the electroweak and strong interactions appear indeed rooted in the same theoretical frame including also the basic principles of special and general relativity along with the gravity force.

1 Introduction

The state of a classical particle is specified by its coordinates and momentum; the dynamical variables x, p_x, y, p_y, z, p_z, assumed known at any time, define the 6-dimensional space usually called "phase space". Knowing the state of a particle means determining these six quantities that describe its motion and energy. Since the state of a classical system is identified by the distribution of corresponding points in the phase space, any finite volume $V_{ps} = (\delta x\delta y\delta z)(\delta p_x\delta p_y\delta p_z)$ should seemingly contain an infinite number of states. Because of the uncertainty principle, however, these six quantities are not simultaneously known; the impossibility of defining the corresponding points in the phase space compels instead introducing a lower limit to the volume of phase space physically significant. Since such an elementary volume has size $V^o_{ps} = (dxdydz)(dp_xdp_ydp_z) = \hbar^3$, any finite volume V_{ps} enclosing measurable combinations of coordinates and conjugate momenta consists of a finite number V_{ps}/V^o_{ps} of elementary volumes. The quantum uncertainty was inferred by W. Heisenberg as a consequence of the operator formalism of wave mechanics, on which relies the quantum theory: the wave function $\psi = \psi(x, t)$ replaces the lack of definable quantum values of x concurrently associable to the conjugate p_x. However most physicists believe unsatisfactory a theory based on the wave function ψ without direct physical meaning [1]; indeed $\psi\psi^*$ only has the statistical meaning of probability density and contains the maximum information obtainable about a physical system. The wave function characterizes a pure state, represented by a single "ket" vector to which corresponds a well defined eigenvalue, whereas in general a particle is found in a mixture of states; so the result of a measurement on a quantum state represents a probability distribution of finding the particle in a given volume of phase space. The density matrix is the mathematical tool to describe mixed quantum states by means of a distribution function of coordinates and momenta. Owing to the statistical character of the knowledge we can afford in the quantum world, the Wigner function $W(x, p)$ [2] aims to represent a quantum state in terms of a joint probability distribution involving both coordinates and momenta, in formal analogy with the classical statistics; the former is therefore a correction to the latter. The quantum x and p distributions are appropriately described by the respective marginal distributions $\int_{-\infty}^{+\infty} W(x, p)dp$ and $\int_{-\infty}^{+\infty} W(x, p)dx$ under the normalization condition $\int_{-\infty}^{+\infty}\int_{-\infty}^{+\infty} W(x, p)dpdx = 1$, whereas the expectation value for any operator function is weighed by $W(x, p)$ as $\int_{-\infty}^{+\infty}\int_{-\infty}^{+\infty} W(x, p) f(x, p)dpdx$. Other relevant features of $W(x, p)$, well known [3], are omitted here for brevity. Also the Wigner function, however, although providing significant information about the quantum states, presents conceptual difficulties: it is not a real probability distribution in the classical sense, it is a quasi-probability that can even take negative values; moreover it can represent the average value of an observable but not, in general, also its higher power moments.

To bypass both these difficulties inevitably inherent the wave formalism, the present theoretical model implements an approach conceptually different: it exploits directly the statistical formulation of quantum uncertainty, which therefore becomes itself a fundamental assumption of the model and reads in one space dimension

$$\Delta x\Delta p_x = n\hbar = \Delta t\Delta\varepsilon. \qquad (1,1)$$

This set of $2n$ equation disregards since the beginning the local dynamical variables of the particles forming the quantum system and simply counts its number n of allowed states. Are therefore required the following positions

$$x_i \to \Delta x_i, \qquad t \to \Delta t, \qquad i = 1..3. \qquad (1,2)$$

No hypotheses are made about the uncertainty ranges, which are by definition unknown, unknowable and arbitrary. In quantum mechanics the square complex wave function of space and time variables contains the maximum information about a quantum system, which has therefore probabilistic character. The present model intends instead starting from a *minimal* information about any quantum system, still based on the failure of the physical concept of points definable in the quantum phase space but trusting on the idea that a minimum information is consistent with the maximum generality: despite the knowledge of one dynamical variable only is in principle allowed even in the quantum world, the present

model disregards "a priori" the local values of both conjugate dynamical variables. This means renouncing even to the concept of probability density provided by the wave function of a particle, while also disregarding the related concept of wave packet to describe its propagation; in the present model it is only possible to say that if the particle moves during a time range Δt throughout its uncertainty range Δx, then its average velocity component is $v_x = \Delta x/\Delta t$ regardless of any local feature of its actual delocalization motion. So eqs (1,1) require by definition $\Delta\varepsilon = v_x \Delta p_x$. In fact the positions (1,2) ignore both local dynamical variables, not as a sort of approximation to simplify some calculation but conceptually and since the early formulation of any quantum problem; accordingly, the delocalization of a quantum particle in its uncertainty range is conceived in its most agnostic form, i.e. waiving any kind of information about its position and motion. Thus, regarded in this way, eqs (1,1) exclude the concept itself of probability density and contextually also the definition of Wigner function linking the Schrodinger equation to the marginal distributions in the phase space; both equations are bypassed along with the concept of wave equation itself. Eqs (1,1) merely list the eigenvalues of pure states, indeed they are a set of equations corresponding to the respective values of n; so they also skip the probability with which in a mixed state each eigenvalue could be measured. Despite waiving themselves the concept of probability density through the positions (1,2), eqs (1,1) enable however also this kind of probabilistic information; it is essential indeed to mention that the wave formalism is obtainable as a corollary of eqs (1,1) [4], which means that all considerations previously introduced are in fact comprised also in the present theoretical model: one infers first from eqs (1,1) the operator formalism and then proceeds as usual. In this way the wave formalism, with its conceptual weakness, loses its rank of fundamental root of our knowledge about the quantum world, becoming indeed a mere by-product of eqs (1,1); yet, even so it still represents an added value to the physical information by introducing the concept of probability density that partially overcomes the total agnosticism of eqs (1,1).

What however about the chance of formulating any physical problem exploiting directly the eqs (1,1) only? Is legitimate the belief that the equations enclosing conceptually the wave formalism as a corollary also enclose the inherent physical information. The question that arises at this point concerns just the real chance of obtaining physical information once abandoning the typical ideas and mathematical tools of wave mechanics: is really redundant the concept of probability density? Several papers have demonstrated the effectiveness of this alternative approach, e.g. [5,6]; moreover, without the need of hypotheses on n and on the uncertainty ranges defined by eqs (1,1), the paper [7] has shown the possibility of extending the mere quantum horizon of these equations, initially concerned, also to the special and general relativity. The positions (1,2) compel focusing the attention on the uncertainty ranges and related numbers of states, i.e. on the phase space, rather than on the specific coordinates of the particles concerned by the particular physical problem. In fact, the local dynamical variables are conceptually disregarded since the beginning in the present model. Put for instance $\Delta x = x - x_o$: if either boundary coordinate, say x_o, is defined by the origin of the coordinate system R, then it determines the position of Δx in R; the other boundary coordinate x determines its size. The crucial point is that both x_o and x are arbitrary, unknown and unknowable by fundamental assumption; the reference system R is therefore "a priori" arbitrary, unspecified and unspecifiable as well, whence the equivalence of all reference systems whenever implementing the positions (1,2) to describe the quantum world. Otherwise stated, eqs (1,1) do not specify any particular reference system because analogous considerations hold for all uncertainty ranges they introduce. Moreover n is itself arbitrary as well; it merely symbolizes a sequence of numbers of allowed states, not some specific value in particular. Let therefore eqs (1,1) be defined in any R and rewrite them as $\Delta x' \Delta p'_x = n' = \Delta\varepsilon' \Delta t'$ in any R': it is self-evident that actually these equations are indistinguishable because n and n' do so as well. Whatever a specific value of n might be in R, any change to n' e.g. because of the Lorentz transformations of the ranges is physically irrelevant: it means replacing an arbitrary integer in the former set with another integer of the latter set. In effect, two examples of calculation reported below highlight that modifying the range sizes from primed to unprimed values does not affect any result, in agreement with their postulated arbitrariness: no range size is expected to appear in the quantum eigenvalues. Hence the eqs (1,1) have general character, regardless of any particular reference system to be appropriately specified; this holds also if R and R' are inertial and non-inertial, since no hypothesis has been assumed about them [7]. On the one hand this entails obtaining the indistinguishability of identical particles as a corollary, regardless of which particle in a set could be that actually delocalized in a given uncertainty range; indeed no particle is specifically concerned "a priori". On the other hand it also entails that the properties of motion of the particle, and thus the marginal distributions of its dynamical variables, are disregarded by assumption and skipped by consequence when formulating any physical problem. To better understand the following of the paper, these remarks are now exemplified examining shortly the non-relativistic quantum angular momentum $\mathbf{M}$, on the one side to highlight how to exploit the positions (1,2) and on the other side to show why the minimal information accessible through eqs (1,1) is in fact just that available through the usual operator formalism of wave mechanics.

Consider the classical component $M_w = \mathbf{r} \times \mathbf{p} \cdot \mathbf{w}$ of $\mathbf{M}$ along an arbitrary direction defined by the unit vector $\mathbf{w}$, being $\mathbf{r}$ the radial distance of any particle from the origin of an arbitrary reference system and its momentum. The positions (1,2) compel $\mathbf{r} \to \Delta\mathbf{r}$ and $\mathbf{p} \to \Delta\mathbf{p}$ and enable the

number l of states to be calculated only considering the total ranges $\Delta\mathbf{r}$ and $\Delta\mathbf{p}$ of distances and momenta physically allowed to the particle, about which no hypothesis is necessary; let us show that the random local values $\mathbf{r}$ and $\mathbf{p}$ themselves have instead no physical interest. So $M_w = (\Delta\mathbf{r} \times \Delta\mathbf{p}) \cdot \mathbf{w} = (\mathbf{w} \times \Delta\mathbf{r}) \cdot \Delta\mathbf{p}$, i.e. $M_w = \Delta\mathbf{W} \cdot \Delta\mathbf{p}$, where $\Delta\mathbf{W} = \mathbf{w} \times \Delta\mathbf{r}$. If and $\Delta\mathbf{W}$ are orthogonal, then $M_w = 0$; else, rewriting $\Delta\mathbf{W} \cdot \Delta\mathbf{p}$ as $(\Delta\mathbf{p} \cdot \Delta\mathbf{W}/\Delta W)\,\Delta W$ with $\Delta W = |\Delta\mathbf{W}|$, the component $\pm\Delta p_W = \Delta\mathbf{p} \cdot \Delta\mathbf{W}/\Delta W$ of $\Delta\mathbf{p}$ along $\Delta\mathbf{W}$ yields $M_w = \pm\Delta W \Delta p_W$.

Thus, according to eqs (1,1), $M_w = \pm l\hbar$, being l the usual notation for the number of states of the angular momentum. As expected, M_w is a multi-valued function because of the uncertainties initially postulated for $\mathbf{r}$ and $\mathbf{p}$. One component of $\mathbf{M}$ only, e.g. along the z-axis, is knowable; repeating the same approach for the y and x components would trivially mean changing $\mathbf{w}$. Just this conclusion suggests that the average values $< M_x^2 >$, $< M_y^2 >$ and $< M_z^2 >$ should be equal; so the quantity of physical interest to describe the properties of quantum angular momentum is l, as a function of which M^2 is indeed inferred as well. The components averaged over the possible states summing $(l\hbar)^2$ from $-L$ to $+L$, where L is an arbitrary maximum value of l, yield $< M_i^2 >= \sum_{l_i=-L}^{l_i=L} (\hbar l)^2/(2L{+}1)$ and thus $M^2 = \sum_{i=1}^{3} < M_i^2 >= L(L{+}1)\hbar^2$.

The physical definition of angular momentum is enough to find quantum results completely analogous to that of the wave mechanics even disregarding any local detail about the angular motion. This result has been reminded here as it introduces several significant considerations useful in the following: (i) eqs (1,1) and the positions (1,2) plug the classical physics into the quantum world; (ii) no hypothesis is necessary about the motion of the particle nor about its wave/matter nature to infer the quantum result; (iii) trivial algebraic manipulations replace the solution of the pertinent wave equation; (iv) the result inferred through eqs (1,1) only is consistent with that of the wave mechanics; (v) the local distance between the particles concerned in the angular motion does not play any role in determining l; (vi) the number of allowed states plays actually the role of angular quantum number of the operator formalism of wave mechanics; (vii) the amount of information accessible for the angular momentum is not complete like that of the classical physics, but identical to that of the wave formalism; (viii) eqs (1,1) rule out "a priori" any chance of hidden variables hypothetically encodable in the wave function, i.e. local values of any kind that could in principle enhance our knowledge about M_w and M^2 to obtain a more complete description of the angular quantum system; (ix) the eigenvalues, i.e. the physical observables, are actually properties of the phase space rather than properties of specific particles, whence the indistinguishability of identical particles here inferred as a corollary of eqs (1,1); (x) the numbers of states are here simply counted; (xi) the positions (1,2) are consistent with the concept of classical coordinate in the limit case $\Delta x \to 0$, which means that the random local variable $x_o \le x \le x_1$ tends to a classical local value uniquely and exactly defined; (xii) the total arbitrariness of the boundary values of the ranges is necessary to ensure that any local value is allowed for the corresponding classical variables; (xiii) the range sizes do not play any role in determining the eigenvalues of angular momentum, their conceptual reality, i.e. the total uncertainty about both conjugate dynamical variables of a quantum particle, is the unique hypothesis of the present model. The same holds of course for any other uncertainty range.

These ideas have been extended and checked in the papers [5,6] also for more complex quantum systems like hydrogenlike and many electron atoms/ions and diatomic molecules; also these papers allowed concluding that eqs (1,1) efficiently replace the standard approach of wave mechanics, without requiring the concept of probability density and thus without need of calculating marginal distributions in the phase space through the Wigner functions. In these papers the interaction is described via the Coulomb potential energy between charged particles; in other words, one assumes already known the Coulomb law to calculate for instance the energy levels of hydrogenlike atoms. This point is easily highlighted considering for simplicity the non-relativistic hydrogenlike energy levels; also this topic, already introduced in [5], is reported here for completeness.

Assuming the origin O of an arbitrary reference system R on the nucleus, the classical energy is $\varepsilon = p^2/2m - Ze^2/r$ being m the electron mass. Since $p^2 = p_r^2 + M^2/r^2$, the positions (1,2) $p_r \to \Delta p_r$ and $r \to \Delta r$ yield $\varepsilon = \Delta p_r^2/2m + M^2/2m\Delta r^2 - Ze^2/\Delta r$. Two numbers of states, i.e. two quantum numbers, are expected because of the radial and angular uncertainties. Eqs (1,1) and the previous result yield $\varepsilon = n^2\hbar^2/2m\Delta r^2 + l(l+1)\hbar^2/2m\Delta r^2 - Ze^2/\Delta r$ that reads $\varepsilon = \varepsilon_o + l(l+1)\hbar^2/2m\Delta r^2 - E_o/n^2$ with $E_o = Z^2e^4m/2\hbar^2$ and $\varepsilon_o = (n\hbar/\Delta r - Ze^2m/n\hbar)^2/2m$. Minimize ε putting $\varepsilon_o = 0$, which yields $\Delta r = n^2\hbar^2/Ze^2m$ and $\varepsilon = [l(l+1)/n^2 - 1]E_o/n^2$; so $l \le n-1$ in order to get $\varepsilon < 0$, i.e. a bound state. Putting thus $n = n_o + l + 1$ one finds the electron energy levels $\varepsilon_{el} = -E_o/(n_o + l + 1)^2$ and the rotational energy $\varepsilon_{rot} = l(l+1)E_o/n^4$ of the atom as a whole around O. Hold also here all considerations introduced for the angular momentum, in particular it appears that the range sizes do not play any role in determining the energy levels. The physical meaning of Δr, related to the early Bohr radius, appears noting that

$$\varepsilon_{el} = -\frac{E_o}{n^2} = -\frac{Ze^2}{2\Delta r}, \quad \Delta r = \frac{n^2\hbar^2}{Ze^2m}, \quad E_o = \frac{Z^2e^4m}{2\hbar^2}, \quad (1,3)$$

i.e. ε_{el} is due to charges of opposite sign delocalized within a diametric distance $2\Delta r$ apart. As previously stated, nucleus and electron share a unique uncertainty radial range: in general, the greater m, the closer its delocalization extent around the nucleus. Also note that n and l are still properties of the phase space, but now they describe the whole quantum sys-

tem "nucleus + electron" rather than the nucleus and the electron separately. Since the first eq (1,3) does not depend explicitly on the kind of particles forming the concerned hydrogenlike atom, m or the reduced mass are actually hidden into Δr; it is possible to link ε_{el} to the known condition $n\lambda = 2\pi\Delta r$, according which an integer number of steady electron wavelengths is defined along a circumference of radius Δr. For such electron waves one finds

$$\varepsilon_{el} = -\frac{\pi Z e^2}{n\lambda} = -\frac{\alpha}{n}\frac{Z p_\lambda c}{2}, \quad p_\lambda = \frac{h}{\lambda}, \quad \alpha = \frac{e^2}{\hbar c}. \qquad (1,4)$$

Note that introducing α to express the quantum energy levels compels defining the De Broglie momentum. Even in this form ε_{el} is still related to the reduced mass of the system, which can be introduced via the momentum p_λ; thus eq (1,4) holds in general for any system of charges. Moreover, the factor $Z/2$ apart, appears interesting that the energy levels of the system ε_{el} are linked to the kinetic energy $p_\lambda c$ of the running electron wave circulating along the circumference of radius Δr via the coefficient α/n. On the one hand, this result emphasizes the electromagnetic character of the interaction between electron and nucleus; on the other hand, the key role of the quantum uncertainty in determining the allowed energy levels of eqs (1,3) also evidences the kind of interaction itself. The more general question that arises at this point is therefore: do eqs (1,1) provide themselves any hint also about the physical essence of the fundamental interactions? The standard model [8-11] provides a satisfactory description of the fundamental forces of nature. So the present paper does not aim to replicate the electro-weak model or the chromodynamics, which indeed would be useless and unexciting; nevertheless seems useful to propose a simplified approach aimed to show (i) that the fundamental interactions are inferable from eqs (1,1) only and (ii) that exists a unique conceptual root common to all fundamental interactions. This task is in effect particularly valuable because the present model has already accounted for the gravity force [7] and for the basic principles of special and general relativity.

The purpose of the paper is to examine the ability of eqs (1,1) to describe also other kinds of possible interactions and their relative strengths at comparable energies; it will be also shown that further information is obtained about the vector bosons associated with the respective kinds of interactions. Therefore the worth of the present paper rests mostly on the chance of finding concepts today known as fingerprints of the electroweak and strong interactions in the frame of a unique logical scheme based on the quantum uncertainty and including the relativity. The paper [7] has somewhat concerned the electromagnetic interactions, while also showing that all concepts of quantum wave formalism are indeed obtained through the present approach. Here we concern in particular the weak and strong interactions between nuclear and subnuclear particles. The next sections will describe the possible features of these interactions.

2 Physical background of the interactions

Let us show that the concept of interaction relies in the frame of the present model entirely on eqs (1,1). Consider first an isolated particle of mass m and momentum component p_x^∞ free to move in an ideal infinite range. When confined in a time-space uncertainty range Δx, however, its energy changes by an amount $\Delta\varepsilon$ given by

$$\Delta p_x^2/2m = (n\hbar)^2/2m\Delta x^2, \qquad \Delta p_x = p_x^{conf} - p_x^\infty;$$

i.e. Δp_x is by definition the range including any change of local momentum component p_x occurring when the free particle turns from a non-confined to a confined state within Δx.

Since no process occurs instantaneously in nature, let Δt be the confinement time range corresponding to Δp_x: to the confinement process corresponds thus the arising of a force field whose component $\Delta F_x = \Delta p_x/\Delta t = F_x^{conf} - F_x^\infty$ is related to $\Delta\varepsilon$, being clearly $\Delta F_x = \Delta\varepsilon/\Delta x = \Delta p_x^2/2m\Delta x^3$. By definition ΔF_x includes any random $F_x^\infty \le F_x \le F_x^{conf}$: in the present model the local dynamical variables are replaced by corresponding ranges of values, so the classical force F_x at the local coordinate x is replaced by a range of possible forces active within Δx. Actually the result $\Delta p_x/\Delta t = \Delta\varepsilon/\Delta x$ could have been inferred directly from eqs (1,1) without need of any remark; yet these considerations highlight that a force field in a space time uncertainty range is the only information available on the particle once accepting the eqs (1,1) as the unique assumption of the model.

Clearly, once concerning one particle only, energy and force component cannot be related to any form of interaction; rather both have mere quantum origin. Also, $\Delta\varepsilon$ and ΔF_x tend obviously to zero for $\Delta x \to \infty$; hence if p_x^∞ changes to p_x^{conf} concurrently with the arising of a force component acting on the particle, then p_x^∞ must be constant by definition as it represents the momentum of the particle before its confinement driven perturbation. This again appears from the standpoint of eqs (1,1): $\Delta x \to \infty$ requires $\Delta p_x \to 0$ for any finite number of states regardless of Δt. Since an uncertainty range infinitely small tends to a unique classical value of its corresponding quantum random variable and since this holds regardless of Δt, then the limit value must be a constant: so $p_x^\infty = const$ corresponds by necessity to $F_x^\infty = 0$.

Despite the present model allows reasoning on ΔF_x only, a first corollary is the inertia principle that holds for a lonely particle in an infinite space time delocalization range. Other interesting consequences follow for any finite $\Delta x = x_2 - x_1$: the notation emphasizes that instead of considering the particle initially in an infinite unconfined range, we are now interested to describe its behavior in a confined state, e.g. in the presence of two infinite potential walls Δx apart. Clearly this means introducing the corresponding $\Delta p_x = p_2^{conf} - p_1^{conf}$: again the eqs (1,1) compel writing $\Delta\varepsilon/\Delta x = \Delta p_x^2/2m\Delta x^3$ when p_x^∞ has turned into a local $p_1^{conf} \le p_x \le p_2^{conf}$, which entails once more $\Delta F_x = \Delta p_x/\Delta t$ within Δx. These ideas are

now extended to the interaction forces. Rewrite first the force field component $\Delta\varepsilon/\Delta x = \Delta p_x^2/2m\Delta x^3$ of a particle confined within Δx as follows

$$\Delta F_x = \frac{\hbar^2}{2}\frac{n}{m}\frac{n}{V}, \qquad V = \Delta x^3. \tag{2,1}$$

Even the one-dimensional case defines the delocalization volume V because, being Δx, Δy and Δz arbitrary, any value allowed to $\Delta x\Delta y\Delta z$ is also allowed to Δx^3. Is crucial the fact that the range of each force component is proportional to n/m, number of allowed states per unit mass, times n/V, number of allowed states per unit delocalization volume. Consider now two free particles a and b in their own uncertainty ranges Δx_a and Δx_b; hold separately for them the relationships $\Delta\varepsilon_a = (n_a\hbar)^2/2m_a\Delta x_{xa}^2$ and $\Delta\varepsilon_b = (n_b\hbar)^2/2m_b\Delta x_{xb}^2$. These particles are non-interacting, as their n_a and n_b are assumed independent each other like Δx_a and Δx_b themselves; nothing in these equations accounts for the most typical and obvious consequence of any kind of interaction, i.e. some relationship between their allowed states or between their delocalization ranges. Two free particles do not share by definition any kind of link, any possible coincidence of allowed states would be accidental and transient only. Consider now their possible interaction; a reasonable chance of linking their allowed states is to assume, for instance, that the particles share the same uncertainty range. If Δx is unique for both particles, then their allowed states must be somehow linked because of eqs (1,1); in other words, even being still $n_a \neq n_b$, the random values of local momentum components p_{xa} and p_{xb} are subjected to the constrain $n_a/\Delta p_{xa} = n_b/\Delta p_{xb} = \Delta x/\hbar$. Note for instance that Δr of eq (1,3) includes by definition all possible distances between electron and nucleus, which implicitly means that both particles share the same uncertainty range where the interaction occurs; so n and l characterizing the electron energy levels of the hydrogenlike system result from the change of the early quantum numbers, e.g. n^{free} and $l^{free} = 0$, owned by each particle independently of the other before interaction. In this respect two relevant points are: (i) the interaction driven change δn of the number n of states and (ii) the physical meaning of the related $\delta[(n/m)(n/V)]$.

As concerns the point (i), consider $\Delta\varepsilon\Delta t = n\hbar$ in an arbitrary reference system R and let n be allowed to change from any initial value n_1 to any successive value n_2 during a fixed time range Δt; whatever n_1 and n_2 might be, this is admissible because Δt is arbitrary. The notation emphasizes that a given value of $\delta n = n_2 - n_1$ is obtainable regardless of the initial value n_1 because n_2 is arbitrary; so $\delta n = 1, 2, ..$ anyway, regardless of the specific value of n_1. Calculate next the change $\delta\Delta\varepsilon$ of $\Delta\varepsilon$ as a function of δn during Δt, which reads now $(\Delta\varepsilon_{n_2} - \Delta\varepsilon_{n_1})/\Delta\varepsilon_{n_1} = \delta n/n_1$ with obvious meaning of symbols. Note that in general the series expansion of $\log(\Delta\varepsilon)$ around $\log(\Delta\varepsilon_{n_1})$ reads

$$\log(\Delta\varepsilon_{n_2}) = \log(\Delta\varepsilon_{n_1}) + \frac{\Delta\varepsilon_{n_2} - \Delta\varepsilon_{n_1}}{\Delta\varepsilon_{n_1}} - \frac{1}{2}\left(\frac{\Delta\varepsilon_{n_2} - \Delta\varepsilon_{n_1}}{\Delta\varepsilon_{n_1}}\right)^2 + ..$$

so that

$$\log\left(\frac{\Delta\varepsilon_{n_1+\delta n}}{\Delta\varepsilon_{n_1}}\right) = \frac{\delta n}{n_1} - \frac{1}{2}\left(\frac{\delta n}{n_1}\right)^2 + \frac{1}{3}\left(\frac{\delta n}{n_1}\right)^3 - ..$$

$$\Delta\varepsilon_{n_1} = \frac{n_1\hbar}{\Delta t}, \quad \delta n = 1, 2, \ldots \tag{2,2}$$

This equation describes the size change of the energy range $\Delta\varepsilon_{n_1}$ as long as the number of allowed states increases with respect to the initial value n_1: so $\Delta\varepsilon_{n_1+\delta n}$ with $\delta n = 1$ describes the first increment of energy range size with respect to $\Delta\varepsilon_{n_1}$, then $\delta n = 2$ the next size increment and so on; in short, eq (2,2) describes how are modified the random local values $\varepsilon_{n_1+\delta n}$ included in $\Delta\varepsilon_{n_1+\delta n}$ at δn progressively increasing. Instead $\Delta\varepsilon_{n_1}$ plays here the role of a fixed reference range with respect to which is calculated $\Delta\varepsilon_{n_1+\delta n}$. For reasons that will be clear in the next section 5, it is mostly interesting to examine the particular case of n_1 such that

$$\Delta\varepsilon_{n_2} - \Delta\varepsilon_{n_1} << \Delta\varepsilon_{n_1}, \qquad \delta n/n_1 << 1. \tag{2,3}$$

Let us truncate thus the series expansion (2,2) at the first order of approximation under the assumption (2,3) and simplify the notation putting $i = \delta n$; one finds (i=1,2,...)

$$n_1 \log\left(\frac{\Lambda_i}{\Lambda}\right) = i, \qquad \Lambda_i = \Delta\varepsilon_{n_1+\delta n}, \qquad \Lambda = \Delta\varepsilon_{n_1}. \tag{2,4}$$

Despite the generality of eqs (2,2), is particularly significant for the purposes of the present paper the case of a quantum system consisting of an arbitrary number of particles, each one delocalized in its own uncertainty range: if these latter are non-interacting, then let the energy of the system be included within the range $\Delta\varepsilon_{n_1}$ and be n_1 its total number of states; if instead all particles are delocalized in the same space-time range, then their interaction changes the energy range of the system to $\Delta\varepsilon_{n_1+\delta n}$ characterized of course by a new number of states $n_2 = n_1 + \delta n$.

As concerns the point (ii), we expect according to eq (2,1) that from $\Delta\varepsilon_a$ and $\Delta\varepsilon_b$ of the two free particles follow because of the interaction the changes $\delta\Delta\varepsilon_a = (\hbar^2/2)\delta(n_a^2/m_a\Delta x_a^2)$ and $\delta\Delta\varepsilon_b = (\hbar^2/2)\delta(n_b^2/m_b\Delta x_b^2)$. The expressions of the corresponding changes of the initial confinement force components $\Delta F_{xa} = \Delta\varepsilon_a/\Delta x_a$ and $\Delta F_{xb} = \Delta\varepsilon_b/\Delta x_b$ from the non-interacting to the interacting state read thus

$$\delta\Delta F_{xa} = (\hbar^2/2)\delta\left[(n_a/m_a)(n_a/V_a)\right]$$

$$\delta\Delta F_{xb} = (\hbar^2/2)\delta\left[(n_b/m_b)(n_b/V_b)\right].$$

These equations agree with the previous idea, i.e. the forces are related to changes of the allowed numbers of states per unit mass and delocalization volumes of the particles a and b: in effect the interaction between two particles consists of forces acting on both of them and requires that the respective numbers of states are affected as well. More precisely

$\delta[(n/m)(n/V)]$ means that are modified during the interaction not only the states allowed to the particles themselves, but also that of the delocalization space surrounding them. Clearly the former are consequences of the latter. In other words, the fact that $\delta(n/m)$ requires explicitly also the concurrent $\delta(n/V)$ compels thinking: (i) that a particle interacts with another particle because it generates a field that propagates outwards through the space volume V and (ii) that just in doing so this field changes the number of states allowed to the other particle; i.e. the changes of number of states of each particle are somehow correlated, as previously stated. Since no event occurs instantaneously in nature, $\delta(n/V)$ requires an appropriate time range to be realized, i.e. the propagation rate is finite in agreement with the existence of an upper limit obliged by eqs (1,1) [7]; in this way the interaction exchanges information about physical features and strength of the related force between particles. The most natural way to acknowledge this way of regarding two interacting particles is to admit that they exchange intermediate virtual particles that propagate, whence $\delta(n/V)$, and carry the necessary information that affects in turn the real particles themselves, whence $\delta(n/m)$; indeed n defining n/V is the same as that defining n/m, i.e. the change $\delta(n/m)$ of states allowed to the particle is actually just that $\delta(n/V)$ of the space around it. Strictly speaking, however, one should say more appropriately space-time, and not simply space: indeed Δx defining V in eq (2,1) is actually $\Delta x = \Delta x(\Delta t)$ because of eqs (1,1) themselves. So the finite time range required for $\delta(n/m)$ to occur is nothing else but the finite time range required to propagate $\delta(n/V)$ and to come back, i.e. to allow exchanging the interaction carriers. Interaction force and propagation of force carriers through V are therefore according to eq (2,1) two basic aspects of the interaction. In principle these carriers could be massive or massless, in which case one expects $(\hbar^2c^2)\delta[(n/\varepsilon)(n/V)]$, but they must have anyway boson character in order that the aforesaid forces affect the allowed states of the interaction partners while minimizing their exchange energy. It has been already demonstrated in [7] that as a consequence of eqs (1,1) integer or half-integer spin particles have a different link to the respective numbers of allowed states: an arbitrary number of the former can be found in a given quantum state, instead one particle only of the latter kind can be found in a given quantum state. Consider a multi-body interaction, where an arbitrary number of force carriers is to be expected: fermion carriers would require a corresponding number of quantum states with energy progressively increasing, whereas a unique ground state allows any number of boson carriers; as it will be shown below, the former case would be incompatible with a unique amount of energy to be transferred between all interacting particles and thus with at a minimum transfer energy. The corpuscles that mediate the fundamental forces of nature are indeed well known in literature as vector bosons, which also suggests the existence of a pertinent boson energy field. An interesting consequence of eq (2,1) comes from the chance of rewriting it as $(m/n\hbar)\Delta F_x = (\hbar/2)(n/V)$. Note that at left hand side appears the ratio $\hbar/m$ having physical dimensions of diffusion coefficient; write therefore $\Delta F_x = D^* n\hbar/2V$ with $D^* = n\hbar/m$. Moreover the fact that the physical dimensions of F/D^* are $mass/(length \times time)$ suggests the position

$$\frac{\Delta F_x}{D^*} = \frac{\hbar}{2}\frac{n}{V} = \frac{du_\omega}{d\omega}, \quad D^* = \frac{n\hbar}{m}, \tag{2,5}$$

having at the moment mere formal meaning: if ω represents a frequency and u_ω an energy density, the physical dimensions of both sides are $energy \times time/volume$. So $\Delta F_x = D^* du_\omega/d\omega$ agrees with the idea that the force field is due to a diffusion-like flux of particles. This appears properly handling $du_\omega/d\omega$: indeed it is possible to write $du_\omega/d\omega = \omega V d\mathrm{C}/dx$ once more via dimensional requirement, being $\mathrm{C} = m/V$ or $\mathrm{C} = \varepsilon/c^2V$ the concentration of massive or massless carriers. Hence $\Delta F_x = \omega V D^* d\mathrm{C}/dx$ i.e. $\Delta F_x = -\omega V J_x$; the minus sign means of course an incoming flux of messenger particles if $J_x > 0$, yet both signs possible for $d\mathrm{C}$ reveal a complex fluctuation driven space distribution of interaction carriers randomly moving forwards and backwards between the real particles. This result is easily understood: in a volume V where are delocalized interacting particles, boson carriers with density C are exchanged at frequency ω according to a Fick-like law that generates the force field ΔF_x; the flow J_x of vector bosons crosses an ideal plane perpendicular to the flow moving at rate $\omega\Delta x$ consistently with an energy $\Delta F_x \Delta x/V$ per unit volume. The diffusion coefficient of the bosons is quantized. In [12] has been demonstrated the quantum nature of the diffusion process and also the link between particle flow and concentration gradient driven Fick's law, as a consequence of which the statistical nature of the entropy also follows; this latter result is further inferred in the next section 7 in an independent way, see eqs (7,7). Eq (2,5) is immediately verifiable considering the cubic volume $V = \Delta x^3$ of space of eq (2,1) filled with photons. Let $\Delta x = \lambda$ be the longest wavelength allowed in V to a steady electromagnetic wave with nodes at the opposite surfaces of the cube, whose side is therefore $\lambda/2$; thus $V = (\lambda/2)^3$, whereas $u_\omega = (\hbar\omega/2)/V$ is the corresponding zero point energy density of the oscillating electromagnetic field. So, with $\lambda = c/\nu$ one finds $du_\omega = 4n(\nu/c)^3\hbar d\omega$; since by definition $\hbar d\omega = h d\nu$, and thus $du_\omega = (2\pi)^{-1} du_\nu$, this result reads $du_\nu = (8\pi(\nu/c)^3 h d\nu)n$. In section 7 it will be shown that the number of states n allowed to the photons trapped within the cube is given by $(\exp(h\nu/kT) - 1)^{-1}$, whence the well known result

$$\frac{du_\nu}{d\nu} = \frac{8\pi h\nu^3}{c^3}n, \qquad n = \frac{1}{\exp(h\nu/kT) - 1}. \tag{2,6}$$

It is interesting the fact that the black body law comes immediately from the same idea that shows the existence of messenger bosons mediating the interaction between particles. Clearly Δx^3 represents the black body volume.

Recall now that, in agreement with the arbitrariness of n, the ranges of eqs (1,1) can be regarded as arbitrary functions of time through Δt; read for instance $\Delta x = x - x_o$ with $x = x(\Delta t)$ and $x_o = x_o(\Delta t)$, being in general $x(\Delta t)$ and $x_o(\Delta t)$ different time functions. Of course no hypothesis is necessary about these functions, which are undefined and undefinable. Hence the size of Δx is in general an arbitrary function of time itself, whereas the concept of derivative relies in the frame of eqs (1,1) only as mere ratio of uncertainty ranges. This idea generalizes the previous definition of force field $\Delta F_x = F_x^{conf} - F_x^{\infty}$. For instance $\Delta p_x/\Delta t$ takes the physical meaning of force field component $\Delta\varepsilon/\Delta x$ generated within Δx by the change rate of all p_x compatible with Δp_x during Δt, whatever the physical reason affecting p_x might be. Moreover, being the range sizes arbitrary, these ratios can even take the local physical meaning elucidated by the familiar notations $\Delta\varepsilon \to d\varepsilon$, $\Delta t \to dt$ and $\Delta p_x \to dp_x$. In other words, the local concept of derivative is here a particular case of that of ratio of arbitrarily sized uncertainty ranges. There is no contradiction between $\Delta\varepsilon/\Delta t$ and $d\varepsilon/dt$, which have both mere conceptual meaning and in fact are both indeterminable: the former because of the arbitrariness of the range boundaries, the latter because the local variables p_x and t around which shrink the respective ranges are arbitrary as well. The consistency of this position with the concept of covariancy has been concerned in [7]; in this paper and in [4] has been also shown that just the evanescent concept of distance required by the agnostic positions (1,2) in fact determines the non-locality of the quantum world. Exploit now eqs (1,1) to calculate in any reference system R an arbitrary size change $d\Delta p_x$ of $\Delta p_x = p_x - p_{ox}$ as a function of that, $d\Delta t$, of the time uncertainty range Δt, assuming that n remains constant during $d\Delta t$; hence during $d\Delta t$ the size of Δx necessarily changes by an amount $d\Delta x$ as well. Of course this reasoning can be reversed: a force field arises within the space-time range Δx because of its deformation $d\Delta x$ that in turn, because of eqs (1,1), requires the momentum range Δp_x deformation as well [7]. Is evident the link of these ideas with the foundations of relativity. Differentiating eqs (1,1) and dividing by $d\Delta t$, one finds $d\Delta p_x/d\Delta t = -(n_x\hbar/\Delta x^2)(d\Delta x/d\Delta t)$. Of course, in R' one would obtain $d\Delta p'_x/d\Delta t' = -(n'_x\hbar/\Delta x'^2)(d\Delta x'/d\Delta t')$; yet any consideration carried out about the unprimed equation can be identically carried out on the primed equation. In the present model there is no local value defined in R that changes into a new value in R', while any uncertainty range undefined in R remains undefined in R' too; so considering primed and unprimed range sizes means actually renaming a unique undefined range. The same holds of course for the ratios of any two ranges. If in particular $\Delta t = t - t_o$ is defined with constant t_o, since actually even this latter could be itself a function of t without changing anything so far introduced, then one finds in any R

$$\frac{d\Delta p_x}{dt} = -\frac{n_x\hbar}{\Delta x^2}v'_x = F_x - F_{ox}, \qquad (2,7)$$

$$F_x = \dot{p}_x, \qquad F_{ox} = \dot{p}_{ox}, \qquad v'_x = \frac{d\Delta x}{d\Delta t}.$$

Having replaced any local distance x with the uncertainty range Δx including it, the local force F_x is replaced by a corresponding range ΔF_x including local values of force. The notation n_x emphasizes that the arbitrary number n of states refers here to the x components of $\Delta\mathbf{p}$, $\mathbf{v}'$, $\mathbf{F}$ and $\mathbf{F}_o$; of course are likewise definable n_y and n_z too. Moreover note that v'_x is conceptually different from v_x introduced in section 1: despite both have formally physical dimensions of velocity, the latter only is the actual average velocity of any real particle traveling through its delocalization range Δx during Δt, the former is the deformation extent $d\Delta x$ of Δx during the time increment $d\Delta t$. So v_x is self-defined without need of further considerations, the physical meaning of v'_x is instead strictly related to that of F_x concurrently inferred. This distinction is inherent the character of the present theoretical model that, as previously remarked, concerns the uncertainty ranges of the phase space where any particle could be found rather than the particle itself; however the examples of the angular momentum and hydrogenlike energy levels have shown that working on the uncertainty ranges that define a physical property allows to gain information on the related behavior of the particle and on the given law itself. Eqs (2,7), reported here for clarity, have been early introduced in [7] and therein exploited to infer as a corollary in the particular case of constant p_{ox} (i) the equivalence principle of general relativity, (ii) the coincidence of gravitational and inertial mass and then (iii) the Newton gravity law as a particular case; actually this law results to be the first order approximation of a more general equation allowing to calculate some interesting results of general relativity, for instance the perihelion precession of planets.

Also in the present model, therefore, the deformation of the space time quantum delocalization range entails the arising of a force as a corollary of eqs (1,1). In this paper we propose a further way of handling eq (2,7): in agreement with the purpose of this paper, i.e. to infer various forms of interaction between particles from a common principle, it is enough to rewrite eqs (2,7) in different ways and examine the respective consequences. The fine structure constant α enables $\hbar$ to be eliminated from eqs (2,7), which read in c.g.s. units for simplicity

$$F_x - F_{ox} = \pm\frac{e'e}{\Delta x^2}, \qquad e' = \pm\frac{n_x v'_x}{\alpha c}e. \qquad (2,8)$$

Here $\Delta F_x = F_x - F_{ox}$ is the force field between two charges e and e' interacting through their linear charge densities $e/\Delta x$ and $e'/\Delta x$: i.e. even the electric interaction force relies on a physical basis similar to that of the gravity force. The double sign accounts for both chances that Δx expands or shrinks at deformation rate $\pm v'_x$, which is a decisive parameter to express the respective states of charge. If $v'_x = 0$ then $e' = 0$, i.e. it corresponds to a chargeless particle; of course the related electric force is null, i.e. $F_x = F_{ox}$ accounts for

other forces possibly acting on the particle, for instance the gravity; this case, concerned in [7] to emphasize the link between quantum theory and relativity, is skipped here. Moreover holds an obvious boundary condition on n_x, i.e. a value of n_x must necessarily exist such that $e' = \pm e$. Be n' this value such that by definition $n'v'_x = \alpha c$; being n'_x arbitrary integer and v'_x arbitrary as well, this position is certainly possible. Then

$$e' = \pm(n_x/n')e. \qquad (2,9)$$

Here the double sign agrees with the chances allowed for e depending on the expansion or contraction of Δx. It is reasonable to assume that $n' = 3$; considering also the deformation rates $\pm v'_y$ and $\pm v'_z$ of Δy and Δz defined likewise to v'_x, the number of states is actually counted as $n' = n_x + n_y + n_z$ with ground values $n_x = n_y = n_z = 1$, while being $1 \leq n_{xi} \leq n'$ depending on the number of respective force components $F_{xi} - F_{oxi}$ actively contributing to n'. Consider first the x-component, eq (2,7), only. If $n_x = n' = 3$, then $e'_{(3)} = \pm e$ corresponds to electron and proton charges; $F_x - F_{ox}$ of eq (2,8) is the related Coulomb force component. The case $n_x = 2$ yields $e'_{(2)} = \pm(2/3)e$, whereas $n_x = 1$ yields $e'_{(1)} = \pm(1/3)e$; accordingly $F_x - F_{ox}$ must have a characteristic physical meaning that will be concerned in section 5. The same result would be obtained considering the y or z components corresponding to eq (2,7). Hence fractional charges are in principle to be expected in nature. It is easy guess how many particles with fractional charges, the well known quarks, are to be expected. Consider the four chances corresponding to the double signs of $e'_{(1)}$ and $e'_{(2)}$ and the three deformation rates v'_x, v'_y and v'_z; the previous discussion has exemplified the link of e' with v'_x only, yet an analogous reasoning holds of course also for v'_y and v'_z. Instead three different situations are in general compatible with $e'_{(1)}$ and $e'_{(2)}$ when (i) $v'_x \neq 0$ only, (ii) $v'_x \neq 0$ and $v'_y \neq 0$ only, (iii) $v'_x \neq 0$ and $v'_y \neq 0$ along with $v'_z \neq 0$ too. Since n_x, n_y, n_z are independent and arbitrary, one could replace the second eq (2,8) for instance with $\pm n_x v'_x/\alpha c \pm n_y v'_y/\alpha c$, obtaining thus $\pm(n_x \pm n_y)/n'$ as done to infer eq (2,9); then one could combine n_x and n_y in order to obtain again ratios having the same values $\pm 1/3$ and $\pm 2/3$ previously found, but involving now both v'_x and v'_y instead of v'_x only. Analogous considerations hold for the case (iii) that involves also v'_z. In (i) the vector $\mathbf{F} - \mathbf{F}_o$ is oriented along one of the axes, here the x-axis, in (ii) it lies on one coordinate plane, here the $x-y$ plane; the components of $\mathbf{F} - \mathbf{F}_o$ arbitrarily oriented correspond in general to (iii), whereas a null vector is instead related to $\mathbf{v}' = 0$ i.e. $e' = 0$. Anyway, whatever the linear combination of v'_x, v'_y and v'_z might be, it is reasonable to think that these ways of inferring $e'_{(1)}$ and $e'_{(2)}$ are physically different from that involving v'_x only; otherwise stated, to the various ways of finding a given kind of charge correspond different particles. With the aforesaid 3 chances for each sign of $e'_{(1)}$ and $e'_{(2)}$ we expect therefore a variety of 12 particles in total. Since this number is reasonably expected to include particles and antiparticles, a sensible conclusion is that we should have 6 quarks and 6 antiquarks: for instance, to the $(n_x - n_y)e/n'$ quark charge corresponds the $(n_y - n_x)e/n'$ antiquark charge. Now the first problem is how to sort the charge signs between particles and antiparticles; in principle one could think the former as the ones having $e'_{(1)} = +e/3$ and $e'_{(2)} = +2e/3$, the latter as the ones with both negative signs. In this way, however, considering all values of charges compatible with n from 1 to n', one should conclude that in nature the mere charge signs discriminate particles and antiparticles. Since this is not the case, it is more sensible to expect that $e'_{(1)} = -e/3$ and $e'_{(2)} = +2e/3$, for instance, identify quarks whereas the inverted signs identify the corresponding antiquarks: likewise exist as a particular case particles with either integer charge whose antiparticles have either opposite charge.

Moreover if two charge states $-e/3$ and $+2e/3$ are consistent with six particles physically distinguishable, then each quark requires three chances of a new property, which is indeed well known and usually called color charge: each quark can exist in three quantum states, i.e. it can take three different color states. Being the quarks characterized by several quantum numbers, this way of justifying their number does not mean a specific color uniquely assigned to each one of them; rather it means introducing a number of internal freedom degrees of color that make two fractional charges consistent with six distinguishable particles. Anyway, since also anti-quarks exist for which hold the same considerations, three anti-colors must exist too.

Eventually, let us calculate how many kinds of bosons are necessary to describe the interactions between quarks via boson exchanges able to modify their initial color states. Consider for instance a charmed meson identically symbolized as $\{c\bar{c}\}$ or $\{\bar{c}c\}$ and assume that each boson mediating the quark interaction is specifically entrusted with changing one couple color-anticolor only: let for instance the exchange of one boson turn r into $\bar{r}$ and vice-versa. The mesons $\{c\bar{c}\}$ and $\{\bar{c}c\}$, formally obtained by quark-antiquark and antiquark-quark exchanges, are clearly identical and indistinguishable. Imagine therefore of turning all colors of c, whatever they might be, into the corresponding anticolors of $\bar{c}$, whose anticolors are at once turned into the respective colors. How many exchanges of color states into the respective anticolor states are consistent with the identity of $c\bar{c}$ and $\bar{c}c$? Given two objects, c and $\bar{c}$, each one of which can be found in three quantum states, the three colors, the trivial answer is 2^3; eight exchanges are not only enough to turn all color states of c into the respective anticolor states, which means by definition obtaining $\bar{c}$ from c, but also purposely necessary, as each single exchange generates a new quantum configuration of states physically distinguishable from that previously existing. Since a total of eight color-anticolor exchanges are required to account for as many different configurations, eight is also the number of different bosons required to make the aforesaid couple of identical mesons effectively indistinguishable. These different chances

of interaction, each one characterized by its own specific energy, should be someway correlated to and described by the existence of as many such particles representing the possible exchanges, i.e. just eight vector bosons. Also these particles are well known and usually called gluons. Is this reasoning extensible also to three-quark particles like neutron or proton? The quark-gluon plasma of these latter is necessarily more complex than that of the mesons, so the question arises whether the 8 gluons previously introduced are enough to describe also such three quark systems. Consider the proton uud and the antiproton $\overline{uu}\overline{d}$. The conversion $uu \to \overline{uu}$ has been already described. As concerns $d \to \bar{d}$, still holds an analogous reasoning: a specific kind of gluon undertakes to change one color into the anticolor, another kind of gluon does the same with another color and so on. However the kind of gluon exchanges that turns red into antired of the quark u cannot differ from that acting similarly on the quark d: it would mean that each gluon "recognizes" its own quark on which to act, i.e. we should admit that different $\delta(n/m)$ require different $\delta(n/V)$ depending on the respective m. But nothing in the previous eq (2,1) allows this conclusion, rather it seems true exactly the contrary because Δx defining V has nothing to do with m therein delocalized: indeed, as above stated, the indistinguishability of identical particles is just due to the possibility that any particle could be found in a given range. So it is more reasonable to think that each kind of gluon exchange affects a specific color, not the color of specific quark only; otherwise stated, the total number of gluons in a nucleon is greater than that in a meson without necessarily compelling a new kind of gluons, i.e. any gluon in the tree-quark system turns one specific color regardless of whether that color is of a quark d or u. This way of thinking allows that the gluons transmit the interaction between different quarks modifying their $\delta(n/m)$, i.e. their color quantum states, regardless of m. So, when counting the number of different gluons that allow the three-quark particle/ antiparticle exchanges the result is the same as that previously computed.

These short remarks are enough for the purposes of the present paper; further considerations on other properties like strangeness, isospin and so on, whose conservation rules are necessary for instance to describe the decay of complex particles consisting of two or three quarks, are well known and thus omitted here for brevity. The remainder of the paper aims to describe the fundamental interactions by implementing the ideas hitherto exposed.

3 The quantum interactions

Divide all sides of eqs (1,1) by $e^2\Delta x$ and recall that in general $\Delta p_x = (v_x/c^2)\Delta\varepsilon$. An intuitive hint to this equation, already concerned in [7] and important also for the present purposes, is quickly reported here for completeness. Let in an arbitrary reference system R a photon travel at speed c through an arbitrary delocalization range $\Delta x^{(c)}$, so that eqs (1,1) read $\Delta x^{(c)}\Delta p_x^{(c)} = n^{(c)}\hbar = \Delta t^{(c)}\Delta\varepsilon^{(c)}$; the superscripts emphasize that the ranges are sized in order to fulfill this delocalization condition during an appropriate time range $\Delta t^{(c)}$. Then $c\Delta p_x^{(c)} = \Delta\varepsilon^{(c)}$. To find how scale the sizes of the momentum and energy ranges with respect to $\Delta p_x^{(c)}$ and $\Delta\varepsilon^{(c)}$ in the case of a massive particle traveling at slower rate $v_x < c$ through $\Delta x^{(c)}$, write $\Delta x^{(c)}\Delta p_x^{(v)} = n^{(v)}\hbar = \Delta t^{(c)}\Delta\varepsilon^{(v)}$. Since neither v_x nor c appear explicitly in this equation, it is also possible to write $n^{(v)}\hbar = \Delta t^{(c)}\Delta\varepsilon^{(c)} = \Delta t^{(v)}\Delta\varepsilon^{(v)}$; this is indeed true if $\Delta t^{(c)}$ and $\Delta\varepsilon^{(c)}$ scale like $\Delta t^{(v)} = (c/v_x)\Delta t^{(c)}$, as it is reasonable, and $\Delta\varepsilon^{(v)} = (v_x/c)\Delta\varepsilon^{(c)}$. Replacing these positions in the former equation yields $\Delta x^{(c)}\Delta p_x^{(v)} = \Delta t^{(c)}(v_x/c)\Delta\varepsilon^{(c)}$ whence $c\Delta p_x^{(v)} = (v_x/c)\Delta\varepsilon^{(c)}$. Actually the superscripts can be omitted because they do not identify particular range sizes; both $\Delta p_x^{(v)}$ and $\Delta\varepsilon^{(c)}$ are indeed arbitrary like v_x itself. The superscripts are also irrelevant as concerns the functional relationship between the local values of the respective variables, which reads $p_x = (v_x/c^2)\varepsilon$ regardless of how the respective uncertainty ranges are defined. Note that p_x and ε, exactly determined in classical physics and in relativity, are instead here random values within the respective uncertainty ranges. Also note that an identical reasoning in R' solidal with the particle would yield $p'_x = (v'_x/c^2)\varepsilon'$: this is therefore a quantum expression relativistically invariant. This kind of reasoning has been carried out in [7] to show the connection between quantum mechanics and relativity. Now instead consider for the next discussion the following equations directly inferred from eqs (1,1)

$$\frac{n\hbar v_x}{\Delta x} = \Delta\varepsilon, \qquad v_x = \frac{\Delta x}{\Delta t}, \qquad v_x \le c. \tag{3,1}$$

The last position does not merely emphasize a feature in principle expected for any velocity, it takes a special relevance in the present context. Being $\Delta\varepsilon$ and Δx arbitrary, one could write $\Delta p_x = \Delta\varepsilon^o v_x^o/c^2$ too, with v_x^o and $\Delta\varepsilon^o$ still fulfilling the given Δp_x. The total arbitrariness of the range sizes plays a key role in the following reasoning based on $v_x\Delta\varepsilon = v_x^o\Delta\varepsilon^o$: if $v_x = c$, then necessarily $v_x^o < c$ and $\Delta\varepsilon^o > \Delta\varepsilon$. Examine step by step this point writing identically eq (3,1) as follows

$$\frac{e^2}{\Delta x} = \frac{\alpha}{n}\frac{v_x^o}{c}\Delta\varepsilon^o, \qquad \frac{v_x v_x^o}{c^2} = \frac{\Delta\varepsilon}{\Delta\varepsilon^o}, \qquad \Delta\varepsilon \le \Delta\varepsilon^o. \tag{3,2}$$

The last position emphasizes that both chances $\Delta\varepsilon^o = \Delta\varepsilon$ and $\Delta\varepsilon^o \neq \Delta\varepsilon$ are equally possible. If $\Delta\varepsilon = \Delta\varepsilon^o$, then $v_x = v_x^o$ compels concluding $v_x = v_x^o = c$ only; so eqs (2,7) and (3,2) yield $e^2/\Delta x = \chi\Delta\varepsilon$, being $\chi = \alpha/n$ a proportionality factor. This means correlating the potential energy $e^2/\Delta x$ of two electric charges to $\Delta\varepsilon$, introduced through Δp_x and thus having the meaning of kinetic energy range. On the one hand $\Delta\varepsilon^o \neq \Delta\varepsilon$ requires different v_x^o and v_x, thus both velocities or at least either of them smaller than c, whence the inequality; on the other hand, relating the physical meaning of the velocities hitherto introduced to that of the boson carriers that

mediate the interaction force between particles: $v_x^o = c$ requires massless bosons, $v_x^o < c$ massive bosons. Therefore the arbitrariness of $\Delta\varepsilon$ and $\Delta\varepsilon^o$ justifies the conclusion that either chance of range sizes prospects different results for eqs (3,2) and (3,1), despite their common origin from eqs (1,1). Two questions arise at this point: (i) whether these equations describe two different interactions or two different appearances of a unique interaction, (ii) whether or not it is possible to infer from both equations a relationship like $e^2/\Delta x = \chi\Delta\varepsilon$ despite their formal difference. The answers rely on the fact that in eq (3,2) appears explicitly the Coulomb charge e inherent the definition of α, in eq (3,1) it does not necessarily hold; nothing compels assuming that even the energy $n\hbar v_x/\Delta x$ is by necessity referable to a Coulomb energy.

If $n\hbar v_x/\Delta x$ does, then the common origin of these equations from eqs (1,1) is a good reason to expect that the chances of massive or massless vector bosons are merely two different ways of manifesting a unique kind of interaction; rewriting the inequality as $\Delta\varepsilon^o = \Delta\varepsilon + \delta\varepsilon$, with $\delta\varepsilon \geq 0$ of course arbitrary like $\Delta\varepsilon$ and $\Delta\varepsilon^o$, both chances are in principle acceptable depending on the amount of energy at which the interaction occurs. In other words $\delta\varepsilon > 0$ is an additional energy range motivated by the arbitrariness of $\Delta\varepsilon$, which indeed admits introducing also $\Delta\varepsilon^o$ too, and justifying the presence of massive vector bosons. By consequence the chance of finding a unique link like $e^2/\Delta x = \chi\Delta\varepsilon$ between potential and kinetic energies is to be reasonably expected; so, fixing an arbitrary $\Delta\varepsilon$ allows assessing via χ the relative strengths of both interactions at comparable values of $\Delta\varepsilon$ and respective characteristic lengths Δx. The physical consequences of this reasoning are exposed in section 4.

If instead $n\hbar v_x/\Delta x$ is an energy not referable to that between integer charges, in fact nothing hinders thinking that it is directly related to the aforesaid fractional charges; according to eq (2,8), $v_x = \Delta x/\Delta t$ is physically different from $v'_x = d\Delta x/d\Delta t$. Then eq (3,1) describes an interaction prospectively different from that of eq (3,2); so the former equation must be considered regardless of the latter to check what kind of physical information follows from the considerations of section 2. Also the consequences inferred from these equations are expectedly different; in particular the link χ between potential and kinetic energies should be reasonably different in either case just mentioned. In other words, χ can be compared for similar $e^2/\Delta x$ and $\Delta\varepsilon$ to characterize the relative strengths of the various kinds of interactions. The physical consequences of this reasoning are exposed in section 5.

These are the key ideas to be further highlighted below. The dual way of elaborating a unique principle, the statistical formulation of quantum uncertainty, has an intrinsic physical meaning coherent with the purposes of the present paper, i.e. to demonstrate that kinds of interaction apparently different are in fact consequences of a unique principle. In other words, eqs (3,2) and (3,1) are the starting point to distinguish two cases, which will be discussed separately under the only conceptual constraint of being mutually self-consistent. The following sections 4 and 5 aim to outline the respective ways to link the potential and kinetic energies.

4 The interaction according to eqs (3,1) and (3,2)

The following discussion concerns the ways to reduce the eqs (3,1) and (3,2), regarded together, to the form $e^2/\Delta x = \chi\Delta\varepsilon$ in both cases $\delta\varepsilon = 0$ and $\delta\varepsilon > 0$. Consider first $\delta\varepsilon = 0$, which requires $v_x^o = v_x = c$ and thus massless boson carriers. So the unique result possible is

$$\frac{e^2}{\Delta x} = \chi_{em}\Delta\varepsilon, \qquad \chi_{em} = \frac{\alpha}{n}. \tag{4,1}$$

Here α/n emphasizes the electromagnetic interaction in analogy with eq (1,4).

The further chance $\delta\varepsilon > 0$ requiring the condition $v_x^o < c$ prospects instead the presence of massive boson carriers; thus $\delta\varepsilon > 0$, related to the formation of massive carriers, represents reasonably the energy gap with respect to the former case of eq (4,1) involving massless carriers only. While heavy vector bosons are the physical consequence of the concurring inequalities $v_x^o < c$ and $\delta\varepsilon > 0$, the arbitrariness of v_x^o prevents the possibility of deciding a priori either chance for $\delta\varepsilon$ and compels the conclusion that a unique kind of interaction is actually compatible with both chances. It will be shown that the interaction energy related to the possible size of Δx discriminates either chance. Despite both chances are incorporated into a unique conceptual frame, further considerations are necessary in this case. Write the first eq (3,2) as follows

$$\frac{e^2}{\Delta x} = \frac{\alpha^2}{n^2}\frac{\Delta\varepsilon^o}{q^o}, \qquad q^o = \frac{e^2}{n\hbar v_x^o}, \qquad v_x < c. \tag{4,2}$$

Since eqs (3,2) require $\Delta\varepsilon^o/q^o = (c/v_x)(n/\alpha)\Delta\varepsilon$, the obvious inequality

$$(n/\alpha)^2 > v_x/c \tag{4,3}$$

yields $\Delta\varepsilon^o/q^o > (\alpha/n)\Delta\varepsilon$. Hence a value $q_w > q^o$ certainly exists such that

$$\Delta\varepsilon^o/q_w = (\alpha/n)\Delta\varepsilon. \tag{4,4}$$

Replacing this result into the first eq (4,2), one finds

$$\frac{e^2}{\Delta x_w} = \chi_w\Delta\varepsilon, \qquad \chi_w = \left(\frac{\alpha}{n}\right)^3, \qquad \Delta x_w = \frac{q_w}{q^o}\Delta x. \tag{4,5}$$

The first equation is formally analogous to eq (4,1) a scale factor q_w/q^o for Δx apart, while α/n is replaced by the much smaller quantity $(\alpha/n)^3$; hold however for χ_w considerations analogous to that previously carried out for χ_{em}, i.e. it links kinetics and potential energies. The explicit form of the inequality (4,3) reads $(n\hbar c)^2 > e^4(v_x/c)$, so that $(n\hbar c/\Delta x)^2 > (e^2/\Delta x)^2(v_x/c)$ and thus $(c\Delta p_x)^2 > (e^2/\Delta x)^2(c\Delta\varepsilon/v_x^o\Delta\varepsilon^o)$; as $c\Delta p_x = \Delta\varepsilon^o v_x^o/c$, i.e. $c\Delta p_x = (q_w v_x^o\alpha/nc)\Delta\varepsilon$ according to eq (4,4), the inequality (4,3) reads

$$(\zeta\Delta\varepsilon)^3 > (e^2/\Delta x)^2\Delta\varepsilon, \qquad \zeta = \frac{q_w v_x^o\alpha}{nc} = w\left(\frac{n}{\alpha}\right)^2. \tag{4,6}$$

Hence an energy $\varepsilon_0 > 0$ certainly exists such that

$$\zeta^3\Delta\varepsilon^3 - (e^2/\Delta x)^2\Delta\varepsilon - \varepsilon_0^3 = 0. \quad (4,7)$$

Regarding ζ as a constant through an appropriate choice of q_w, not yet specified and here accordingly defined, let us solve the eq (4,7) in order to introduce three real sizes $\Delta\varepsilon_j$, $j = 1, 2, 3$. Note that this does not mean assigning definite values to the size of $\Delta\varepsilon$, which remains indeed arbitrary and unknown like any uncertainty range because of Δx; solving eq (4,7) means examining the physical information consistent with some particular range sizes that fulfil the inequality (4,6). One finds

$$\varepsilon_0 = \left(\frac{2\sqrt{3}}{9}\right)^{1/3}\zeta^{-1/2}\frac{e^2}{\Delta x}, \qquad \Delta\varepsilon_1 = \frac{2}{\zeta^{3/2}\sqrt{3}}\frac{e^2}{\Delta x}, \quad (4,8)$$

$$\Delta\varepsilon_{2,3} = \Delta\varepsilon_2 = \Delta\varepsilon_3 = -\frac{1}{\zeta^{3/2}\sqrt{3}}\frac{e^2}{\Delta x}.$$

The former equation is the condition to make null the imaginary parts of the roots $\Delta\varepsilon_2$ and $\Delta\varepsilon_3$ that, as emphasized by the last equation, result by consequence coincident. As expected, all quantities expressed here as a function of Δx are in fact arbitrary like this latter. The constant ζ can be eliminated from the equations; so

$$\frac{\Delta\varepsilon_1}{\varepsilon_0} = \frac{2}{\zeta\sqrt{3}}\left(\frac{9}{2\sqrt{3}}\right)^{1/3}, \qquad \frac{\Delta\varepsilon_1}{\varepsilon_0^3} = \frac{3}{(e^2/\Delta x)^2}, \quad (4,9)$$

$$\frac{e^2}{\Delta x} = \varepsilon_0\sqrt{3\frac{\varepsilon_0}{\Delta\varepsilon_1}}.$$

It is interesting to rewrite eq (4,7) as $(\zeta^3\Delta\varepsilon^2 - (e^2/\Delta x)^2)\Delta\varepsilon = \varepsilon_0^3$, which yields

$$\Delta t = n\hbar\zeta^3\frac{(e^2/\Delta x)^2}{\varepsilon_0^3}\left[\left(\frac{\Delta\varepsilon}{e^2/\Delta x}\right)^2 - \zeta^{-3}\right].$$

In this way $\Delta\varepsilon^3$ splits into a multiplicative factor $\Delta\varepsilon$, related to Δt through eqs (1,1), times a factor merging together $\Delta\varepsilon^2$ and $(e^2/\Delta x)^2$. Let us specify in particular Δx as Δx_w of eq (4,5); owing to the last eq (4,9), one finds then

$$\Delta t_w = \frac{3n\hbar\zeta^3}{\Delta\varepsilon_{1w}}\left[\left(\frac{n^3}{\alpha^3}\right)^2 - \zeta^{-3}\right], \quad \Delta\varepsilon_{1w} = \frac{2}{\zeta^{3/2}\sqrt{3}}\frac{e^2}{\Delta x_w}. \quad (4,10)$$

Despite Δx is unknown and arbitrary by definition, when it is specified as the range Δx_w purposely pertinent to eq (4,5) the former equation takes the form $\Delta t \propto (n/\alpha)^6$ plus a term $\tau = 3n\hbar/\Delta\varepsilon_{1w}$. If $\Delta\varepsilon_{1w}$ and n are large enough so that $\tau << (n/\alpha)^6$, then Δt_w and the factor χ_w linking $e^2/\Delta x_w$ and $\Delta\varepsilon$ of eq (4,5) fulfill the well known condition

$$\Delta t_w \propto \chi_w^{-2}.$$

Note now that

$$\Delta\varepsilon_1 + \Delta\varepsilon_2 + \Delta\varepsilon_3 = 0 \quad (4,11)$$

and that eq (4,7) is directly related to $v_x^o/c < 1$ because it comes from the inequalities (4,2) and (4,3). Moreover each energy range by definition introduces its own random value of energy; this suggests that are related to eq (4,5) three characteristic energies, i.e. three corresponding massive particles, whose energies are by definition included within the uncertainty ranges of eqs (4,11).

Consider in general three energy ranges $\Delta\varepsilon_j = \varepsilon_j' - \varepsilon_j''$, being $j = 1..3$, of course with both ε_j' and ε_j'' arbitrary and unknown; define then the energies η_j included within them as $\eta_j = (\varepsilon_j' + \varepsilon_j'')/2$, i.e. as average values of the respective boundary values. It is immediate to realize that the condition $\sum\Delta\varepsilon_j = 0$ is compatible with $\sum\eta_j \neq 0$; indeed $\sum(\varepsilon_j' - \varepsilon_j'')/2 = 0$ reads identically $\sum(\varepsilon_j' + \varepsilon_j'')/2 - \sum\varepsilon_j'' = 0$, whence in general $\sum\eta_j = \sum\varepsilon_j'' \neq 0$. Repeat this reasoning regarding η_j as the average values of the specific energy ranges of eq (4,11). The fact that $\eta_{tot} = \eta_1 + \eta_2 + \eta_3 \neq 0$ agrees with the idea of interaction energy; indeed no constrain could be definable for three independent free particles. On the one hand the chance of replacing any quantum range with its average, as done here for $\Delta\varepsilon_j$ and η_j, has a general valence because the range sizes are arbitrary, undefined and undefinable like the average value inferred from their boundaries. Since any value allowed to the former is also allowed to the latter, considering η_j instead of $\Delta\varepsilon_j$ does not exclude the point of view of eqs (1,1): replacing an arbitrary value with another arbitrary value corresponds to replace n with n', which is however immaterial because both symbolize sets of integer values and not specific values. On the other hand the ranges (4,11), regarded all together, fulfill globally the energy conservation regardless of whether $\Delta\varepsilon_j \neq 0$ or $\Delta\varepsilon_j = 0$; as just shown, however, the same does not necessarily hold for η_{tot}. To make also this latter compliant with the eq (4,11), let us assume therefore that η_{tot} has a finite lifetime of the order of $\hbar/\eta_{tot}$. Let Δt_w be this lifetime. In agreement with eq (4,10), during Δt_w the sum $\sum\Delta\varepsilon_j$ is still globally null likewise as before and after their actual transient appearance; in this way the massive particles concerned by the respective energy ranges are jointly involved as concurrent physical properties inherent eq (4,5) and thus the present kind of interaction. The physics of the weak interactions is well known. Here, as a significant check of these ideas, we propose a simple energy balance to infer the energies η_j and thus η_{tot} exploiting just the requirement that the η_j must be regarded all together.

A possible interpretation of the equal sizes and negative signs of $\Delta\varepsilon_2$ and $\Delta\varepsilon_3$, despite in the present model the ranges are always introduced positive by definition, is that their sum with $\Delta\varepsilon_1$ equal to zero requires interacting particles; as explained in section 2, no relationship would be possible by definition for free particles. Let two of them, say η_2 and η_3,

interact in order to release the energy necessary to form also η_1. The fact that $\eta_2 = \eta_3$ because of $\Delta\varepsilon_2 = \Delta\varepsilon_3$ means that their interaction occurs regarding identically either of them in the field of the other one; together, therefore, these particles provide the energy necessary to allow the kind of interaction here concerned. The simplest hypothesis is that the particles η_2 and η_3 have charges of opposite signs whereas η_1 is neutral, thus fulfilling the global charge conservation before, during and after their lifetime; if so, the energy gain of Coulomb energy at an appropriate interaction distance justifies also the neutral particle η_1. In this way the model allows the existence of three range sizes whose finite lifetimes agree with the finite values of the respective heavy bosons η_j. This conclusion is summarized as follows

$$\eta_{tot} = \eta_1 + (\eta_2 + \eta_3), \qquad \eta_2 = \eta_3.$$

The second equation emphasizes that actually η_2 and η_3 form a Coulomb system of charges, whose energy transient uniquely defined likewise ε_{el} of eq (1,4) characterizes the present kind of interaction. This idea suggests to estimate η_{tot} just computing the energy levels of the system of charges η_2 and η_3 by analogy with that of a hydrogenlike atom. Exploit for simplicity the previous non-relativistic equations (1,3) and (1,4); owing to the generality of these equations, there is no reason to exclude that analogous considerations hold at least approximately also here putting of course the charge $Z = 1$ and describing the system of charged bosons η_2 and η_3 as due to $-\varepsilon_{el} = \pi e^2/n\lambda$. It is necessary to take into account however that now also the neutral particle η_1 contributes to η_{tot}, in agreement with the idea of regarding the particles all together. Guess first according to eqs (4,8) that the mass of η_1 should have the same order of magnitude of η_2 and η_3, so that $\eta_{tot} \approx 3\eta_2$; the chance of identifying η_{tot} with $-\varepsilon_{el}$ is consistent with this idea simply putting

$$\eta_{tot} = \pi\eta_2, \quad \eta_2 = \eta_3 = e^2/n\lambda, \quad \eta_1 = (\pi - 2)e^2/n\lambda. \quad (4,12)$$

In other words, eq (1,4) suggests that the expected coefficient ≈ 3 must be actually regarded as π. Despite the non-relativistic reasoning, these conclusions are correct because confirmed by the experience. The experimental masses of the $W^{\pm}$ and Z^0 vector bosons are $m_{W^{\pm}} = 80.39$ GeV and $m_{Z^0} = 91.19$ GeV respectively, for a total mass of $m_{tot} = 251.97$ GeV; in effect

$$m_{tot} = 3.134\, m_{W^{\pm}} \qquad m_{Z^0} = 1.134\, m_{W^{\pm}}$$

are compatible with the values expected for π and $\pi - 2$. Trivial considerations show that the reduced Compton lengths $\bar{\lambda}$ of the vector bosons consistent with $e^2/n\lambda$ are $\bar{\lambda}_{\eta_1} = n\lambda/((\pi - 2)\alpha)$ and $\bar{\lambda}_{\eta_2} = \bar{\lambda}_{\eta_3} = n\lambda/\alpha$, having introduced explicitly the masses $m_j = \eta_j/c^2$. These results are confirmed considering the zero point energy $\Delta p_j^2/2m_j$ of the vector bosons η_j, where $\Delta p_j = p_2 - p_1$ is the gap between its momentum p_2 after confinement within a given delocalization range Δx_w and its initial momentum p_1 in an ideal unconfined state; hence the corresponding energy gap after confinement within Δx_w resulting from the x, y and z components is $\Delta p_j^2/2m_j = 3(n^2\hbar^2/2m_j\Delta x_w^2)$. Assume now that the confinement energy $\Delta p_j^2/2m_j$ is just the energy $\eta_j = m_j c^2$ itself that determines the space-time scale of this kind of interaction, i.e.

$$\eta_j = \frac{3}{2}\frac{c^2\Delta p_j^2}{\eta_j}; \quad (4,13)$$

then $\Delta x_w = (3/2)^{1/2} n\hbar c/\eta_j$, i.e. for η_2 and η_3

$$\Delta x_w = (3/2)^{1/2} n^2 \lambda(\hbar c/e^2). \quad (4,14)$$

For $n = 1$ therefore Δx_w coincides with $\bar{\lambda}_{\eta_2} = \bar{\lambda}_{\eta_3}$ a trivial numerical factor $\sqrt{3/2}$ apart; an identical conclusion holds of course for η_1 too, the numerical factor $(\pi - 2)\sqrt{3/2}$ apart. This confirms the assumed link between delocalization extent and energy of the force carriers, which allows identifying $\eta_{tot} = -\varepsilon_{el}$ in agreement with eq (1,3).

Put first $n = 1$ in eqs (4,12). The value of λ corresponding to the energies of the particles η_2 and η_3 is $\lambda = 1.79\times10^{-20}$ m, so that $\bar{\lambda}_{\eta_2} = \bar{\lambda}_{\eta_3} = 2.45 \times 10^{-18}$ m and $\bar{\lambda}_{\eta_1} = 2.15 \times 10^{-18}$ m; the characteristic range Δx_w of interaction is thus of the order of 10^{-18} m. Since the classical proton radius $r_p = e^2/m_p c^2$ is about 0.8768 fm according to recent measurements [13], the above energies concern a sub-nuclear scale interaction; vice-versa, one could estimate the correct scale of energy of the vector bosons requiring an interaction that occurs at the sub-nuclear extent at which one calculates $\chi_w = \alpha^3 = 3.9 \times 10^{-7}$.

So far we have considered $n = 1$. What however about $n > 1$? First of all, Δx_w becomes n times larger than the aforesaid Compton lengths of η_j; this deviation means a longer range allowed to the interaction. Moreover, according to eqs (4,12) $\eta_{tot} \to 0$ for $n \to \infty$; at this limit the aforesaid space scale of interaction is inconsistent with the corresponding energies of massive boson carriers, which therefore should expectedly require an appropriate threshold energy to be activated. For $n \to \infty$ is thus allowed the less energy expensive and longer range interaction with $\delta\varepsilon = 0$ only, in agreement with the initial idea that $\delta\varepsilon \neq 0$ is related to the boson masses. This conclusion is intuitively clear, but what about the energy threshold? According to the eqs (4,12) the energies η_1, η_2 and η_3 downscale with n, whereas according to eq (4,14) Δx_w upscales with n^2; so the lower threshold for the existence of massive bosons, i.e. for the validity of these equations themselves, concerns n of $\eta_{tot}^{(n)} = -\varepsilon_{el}(Z = 1, n) = (\pi/n)e^2/\lambda$: it is required that the interaction distance of the hydrogenlike system of charges enable the energy to create vector bosons. The inequality $\eta_{tot}^{(n)} > e^2/\lambda$, which holds for $n \leq 3$, ensures that, whatever the masses $\eta_2^{(n)}$ and $\eta_3^{(n)}$ might be, the energy gain due to their Coulomb interaction accounts not only for the energy e^2/λ of the system of charged particles themselves but also for the surplus required by the neutral particle $\eta_1^{(n)}$. Clearly the threshold corresponds to the

value $\eta^{(3)}_{tot} = (\pi/3)e^2/\lambda$, i.e. about 81 GeV; the corresponding Compton lengths of the bosons are $\lambda^{(3)}_{\eta_2} = \lambda^{(3)}_{\eta_3} = 3\lambda/\alpha$ and $\lambda^{(3)}_{\eta_1} = 3\lambda/((\pi-2)\alpha)$. In fact even for $n = 3$ these lengths are of the order of 10^{-17} m, i.e. still consistent with a subnuclear range. At energy below this threshold, i.e. $n \geq 4$, eq (4,1) only describes the interaction. Of course the most favorable condition for this interaction to occur is that with $n = 1$, which ensures the maximum binding energy given by eq (4,12) and corresponds to the shortest interaction distance and maximum values of the three boson masses in fact experimentally detected. The model admits however even the possible existence of lighter bosons. In conclusion, the different energy scales characterize the features of eqs (4,1) or (4,5) because of different values of n; both equations describe however the same kind of interaction.

5 The interaction according to eq (3,1)

The starting point of this section is the eq (3,1) that reads

$$\frac{n\hbar v_x}{\Delta x} = \chi_s \Delta\varepsilon, \qquad \chi_s = 1. \tag{5,1}$$

The lack of coefficient at right hand side of eq (3,1) is tentatively interpreted here as the presence of coefficient $\chi_s = 1$. Being v_x and n arbitrary, it is certainly possible to introduce a proportionality constant ξ defined as $n\hbar v_x = \xi e^2$; so eq (3,1) reads $(\xi e^2/\Delta x)/\Delta\varepsilon = 1$. Usually a proportionality constant linking two quantities that fulfill a given condition or a given physical law is of the order of the unity, unless some specific reason compels an appropriate hypothesis about its actual order of magnitude. Since here even Δx and $\Delta\varepsilon$ are arbitrary, however, it is difficult to guess a valid reason to compel ξ very different from the unity. So, in terms of order of magnitude, the position $\xi \approx 1$ seems reasonable although not thoroughly demonstrated, whence the tentative conclusion quoted in eq (5,1). On the other hand, once having reduced this equation to the form $(e^2/\Delta x)/\Delta\varepsilon = \chi_s$, one can compare $\chi_s = \xi^{-1} \approx 1$ with $\chi_{em} \approx \alpha$ and $\chi_w \approx \alpha^3$ defined by the equations (4,1) and (4,5) formally similar, of course under the assumption that the ranges at left hand sides defining these values are comparable as well. Even without a specific reason to exclude the plain idea $\chi_s \approx 1$, a better assessment of this conclusion appears however necessary: the lack of e^2 at left hand side, replaced by $n\hbar v_x$, allows handling eq (5,1) in order to introduce the interaction between the fractional charges concerned in section 2; but this chance, suggested by eqs (2,8) and (2,9) that anyway do no exclude themselves $\xi \approx 1$, is justified only revising the term $e^2/\Delta x$.

Consider again the eq (2,7) $F_x = -a'/\Delta x^2 + F_{ox}$ with $a' = n\hbar v'_x$ in the simplest case where both a' and $\dot{p}_{ox} = F_{ox}$ are constants. Actually these constants could likely be first order approximations only of series developments whose higher order terms are neglected; yet, even this approximate meaning of the eq (2,7) is enough for the present discussion. Assuming $F_{ox} < 0$ likewise as the first addend in order to describe an attractive force, F_x is compatible with a potential energy U_i of the i-th quark having the form

$$U_i = -\frac{a}{\Delta x} + b\Delta x + U_0 \tag{5,2}$$

being U_0, a and b appropriate integration constants; the latter is clearly related to F_{ox}. Considering $\Delta U_i = U_i - U_0$ one recognizes a well know formula, the so called "asymptotic freedom", describing the interaction between quarks; of course in the present model where any local distance x randomly included by its quantum uncertainty range is replaced by a range of distances Δx, the local value of potential energy U_i turns into a range ΔU_i of allowed values. Let us examine the eq (5,2) in two particular cases where (i) $a/\Delta x \approx b\Delta x$ and (ii) $a/\Delta x \approx U_0$; the arbitrary size of Δx justifies in principle both chances. The former case holds when $\Delta x^{(\mathrm{i})} \approx \sqrt{a/b}$ and yields $U^{(\mathrm{i})}_i \approx U_0$; according to the chance (ii) $\Delta x^{(\mathrm{ii})} \approx a/U_0$ yields instead $U^{(\mathrm{ii})}_i \approx b\Delta x^{(\mathrm{ii})} = ba/U_0$. This means that a delocalization extent of the system quark + gluons around $\Delta x^{(\mathrm{i})}$ the potential energy is approximately of the order of U_0, around a range $\Delta x^{(\mathrm{ii})}$ the potential energy increases linearly with Δx. Define a and b in agreement with eqs (2,8) and (2,9) in order that eq (5,2) takes a reasonable form. Put a proportional to the electric charge $c_i^2 = (\pm(n_i/n')e)^2$, i.e. $a = a_o c_i^2$ via the proportionality constant a_o; also, let analogously be b proportional to the color quantum number C_j, i.e. $b = b_o C_j^2$ with $j = 1 \cdot \cdot 3$. The subscripts symbolize the i-th quark in the j-th color quantum state; in this way $b = 0$ for a colorless Coulomb particle with $n_i = n'$, in which case the eq (5,2) turns, according to eq (2,9), into the classical potential energy $-e^2/\Delta x' + U_0$ of two Coulomb charges attracting each other. This reasoning suggests that the color quantum number should have the form $C_j = f_{j1}(n' - n_i)^2 + f_{j2}(n' - n_i)^4 + \cdot\cdot$, where f_{j1} and f_{j2} are appropriate coefficients of series expansion fulfilling the actual value of C_j whatever it might be; it is interesting the fact that the electric charge depends on n_i/n', the color charge on $n' - n_i$. As concerns $\Delta x' = \Delta x/a_o$, note that multiplying the size of Δx by any factor yields a new range still arbitrary and thus still compliant with eqs (1,1); for the same reasons introduced in the previous section, i.e. because any size possible for Δx is allowed to $\Delta x'$ as well, the notation $\Delta x'$ means in fact nothing else but renaming Δx. In summary, the Coulomb potential appears to be a particular case of eq (5,2), whose local features are described by the aforesaid chances; the expressions of $U^{(\mathrm{i})}_i$ and $U^{(\mathrm{ii})}_i$ are

$$\begin{gathered} \Delta x^{(\mathrm{i})} = \sqrt{\frac{a}{b}}, \qquad U^{(\mathrm{i})}_i = U_0, \\ a = l_a\varepsilon_a\left(\frac{c_i}{e}\right)^2, \qquad b = \frac{\varepsilon_b}{l_b}C_j^2, \\ \Delta x^{(\mathrm{ii})} = \frac{a}{U_0}, \\ U^{(\mathrm{ii})}_i = \frac{ab}{U_0} = \frac{\varepsilon_a\varepsilon_b}{U_0}\frac{l_a}{l_b}\left(\frac{c_iC_j}{e}\right)^2 = b\Delta x^{(\mathrm{ii})}. \end{gathered} \tag{5,3}$$

The constant energies ε_a and ε_b together with the constant lengths l_a and l_b describe the physical dimensions of a and b without need of proportionality factors. Note that $l_b \to \infty$, compels $\Delta x^{(\mathrm{i})} \to \infty$ and $b \to 0$; as the color is introduced by b, this agrees with a constant Coulomb potential $U_i^{(\mathrm{i})} = U_0$ of a colorless particle. By definition therefore $l_a\varepsilon_a = e^2$ for $n_i/n' = 1$, whereas it is expected to take a different value for $n_i/n' < 1$: the new value of $l_a\varepsilon_a/e^2$ when e^2 is replaced by $(n_i/n')e^2$ is known in the literature as $\alpha_s \approx 1$. In summary, eqs (5,3) yield

$$U_i^{(\mathrm{i})} = U_0, \quad U_i^{(\mathrm{ii})} = U_0'\left(\frac{c_i}{e}\right)^2, \quad U_0' = \frac{\alpha_s\varepsilon_b e^2 C_j^2}{l_b U_0}. \qquad (5,4)$$

Appears here once more the importance of the delocalization range Δx: in eq (4,14) Δx_w controlled either appearance of the electroweak interaction, in eqs (5,3) two different range sizes $\Delta x \approx \Delta x^{(\mathrm{i})}$ or $\Delta x \approx \Delta x^{(\mathrm{ii})}$ emphasize either feature of U_i: in (ii) it depends upon the fractional charge, in (i) it does not because $-a/\Delta x$ is balanced by $b\Delta x$ despite both terms describe attractive force.

Let us concern now eq (5,2) in a more general way. The features of U_i as a function of Δx are related to $\delta[(n/m)(n/V)]$ because Δx defines V, eq (2,1), and also because the eq (5,2) comes directly from ΔF_x of eq (2,7). What is distinctive here with respect to the gravitational or Coulomb interaction is the mere fact of having put $F_{ox} \neq 0$; so the consequent form of U_i with $b \neq 0$ describes a peculiar kind of attractive force that increases with Δx. Another remarkable point is that ΔF_x is not necessarily that between different quarks only, because eq (2,7) concerns a mere effect of confinement that holds even for an isolated quark; rather it seems more appropriate to think that the interaction between different quarks strictly replicates an intrinsic feature of the potential energy due to the confinement effect even of a single particle, which also involves its messenger bosons. In fact, in the present model Δx is by definition the delocalization range of one particle; the arising of any form of interaction is due to the presence of a further particle that possibly shares the same delocalization range. In general the number of states within a system of interacting particles is related to their energy, to their masses and to the whole space volume in which they are delocalized: eq (2,2) shows indeed that if n_1 is the number of states of the system with its particles supposed non-interacting, then δn is the change consequent to their interaction, while $\Delta\varepsilon_{n_1+\delta n}$ is the concurrent energy change from the initial $\Delta\varepsilon_{n_1}$. According to the considerations of section 2, in the present case V is the time space delocalization volume of one quark and its interaction messengers, the gluons. If a further quark could share this V, then the quarks interact. If the delocalization volume V is filled with gluons of both quarks mediating their interaction, then the change $\delta(n/V)$ stimulates a question: are the particles that mediate the interaction interacting themselves? Clearly, from the standpoint of eqs (2,7) and (5,2) this question holds even for one quark only within V. A positive answer would explain why ΔF_x increases when pulling apart the interacting quarks, e.g. of a nucleon or meson, or even a lonely quark and its gluon system; in the latter case a greater delocalization range describes indeed the chance of mowing away the gluons from their own quark, which however increases the energy of the system. To emphasize how the position $F_{ox} \neq 0$ answers the question, suppose that the quark-gluon and gluon-gluon interactions does not allow distinguishing the interaction between a quark and "its own" gluons from that of these latter with another identical quark; this would mean distinguishing identical particles, which is however forbidden by eqs (1,1) [7]. If the gluons are not mere interaction messengers but rather self-interacting messengers, then eq (5,2) describes the asymptotic freedom simply as a feature of one quark and its own system of gluons, i.e. even without necessarily requiring a further quark; otherwise stated, a net splitting of gluons from a quark interferes even with their propensity to follow another quark. The concept of asymptotic freedom is linked to the energy constrain that explains why do not exist bare quarks without gluons and bare gluons without quarks. Calculate the change of U_i as a function of Δx as $\Delta U_i = (\partial U_i/\partial\Delta x)\Delta x$ at the first order; the force field $\Delta F_x = -\partial U_i/\partial\Delta x$ acting on quark and its gluon system delocalized in Δx can be calculated in particular at the delocalization extents $\Delta x^{(\mathrm{i})}$ or $\Delta x^{(\mathrm{ii})}$. Replacing here the previous results, one finds $\Delta F_x^{(\mathrm{i})} = -2b$ and $\Delta F_x^{(\mathrm{ii})} = -b(1 + U_0/U^{(\mathrm{ii})})$.

It will be shown in the next section that $U_0' \approx 2U_0 \approx 1\,\mathrm{MeV}$; so, being U_i a monotonic function of Δx, results $\Delta x^{(\mathrm{ii})} \lesssim \Delta x^{(\mathrm{i})}$ because $U_i^{(\mathrm{ii})} \lesssim U_i^{(\mathrm{i})}$ according to eq (5,4). If $\Delta x^{(\mathrm{ii})}$ is of the order of the proton radius, i.e. 10^{-15} m, then according to eq (5,3) b results of the order of 1 GeV/fm, as it is well known. Then, inside a proton the force field at (i) is about twice than that at (ii); of course $b\Delta x$ further increases for $\Delta x > \Delta x^{(\mathrm{i})}$, i.e. outside the actual radius of the proton. This means that extending delocalization range of the quark/gluon system from $\Delta x^{(\mathrm{ii})}$ to $\Delta x^{(\mathrm{i})}$ and then to any $\Delta x > \Delta x^{(\mathrm{i})}$, i.e. allowing quark and gluons to have more space to move apart each other, corresponds to a greater energy; this is not surprising once having found that $U_i^{(\mathrm{ii})}$ is already in the region of linear increase of U_i as a function of Δx. The dependence of U_i on Δx is trivially self-evident; the reasoning about $\Delta x^{(\mathrm{ii})}$ and $\Delta x^{(\mathrm{i})}$ allows to quantify this evidence with specific reference to the sub-nuclear length scale.

The behavior of U_i and the concept of asymptotic freedom equation are straightforward consequences of eq (2,7) and thus of eqs (1,1); this feature of the strong interaction is indeed characterized by the concept of uncertainty, which in particular prevents specifying the actual size of Δx. From the present standpoint only, therefore, no kind of correlation appears in principle between quark generations and chances (i) and (ii) inherent the eq (5,2). Yet, it seems intuitive that either chance for Δx and thus either behavior of potential energy should be selectively related to the energies characteristic of

the three generations of quarks. This supposition will be confirmed in the next section, at the moment one must only admit that both chances are allowed to occur.

Now let us revert to the opening question of this section, i.e. how to regard the energy term $n\hbar v_x/\Delta x$ and χ_s of eq (5,1). The conceptual analogy of χ_s with χ_{em} and χ_w of eqs (4,1) and (4,5) was in principle legitimated by the arbitrariness of v_x in defining $(e^2/\Delta x)/\Delta\varepsilon = \chi_s$ with χ_s expectedly of the order of the unity. Exploit now eq (2,2), for simplicity regarded again at the first order only

$$n_1 = \frac{\delta n}{\delta \log(\Delta\eta')}, \quad \delta \log(\Delta\eta') = \log(\Delta\varepsilon_{n_1+\delta n}) - \log(\Delta\varepsilon_{n_1}),$$

introducing two further energy uncertainty ranges $\Delta\varepsilon_o$ and $\Delta\varepsilon$ whose sizes are by definition intermediate between that of $\Delta\varepsilon_{n_1}$ and that of $\Delta\varepsilon_{n_1+\delta n}$, i.e. $\Delta\varepsilon_{n_1} \le \Delta\varepsilon_o < \Delta\varepsilon \le \Delta\varepsilon_{n_1+\delta n}$. Hence eq (2,2) rewritten as a function of these new ranges takes the form

$$\begin{gathered} \gamma n_1 = \frac{\zeta\delta n}{\delta \log(\Delta\eta)}, \quad \gamma = \gamma(\Delta\eta), \quad \zeta = \zeta(\Delta\eta), \\ \delta \log(\Delta\eta) = \log(\Delta\varepsilon) - \log(\Delta\varepsilon_o). \end{gathered} \tag{5,5}$$

Now $\Delta\varepsilon_o$ plays the role of fixed reference energy range, likewise as the early $\Delta\varepsilon_{n_1}$ did. The correction coefficients γ and ζ account for the fact that n_1 and $\delta n = n_2 - n_1$ were early defined for $\Delta\varepsilon_o \equiv \Delta\varepsilon_{n_1}$ and $\Delta\varepsilon \equiv \Delta\varepsilon_{n_1+\delta n}$, being therefore $\gamma = 1$ and $\zeta = 1$; having changed the ranges at right hand sides, clearly γ and ζ must be replaced here by γn_1 and $\zeta\delta n$ with $\gamma \neq 1$ and $\zeta \neq 1$, whence their definitions of functions of $\Delta\varepsilon$ once having fixed $\Delta\varepsilon_o$. So the previous eq (2,2) becomes a particular case of the present result (5,5), which reads now

$$\begin{gathered} \beta(\Delta\eta) = \frac{\delta g}{\delta \log(\Delta\eta)}, \quad \beta(\Delta\eta) = \gamma n_1, \\ \delta g = \zeta n_2 - \zeta n_1 = \delta(\zeta n). \end{gathered} \tag{5,6}$$

The third equation is interesting as it defines the new range δg. Let the function ζ be someway proportional to $\Delta\eta$, i.e. let ζ decrease with $\Delta\eta$; also, consider the particular case where $\Delta\eta$ is so small that the notation δg can replaced by the familiar differential symbol dg whatever the actual δn might be. Being the range sizes arbitrary, this position about δg is not a hypothesis; it focuses the attention on a particular chance of $\Delta\eta$ that must be taken into account simply because it is allowed and thus to be actually expected. Since a smaller and smaller uncertainty range identifies better and better a local value of the random variable included by its boundaries, $\delta \log(\Delta\eta)$ tends to $d \log(\eta)$; hence the former equation (5,6) tends to the known beta function $\beta(\eta) = dg/d \log(\eta)$ defining the coupling constant g at the energy scale defined by η. This particular limit case helps thus to understand the physical meaning of the ratio in the first eq (5,6), merely written as a function of ranges instead of local values. It is clear the interest to take now $\Delta\eta$ comparable with $\Delta\varepsilon$ of eq (4,1) and (4,5) in order to infer from $\beta(\Delta\eta)$ the function $g(\Delta\eta) \equiv \chi_s$ to be compared with the respective χ_{em} and χ_w. The next task is to calculate the first eq (5,6) in order to confirm that χ_s is of the order of the unity. To this purpose let us expand β in series of powers of δg, i.e. $\beta = \beta_o + \beta_1\delta g + \beta_2\delta g^2 + \cdots$: the coefficient β_o must be equal to zero because of eqs (5,6), whereas $\beta_1 = 0$ as well to fulfill the reasonable condition $\partial\beta/\partial(\delta g) = 0$ of minimum β for $\delta g = 0$. Hence $\beta = \beta_2\delta g^2$, neglecting the higher order terms, requires $\delta g = (\beta_2\delta \log(\Delta\eta))^{-1}$; this appears replacing $1/(\delta \log(\Delta\eta))$ in eq (5,6), which indeed turns into $\beta(\Delta\eta) = \beta_2(\delta g)^2$. According to the fourth eq (5,5), $\delta g = \beta_2/(\log(\Delta\varepsilon/\Delta\varepsilon_o))$ is reducible to the well known form

$$\delta g = \frac{\xi}{\zeta \log(\Delta\eta^2/\Delta\varepsilon_o^2)}, \quad \frac{2\zeta}{\xi} = \beta_2, \quad \Delta\varepsilon_o \approx 0.2 \text{ GeV}. \tag{5,7}$$

The order of magnitude of $\Delta\varepsilon_o$ is easily justified recalling the eq (2,5) of section 2 and the conclusions thereafter inferred: $\Delta\varepsilon_o$ implies that to $\Delta t \approx \hbar/\Delta\varepsilon_o$ corresponds the path $\delta x \approx \hbar c/\Delta\varepsilon_o$ of gluons moving at the light speed to carry the interaction between quarks. The given value of $\Delta\varepsilon_o$ is therefore consistent with the order of magnitude $\delta x \approx 10^{-15}$ m previously quoted for the strong interaction. The result (5,7) and the value of $\Delta\varepsilon_o$ are well known outcomes of quantum chromodynamics; further considerations, in particular about the constants ξ and ζ, are omitted for brevity. This paper aims indeed to show the consistency of the present model based uniquely on eqs (1,1) with the standard features of the strong interactions, not to repeat known concepts.

6 The quark and lepton masses

This section consists of two parts, the first of which concerns the ability of eq (2,4) to describe the ideal masses of isolated quarks. Correlating these masses to the energy ranges $\Lambda_i \equiv \Delta\varepsilon_{n_1+\delta n}$ is in principle sensible first of all regarding the various quarks as a unique class of particles: there would be no reason to expect that different kinds of particles of dissimilar nature are all described by a unique law simply changing a unique distinctive index, here represented by $i \equiv \delta n$. Moreover must hold for the energies of the various quarks a common sort of functional dependence upon δn like that of $\Delta\varepsilon_{n_1+\delta n}$. Eventually, this dependence must still hold even replacing these ranges with the respective average energies $< \varepsilon_{n_1+\delta n} >$ calculated as described in section 4. This last requirement suggests correlating the quark masses with these averages in agreement with the eq (2,4), tanks to the fact that both $< \varepsilon_{n_1+\delta n} >$ and $\Delta\varepsilon_{n_1+\delta n}$ are consistent with their own δn. Indeed an incremental index δn representing the quark energies is defined replacing in eq (2,2) $\log(\Delta\varepsilon_{n_2})$ and $\log(\Delta\varepsilon_{n_1})$ with $\log(< \varepsilon_{n_1} >)$ and $\log(< \varepsilon_{n_2} >)$; a procedure completely analogous yields an equation of the average quantities fully corresponding to eq (2,4). The second point has been explained: the self-interaction of quarks justifies in principle δn

simply admitting that the various quarks are characterized by different self-interaction strengths and thus by distinctively different values of δn. So the critical step is the first one, i.e. whether or not ΔF_x of eq (2,5) really governs the self-interactions of all quarks in order that all of them are related to a unique law (2,4) of δn. This means in practice: (i) regarding one quark delocalized in its own uncertainty range; (ii) thinking that various quarks are characterized by different $\delta(n/m)$ because of their own kind of self-interaction; (iii) assuming that in fact the eq (2,4) accounts for the different numbers of states that characterize uniquely the various quarks. If the functional dependence described by the eq (2,4) is consistent with the three points just mentioned, then Λ_i describes the ideal masses of the quarks as a function of i; also, the point (ii) shows that the energies of this class of particles are really related to their number of allowed states through the self-interaction between quark and gluons.

The estimated masses Q_i of the quarks quoted in literature [14] are reported here:

$$\begin{array}{l} Q_u = 1.7 \leftrightarrow 3.3 \text{ MeV} \\ Q_d = 4.1 \leftrightarrow 5.8 \text{ MeV} \\ Q_s = 80 \leftrightarrow 130 \text{ MeV} \\ Q_c = 1.18 \leftrightarrow 1.34 \text{ GeV} \\ Q_b = 4.13 \leftrightarrow 4.85 \text{ GeV} \\ Q_t = 170.7 \leftrightarrow 173.3 \text{ GeV} \end{array} \qquad (6,1)$$

The mass interval of the "b" quark actually merges two intervals, that reported for the $\overline{MS}$ "mass-independent subtraction scheme" and that of the "1S mass" scheme [14]; the respective mass intervals are $4.19^{+0.18}_{-0.06}$ GeV and $4.67^{+0.18}_{-0.06}$ GeV [15].

It is known that these literature data represent estimates instead of experimental values, as actually isolate quarks do not exist; because of their confinement, the masses are indirectly inferred from scattering experiments. In fact the masses depend on their different combinations in various hadrons and mesons. So the values quoted above must be regarded with carefulness when compared with the results of theoretical calculations. Nevertheless the intervals of values (6,1) do not overlap, which suggests that their order of magnitude is somehow related to and thus at least indicative of the ideal masses of isolated quarks; by consequence it seems also sensible to expect that the sought values of quark masses should fall within these intervals. In lack of further information, therefore, exploit the intervals (6,1) to calculate the average values Q_i:

$$\begin{array}{l} {Q_u}^{(2/3)} = 2.50 \text{ MeV} \\ {Q_d}^{(-1/3)} = 4.95 \text{ MeV} \\ {Q_s}^{(-1/3)} = 105 \text{ MeV} \\ {Q_c}^{(2/3)} = 1.26 \text{ GeV} \\ {Q_b}^{(-1/3)} = 4.49 \text{ GeV} \\ {Q_t}^{(2/3)} = 172 \text{ GeV} \end{array} \qquad (6,2)$$

The superscripts indicate the charges of the respective quarks. These averages have neither specific physical meaning nor come from some particular assumption, they merely represent preliminary starting points defined within realistic intervals; thus their worth is that of reasonable inputs to carry out calculations. The validity of the results inferred in this way relies mostly on their self-consistency; the only initial information is that any sensible output calculated starting from the values (6,2) should expectedly fall within the intervals (6,1). Regard therefore the available data as mere reference values to clarify with the help of eq (2,4) what do Q_i vs i might actually mean in the present context. According to the reasoning carried out in the previous section let us try preliminarily to correlate Q_i with Λ_i putting $\Lambda_i/\Lambda = ((Q_i/U_i)/q)^{1/b}$, where q is a proportionality constant and b a coefficient to be determined by successive calculations; this coefficient fulfills the chance that if $< \Delta\varepsilon_{n_2} > \approx < \Delta\varepsilon_{n_1} >$, i.e. $< \varepsilon_{n_2} > \approx < \varepsilon_{n_1} >$, then the corresponding ratio $(Q_i/U_i q)^{1/b}$ with increasing b anyway matches the limit behavior of Λ_i/Λ whatever q and U_i might be. Initially U_i is justified as mere dimensional factor to be determined; the next results will show that actually it results to be just the potential energy of eq (5,2). Let us sort now the various Q_i by increasing value to check if really the estimated quark masses fulfill the logarithmic dependence of eq (2,4) upon the incremental number of states i, which therefore takes from now on values from 1 to 6. In this way each mass is progressively related to its own increasing i. This expectation is indeed reasonable because $i \equiv \delta n$ defines $\Lambda_i \equiv < \varepsilon_{n_1+\delta n} >$ with respect to a ground reference state number, to which corresponds the reference energy range $\Lambda \equiv < \varepsilon_{n_1} >$. Being by definition $\Lambda_i \equiv \Lambda$ for $\delta n = 0$, one also expects that holds for the eq (2,4) the boundary condition

$$Q_0/U_0 \equiv q \qquad i = 0 \qquad (6,3)$$

whatever b might be; this fact justifies the proposed notation. When handling sets of data, regression calculations are in general needed; the outcomes of these calculations are usually expressed as power series development of an appropriate parameter. Implementing the linear eq (2,4) with the values (6,2) as a function of i, means therefore calculating the best fit coefficients a and b of the form $\log(Q_i/U_i) = a + ib$; clearly n_1 has been included in the regression coefficients. This is easily done regarding Λ_i and Λ of eq (2,4) as follows

$$\log(Q_i/U_i) = a + bi, \qquad a = \log(q), \qquad 1 \le i \le 6. \qquad (6,4)$$

The factor q linking U_i to the reference energy Λ is determined by the boundary condition (6,3); this holds of course even in the presence of higher order terms. The plain first order approximation decided for i agrees with the intent of the present paper: to describe the quarks through an approach as simple as possible and compatible with the minimum amount of input data needed for an unambiguous assessment of re-

sults. So, owing to eqs (5,3) and (5,4), one expects

$$a + bi = \begin{cases} \log(Q_i/U_0) \\ \log\left(Q_i/U_0'(c_i/e)^2\right) \end{cases} \qquad U_0' = \frac{\alpha_s \varepsilon_b e^2 C_j^2}{l_b U_0} \qquad (6,5)$$

Now the Δx-dependent behavior of U_i can be checked: if these equations of U_i and the position $\Lambda_i/\Lambda \propto (Q_i/U_i)^{1/b}$ are correct, then both chances (5,3) should somehow appear when exploiting the logarithmic law. A series of plots shows this point step by step starting from the raw data (6,2).

The various Q_i are preliminarily plotted vs i taking all U_i equal to a constant; this first result is reported in fig 1. The boxes represent the input data, the letters between {} identify the quarks, the dot lines describe tentatively their possible connection; the best fit dashed line has a mere indicative meaning of preliminary reference trend. The various points are not completely random, rather they roughly follow an identifiable increase with i. It appears that couples of the various Q_i lie along three lines reasonably parallel each other; so, according to eq (6,4), these lines should be characterized by a unique best fit coefficient b and differ by the coefficient a only. Yet, since each line must be handled in order to fulfill the condition (6,3), the different a are irrelevant: indeed the three regression lines $\log(Q_i) = a_k + bi$, with $k = 1..3$, must be actually plotted as $\log(Q_i/q_k) = bi$ putting $a_k = \log(q_k)$. In effect the fig 2 shows that once having forced the three dotted connections to cross the origin, all quark masses are perfectly aligned along a unique best fit line, whose regression coefficients are: $a_k = 4.7,\ 5.1,\ 5.4$; the respective values of b range between 0.967 and 0.985, i.e. it is reasonably unchanged. Clearly are here concerned the masses of isolated quarks, since the raw data (6,2) have been plotted one by one independently each other. The relevant conclusion is that of having confirmed the validity of eq (2,4) and (2,1): Δx has physical meaning of delocalization range of a unique quark. Considering that the masses spread over 5 orders of magnitude, the result is certainly interesting. If one would calculate the masses of quarks through this plot, however, four constants must be known: three a_k and b: too many, to consider physically meaningful this way of exploiting eq (2,4). The worth of fig 2 is merely heuristic. It must be noted, however, that significant information about b can be obtained through very simple considerations. In the linear regression (6,4), the best fit coefficient b weights the increase of $\log(Q_i)$ as a function of the incremental number of states i. Consider in particular the highest mass Q_6 of the top quark, corresponding to $i = 6$: the greater b, the greater the calculated value of Q_6. So b is expected to be proportional to Q_6. Moreover for the same reason b controls also the masses of lighter quarks for $i < 6$; the link of Q_6 with the masses of all quarks, inherent the plot of fig 2, suggests that the proportionality constant should reasonably have form and physical dimensions somehow related to all quark masses. Put therefore $b = (\sum_{i=1}^{6} Q_i)^{-1} Q_6$,

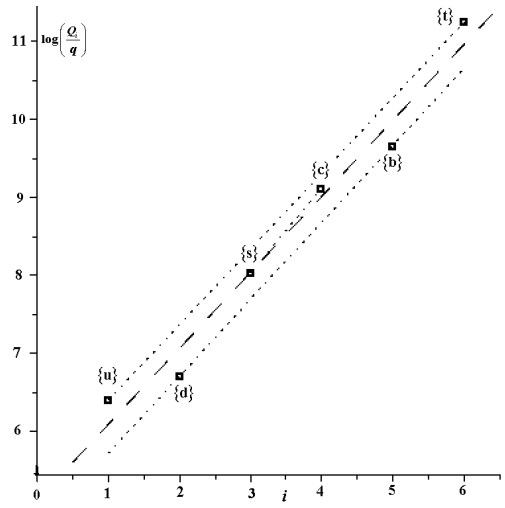

Fig. 2: Plot of $\log(Q_i/q_k)$ vs i; three values of q_k calculated via the boundary condition (6,3) enable a unique trend line of the quark masses with a unique constant U_0.

in which case Q_6 is normalized with respect to the total energy of all possible states allowed between $\Delta\varepsilon_{n_1}$ and $\Delta\varepsilon_{n_1+\delta n}$. Hence the estimates (6,2) yield

$$\frac{Q_6}{\sum_{i=1}^{6} Q_i} = 0.967.$$

In effect, the value of b calculated in this way is very close to that determined in (6,6) via best fit regression.

Yet even three input data to calculate the quarks masses

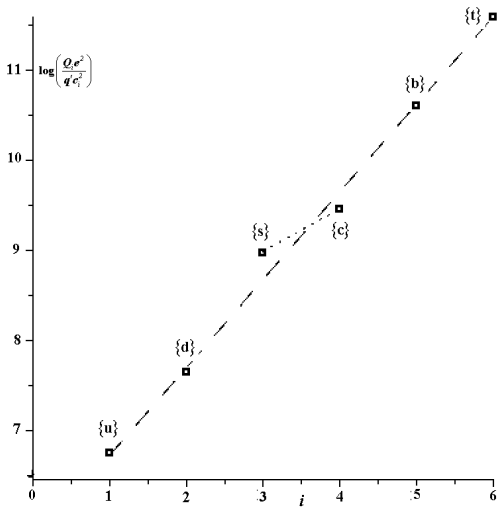

Fig. 4: Plot of $\log(Q_i^*/q')$ vs i with $Q_i^* = Q_i/x_i^2$: here $x_i = const$ for the quarks {c} and {s} and $x_i = c_i/e$ for the other quarks.

Fig. 5: Plot of $\log(Q_i^*/q_k')$ vs i; x_i are defined in fig 4, q_k', with $k = 1, 2$, are calculated in order to fulfil the condition (6,3).

are still too many; certainly there is something else not yet evidenced by the plot of fig 2. Moreover this result, while showing that the idea of concerning the masses of isolated quarks is basically correct, does not highlight anything about the potential energies U_i of eqs (6,5), at the most it could account for U_0 only. Since the idea of considering Q_i/q_k is theoretically too naive, let us regard the various Q_i all together. If so however, despite the previous warnings, the plot of fig 1 is unsatisfactory; owing to the logarithmic ordinate scale, the deviations of the various Q_i from the best fit line are markedly large. Seems however decipherable an unambiguous configuration of these points; this plot prospects the chance of better results. An improved connection between quark masses and i must have exclusively physical valence: here the problem does not concern a random dispersion of experimental measurement errors, but the relationship between masses of isolated quarks and bound quarks on the basis of data extrapolated from the experience; the challenge is to extract the former from the latter trusting to their initial order of magnitude only. The fig 3 reports a new plot where the ratios $(Q_i/U_0)/q$ are replaced by the respective $Q_i e^2/q'c_i^2$, being c_i the electric charges of the various quarks; e is clearly introduced for dimensional reasons. The chance $Q_i e/qc_i$ is not mentioned because found of scarce interest after preliminary checks. From a numerical point of view, therefore, the plain Q_i are now corrected by fractional charge factors $(-1/3)^2$ and $(2/3)^2$. In this way the logarithmic terms are handled exactly as before, which allows the comparison with the former plot: the figure 3 reports again a new best fit line. Now the linear trend of $\log(Q_i e^2/q'c_i^2)$ as a function of i is significantly better than that of fig 1; the {s} and {c} quarks only, both second generation quarks, deviate appreciably from the best fit line; their calculated values consistent with the linear best fit trend are respectively 51 MeV and 1.9 GeV, well outside the literature intervals (6,1). Considering that the orders of magnitude calculated are however globally correct, two chances are in principle admissible: either the literature estimates of the masses of these quarks must be replaced by the values calculated here or some further physical reason, not yet taken into account, enables to modify just these values and align them with the others. The former option is in principle acceptable according to the previous warnings on the literature quark masses, but would conflict with the plot of fig 1: both masses of these quarks were correctly aligned on a similar best fit line before introducing the correction due to their electric charges. So the

latter option seems more stimulating.

Replace therefore $Q_i e^2/q' c_i^2$ of the quarks {c} and {s} only with $Q_i/const$. This idea works well defining *const* appropriately, i.e. in order to fit Q_i of these two quarks to the main best fit line of the other quarks. The fig 4 reports the same data of fig 3, yet replacing e^2/c_i^2 of the quarks {s} and {c} only with a unique value not dependent on c_i; now Q_i^*/q' with $Q_i^* = Q_i/x_i^2$ includes both chances through x_i. The ideal line joining these quark masses is reasonably parallel to the four quark best fit line, i.e. the plot of these two quarks differs trivially from that of the other quarks by the value of the constant a only. As before, in fact this means admitting two values of a: one for the main best fit line, another one for the second generation quark best fit line; of course both values must make the best fit lines compliant with the condition (6,3) via a unique b. The result is shown in fig 5: despite replacing c_i/e with a unique constant is certainly an approximation, nevertheless all quark masses are reasonably represented by a unique eq (2,4). In conclusion, the path from fig 1 to fig 5 was aimed to verify that effectively the logarithmic law (2,4) is expressed via the ratio Q_i/U_i vs the incremental number i of states. The plot of the quark masses Q_i is described by the following equation

$$\begin{array}{lll} \log\left(\dfrac{Q_i^*}{Q_0}\right) = bi & Q_i^* = \dfrac{Q_i}{x_i^2} & b = 0.9723 \\ x_i = c_i/e & Q_0 = 0.556 \text{ MeV} & 1^{st}, 3^{rd} \text{ gen.} \\ x_i = 0.3644 & Q_0 = 1.118 \text{ MeV} & 2^{nd} \text{ generation} \end{array} \qquad (6,6)$$

So b is very similar to that of fig 2. The double value of U_0 corresponds to the two regression constants a allowing to merge the best fit lines of fig 4 according to the condition (6,3); Q_i^* plays the role of an "effective mass" of quarks. The reliability of the results inferred from the plots is assessed recalculating via eqs (6,6) the quark masses and comparing them to the starting values (6,2); one finds $2.32,\ 5.44,\ 1.22 \times 10^2,\ 1.14 \times 10^3,\ 4.50 \times 10^3,\ 1.69 \times 10^5$ MeV that agree reasonably with the literature intervals (6,1). As mentioned at the beginning of this section, this is the basic requirement to be fulfilled. To assess this result also note however that the values (6,2) do not have the rank of experimental data, to be necessarily matched as exactly as possible; as stated before, they have a mere indicative meaning of reference values. Hence the conclusion is that the eqs (6,6) yield a sensible result, while having also the merit of verifying the positions (6,5) strictly related to eqs (5,3). But the most interesting remark concerns U_i, which depends explicitly on the charges c_i in the first and third generation of quarks only; in the second generation it does not, which brings to mind the respective limit cases introduced in eqs (5,3) and further emphasized in eqs (6,5). The generations of quarks are indeed described by $\log(Q_i/U_i) = bi$ with U_i defined by the following equations

$$\begin{array}{ll} U_i^{(\mathrm{ii})} = 0.556(c_i/e)^2 \text{ MeV} & 1^{st}, 3^{rd} \text{ generation,} \\ U_i^{(\mathrm{i})} = 0.148 \text{ MeV} & 2^{nd} \text{ generation.} \end{array}$$

The superscripts are assigned to the generations of quarks by comparison with eqs (5,4) and (6,5); so $U_0 = 0.148$ MeV and $U_0' = 0.556$ MeV.

Some further remarks on this result are also useful. The first concerns the plots of figs 2 and 5: despite the former has been obtained from $\log(Q_i/q_k)$ and the latter from $\log(Q_i/U_i)$ that involves the potential energy, both plots look like and fit surprisingly well the logarithmic law (2,4) despite the quark masses spread over 5 orders of magnitude. These plots are not trivial duplicates: it is interesting the fact that Q_i/U_i takes both forms $Q_i(e/c_i)^2$ and $Q_i/const$, while are determined U_0 and U_0'. On the one hand is remarkable the fact of having identified the mass range as the reason that discriminates the chances (i) and (ii) of eqs (6,5): indeed the mass range of the second generation of quarks is well defined with respect to that of the first and third generations. On the other hand, the fact that both chances are merged in the same plot is itself a further fingerprint of the quantum uncertainty, early introduced because of the mere arbitrariness of Δx. The third remark confirms the fact that Δx is not necessarily the distance between two quarks, it can also be the delocalization range of one quark only; the fact that the plot of fig 5 overlaps very well that of fig 2 shows that even isolated quarks must be regarded as self-interacting and that the interaction potential energy between quarks, the well known eq (5,2) is a replica of the self-interaction potential energy. This conclusion, also supported by the fact that the plot of fig 5 is better than that of fig 1 by introducing Q_i/c_i^2 and not Q_i/c_i, explains why eq (5,2) describing the interaction between different quarks holds also for isolated quarks. The fourth remark concerns the values of the constants U_0 and U_0' reported in eqs (6,6), which describe the asymptotic freedom introduced in the previous section.

Note eventually that the considerations hitherto carried out have assumed already known the quark masses; also, in eqs (6,6) appear several constants to be known "a priori" to carry out the calculations. Moreover, the literature estimates (6,1) appear now as values well configured in the frame of eq (2,4) but not directly supported by experimental measurements. In this respect, a sound proof of their meaning would be to calculate them contextually to other well known and well determined particle mass. The merit of this first part of the section is to have checked the eqs (5,2) and (5,3) via the logarithmic law of eq (2,4). Yet it is also possible to extend further this idea considering together both lepton and quark masses. Indeed a simple question arises at this point: does the eq (6,4) hold also for the leptons? The fact that quarks and leptons are both fundamental bricks of matter suggests the idea that the eq (6,4) could hold for both classes of particles. Moreover note an interesting coincidence: the number of leptons is 6, like that of the quarks. Is this a mere accident or is there some correlation between each quark and each lepton? The next part of the section will show that considering together both kinds of particles allows obtaining all of their

masses as a consequence of a unique principle.

The literature data on the masses L_i of the 6 leptons are summarized here:

$$\begin{array}{l} e \to 0.51 \text{ MeV}, \quad \mu \to 105.66 \text{ MeV}, \\ \tau \to 1776.84 \text{ MeV}, \quad \nu_e \to \ < 2.2 \text{ eV}, \\ \nu_\mu \to < 170 \text{ KeV}, \quad \nu_\tau \to \ < 15.5 \text{ MeV}. \end{array} \tag{6,7}$$

The difficulty of comparing calculated and experimental masses concerns now the neutrinos, because of their very scarce interaction with matter and because the neutrino flavor eigenstates are not the same as the mass eigenstates due to the neutrino oscillations [17]. However, being the masses of electron, muon and tau well known, the strategy to carry out the next calculations is: (i) to assume preliminarily the eq (6,4) for the masses of the leptons; (ii) to fit the masses of the neutrinos to the profile required by the logarithmic law via an appropriate correction factor downscaling their upper limit values (6,7); (iii) to look for a unique best fit calculation including both leptons and quarks; (iv) to infer some conclusion about the physical meaning of such a result.

Since the most important task of this section is to find a correlation between the lepton and quark masses previously determined and to confirm the validity of the previous results, the approach proposed here does not concern directly eq (2,4) rewritten in the form (6,4) $\log(L_i) = a' + b'i$ involving the lepton masses only; rather we start looking since the beginning for a connection between L_i and Q_i. Let us show first of all that such a link actually exists, i.e. that are physically sensible logarithmic laws having the forms $\log\left(Q_i^*\right) \pm \log(L_i)$ with Q_i^* defined in eqs (6,6). From $\log(Q_i^*) = a_Q + bi + ci^2 + \cdot\cdot$ and $\log(L_i) = a_L + b'i + c'i^2 + \cdot\cdot$, with $a_Q = \log(Q_0)$ and $a_L = \log(L_0)$ regression constants, one finds first $\log(Q_i^*) \pm \log(L_i) = a_Q \pm a_L + (b \pm b')i + (c \pm c')i^2 + \cdot\cdot$; the higher powers of i have been skipped for brevity, whereas the dimensional factors Q_0 and L_0 are included in the constants a_Q and a_L as in eq (6,4). The fig 6 evidences that the idea of plotting $\log(Q_i^*) + \log(L_i)$ and $\log(Q_i^*) - \log(L_i)$ vs i is sensible: in fact both curves are reasonably definable through appropriate best fit coefficients. To obtain these plots, the neutrino masses, quoted in literature through the respective upper limits only, have been downscaled to the following values

$$\nu_e = 1.802 \text{ eV}, \nu_\mu = 3481.6 \text{ eV}, \nu_\tau = 1.549 \times 10^7 \text{ eV}. \tag{6,8}$$

Moreover the various L_i have been sorted by increasing mass like the respective Q_i^*. This sorting criterion establishes a one-to one correspondence between leptons and quarks that reads

$$\begin{array}{lcccccc} \textit{leptons} & \nu_e & \nu_\mu & e & \nu_\tau & \mu & \tau \\ & \updownarrow & \updownarrow & \updownarrow & \updownarrow & \updownarrow & \updownarrow \\ \textit{quarks} & u & d & s & c & b & t \end{array} \tag{6,9}$$

Before commenting this correspondence and confirming the validity of eq (2,4) also for the leptons, let us repeat here preliminarily the reasoning previously carried out for the quarks. Calculate $(\sum_{i=1}^6 L_i)^{-1} L_6$ exploiting the values (6,7) and (6,8); one finds

$$\frac{L_6}{\sum_{i=1}^6 L_i} = 0.935 \qquad \left(\frac{Q_6}{\sum_{i=1}^6 Q_i}\right)^2 = 0.936$$

which shows that the lepton equation is related to that of the quarks. To explain this result assume that the normalized values of L_6 and Q_6 are correlated, i.e. $L_6/\sum_j L_j = b' Q_6/\sum_j Q_j$, being b' a constant; imposing then $b' = b$, in order that also $L_6/\sum_j L_j$ be proportional to b of eq (6,5) for the same aforesaid reasons, one finds the given result. These considerations put a constrain on the best fit coefficients of Q_i and L_i vs i. The fig 6 suggests the reasonable chance of introducing a further arbitrary constant b_o that defines the more general linear combinations $\log\left(Q_i^*\right) \pm b_o \log(L_i) = a''_Q \pm b_o a''_L + b''_\pm i + \cdot\cdot$. Hence, multiplying side by side these equations and collecting the constants at right hand side, it must be also true that

$$(\log(Q_i^*))^2 - b_o^2 (\log(L_i))^2 = a''^2_Q - b_o^2 a''^2_L + \cdot\cdot$$

skipping even the first power of i. In effect the advantage of having introduced the arbitrary coefficient b_o is that it can be defined in order to make even the first order term negligible with respect to the constant term, whence the notation reported here; so, neglecting all powers of i, the right hand side reduces to a constant. The last equation reads thus

$$(\log(Q_i^*))^2 = a + (\log(L_i))^2 b, \quad a = a''^2_Q - b_o^2 a''^2_L, \quad b = b_o^2.$$

Now implement again the input data listed in (6,7), (6,8) and (6,2) to check if this last equation correlates sensibly the sets of leptons and quark masses via two constants a and b

Fig. 6: Plot of $\log(Q_i^*/Q_0) \pm \log(L_i/L_0)$ vs i; Q_0 and L_0 are dimensional best fit constants. Q_0 is defined in eqs (6,6).

only; these constants are clearly best fit coefficients that describe the correspondence (6,9). If the zero order approximation just introduced is correct, then trivial regression calculations should yield a sensible statistical correlation of all masses. The best fit coefficients consistent with the zero order approximation of the last equation are

$$a = 45.49178521, \qquad b = 1.039628847. \tag{6,10}$$

So the best fit equation is

$$\log\left(Q_i^{bf}/x_i^2\right) = \pm\sqrt{a + b(\log(L_i))^2};$$

the notation stresses that Q_i^* of eqs (6,6) are replaced by values Q_i^{bf} of Q_i determined by the regression, while the various x_i are of course still that defined in eq (6,6). This result is readily checked calculating

$$Q_i^{bf} = x_i^2 \times 10^{\pm\sqrt{a+b\left(\log(L_i)\right)^2}} \tag{6,11}$$

via the respective lepton masses L_i listed in (6,7), (6,8) and comparing with Q_i reported in (6,1). Note that, because of the exponentials, the decimal places of the regression coefficients are important to reproduce the results of the following calculations. All of the values calculated with the positive sign in eq (6,11)

$$\begin{array}{ll} Q_u^{bf} = 2.50\times10^6 \text{ eV} & Q_d^{bf} = 4.97\times10^6 \text{ eV} \\ Q_s^{bf} = 1.08\times10^8 \text{ eV} & Q_c^{bf} = 1.22\times10^8 \text{ eV} \\ Q_b^{bf} = 4.45\times10^9 \text{ eV} & Q_t^{bf} = 1.75\times10^{11} \text{ eV} \end{array} \tag{6,12}$$

fit surprisingly well the values (6,2) and, mostly important, fall within the estimated intervals (6,1); it is worth noticing that the agreement is much better than that obtained through eqs (6,6). A further remark in this respect is the following. When carrying out the regression calculations with random input data, have been traced the percent deviations of the resulting values of quark and lepton masses with respect to the respective input values; the best self-consistency was found with the true data; the conclusion is that the regression is not mere calculation procedure, but rather a real physical representation of the masses. This also supports the idea that the average values (6,2) of the estimated intervals (6,1) could have an actual physical meaning. Yet are also allowed the following results calculated with the minus sign

$$\begin{array}{ll} q_u^{bf} = 7.91\times10^{-8} \text{ eV} & q_d^{bf} = 2.48\times10^{-9} \text{ eV} \\ q_s^{bf} = 1.64\times10^{-10} \text{ eV} & q_c^{bf} = 1.45\times10^{-11} \text{ eV} \\ q_b^{bf} = 2.77\times10^{-12} \text{ eV} & q_t^{bf} = 1.13\times10^{-12} \text{ eV} \end{array} \tag{6,13}$$

The former set of energies has a literature check through the estimates (6,1), the latter set does not; yet there is no reason to exclude the values (6,13), whose physical meaning will appear shortly. In the latter case the subscripts have a formal physical meaning only, merely reminiscent of the respective quark masses (6,12); nevertheless, it is possible to show the key role of these further energies for the physics of quarks and leptons.

Any statistical regression concerns by definition whole sets of values; here eq (6,11) correlates all masses of leptons and that of all quarks reported in (6,2) and (6,7), (6,8) according to their representation (6,9). The best fit coefficients (6,10) are therefore the fingerprint of *all* masses. Various simulations have been indeed carried out (i) altering deliberately some selected input values of either set of masses, (ii) altering either whole set of masses and (iii) altering both whole sets of masses by means of arbitrary multiplicative factors to find out how the corresponding results are affected; the results, compared with that of eq (6,11) obtained from true values, confirm of course that anyway the new regression coefficients differ from (6,10). The obvious conclusion is that, for some specific reason, just the quoted coefficients (6,10) identify uniquely the fundamental masses of our universe: a is related to their measure units, as previously explained, b controls instead the link between quarks and lepton masses at increasing values of i. Actually one coefficient only is enough to identify all masses; the other is merely associated to it, being concurrently calculated. Otherwise stated, one could assume as a fundamental assumption one of these coefficients only, the other one results consequently determined by the unique set of quark and lepton masses consistent with the former one. Is clear the importance of understanding the specific physical meaning of the particular couple of coefficients (6,10) able to account for the fundamental masses of our universe as a function of *one* predetermined input. Besides the numerical calculation of these masses, however, it seems reasonable to expect that some physical idea is still hidden in eq (6,11).

To investigate this point consider the following equation

$$q_i^o = x_i^2 \times 10^{\pm\sqrt{a+\left(\log(L_i)\right)^2}} \tag{6,14}$$

inferred from (6,11) leaving unchanged a while replacing instead b with the unity. This equation results formally from $\left(\log(q_i^o)\right)^2 = (\log(L_i))^2 + a$, which is interesting because q_i^o and L_i can be interchanged simply changing the sign of a but not its absolute value. Of course the various q_i^o so defined are no longer quark masses; being still related to the respective true lepton masses L_i, however, also q_i^o are somehow related to Q_i.

It is very significant to regard eqs (6,14) thinking Q_i correlated to L_i, which in turn are correlated to q_i^o via one additive constant a only.

So far the experimental masses of quarks and leptons have been introduced as a matter of fact, thus finding that a unique equation, (6,11), accounts for all of them simply postulating a well defined and unique couple of regression constants. Eq (6,14) adds to this standpoint a new perspective: the existence

of a field whose quanta are related to the q_i^o, as a function of which are first calculated L_i via eq (6,14) and then Q_i via eq (6,11). The number of input data confirms that highlighted before, i.e. the quoted value of a only; the masses of both quarks and leptons appear then as consequences of a unique kind of particles, just the q_i^o, since the only possible regression of L_i with Q_i consistent with the given a is that with the concurrent value b. This explains why q_i^o have been defined keeping a and changing b only; even without appearing explicitly appearing in eq (6,14), we know that the latter is required to be just that consistent with the former.

Note now that also eq (6,14) allows two sets of of values, q_i^{o+} and q_i^{o-}, defined by either possible sign of the exponential; it is easy to realize that, likewise as the values (6,12) and (6,13), also now from a numerical point of view $q_i^{o+} >> q_i^{o-}$. This appears regarding all q_i^o together: the resulting total energies corresponding to the positive and negative signs are $\sum_{i=1}^{6} q_i^{o+} = 1.29 \times 10^{11}$ eV and $\sum_{i=1}^{6} q_i^{o-} = 8.189 \times 10^{-8}$ eV. Define therefore the linear combination $q_i^{o+} - q_i^{o-}$ and sum together all i-th terms; one obtains again a total energy

$$\varepsilon_H = 129 \text{ GeV}.$$

Regardless of the numerical values, however, the physical meaning of each term $q_i^{o+} - q_i^{o-}$ is profoundly different from that of the terms q_i^{o+} and q_i^{o-} regarded separately: the masses m_i, charges c_i, spins s_i, colors C_i and so on of these virtual particles, expectedly the same for q_i^{o+} and q_i^{o-} whatever they might be as a consequence of eq (6,14), subtract each other and thus do no longer appear in $q_i^{o+} - q_i^{o-}$. This point is easily highlighted and explained. Actually the eq (6,14) establishes the numerical values of the new energies q_i^{o+} and q_i^{o-}, not their specific forms about which nothing has been hypothesized or is known. The most natural way to regard these quantities, in full line with the basic ideas of the present model, is to relate the various q_i^o to appropriate energy uncertainty ranges as done in eq (2,4); this means assuming for instance

$$q_i^{o+} = \varepsilon_i^+(m_i, c_i, s_i, C_i, ..) - \varepsilon_i^+(0, 0, 0, 0, ..)$$
$$q_i^{o-} = \varepsilon_i^-(m_i, c_i, s_i, C_i, ..) - \varepsilon_i^-(0, 0, 0, 0, ..)$$

with

$$\varepsilon_i^-(m_i, c_i, s_i, C_i, ..) \approx \varepsilon_i^-(0, 0, 0, 0, ..)$$

as well. As repeatedly stressed, both boundaries of any uncertainty ranges are arbitrary. Here we are interested to consider in particular ranges fulfilling the following condition about the upper boundaries:

$$\varepsilon_i^+(m_i, c_i, s_i, C_i, ..) = \varepsilon_i^-(m_i, c_i, s_i, C_i, ..).$$

These positions agree with $q_i^{o+} >> q_i^{o-}$ and also yield

$$q_i^{o+} - q_i^{o-} = \varepsilon_i^-(0, 0, 0, 0, ..) - \varepsilon_i^+(0, 0, 0, 0, ..)$$

that defines $q_i^{o+} - q_i^{o-}$ as the energy uncertainty range of a massless, spinless, chargeless, colorless,.. virtual particle, having in particular boson character. So, when summing up all these terms one finds a total boson energy having the value just quoted. This peculiar energy that accounts for the lepton and quark masses corresponds to a *composite* particle consisting of the sum of 6 terms $q_i^{o+} - q_i^{o-}$ rather than to a truly elementary particle. This conclusion is supported by the fact that the lifetime Δt_H of such a particle should reasonably result from that of its longest life constituent term with $i = 1$, i.e. $\Delta t_H = \hbar/(q_1^{o+} - q_1^{o-})$; one calculates in this way via eq (6,14)

$$q_1^{o+} - q_1^{o-} = 2.50 \text{ MeV}, \qquad \Delta t_H = 2.63 \times 10^{-22} \text{ s}.$$

These last results are reasonable and fully agree with the outcomes of recent experimental measurements.

7 The quantum statistical distributions

This section investigates further consequences of eq (2,2). This part of the paper is thus significant because just this equation leads to eq (2,4), which has been heavily involved to infer the asymptotic freedom equation (5,7) of quarks and the masses of quarks and leptons; confirming once more eq (2,2) means therefore to correlate these results to another fundamental topic of quantum physics concerned in the present section, i.e. the statistical distributions of quantum particles. Eqs (1,1) link the energy range $\Delta\varepsilon$ including the possible energies of a quantum system to its number n of allowed states: the change of energy range size $\delta\Delta\varepsilon = (\hbar/\Delta t)\delta n$ during a given time rage Δt has been concerned in section 2 to calculate the related change $\delta n = n_2 - n_1$ of n, thus obtaining eq (2,4). In that case n_1 was regarded as a fixed quantity, i.e. as a reference number of states as a function of which to define δn. Now we generalize these ideas: both n_1 and n_2 are allowed to change in a quantum system characterized by an initial number of states n_o. If so $\hbar/\Delta t$ can be identically rewritten as $\hbar/\Delta t = \Delta\varepsilon_{n_1}/n_1$ or $\hbar/\Delta t = \Delta\varepsilon_{n_2}/n_2$, because both right hand sides are equivalent reference states in defining δn. So, being both chances alike as well, it is reasonable to expect that $\hbar/\Delta t \propto K_t/(n_1 n_2)$ with $K_t = K_t(\Delta t)$ proportionality factor having physical dimensions of an energy. This position is possible in principle because Δt is arbitrary; so, whatever n_1 and n_2 might be, certainly exists a time length $\Delta t = \Delta t(n_1, n_2)$ that fulfills the proposed correlation. From a formal point of view, assume that $\Delta\varepsilon/n$ of the system is described during Δt by the linear combination $a_1\Delta\varepsilon_{n_1}/n_1 + a_2\Delta\varepsilon_{n_2}/n_2$, being a_1 and a_2 appropriate time dependent coefficients; if so, then $K_t = a_1 n_2 \Delta\varepsilon_{n_1} + a_2 n_1 \Delta\varepsilon_{n_2}$ is defined just by the equation $\delta\Delta\varepsilon/\delta n = \hbar/\Delta t = K_t/(n_1 n_2)$. Since all quantities at right hand side are arbitrary, for simplicity let us approach the problem in the particular case where K_t is regarded as a constant in the following. This chance is obviously also obtainable defining appropriately a_1 or a_2 or both during Δt. The following discussion will show that even this particular case is far reaching and deserves attention.

Write $n_2 = n_o \pm j$ and $n_1 = \pm j$, being n_o a reference fixed number of states and j a variable integer accounting for the change of n_1 and n_2; of course both n_o and j are arbitrary and independent each other, which yields indeed $n_2 - n_1 = n_o$ or $n_2 - n_1 = n_o \pm 2\delta j$ depending on the signs of j. In this way it is possible to describe a steady system with its n_o initial states or an evolving system where is allowed a new number $n' \neq n_o$ of states; since now both n_1 and n_2 are allowed to change, $\delta n = \pm 2\delta j$. Simplifying the notations, the equation inferred from $\delta\Delta\varepsilon/\delta n = K_t/(n_1 n_2)$ of interest for the following discussion reads

$$\frac{\delta\Delta\varepsilon_j}{\delta j} = \frac{2K}{j(n_o \pm j)}, \qquad \delta j = 1,\ 2,.. \tag{7,1}$$

where K must be intended as the constant replacing K_t previously introduced; it is allowed to take both signs, which is avoids writing explicitly $\pm\delta j$. The notation $\Delta\varepsilon_j$ emphasizes the variable number of states appearing at right hand side. To proceed on, consider the case where both j and n_o are large enough to regard approximately the former as a continuous variable, so that $\delta j << j$; so the left hand side can be handled, for mere computational purposes only, as $d\Delta\varepsilon_j/dj$; hence $\Delta\varepsilon_j$ calculated solving the differential equation, results to be

$$\Delta\varepsilon_j = (K'\varepsilon_o/n_o)\log(n_o/j \pm 1) + const, \quad 2K = -K'\varepsilon_o, \tag{7,2}$$

being *const* the integration constant; K' is an arbitrary dimensionless constant and ε_o an arbitrary constant energy. Consider now two boundary conditions of eq (7,2) concerning the respective limit cases (i) $n_o << j$ and (ii) $n_o >> j$. From a mathematical point of view, note that eq (7,2) is obtained by integration of eq (7,1) with respect to j regardless of n_o; hence one could think the cases (i) and (ii) as due to fixed integration limits on dj for two different values of n_o consistent with either inequality, of course without modifying the result of the integration and the subsequent considerations.

In the case (i) holds $n_o/j + 1$ only; putting $const = 0$ and expanding in series the logarithmic term, the right hand side of eq (7,2) reads

$$\begin{gathered} \Delta\varepsilon_j = \frac{w_j K'\varepsilon_o}{j}, \\ w_j = 1 - \frac{n_o}{2j} + \frac{n_o^2}{3j^2} - \ldots, \quad 0 < w_j < 1. \end{gathered} \tag{7,3}$$

Let j be defined between two arbitrary numbers of states j_1 and $j_2 > j_1$; moreover define now K' in order that the sum of all terms $K'w_j$ introduced in the last equation over all values of j fulfills the following condition

$$j_1 \leq j \leq j_2, \qquad \pi_j = K'w_j, \qquad K'\sum_{j_1}^{j_2} w_j = \sum_{j_1}^{j_2} \pi_j = 1;$$

then the result is

$$\pi_j = \frac{j\Delta\varepsilon_j}{\sum_{j=j_1}^{j_2} j\Delta\varepsilon_j}, \quad \varepsilon_o = \sum_{j=j_1}^{j_2} j\Delta\varepsilon_j, \quad \frac{n_o}{j_1} << 1. \tag{7,4}$$

The inequality ensures that is fulfilled the initial condition of the case (i) concerned here, whereas the first eq (7,4) shows the probabilistic character of π_j resulting from the previous positions.

Consider now the limit case (ii). Despite the second eq (7,3) requires in principle a very large number of series terms to express $n_o/j >> 1$, even tending to infinity, there is no reason to exclude that the second equation (7,4) defining $j\Delta\varepsilon_j$ still holds: being K' arbitrary, it can be still defined in order to fulfill the inequality $K'\Sigma_j(1 - n_o/2j + n_o^2/3j^2 + ..) < 1$ whatever the ratio n_o/j might be. On the one hand this inequality can be accepted in principle even though the series consists of an infinite number of terms; in fact the series does not need to be explicitly computed, which makes plausible also the position $\pi_j = K'w_j$. On the other hand, however, in this way the result $j\Delta\varepsilon_j = K'\varepsilon_o w_j$ is not explicitly inferred: the left hand side of the last inequality is indeed undefined. Otherwise stated, without the straightforward hint coming from the case (i) the eqs (7,4) could have been hypothesized only and then still introduced in the case (ii) as plausible inputs but without explanation. Actually, the assessment of the limit case (i) and the subsequent considerations on $w_j K'$ are the points really significant of the present reasoning: while extending the physical meaning of π_j and $j\Delta\varepsilon_j$ also to the case (ii), they ensure the compatibility of the limit cases (i) and (ii). Once again, the arbitrariness of the numbers of states plays a key role to carry out the reasoning.

Looking back to eq (7,2) and multiplying by j both sides, let us write

$$j\Delta\varepsilon_j = K'\varepsilon_o(j/n_o)\log(n_o/j \pm 1) + const\, j. \tag{7,5}$$

According to eqs (7,4) $j\Delta\varepsilon_j/K'\varepsilon_o = w_j$; so, neglecting 1 with respect to n_o/j in agreement with the present limit case (ii) and summing all terms w_j, eq (7,5) yields

$$W = -\sum_{j=j_1}^{j_2}\left(\frac{j}{n_o}\right)\log\left(\frac{j}{n_o}\right) - \sigma\frac{const}{K'\varepsilon_o}, \qquad \sigma = \sum_{j=j_1}^{j_2} j. \tag{7,6}$$

It is useful now to rewrite eq (7,6) as a function of a new variable ξ_j

$$W = -q\sum_{j=j_1}^{j_2}\xi_j\log(\xi_j), \quad const = -\frac{K'\varepsilon_o}{n_o}\log(q), \quad \xi_j = \frac{j}{n_o q},$$

where q is a proportionality factor not dependent on j; it has been defined according to the second equation to eliminate the second constant addend of eq (7,6). The next step is to define j, so far simply introduced as an arbitrary integer without any hypothesis on its actual values, in order that W has specific physical meaning with reference to a thermodynamic system characterized by a number s of freedom degrees. To this purpose assume that j can take selected values n^s only, with n arbitrary integer. This is certainly possible:

nothing hinders calculating the eq (7,2) as a function of n_o/n^s instead of any j progressively increasing; in this way also the eq (7,6) accordingly calculated takes a specific physical meaning consistent with that of the ratios n^s/n_o. Clearly this does not mean trivially renaming j: now n^s reads $\Delta x\Delta p/\hbar^s$, where $\Delta x = \Delta x_1 \cdot \cdot \Delta x_s$ and $\Delta p = \Delta p_1 \cdot \cdot \Delta p_s$. Since therefore $\Delta x\Delta p$ symbolizes a volume in a s-dimensional phase space, $\Delta x\Delta p/\hbar^s$ represents the number of states allowed in this volume. It is known that this ratio introduces the statistical formulation of the entropy [16]; so putting $const/K'\varepsilon_o$ proportional to a new quantity S_0, one finds

$$S = -q\sum_{n=n_1}^{n_2}\xi_n\log(\xi_n), \qquad S_0 = -q\log(\Omega),$$
$$\frac{const}{K'\varepsilon_o} = \frac{1}{\zeta}\frac{S_0}{q}, \qquad \Omega = q^{\zeta/n_o}. \tag{7,7}$$

The notation of the first sum emphasizes that now j takes values corresponding to the possible n^s. The constant of eq (7,6) has been therefore related in the last equation to S_0. The second equation can be regarded as a particular case of the former when the thermodynamic probabilities ξ_j are all equal; while in eq (7,2) j was an arbitrary number progressively increasing fro j_1 to j_2, in eq (7,7) its relationship to n^s does not exclude the chance of coincident values for equal volumes of phase space. It is well known that the results so far exposed introduce the statistical definition of entropy a trivial proportionality factor apart. Note that this result has been obtained in a very different context [12], i.e. to show the quantum character of the Fick diffusion laws as a consequence of eqs (1,1) only; despite the different topic, the theoretical frame is however exactly the same as that hitherto concerned.

Let us return now to the early eq (7,2). Define as usual the energy range as $\Delta\varepsilon_j = \varepsilon'' - \varepsilon'$, so that the eq (7,2) reads $n_o(const + \varepsilon' - \varepsilon'')/K = \log(n_o/j \pm 1)$. Exploit once again the fact that in general the boundary values of the uncertainty ranges are arbitrary; hence, whatever the sign and values of K and $const$ might be, the left hand side can be rewritten as $(\varepsilon_j - \varepsilon_o)/K$, being of course both ε_j and ε_o still arbitrary. So the number of states j of the eq (7,2) reads

$$j = \frac{n_o}{\exp((\varepsilon_j - \varepsilon_o)/K) \mp 1}, \quad \Delta\varepsilon = \varepsilon_j - \varepsilon_o = n_o(const + \varepsilon' - \varepsilon'').$$

The second equation reports again the starting point from which is inferred the former equation to emphasize that, despite the arbitrariness of the boundary values that define the size of the energy uncertainty range, the specific problem determines the values of physical interest. For instance in eq (2,6) has been inferred the Planck law identifying $\Delta\varepsilon_j$ with $h\Delta\nu_j$; clearly the number of states therein appearing is to be identified here with j, whereas n_o can be taken equal to 1 because the photons are bosons. Here the upper sign requires signs of K and $\varepsilon_j - \varepsilon_o$ such that $(\varepsilon_j - \varepsilon_o)/K > 0$ because the number of states j must be obviously positive; instead the lower sign allows in principle both $\varepsilon_o < \varepsilon_j$ and $\varepsilon_o > \varepsilon_j$, as in effect it is well known. To understand these conclusions, let us exploit the reasonable idea that the number j of states allowed for a quantum system is related to the number N of particles of the system. Recall another result previously obtained exploiting eqs (1,1) [7]: half-integer spin particles can occupy one quantum state only, whereas one quantum state can be occupied by an arbitrary number of integer spin particles. In the former case therefore j is directly related to N, i.e. $j = N$ and $n_o = 1$, in the latter case instead in general $N >> j$ without a specific link between j and N. Yet the arbitrariness of n_o makes j suitable to represent any N also in this case as $N = \sum j = n_o\sum(\exp(\Delta\varepsilon_j/K) - 1)^{-1}$. In the classical case where $\Delta\varepsilon_j >> K$, this equation is the well known partition function.

8 Discussion

After the early papers concerning non-relativistic quantum physics [5,6], the perspective of the eqs (1,1) was extended to the special and general relativity; the gravitational interaction was indeed inferred as a corollary just in the present theoretical frame. The problem of examining more in general also other possible forms of quantum interaction appeared next as a natural extension of these results. This paper aimed indeed to infer some basic concepts on the fundamental interactions possible in nature. Even without ambition of completeness and exhaustiveness, the chance of finding some outstanding features unambiguously typical of the electromagnetic, weak and strong interactions has the heuristic value of confirming the fundamental character of eqs (1,1): seems indeed significant that the weird peculiarities of the quantum world are directly related not only to the physical properties of the elementary particles but also to that of their fundamental interactions, which are described in a unique conceptual frame including also the gravity and the Maxwell equations [7]. Now also the gravitational coupling constant, so far not explicitly concerned, is inferred within the proposed conceptual frame. The starting point is again the eq (2,7) rewritten as follows

$$v'_x = -\frac{\Delta F_x\Delta x^2}{n\hbar}, \qquad v'_x = \frac{d\Delta x}{d\Delta t}, \qquad \Delta F_x = F_x - F_{ox}. \tag{8,1}$$

By means of this equation the paper [7] has emphasized the quantum nature of the gravity force, approximately found equal to $\Delta F_x = Gm_am_b/\Delta x^2$ for two particles of mass m_a and m_b; also, the time dependence of p_x or p_{ox} of $\Delta p_x = p_x - p_{ox}$ was alternatively introduced to infer the equivalence principle of relativity as a corollary. In the present paper, instead, both boundary values of the momentum component range have been concurrently regarded as time dependent to infer the expected potential energy (5,2) of the strong interactions: the reasoning is in principle identical, although merely carried out in a more general way; the form of eq (5,2) comes putting in eq (2,7) both $\dot{p}_x \neq 0$ and $\dot{p}_{ox} \neq 0$, which is the

generalization of the relativistic reasoning carried out in [7]. In fact the eq (2,7), straightforward consequence of eqs (1,1) and thus valid in general, has been reported also in the present paper to better understand these results through its underlying reasoning: what changes is the way it can be exploited to describe specific physical problems, as it has been also emphasized about the physical meaning of v'_x. Now we are interested to implement a particular case of eq (2,7), i.e. the Coulomb law quoted in eq (2,8). The procedure followed below does not need any additional hypothesis with respect to these considerations: it is enough to specify appropriately ΔF_x in eq (8,1).

Consider first the eq (2,8): in the particular case $e' = e$ it yields the Coulomb law $F_x - F_{ox} = \Delta F_x = \pm e^2/\Delta x^2$. Replace this expression into eq (8,1), which reads then

$$v'_x = \pm e^2/n\hbar. \tag{8,2}$$

The ± sign is a trivial feature of the velocity component v'_x along the arbitrary x-axis, it is in fact of scarce interest for the purposes of the present discussion. More interesting is the fact that putting $v'_x = (\alpha/n)c$, as done to infer eq (2,9), one obtains the identity $\alpha/n = e^2/n\hbar c$. This result supports the idea that v'_x/c of eq (8,2) effectively represents a coupling constant: it reads α/n, just the electromagnetic coupling constant found in eq (1,4).

Consider now the gravity force $\Delta F_x = Gm_a m_b/\Delta x^2$ and replace this expression into eq (8,1): so $v'_x = Gm_a m_b/n\hbar$. Comparing this result with the case of the electric force propagating between charged masses, one finds

$$\alpha_G = v'_x/c = Gm_a m_b/n\hbar c. \tag{8,3}$$

Is obvious the reason why the gravitational coupling constant, recognizable at the right hand side, has been formally obtained through elementary considerations identical to that of eq (8,2): the unique eq (8,1) turns into either result simply depending on whether one replaces ΔF_x with $e^2/\Delta x^2$ or $Gm_a m_b/\Delta x^2$. Eqs (8,2) and (8,3) suggest that the gravitational and electromagnetic field propagate at the same rate c: as emphasized when discussing the physical meaning of v_x and v'_x in section 2, the latter is the deformation rate of the space-time range Δx that determines ΔF_x, whereas is instead v_x the real propagation rate of the respective messenger particles in the interaction space-time range Δx; in both cases $\Delta x/\Delta t = c$.

These results are not end points, they have heuristic character. Let us start from eq (8,3) considering for simplicity $m_a = m_b = m$, so that $m = m_P\sqrt{n\alpha_G}$; i.e. any m is proportional to the Planck mass, the proportionality factor being just $\sqrt{n\alpha_G}$. Owing to the small values of α_G, one expects that large values of n are required to fit even small masses. Although α_G depends in general on the specific values of the masses, it is interesting to examine its minimum value corresponding to the particular case where both m_a and m_b represent the lightest elementary particle, the electron neutrino. As concerns the ratio $m_{\nu e}/m_P$ note that $m_{\nu e}$ is a real particle, m_P is a mere definition; so for the former only holds the idea that any particle confined in an arbitrary uncertainty range Δx is characterized in principle by a momentum component gap $\Delta p_x = p_x^{conf} - p_x^{\infty}$ with respect to an ideal unconfined state, see eq (2,1). For the reasoning is irrelevant how an electron neutrino could be confined in practice, because Δx is arbitrary; it could even be the full diameter of the whole universe. It is instead significant in principle that, as already shown in section 4 about the weak interaction boson vectors, it is possible to write for the electron neutrino a delocalization energy $\Delta\varepsilon_{\nu e} = \Delta p_x^2/2m_{\nu e}$ valid for any real object; this reasoning has been in effect exploited in eq (4,13). These considerations aim to conclude that, whatever Δp_x might be, the equation

$$m_{\nu e} = \Delta p_x^2/2\Delta\varepsilon_{\nu e} \qquad \Delta\varepsilon_{\nu e} = m_{\nu e}c^2 \tag{8,4}$$

suggests $m_{\nu e}$ proportional to a reciprocal energy range $\Delta\varepsilon_{\nu e}$ that in turn should be proportional to c^2. If this reasoning is physically sensible, then $m_{\nu e}/m_P \propto c^{-2}$ suggests by consequence $m_{\nu e}/m_P \propto \alpha^2$; since the fine structure constant is proportional itself to c^{-1}, this position simply means including $e^2/\hbar$ into the proportionality constant. Write therefore

$$m_{\nu e}/m_P = \alpha^2/N$$

having called $1/N$ the proportionality constant. The ratio at left hand side is immediately calculated with the help of the first value (6,8), it results equal to 1.5×10^{-28}; the factor $\alpha^2 \approx 5.3\times10^{-5}$ calculates N equal to 3.5×10^{23}, a value surprisingly similar to well known $N = 6.02\times10^{23}$ for the ratio at right hand side. The agreement between these values is really unexpected: while the position $m_{\nu e}/m_P \propto \alpha^2$ could be acceptable at least in principle, is really difficult to understand what the Avogadro number has to do with the present problem. A reasonable idea is to regard α^2/N, perhaps a mere numerical accident, as a whole factor between ordinary mass units and Planck mass units. To support this statement replace in eq (8,4) $\Delta\varepsilon_{\nu e}$ with $m_{\nu e}c^2$, regarded as the average of the boundary values of $\Delta\varepsilon_{\nu e}$; for the following order of magnitude estimate this replacement is acceptable. So, recalling that $\Delta p_x^2 = (n\hbar/\Delta x)^2$ and that actually to calculate $\Delta\varepsilon_{\nu e}$ one should consider $\Delta p_x^2 + \Delta p_y^2 + \Delta p_z^2$, eq (8,4) reads $\Delta x = n\hbar c\sqrt{3/2}/m_{\nu e}c^2$; putting $n = 1$, one finds $\Delta x = 1.3\times10^{-7}$m. Replace now $\Delta\varepsilon_{\nu e}$ with $(N/\alpha^2)\Delta\varepsilon_{\nu e}$: the factor previously found to convert m_{ν_e} into Planck mass units should now convert the energy $\varepsilon_{\nu e}$ from the ordinary units into Plank energy units. Indeed $\Delta x = n\hbar c\sqrt{3/2}\alpha^2/Nm_{\nu e}c^2$ calculated again with $n = 1$ results equal to 1.1×10^{-35}m, which is reasonably comparable with the Planck length $l_P = 1.6\times10^{-35}$m. Actually this result could be expected, because it is based on regarding the energy $\Delta\varepsilon_{\nu e} = \Delta p_x^2/2m_{\nu e}$ as $\Delta\varepsilon_{\nu e} = \Delta p_x^2c^2/2\Delta\varepsilon_{\nu e}$, as already done in section 4; accordingly, this means identifying $\Delta\varepsilon_{\nu e}$ calculated from the confinement uncertainty equation with the mass $m_{\nu e}$

of the particle itself via the factor c^2. This idea was found reasonable to calculate the characteristic length of the weak interaction, eq (4,14), and appears adequate also here because it shows that the conversion factor of m_{ve} into m_P also converts ε_{ve} into E_P.

The main reason for having proposed this result is to stimulate (i) further considerations on the link between α and $\alpha_G^{(ve)}$ and (ii) a greater attention to N when searching fundamental relationships between the constants of nature. Another numerical accident, which is worth noticing here because perhaps of possible interest, concerns the key coefficients (6,10); indeed $\pi a/b = 137.469$, which differs from 137.036 by about 0.3% only. It has been remarked the obvious fact that even small deviations of any lepton or quark mass from the input values (6,2) and (6,7), (6,8) affect the regression coefficients (6,10). So, at least from a numerical point of view, it is sensible to suppose that a very fine-tuning of some among these input values could match exactly the fine structure constant. This optimization is certainly justified: indeed the electron, muon and tau masses only are experimentally known with a degree of accuracy such to exclude any minimum revision; instead, for the reasons previously remarked, there are ample margins of small adjustment for the neutrino and isolate quark masses implemented in the present calculations. On the one hand, such an effort is physically sensible only guessing a good physical reason to expect that the regression coefficients should be actually related to α; on the other hand is evident the interest to provide such an explanation, wholly physical and not merely numerical, of the coefficients that determine the fundamental masses of our universe.

Some further points are still to be better clarified; they pose several questions, some of which are still unanswered. One of them concerns the correspondence (6,9) between leptons and quarks: is it really mere consequence of the increasing order of their masses, thus a mere definition to exploit eq (2,4), or is it actually due to something else still hidden in the correspondence (6,9) and not yet evidenced? But perhaps the most amazing point is that also the leptons fulfill the eq (2,4) just thanks to this correspondence. In the case of quarks, the dependence of their masses on $i \equiv \delta n$ was tentatively explained through the self-interaction of bare quarks with their own clouds of gluons and the self-interaction between these latter: with reference to eq (2,1), a different interaction strength is related both to a dissimilar n/m and to a dissimilar n/V, thus explaining not only the different m of the various quarks but also the equations (5,3) and (6,5). Yet thereafter also the leptons have been handled through the eq (2,4) simply guessing an analogy of behavior for both kinds of fundamental particles of our universe. But, strictly speaking from a physical point of view, why should the lepton masses depend on δn? On the one side the extension of the eq (2,4) certainly works well, because the well known masses of electron, muon and tau particles fit the proposed scheme; the fact of having included these masses among the results calculated through eq (6,10) supports also the values of the masses not experimentally available. On the other side, however, in lack of a self-interaction mechanism characteristic of the quarks only, the question arises: is justified a similar mechanism for the vacuum polarization around the real charges with formation of virtual particle-antiparticle pairs? Does the interaction between these couples of virtual particles/antiparticles surrogate the self-interaction of the quark-gluon plasma? Work is in advanced progress on these points.

Submitted on: December 19, 2012 / Accepted on: December 27, 2012

References

1. Leonhardt U., Paul H. Measuring the quantum state of light. *Progress in Quantum Electronics*, 1995, v. 19, 89–130.
2. Wigner E.P. On the quantum correction for thermodynamic equilibrium. *Physical Review*, 1932, v. 40, 749–759.
3. Allen R.L., Mills D.W. Signal Analysis: Time, Frequency, Scale, and Structure. Wiley-Interscience, NJ, 2004.
4. Tosto S. Spooky action at a distance or action at a spooky distance? *Progress in Physics*, 2012, v. 1, 11–26.
5. Tosto S. An analysis of states in the phase space: the energy levels of quantum systems. *Il Nuovo Cimento B*, 1996, v. 111, 193–215.
6. Tosto S. An analysis of states in the phase space: the diatomic molecules. *Il Nuovo Cimento D*, 1996, v. 18, 1363–1394.
7. Tosto S. Quantum uncertainty and relativity. *Progress in Physics*, 2012, v. 2, 58–81.
8. Glashow S.L. Partial-symmetries of weak interactions. *Nuclear Physics* 1961, v. 22(4), 579–588.
9. Englert F., Brout R. Broken Symmetry and the Mass of Gauge Vector Mesons. *Physical Review Letters*, 1964, v. 13(9), 321–323.
10. Higgs P.W. Broken Symmetries and the Masses of Gauge Bosons. *Physical Review Letters*, 1964, v. 13(16), 508–509.
11. Guralnik G.S., Hagen C.R., Kibble T.W.B. Global Conservation Laws and Massless Particles. *Physical Review Letters*, 1964, v. 13(20), 585–587.
12. Tosto S. Fundamentals of diffusion for optimized applications, Energia, Ambiente, *Innovazione*, 2012, v. 4–5, 94–107.
13. Pohl R. et al. *Nature*, 2010, v. 466, 213–217.
14. Nakamura K. et al., (Particle Data Group), Quarks, 2010, JPG 37, 075021
15. Griffiths D. Introduction to Elementary Particles, Wiley, 1987
16. Landau L., Lifchits E. Physique Statistique (in French), Editions MIR, Moscow, 1967
17. Gonzalez-Garcia M.C., Maltoni M. Phenomenology with massive Neutrinos. *Physics Reports*, 2008, v. 469, 1–129.

Strain Energy Density in the Elastodynamics of the Spacetime Continuum and the Electromagnetic Field

Pierre A. Millette

University of Ottawa (alumnus), Ottawa, Canada. E-mail: PierreAMillette@alumni.uottawa.ca

We investigate the strain energy density of the spacetime continuum in the Elastodynamics of the Spacetime Continuum by applying continuum mechanical results to strained spacetime. The strain energy density is a scalar. We find that it is separated into two terms: the first one expresses the dilatation energy density (the "mass" longitudinal term) while the second one expresses the distortion energy density (the "massless" transverse term). The quadratic structure of the energy relation of Special Relativity is found to be present in the theory. In addition, we find that the kinetic energy pc is carried by the distortion part of the deformation, while the dilatation part carries only the rest-mass energy. The strain energy density of the electromagnetic energy-momentum stress tensor is calculated. The dilatation energy density (the rest-mass energy density of the photon) is found to be 0 as expected. The transverse distortion energy density is found to include a longitudinal electromagnetic energy flux term, from the Poynting vector, that is massless as it is due to distortion, not dilatation, of the spacetime continuum. However, because this energy flux is along the direction of propagation (i.e. longitudinal), it gives rise to the particle aspect of the electromagnetic field, the photon.

1 Introduction

The Elastodynamics of the Spacetime Continuum (*STCED*) is based on the application of a continuum mechanical approach to the analysis of the spacetime continuum [1–3]. The applied stresses from the energy-momentum stress tensor result in strains in, and the deformation of, the spacetime continuum (*STC*). In this paper, we explore the resulting strain energy per unit volume, that is the strain energy density, resulting from the Elastodynamics of the Spacetime Continuum. We then calculate the strain energy density of the electromagnetic field from the electromagnetic energy-momentum stress tensor.

2 Strain energy density of the spacetime continuum

The strain energy density of the spacetime continuum is a scalar given by [4, see p. 51]

$$\mathcal{E} = \frac{1}{2} T^{\alpha\beta} \varepsilon_{\alpha\beta} \tag{1}$$

where $\varepsilon_{\alpha\beta}$ is the strain tensor and $T^{\alpha\beta}$ is the energy-momentum stress tensor. Introducing the strain and stress deviators from (12) and (15) respectively from Millette [2], this equation becomes

$$\mathcal{E} = \frac{1}{2} \left(t^{\alpha\beta} + t g^{\alpha\beta} \right) \left(e_{\alpha\beta} + e g_{\alpha\beta} \right). \tag{2}$$

Multiplying and using relations $e^{\alpha}{}_{\alpha} = 0$ and $t^{\alpha}{}_{\alpha} = 0$ from the definition of the strain and stress deviators, we obtain

$$\mathcal{E} = \frac{1}{2} \left(4te + t^{\alpha\beta} e_{\alpha\beta} \right). \tag{3}$$

Using (11) from [2] to express the stresses in terms of the strains, this expression becomes

$$\mathcal{E} = \frac{1}{2} \kappa_0 \varepsilon^2 + \mu_0 e^{\alpha\beta} e_{\alpha\beta} \tag{4}$$

where the Lamé elastic constant of the spacetime continuum μ_0 is the shear modulus (the resistance of the continuum to *distortions*) and κ_0 is the bulk modulus (the resistance of the continuum to *dilatations*). Alternatively, again using (11) from [2] to express the strains in terms of the stresses, this expression can be written as

$$\mathcal{E} = \frac{1}{2\kappa_0} t^2 + \frac{1}{4\mu_0} t^{\alpha\beta} t_{\alpha\beta}. \tag{5}$$

3 Physical interpretation of the strain energy density

The strain energy density is separated into two terms: the first one expresses the dilatation energy density (the "mass" longitudinal term) while the second one expresses the distortion energy density (the "massless" transverse term):

$$\mathcal{E} = \mathcal{E}_{\parallel} + \mathcal{E}_{\perp} \tag{6}$$

where

$$\mathcal{E}_{\parallel} = \frac{1}{2} \kappa_0 \varepsilon^2 \equiv \frac{1}{2\kappa_0} t^2 \tag{7}$$

and

$$\mathcal{E}_{\perp} = \mu_0 e^{\alpha\beta} e_{\alpha\beta} \equiv \frac{1}{4\mu_0} t^{\alpha\beta} t_{\alpha\beta}. \tag{8}$$

Using (10) from [2] into (7), we obtain

$$\mathcal{E}_{\parallel} = \frac{1}{32\kappa_0} \left[\rho c^2 \right]^2. \tag{9}$$

The rest-mass energy density divided by the bulk modulus κ_0, and the transverse energy density divided by the shear modulus μ_0, have dimensions of energy density as expected.

Multiplying (5) by $32\kappa_0$ and using (9), we obtain

$$32\,\kappa_0\,\mathcal{E} = \rho^2 c^4 + 8\,\frac{\kappa_0}{\mu_0}\,t^{\alpha\beta}t_{\alpha\beta}. \tag{10}$$

Noting that $t^{\alpha\beta}t_{\alpha\beta}$ is quadratic in structure, we see that this equation is similar to the energy relation of Special Relativity [5, see p. 51] for energy density

$$\hat{E}^2 = \rho^2 c^4 + \hat{p}^{\,2} c^2 \tag{11}$$

where $\hat{E}$ is the total energy density and $\hat{p}$ the momentum density.

The quadratic structure of the energy relation of Special Relativity is thus found to be present in the Elastodynamics of the Spacetime Continuum. Equations (10) and (11) also imply that the kinetic energy pc is carried by the distortion part of the deformation, while the dilatation part carries only the rest mass energy.

This observation is in agreement with photons which are massless ($\mathcal{E}_{\|} = 0$), as will be shown in the next section, but still carry kinetic energy in the transverse electromagnetic wave distortions ($\mathcal{E}_{\perp} = t^{\alpha\beta}t_{\alpha\beta}/4\mu_0$).

4 Electromagnetic strain energy density

The strain energy density of the electromagnetic energy-momentum stress tensor is calculated. Note that Rationalized MKSA or SI (Système International) units are used in this paper as noted previously in [3]. In addition, the electromagnetic permittivity of free space ϵ_{em} and the electromagnetic permeability of free space μ_{em} are written with "em" subscripts as the "0" subscripts are used in the spacetime constants. This allows us to differentiate between μ_{em} and μ_0.

Starting from the symmetric electromagnetic stress tensor [6, see pp. 64–66]

$$\Theta^{\mu\nu} = \frac{1}{\mu_{em}}\left(F^{\mu}{}_{\alpha}F^{\alpha\nu} + \frac{1}{4}\,g^{\mu\nu}F^{\alpha\beta}F_{\alpha\beta}\right) \equiv \sigma^{\mu\nu}, \tag{12}$$

with $g^{\mu\nu} = \eta^{\mu\nu}$ of signature $(+---)$, and the field-strength tensor components [6, see p. 43]

$$F^{\mu\nu} = \begin{pmatrix} 0 & -E_x/c & -E_y/c & -E_z/c \\ E_x/c & 0 & B_z & -B_y \\ E_y/c & -B_z & 0 & B_x \\ E_z/c & B_y & -B_x & 0 \end{pmatrix} \tag{13}$$

and

$$F_{\mu\nu} = \begin{pmatrix} 0 & E_x/c & E_y/c & E_z/c \\ -E_x/c & 0 & B_z & -B_y \\ -E_y/c & -B_z & 0 & B_x \\ -E_z/c & B_y & -B_x & 0 \end{pmatrix}, \tag{14}$$

we obtain [6, see p. 66] [7, see p. 141],

$$\begin{aligned} \sigma^{00} &= \tfrac{1}{2}\left(\epsilon_{em}E^2 + \tfrac{1}{\mu_{em}}B^2\right) = \tfrac{1}{2}\epsilon_{em}\left(E^2 + c^2B^2\right) \\ \sigma^{0j} &= \sigma^{j0} = \tfrac{1}{c\mu_{em}}\,(E\times B)^j = \epsilon_{em}c\,(E\times B)^j = \tfrac{1}{c}S^j \\ \sigma^{jk} &= -\left(\epsilon_{em}E^jE^k + \tfrac{1}{\mu_{em}}B^jB^k\right) + \tfrac{1}{2}\delta^{jk}\left(\epsilon_{em}E^2 + \tfrac{1}{\mu_{em}}B^2\right) \\ &= -\epsilon_{em}\left[\left(E^jE^k + c^2B^jB^k\right) - \tfrac{1}{2}\delta^{jk}\left(E^2 + c^2B^2\right)\right] \end{aligned} \tag{15}$$

where S^j is the Poynting vector, and where we use the notation $\sigma^{\mu\nu} \equiv \Theta^{\mu\nu}$ as a generalization of the σ^{ij} Maxwell stress tensor notation. Hence the electromagnetic stress tensor is given by [6, see p. 66]:

$$\sigma^{\mu\nu} = \begin{pmatrix} \frac{1}{2}\epsilon_{em}\left(E^2+c^2B^2\right) & S_x/c & S_y/c & S_z/c \\ S_x/c & -\sigma_{xx} & -\sigma_{xy} & -\sigma_{xz} \\ S_y/c & -\sigma_{yx} & -\sigma_{yy} & -\sigma_{yz} \\ S_z/c & -\sigma_{zx} & -\sigma_{zy} & -\sigma_{zz} \end{pmatrix}, \tag{16}$$

where σ^{ij} is the Maxwell stress tensor. Using the relation $\sigma_{\alpha\beta} = \eta_{\alpha\mu}\eta_{\beta\nu}\sigma^{\mu\nu}$ to lower the indices of $\sigma^{\mu\nu}$, we obtain

$$\sigma_{\mu\nu} = \begin{pmatrix} \frac{1}{2}\epsilon_{em}\left(E^2+c^2B^2\right) & -S_x/c & -S_y/c & -S_z/c \\ -S_x/c & -\sigma_{xx} & -\sigma_{xy} & -\sigma_{xz} \\ -S_y/c & -\sigma_{yx} & -\sigma_{yy} & -\sigma_{yz} \\ -S_z/c & -\sigma_{zx} & -\sigma_{zy} & -\sigma_{zz} \end{pmatrix}. \tag{17}$$

4.1 Calculation of the longitudinal (mass) term

The mass term is calculated from (7) and (17) of [2]:

$$\mathcal{E}_{\|} = \frac{1}{2\kappa_0}\,t^2 = \frac{1}{32\kappa_0}\,(\sigma^{\alpha}{}_{\alpha})^2. \tag{18}$$

The term $\sigma^{\alpha}{}_{\alpha}$ is calculated from:

$$\begin{aligned} \sigma^{\alpha}{}_{\alpha} &= \eta_{\alpha\beta}\sigma^{\alpha\beta} \\ &= \eta_{\alpha0}\sigma^{\alpha0} + \eta_{\alpha1}\sigma^{\alpha1} + \eta_{\alpha2}\sigma^{\alpha2} + \eta_{\alpha3}\sigma^{\alpha3} \\ &= \eta_{00}\sigma^{00} + \eta_{11}\sigma^{11} + \eta_{22}\sigma^{22} + \eta_{33}\sigma^{33}. \end{aligned} \tag{19}$$

Substituting from (16) and the metric $\eta^{\mu\nu}$ of signature $(+---)$, we obtain:

$$\sigma^{\alpha}{}_{\alpha} = \frac{1}{2}\,\epsilon_{em}\left(E^2 + c^2B^2\right) + \sigma_{xx} + \sigma_{yy} + \sigma_{zz}. \tag{20}$$

Substituting from (15), this expands to:

$$\begin{aligned} &\sigma^{\alpha}{}_{\alpha} = \tfrac{1}{2}\,\epsilon_{em}\left(E^2 + c^2B^2\right) + \epsilon_{em}\left(E_x{}^2 + c^2B_x{}^2\right) + \\ &+\epsilon_{em}\left(E_y{}^2 + c^2B_y{}^2\right) + \epsilon_{em}\left(E_z{}^2 + c^2B_z{}^2\right) - \\ &-\tfrac{3}{2}\,\epsilon_{em}\left(E^2 + c^2B^2\right) \end{aligned} \tag{21}$$

and further,

$$\sigma^{\alpha}{}_{\alpha} = \tfrac{1}{2}\,\epsilon_{em}\left(E^2 + c^2B^2\right) + \epsilon_{em}\left(E^2 + c^2B^2\right) - \\ -\tfrac{3}{2}\,\epsilon_{em}\left(E^2 + c^2B^2\right). \tag{22}$$

Hence

$$\sigma^{\alpha}{}_{\alpha} = 0 \tag{23}$$

and, substituting into (18),

$$\mathcal{E}_{\parallel} = 0 \tag{24}$$

as expected [6, see pp. 64–66]. This derivation thus shows that the rest-mass energy density of the photon is 0.

4.2 Calculation of the transverse (massless) term

The transverse term is calculated from (8), viz.

$$\mathcal{E}_{\perp} = \frac{1}{4\mu_0}\, t^{\alpha\beta} t_{\alpha\beta}. \tag{25}$$

Given that $t = \frac{1}{4}\sigma^{\alpha}{}_{\alpha} = 0$, then $t^{\alpha\beta} = \sigma^{\alpha\beta}$ and the terms $\sigma^{\alpha\beta}\sigma_{\alpha\beta}$ are calculated from the components of the electromagnetic stress tensors of (16) and (17). Substituting for the diagonal elements and making use of the symmetry of the Poynting component terms and of the Maxwell stress tensor terms from (16) and (17), this expands to:

$$\sigma^{\alpha\beta}\sigma_{\alpha\beta} = \tfrac{1}{4}\,\epsilon_{em}^2\left(E^2 + c^2B^2\right)^2 + \\ +\epsilon_{em}^2\left[\left(E_xE_x + c^2B_xB_x\right) - \tfrac{1}{2}\left(E^2 + c^2B^2\right)\right]^2 + \\ +\epsilon_{em}^2\left[\left(E_yE_y + c^2B_yB_y\right) - \tfrac{1}{2}\left(E^2 + c^2B^2\right)\right]^2 + \\ +\epsilon_{em}^2\left[\left(E_zE_z + c^2B_zB_z\right) - \tfrac{1}{2}\left(E^2 + c^2B^2\right)\right]^2 - \\ -2\left(S_x/c\right)^2 - 2\left(S_y/c\right)^2 - 2\left(S_z/c\right)^2 + \\ +2\left(\sigma_{xy}\right)^2 + 2\left(\sigma_{yz}\right)^2 + 2\left(\sigma_{zx}\right)^2. \tag{26}$$

The E-B terms expand to:

$$\text{EBterms} = \epsilon_{em}^2\left[\tfrac{1}{4}\left(E^2 + c^2B^2\right)^2 + \right. \\ +\left(E_x{}^2 + c^2B_x{}^2\right)^2 - \left(E_x{}^2 + c^2B_x{}^2\right)\left(E^2 + c^2B^2\right) + \\ +\left(E_y{}^2 + c^2B_y{}^2\right)^2 - \left(E_y{}^2 + c^2B_y{}^2\right)\left(E^2 + c^2B^2\right) + \\ +\left(E_z{}^2 + c^2B_z{}^2\right)^2 - \left(E_z{}^2 + c^2B_z{}^2\right)\left(E^2 + c^2B^2\right) + \\ \left.+\tfrac{3}{4}\left(E^2 + c^2B^2\right)^2\right]. \tag{27}$$

Simplifying,

$$\text{EBterms} = \epsilon_{em}^2\left[\left(E^2 + c^2B^2\right)^2 - \left(E_x{}^2 + c^2B_x{}^2 + \right.\right. \\ +E_y{}^2 + c^2B_y{}^2 + E_z{}^2 + c^2B_z{}^2\left)\left(E^2 + c^2B^2\right) + \right. \\ +\left(E_x{}^2 + c^2B_x{}^2\right)^2 + \left(E_y{}^2 + c^2B_y{}^2\right)^2 + \\ \left.+\left(E_z{}^2 + c^2B_z{}^2\right)^2\right] \tag{28}$$

which gives

$$\text{EBterms} = \epsilon_{em}^2\left[\left(E^2 + c^2B^2\right)^2 - \left(E^2 + c^2B^2\right)^2 + \right. \\ +\left(E_x{}^2 + c^2B_x{}^2\right)^2 + \left(E_y{}^2 + c^2B_y{}^2\right)^2 + \\ \left.+\left(E_z{}^2 + c^2B_z{}^2\right)^2\right] \tag{29}$$

and finally

$$\text{EBterms} = \epsilon_{em}^2\left[\left(E_x{}^4 + E_y{}^4 + E_z{}^4\right) + \right. \\ +c^4\left(B_x{}^4 + B_y{}^4 + B_z{}^4\right) + \\ \left.+2c^2\left(E_x{}^2B_x{}^2 + E_y{}^2B_y{}^2 + E_z{}^2B_z{}^2\right)\right]. \tag{30}$$

Including the E-B terms in (26), substituting from (15), expanding the Poynting vector and rearranging, we obtain

$$\sigma^{\alpha\beta}\sigma_{\alpha\beta} = \epsilon_{em}^2\left[\left(E_x{}^4 + E_y{}^4 + E_z{}^4\right) + c^4\left(B_x{}^4 + B_y{}^4 + \right.\right. \\ \left.+B_z{}^4\right) + 2c^2\left(E_x{}^2B_x{}^2 + E_y{}^2B_y{}^2 + E_z{}^2B_z{}^2\right)\Big] - \\ -2\epsilon_{em}^2c^2\left[\left(E_yB_z - E_zB_y\right)^2 + \left(-E_xB_z + E_zB_x\right)^2 + \right. \\ \left.+\left(E_xB_y - E_yB_x\right)^2\right] + 2\epsilon_{em}^2\left[\left(E_xE_y + c^2B_xB_y\right)^2 + \right. \\ \left.+\left(E_yE_z + c^2B_yB_z\right)^2 + \left(E_zE_x + c^2B_zB_x\right)^2\right]. \tag{31}$$

Expanding the quadratic expressions,

$$\sigma^{\alpha\beta}\sigma_{\alpha\beta} = \epsilon_{em}^2\left[\left(E_x{}^4 + E_y{}^4 + E_z{}^4\right) + c^4\left(B_x{}^4 + B_y{}^4 + \right.\right. \\ \left.+B_z{}^4\right) + 2c^2\left(E_x{}^2B_x{}^2 + E_y{}^2B_y{}^2 + E_z{}^2B_z{}^2\right)\Big] - \\ -2\epsilon_{em}^2c^2\left[E_x{}^2B_y{}^2 + E_y{}^2B_z{}^2 + E_z{}^2B_x{}^2 + B_x{}^2E_y{}^2 + \right. \\ +B_y{}^2E_z{}^2 + B_z{}^2E_x{}^2 - 2\left(E_xE_yB_xB_y + E_yE_zB_yB_z + \right. \\ \left.\left.+E_zE_xB_zB_x\right)\right] + 2\epsilon_{em}^2\left[\left(E_x{}^2E_y{}^2 + E_y{}^2E_z{}^2 + \right.\right. \tag{32}$$

$$+E_z{}^2E_x{}^2\Big) + 2c^2\left(E_xE_yB_xB_y + E_yE_zB_yB_z + \right.$$
$$\left.+E_zE_xB_zB_x\right) + c^4\left(B_x{}^2B_y{}^2 + B_y{}^2B_z{}^2 + B_z{}^2B_x{}^2\right)\Big]$$

Grouping the terms in powers of c together,

$$\begin{aligned}\frac{1}{\epsilon_{em}^2}\,\sigma^{\alpha\beta}\sigma_{\alpha\beta} = &\Big[\left(E_x{}^4 + E_y{}^4 + E_z{}^4\right) + 2\left(E_x{}^2E_y{}^2 + \right.\\ &\left.+E_y{}^2E_z{}^2 + E_z{}^2E_x{}^2\right)\Big] + 2c^2\Big[\left(E_x{}^2B_x{}^2 + E_y{}^2B_y{}^2 + \right.\\ &\left.+E_z{}^2B_z{}^2\right) - \left(E_x{}^2B_y{}^2 + E_y{}^2B_z{}^2 + E_z{}^2B_x{}^2 + B_x{}^2E_y{}^2 + \right.\\ &\left.+B_y{}^2E_z{}^2 + B_z{}^2E_x{}^2\right) + 4\left(E_xE_yB_xB_y + E_yE_zB_yB_z + \right.\\ &\left.+E_zE_xB_zB_x\right)\Big] + c^4\Big[\left(B_x{}^4 + B_y{}^4 + B_z{}^4\right) + \\ &+2\left(B_x{}^2B_y{}^2 + B_y{}^2B_z{}^2 + B_z{}^2B_x{}^2\right)\Big].\end{aligned} \tag{33}$$

Simplifying,

$$\begin{aligned}\frac{1}{\epsilon_{em}^2}\,\sigma^{\alpha\beta}\sigma_{\alpha\beta} = &\left(E_x{}^2 + E_y{}^2 + E_z{}^2\right)^2 + \\ &+2c^2\left(E_x{}^2 + E_y{}^2 + E_z{}^2\right)\left(B_x{}^2 + B_y{}^2 + B_z{}^2\right) - \\ &-2c^2\Big[2\left(E_x{}^2B_y{}^2 + E_y{}^2B_z{}^2 + E_z{}^2B_x{}^2 + \right.\\ &\left.+B_x{}^2E_y{}^2 + B_y{}^2E_z{}^2 + B_z{}^2E_x{}^2\right) - 4\left(E_xE_yB_xB_y + \right.\\ &\left.+E_yE_zB_yB_z + E_zE_xB_zB_x\right)\Big] + c^4\left(B_x{}^2 + B_y{}^2 + B_z{}^2\right)^2\end{aligned} \tag{34}$$

which is further simplified to

$$\begin{aligned}\frac{1}{\epsilon_{em}^2}\,\sigma^{\alpha\beta}\sigma_{\alpha\beta} = &\left(E^4 + 2c^2E^2B^2 + c^4B^4\right) - \\ &-4c^2\Big[\left(E_yB_z - B_yE_z\right)^2 + (E_zB_x - B_zE_x)^2 + \\ &+\left(E_xB_y - B_xE_y\right)^2\Big].\end{aligned} \tag{35}$$

Making use of the definition of the Poynting vector from (15), we obtain

$$\begin{aligned}\sigma^{\alpha\beta}\sigma_{\alpha\beta} = &\epsilon_{em}^2\left(E^2 + c^2B^2\right)^2 - \\ &-4\epsilon_{em}^2c^2\left[(E\times B)_x{}^2 + (E\times B)_y{}^2 + (E\times B)_z{}^2\right]\end{aligned} \tag{36}$$

and finally

$$\sigma^{\alpha\beta}\sigma_{\alpha\beta} = \epsilon_{em}^2\left(E^2 + c^2B^2\right)^2 - \frac{4}{c^2}\left(S_x{}^2 + S_y{}^2 + S_z{}^2\right). \tag{37}$$

Substituting in (25), the transverse term becomes

$$\mathcal{E}_\perp = \frac{1}{4\mu_0}\left[\epsilon_{em}^2\left(E^2 + c^2B^2\right)^2 - \frac{4}{c^2}\,S^2\right] \tag{38}$$

or

$$\mathcal{E}_\perp = \frac{1}{\mu_0}\left[U_{em}{}^2 - \frac{1}{c^2}\,S^2\right] \tag{39}$$

where $U_{em} = \frac{1}{2}\,\epsilon_{em}\,(E^2 + c^2B^2)$ is the electromagnetic field energy density.

4.3 Electromagnetic field strain energy density and the photon

$\boldsymbol{S}$ is the electromagnetic energy flux along the direction of propagation [6, see p. 62]. As noted by Feynman [8, see pp. 27-1–2], local conservation of the electromagnetic field energy can be written as

$$-\frac{\partial U_{em}}{\partial t} = \nabla\cdot\boldsymbol{S}, \tag{40}$$

where the term $\boldsymbol{E}\cdot\boldsymbol{j}$ representing the work done on the matter inside the volume is 0 in the absence of charges (due to the absence of mass [3]). By analogy with the current density four-vector $j^\nu = (c\varrho, \boldsymbol{j})$, where ϱ is the charge density, and $\boldsymbol{j}$ is the current density vector, which obeys a similar conservation relation, we define the Poynting four-vector

$$S^\nu = (cU_{em}, \boldsymbol{S}), \tag{41}$$

where U_{em} is the electromagnetic field energy density, and $\boldsymbol{S}$ is the Poynting vector. Furthermore, as per (40), S^ν satisfies

$$\partial_\nu S^\nu = 0. \tag{42}$$

Using definition (41) in (39), that equation becomes

$$\mathcal{E}_\perp = \frac{1}{\mu_0c^2}\,S_\nu S^\nu. \tag{43}$$

The indefiniteness of the location of the field energy referred to by Feynman [8, see p. 27-6] is thus resolved: the electromagnetic field energy resides in the distortions (transverse displacements) of the spacetime continuum.

Hence the invariant electromagnetic strain energy density is given by

$$\mathcal{E} = \frac{1}{\mu_0c^2}\,S_\nu S^\nu \tag{44}$$

where we have used $\rho = 0$ as per (23). This confirms that S^ν as defined in (41) is a four-vector.

It is surprising that a longitudinal energy flow term is part of the transverse strain energy density i.e. S^2/μ_0c^2 in (39). We note that this term arises from the time-space components of (16) and (17) and can be seen to correspond to the transverse displacements along the *time-space* planes which are folded along the direction of propagation in 3-space as the Poynting vector. The electromagnetic field energy density term $U_{em}{}^2/\mu_0$ and the electromagnetic field energy flux term S^2/μ_0c^2 are thus combined into the transverse strain energy density. The negative sign arises from the signature $(+---)$ of the metric tensor $\eta^{\mu\nu}$.

This longitudinal electromagnetic energy flux is massless as it is due to distortion, not dilatation, of the spacetime continuum. However, because this energy flux is along the direction of propagation (i.e. longitudinal), it gives rise to the particle aspect of the electromagnetic field, the photon. As shown in [9, see pp. 174-5] [10, see p. 58], in the quantum theory of electromagnetic radiation, an intensity operator derived from the Poynting vector has, as expectation value, photons in the direction of propagation.

This implies that the $(pc)^2$ term of the energy relation of Special Relativity needs to be separated into transverse and longitudinal massless terms as follows:

$$\hat{E}^2 = \underbrace{\rho^2 c^4}_{\mathcal{E}_{\parallel}} + \underbrace{\hat{p}_{\parallel}^2 c^2 + \hat{p}_{\perp}^2 c^2}_{massless\ \mathcal{E}_{\perp}} \tag{45}$$

where $\hat{p}_{\parallel}$ is the massless longitudinal momentum density. Equation (39) shows that the electromagnetic field energy density term ${U_{em}}^2/\mu_0$ is reduced by the electromagnetic field energy flux term $S^2/\mu_0 c^2$ in the transverse strain energy density, due to photons propagating in the longitudinal direction. Thus the kinetic energy is carried by the distortion part of the deformation, while the dilatation part carries only the rest-mass energy, which in this case is 0.

As shown in (9), (10) and (11), the constant of proportionality to transform energy density squared ($\hat{E}^2$) into strain energy density ($\mathcal{E}$) is $1/(32\kappa_0)$:

$$\mathcal{E}_{\parallel} = \frac{1}{32\kappa_0}\left[\rho c^2\right]^2 \tag{46}$$

$$\mathcal{E} = \frac{1}{32\kappa_0}\hat{E}^2 \tag{47}$$

$$\mathcal{E}_{\perp} = \frac{1}{32\kappa_0}\left[\hat{p}_{\parallel}^2 c^2 + \hat{p}_{\perp}^2 c^2\right] = \frac{1}{4\mu_0}\, t^{\alpha\beta} t_{\alpha\beta}. \tag{48}$$

Substituting (39) into (48), we obtain

$$\mathcal{E}_{\perp} = \frac{1}{32\kappa_0}\left[\hat{p}_{\parallel}^2 c^2 + \hat{p}_{\perp}^2 c^2\right] = \frac{1}{\mu_0}\left[{U_{em}}^2 - \frac{1}{c^2}S^2\right] \tag{49}$$

and

$$\hat{p}_{\parallel}^2 c^2 + \hat{p}_{\perp}^2 c^2 = \frac{32\kappa_0}{\mu_0}\left[{U_{em}}^2 - \frac{1}{c^2}S^2\right] \tag{50}$$

This suggests that

$$\mu_0 = 32\kappa_0, \tag{51}$$

to obtain the relation

$$\hat{p}_{\parallel}^2 c^2 + \hat{p}_{\perp}^2 c^2 = {U_{em}}^2 - \frac{1}{c^2}S^2. \tag{52}$$

5 Discussion and conclusion

In this paper, we have analyzed the strain energy density of the spacetime continuum in *STCED* and evaluated it for the electromagnetic stress tensor. We have found that the strain energy density is separated into two terms: the first one expresses the dilatation energy density (the "mass" longitudinal term) while the second one expresses the distortion energy density (the "massless" transverse term). We have found that the quadratic structure of the energy relation of Special Relativity is present in the strain energy density of the Elastodynamics of the Spacetime Continuum. We have also found that the kinetic energy pc is carried by the distortion part of the deformation, while the dilatation part carries only the rest mass energy.

We have calculated the strain energy density of the electromagnetic energy-momentum stress tensor. We have found that the dilatation longitudinal (mass) term of the strain energy density and hence the rest-mass energy density of the photon is 0. We have found that the distortion transverse (massless) term of the strain energy density is a combination of the electromagnetic field energy density term ${U_{em}}^2/\mu_0$ and the electromagnetic field energy flux term $S^2/\mu_0 c^2$, calculated from the Poynting vector. This longitudinal electromagnetic energy flux is massless as it is due to distortion, not dilatation, of the spacetime continuum. However, because this energy flux is along the direction of propagation (i.e. longitudinal), it gives rise to the particle aspect of the electromagnetic field, the photon.

Submitted on January 7, 2013 / Accepted on January 11, 2013

References

1. Millette P.A. On the Decomposition of the Spacetime Metric Tensor and of Tensor Fields in Strained Spacetime. *Progress in Physics*, 2012, v. 4, 5–8.
2. Millette P.A. The Elastodynamics of the Spacetime Continuum as a Framework for Strained Spacetime. *Progress in Physics*, 2013, v. 1, 55–59.
3. Millette P.A. Derivation of Electromagnetism from the Elastodynamics of the Spacetime Continuum. *Progress in Physics*, 2013, v. 2, 12–15.
4. Flügge W. Tensor Analysis and Continuum Mechanics. Springer-Verlag, New York, 1972.
5. Lawden D.F. Tensor Calculus and Relativity. Methuen & Co, London, 1971.
6. Charap J.M. Covariant Electrodynamics, A Concise Guide. The John Hopkins University Press, Baltimore, 2011.
7. Misner C.W., Thorne K.S., Wheeler J.A. Gravitation. W.H. Freeman and Company, San Francisco, 1973.
8. Feynman R.P., Leighton R.B., Sands M. Lectures on Physics, Volume II, Mainly Electromagnetism and Matter. Addison-Wesley Publishing Company, Reading, Massachusetts, 1975.
9. Loudon R. The Quantum Theory of Light, Third Edition. Oxford University Press, Oxford, 2000.
10. Heitler W. The Quantum Theory of Radiation, Third Edition. Dover Publications, Inc, New York, 1984.

Liquid Metallic Hydrogen III. Intercalation and Lattice Exclusion Versus Gravitational Settling and Their Consequences Relative to Internal Structure, Surface Activity, and Solar Winds in the Sun

Joseph Christophe Robitaille* and Pierre-Marie Robitaille†

*P.O. Box 21025, Columbus, Ohio, 43221.
†Department of Radiology, The Ohio State University, 395 W. 12th Ave, Columbus, Ohio 43210, USA.
robitaille.1@osu.edu

Invocation of a liquid metallic hydrogen model (Robitaille P.M. Liquid Metallic Hydrogen: A Building Block for the Liquid Sun. *Progr. Phys*., 2011, v. 3, 60–74; Robitaille P.M. Liquid Metallic Hydrogen II: A Critical Assessment of Current and Primordial Helium Levels in Sun. *Progr. Phys*., 2013, v. 2, 35–47) brings with it a set of advantages for understanding solar physics which will always remain unavailable to the gaseous models. Liquids characteristically act as solvents and incorporate solutes within their often fleeting structural matrix. They possess widely varying solubility products and often reject the solute altogether. In that case, the solute becomes immiscible. "Lattice exclusion" can be invoked for atoms which attempt to incorporate themselves into liquid metallic hydrogen. In order to conserve the integrity of its conduction bands, it is anticipated that a graphite-like metallic hydrogen lattice should not permit incorporation of other elements into its in-plane hexagonal hydrogen framework. Based on the physics observed in the intercalation compounds of graphite, non-hydrogen atoms within liquid metallic hydrogen could reside between adjacent hexagonal proton planes. Consequently, the forces associated with solubility products and associated lattice exclusion envisioned in liquid metallic hydrogen for solutes would restrict gravitational settling. The hexagonal metallic hydrogen layered lattice could provide a powerful driving force for excluding heavier elements from the solar body. Herein lies a new exfoliative force to drive both surface activity (flares, coronal mass ejections, prominences) and solar winds with serious consequences relative to the p–p reaction and CNO cycle in the Sun. At the same time, the idea that non-hydrogen atomic nuclei can exist between layers of metallic hydrogen leads to a fascinating array of possibilities with respect to nucleosynthesis. Powerful parallels can be drawn to the intercalation compounds of graphite and their exfoliative forces. In this context, solar winds and activity provide evidence that the lattice of the Sun is not only excluding, but expelling helium and higher elements from the solar body. Finally, exfoliative forces could provide new mechanisms to help understand the creation of planets, satellites, red giants, and even supernova.

Science is a living thing, not a dead dogma. It follows that no idea should be suppressed. That I totally disagree with what you say, but will defend to the death your right to say it, must be our underlying principle. And it applies to ideas that look like nonsense. We must not forget that some of the best ideas seemed like nonsense at first. The truth will prevail in the end. Nonsense will fall of its own weight, by a sort of intellectual law of gravitation. If we bat it about, we shall only keep an error in the air a little longer. And a new truth will go into orbit.

Cecilia Payne-Gaposchkin [1, p. 233]

1 Introduction

As humanity will always be unable to conduct experiments on the stars, insight into stellar physics can only be gained in four steps: 1) the phase of the solar body must be properly ascertained from observational evidence, 2) the substance of which it is comprised must be identified, 3) stellar data must be acquired, and 4) the properties of earthly materials, whose physics might provide at least some level of understanding relative to astrophysical questions, must be taken into account. While such an approach cannot be assured of definitive conclusions, it can nonetheless provide a framework through which the stars can be "understood". Within this context, solar and stellar observations become paramount, as they alone can offer the necessary clues to build realistic models of the stars. Astrophysical data forms the proper foundation for any mathematical treatment. Devoid of observation, theory lacks guidance and leads to stellar models stripped of physical reality.

The postulate that the solar body exists in a liquid state [2, 3] has substantial implications with respect to internal structure and photospheric activity. To understand how the presence of layered graphite-like liquid metallic hydrogen [2, 3]

might alter our insight relative to the Sun, one must turn towards condensed matter physics and the intriguing phenomena associated with both graphite and liquid metallic hydrogen. The consequences are far reaching, touching upon virtually every aspect of astrophysics and provide an elegant setting through which one can begin to understand the most complex observations. Condensed matter offers many advantages not available to gaseous solar models and numerous facts now support a liquid state [4–20].* For instance, evidence suggests that the solar body and the photosphere are behaving as condensed matter [2, 3, 10, 14, 15, 20]. It is not simply that the photosphere gives the appearance of a surface as a result of opacity changes: it is acting as one [14]. The same can be said of every structural element on the Sun, including sunspots, faculae, and granules [15, 20]. The solar body is also behaving as a liquid in sustaining the oscillations which currently occupy helioseismologists. Seismology is a science of the condensed state [10]. Thus, there can be little doubt that the body of the Sun is condensed matter.

Though Gustav Kirchhoff had promoted the idea that the photosphere was liquid, the prevailing models of the period already focused on the gaseous state [21]. By 1865, condensed matter merely floated on the gaseous solar body [21]. Fragmented liquid or solid surfaces continued to survive as a strange addition to gaseous stars [21], but the idea that they were fully liquid never truly materialized in modern astronomy [21]. Finally, liquid stars were definitively abandoned in the days of Sir James Jeans, their last major advocate [22]. Jeans had been unable to identify a proper structural material for his models [22].

Then, in 1935, Wigner and Huntington proposed that pressurized hydrogen could assume a low energy configuration with graphite-like lattice order (see Fig. 1) [23]. In doing so, they unknowingly provided Jeans with a candidate for the solar substance [2, 3], though it is likely that he remained unaware of their solution's value. A layered graphite-like structure was critical to proper solar modeling, as this lattice configuration was closely linked with the study of thermal emission on Earth [24, 25]. Carbon-based materials, such as graphite and soot, are the closest naturally occurring examples of blackbodies [24, 25]. Consequently, they have continued to be vital in the production of such cavities in the laboratory [24, 25]. Thus, a hydrogen based lattice which could adopt a graphite-like structure provides an interesting framework for assembling the Sun. Wigner and Huntington [23] had endowed astrophysics with the perfect candidate for solar material.

In this work, we wish to briefly highlight some of the astrophysical benefits which accompany a liquid metallic hydrogen [23] model of the Sun [2, 3]. Through the liquid model, not only are features on the solar surface given a proper structural foundation, but the entire set of solar observations becomes easily understood [2, 3, 10, 14, 15, 20]. Unlike the gaseous models and their reliance on magnetic fields to explain all aspects of solar activity, the liquid model can secure answers without recourse to such phenomena. Magnetic fields become an effect, not an underlying cause. At the same time, there are ramifications associated with condensed solar matter, especially with respect to gravitational settling, solar activity, and nucleosynthesis. These should be addressed both in the context of existing gaseous models and of the new liquid models of the stars [2, 3].

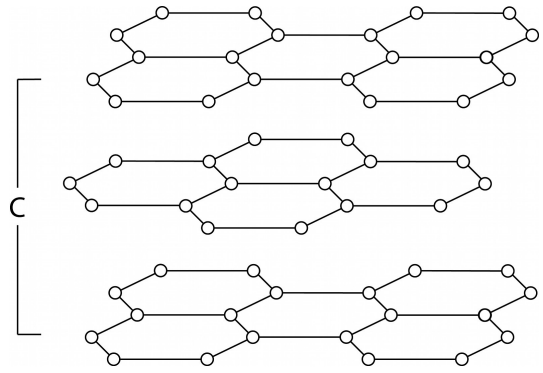

Fig. 1: Schematic representation of the layered hexagonal lattice structure found within graphite and proposed for the liquid metallic hydrogen lattice of the Sun.

2 Solar collapse versus incompressibility

The prevention of solar collapse has always been a central problem with the gaseous models. Theoretical arguments were based on the existence of both gas and radiation pressures in order to balance the masses of the stars against the forces of gravity. In the days of Arthur Stanley Eddington, radiation pressure was believed to play an important role in preventing solar collapse [26]. Over time, this process became generally restricted to supermassive stars [27, p. 180–186]. Solar collapse was prevented by gas pressure [27, p. 132] and radiation thought to contribute only a tiny fraction of the required forces [27, p. 212].

The idea that gas pressure could exist within a star was awkward. On Earth for instance, the atmosphere can be upheld by gas pressure as the planet has a surface through which gas atoms can build positive pressure. Furthermore, the pressure-volume relationship developed using the ideal gas law implied enclosures and rigid surfaces. It was their presence that gave meaning to gas pressure precisely since a rigid compartment defined the volume of interest. But within gaseous stellar models, there are no surfaces. As such, no mechanism exists for speaking of gas pressure.

In his classic text, Donald Clayton would describe the problem as follows: *"The microscopic source of pressure in a perfect gas is particle bombardment.*[1] *The reflection (or*

*The senior author has provided a complete list of his relevant papers to help facilitate the study of this new model.

absorption) of these particles from a real (or imagined) surface in the gas results in a transfer of momentum to that surface. By Newton's second law ($F = dp/dt$)*, that momentum transfer exerts a force on the surface. The average force per unit area is called the pressure. It is the same mechanical quantity appearing in the statement that the quantity of work performed by the infinitesimal expansion of a contained gas is* $dW = PdV$*. In thermal equilibrium in stellar interiors, the angular distribution of particle momenta is isotropic; i.e., particles are moving with equal probabilities in all directions. When reflected from a surface, those moving normal to the surface will transfer larger amounts of momentum than those that glance off at grazing angles*" [28, p. 79]. Clayton's footnote stated: "*In a nonperfect gas strong forces between the particles will represent an additional source or sink of energy for expansions and will therefore contribute to pressure*" [28, p. 79].

There are two problems with Clayton's argument. First, surfaces do not exist within a gaseous Sun. Secondly, by modeling the stars using the ideal gas law, astronomy was requiring elastic collisions between atoms. Yet, if the collisions are elastic, an atom which is moving towards the interior of the Sun could transfer all of its momentum to another atom, without reversing its own direction towards the exterior. In fact, it would simply propel a stationary atom in the interior further inside the Sun. This principle has been well established in the game of billiards. The cue ball can remain completely stationary upon transferring essentially all of its energy to another ball. It is only when a ball hits the banks of the billiard table, or makes use of spin and frictional forces associated with the table surface itself, that it can reverse its momentum. This explains, in the simplest terms, why gas pressure cannot exist within a gaseous Sun devoid of real surfaces and subject to elastic collisions. No net force can be generated with "imaginary surfaces" as the particles have equal probabilities of moving in all directions and transfer their momentum perfectly with no change of direction. A real surface is required to generate a net directional force and such structures cannot exist within a gaseous Sun. Therefore, modern solar models are unable to prevent internal collapse by resorting to gas pressure. In the absence of sufficient radiative forces, gaseous stars collapse.

At the same time, the use of gas models introduced many complications in astronomy. The first was summarized in Eddington's concern regarding internal heating, as stars became increasingly dense: "*I can hardly see how a star which has once got into this compressed condition is ever going to get out of it. . . Imagine a body continually losing heat but with insufficient energy to grow cold*" [29, p. 172]. Ralph H. Fowler would solve Eddington's dilemma. In 1926 [30], he adapted Fermi-Dirac statistics to stellar problems (e.g. [27, p. 118–128]). Stars could now grow cold. Donald Clayton highlighted the salient aspects of Fowler's solution: "*The physical basis for the resolution of this problem is the thermodynamic peculiarity of a degenerate gas: the temperature no longer corresponds to kinetic energy. The electrons in a zero-temperature degenerate gas must still have large kinetic energy if the density is great*" [28, p. 104]. In fact, Fowler's treatment was so theoretically powerful and the arguments so elegant [30], that gaseous stellar models now dominate astronomy. Nonetheless, no mechanism existed for generating gas pressure within Sun-like stars behaving as ideal gases [27, p. 130–132]. Fowler's solution addressed much later stages of stellar evolution [30].

Conversely, liquids are, by their nature, essentially incompressible. Thus, the problem of solar collapse does not occur within the condensed matter context [2, 3], because the layered graphite-like structure of liquid metallic hydrogen (see Fig. 1) would act to uphold the solar mass. Still, it is anticipated that the hexagonal lattice of metallic hydrogen can become slightly compressed with increasing internal solar pressures. The essentially incompressible nature of liquids implies that, while resisting compression, they remain subject to pressure effects to a small extent. Therefore, it is reasonable to anticipate that liquid metallic hydrogen becomes more metallic farther in the solar interior assuming a Type II lattice [2, 3]. The lower pressures of the photosphere would be conducive to supporting a less dense solar lattice (Type-I) with associated decreased metallicity [2, 3]. Conversely, since the Wilson effect [31] implies that sunspots are depressed relative to the photospheric level, it is reasonable to infer the presence of a Type-II lattice with its increased metallicity in these structures [2, 3]. In addition, as facular material is tightly associated with sunspots and may well have been ejected from such regions, it was not unreasonable to extrapolate that their increased metallicity occurs as a result of assuming a Type-II lattice, despite the fact that they appear to float on the photospheric surface [20].

3 Gravitational Settling Versus Restricted Diffusion

Within the context of the gaseous models [32, 33] atoms and ions can diffuse freely within stellar bodies. At the same time, since certain elements are heavier than others, it could be expected that they would slowly move towards the interior of a star through the action of gravitational settling. In fact, such a concept was advanced to explain the lack of helium lines in certain B type stars [34]. Long before, Henry Russell had minimized the idea that heavy elements were gravitationally settling in the Sun: "*It does not appear necessary, therefore, to assume that downward diffusion depletes the sun's atmosphere of the heavier elements, though the possibility of such an influence remains*" [35, p. 59]. Of course, gravitational settling could potentially invalidate all elemental abundances in stellar atmospheres obtained from spectroscopic lines.

Kippenhahn and Weigert discussed both temperature and pressure diffusion (gravitational settling) in their text on "*Stellar Structure and Evolution*" [27, p. 60–61]. They con-

cluded that temperature diffusion was astrophysically irrelevant in the Sun and that diffusion effects were, in general, important only in "special cases" not including the Sun [27, p. 60–61]. Today, the effect of gravitational settling has been included in the calculation of standard solar models [32, 33]. In part, this was because it improved the agreement with the p-mode oscillations from helioseismology: "*One of the principal improvements that has been made in recent years is to include in the calculations the effects of element diffusion. In the absence of an external field, diffusion smooths out variations. However, in the case of the Sun, the stronger pull of gravity on helium and the heavier elements causes them to slowly diffuse downward (towards the solar interior) relative to hydrogen . . . Models that include at least helium diffusion agree with helioseismological determinations of the depth of the convective zone, while neglecting diffusion entirely leads to disagreement with the helioseismological data*" [33]. Gravitational settling was embraced; for gaseous models had no other means of accounting for helioseismological observations.

Within a liquid metallic hydrogen model of the Sun, the free diffusion of the elements becomes highly restricted, as the layered lattice structure of the solar body acts to inhibit the flow of atoms. Rapid diffusion of elements should occur primarily in the layers between the hexagonal liquid metallic hydrogen planes. Such motion may be facilitated by lattice distortions in the hexagonal hydrogen planes in a manner similar to that observed in graphite intercalation compounds.

4 Intercalation and Graphite

Graphite [36–38] can be made to interact with various reagents such that non-carbon atoms occupy lattice points between the hexagonal carbon planes forming intercalation compounds [39–43]. Layered intercalation compounds (see Fig. 2) are created when intraplanar binding forces are much stronger than interplanar forces: "*The most important structural characteristic of graphite intercalation compounds is the occurrence of separate graphite and intercalate layers due to the very strong intraplanar binding and the weak interplanar binding. Thus, the graphite layers retain the basic properties of pristine graphite, and the intercalate layers behave similarly to the parent intercalate material*" [39, p. 36].

In the graphite case, the hexagonal plane excludes non-carbon atoms, the intercalant. In doing so, intercalant atoms can profoundly alter the electrical, thermal, magnetic properties of graphite by acting as electron donors (i.e. Li, K), or acceptors (i.e. $FeCl_3$, HF, BF_3), to the hexagonal plane [39–43]. As a result, graphite intercalation compounds can range from superconductors to insulators [39] with their conductivity often exceeding that of classic metals [43, p. 190]. They consequently occupy an important place in solid state physics. Graphite intercalation compounds can also undergo phase transitions including "*changes in interlayer ordering and changes in intralayer or in-plane ordering, magnetic transitions, and superconductive transition. Structural phase transitions have been induced by variation of the temperature, pressure, and in some cases by variation of the vapour pressure of the intercalant*" [39, p. 55–56]. The presence of intercalated atoms can weaken the interlayer attractive forces within graphite. Since the concentrations of the intercalate can be varied, it is possible to build intercalation compounds wherein many adjacent graphite layers are interrupted by the occasional intercalate layer (see Fig. 3). The stage index, *n*, characterizes the number of graphite layers between intercalation layers (e.g. [39] and [43, p. 88]). In the laboratory, *n* usually ranges from 1 to 10 [39].

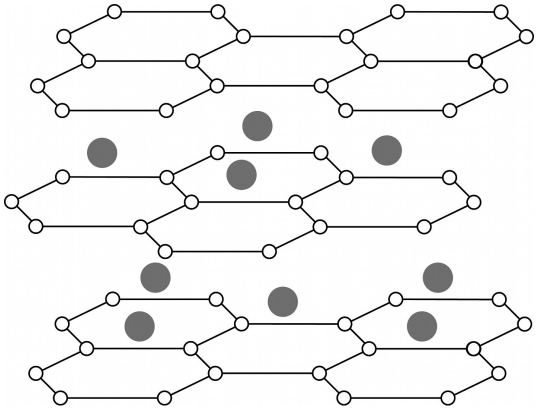

Fig. 2: Schematic representation of an intercalation compound. Non-carbon elements are located between layers of pristine graphite.

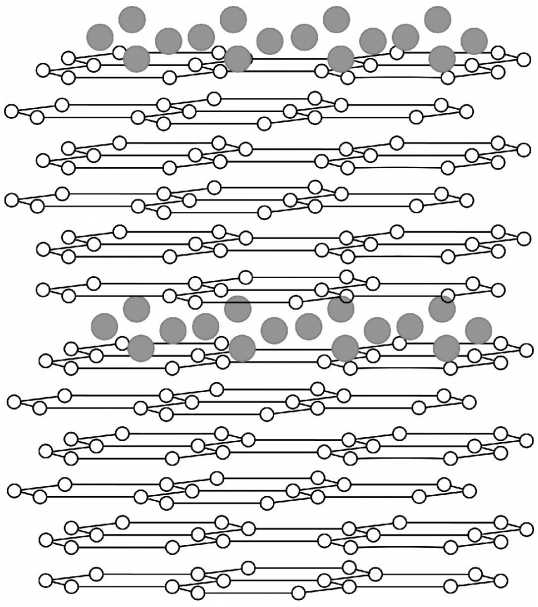

Fig. 3: Schematic representation of the stage index, n, in an intercalate compound, where n = 6.

Graphite intercalation compounds are known to relieve internal strains by undergoing exfoliation [39, p. 9] whereby a great expansion along the c-axis (see Fig. 1) occurs usually due to elevated temperatures [44]. The temperature required for exfoliation is linearly dependent on applied load against the sample [44]. Higher breakaway temperatures, or temperatures of exfoliation, are required under increased pressure. Expansions of the c-axis lattice dimensions of up to a factor of 300 have been reported [44]. These can be violent, even explosive, events wherein layers of material can be torn away from the underlying structure (see e.g. [39, p. 9] and [43, p. 403–413]). They occur as a result of gases being expelled from the graphite intercalated compound. The resultant products are characterized as "*spongy, foamy, low-density, high-surface-area carbon materials*" [43, p. 403].

Martin and Broklehurst [44] performed detailed studies of exfoliation which involved the effect of "*restraining loads on suppressing the onset of exfoliation*" [43, p. 406]. Enoki et al. describe the situation as follows: "*According to [Martin and Broklehurst's] model, the intercalate undergoes a phase change to the vapor phase, forming disk-shaped bubbles of radius* r *and height* I_c *in the interlayer region between graphite planes, with gas pockets accumulating in certain regions where diffusion is facilitated by the presence of defects. Exfoliation then occurs when the gas pressure exceeds the internal stress parallel to the c-axis*" [43, p. 406]. Expressions for the forces involved can be derived, assuming the ideal gas law [44].

Lattice exclusion remains the central lesson of these experiments: the graphite hexagonal planes continue to exclude the intercalate and struggle to remain "*pristine*" even at the cost of exfoliation. Such behavior has strong ramifications when considering the graphite-like liquid metallic hydrogen lattice believed to exist within the Sun [2, 3].

5 Intercalation and Stellar Matter

Graphite's tendency to remain pristine and exclude other elements from its hexagonal plane, even through the process of exfoliation, has important consequences for solar physics. Thermal emission arguments have led Robitaille [2] to postulate that liquid metallic hydrogen in the Sun must adopt a graphite-like layered arrangement. Should this be correct, then liquid metallic hydrogen should be excluding other elements from its hexagonal plane and constantly working to drive them out of the solar body. Such lattice exclusion and the possibility that stars might undergo processes like exfoliation could play a crucial role in at least five separate aspects of solar and stellar dynamics: 1) supplying the driving forces for solar winds, 2) generating the settings for flares, coronal mass ejections, and prominences, 3) accounting for the eleven year solar cycle, 4) providing an alternative explanation for planet and satellite formation, and 5) explaining the existence of red giants and supernovae. Each of these areas could consume many years of study as the liquid metallic hydrogen model of the Sun is adopted. Suffice it, for now, to address these briefly.

5.1 Solar Winds

In modern gaseous models, magnetic fields are thought to be produced by the flow of isolated charged particles within the solar body. In order to prevent collapse, the Sun remains in perfect hydrostatic equilibrium wherein the forces of gravity are balanced by gas and radiation pressure [27, p. 6–7]. However, the preservation of hydrostatic equilibrium severely limits all proposals advanced for the existence of solar winds. An object in equilibrium cannot easily be driving material away from itself.

Conversely, in a condensed model of the Sun, a layered liquid metallic hydrogen lattice exists (see Fig. 1) which is dominated by hexagonal hydrogen planes [2, 3]. Such a lattice restricts the translation of protons within each hexagonal hydrogen layer while permitting electrons to flow in the associated conduction bands [2]. The ability to create conduction bands provides the interatomic binding forces needed to stabilize the hydrogen framework. Proton-proton distances are restricted in order to establish optimal quantum mechanical conditions for these conduction bands. This alone stabilizes the lattice. Since hydrogen atoms possess a single electron and these are restricted to the conduction bands, no conventional bonding can occur. All elements other than hydrogen would be excluded from the hexagonal layer in order to maintain its structural integrity and electronic structure. Protons could be thought of as constantly working to expel elements from the hexagonal planes. This would severely limit the flow of non-hydrogen elements. Each hydrogen layer would act as a barrier to diffusion along the c-axis (see Fig. 1), while providing a channel for rapid elemental diffusion in the region between two hexagonal layers. Herein can be found the driving force for the solar winds and the variable elemental compositions they present due to solar activity [3].

5.2 Flares, Coronal Mass Ejections, and Prominences

In the gaseous models of the Sun, solar flares and coronal mass ejections are considered to be magnetic phenomena [45–48] and are produced by invoking magnetic reconnection [49, 50]. As a gaseous Sun is devoid of a real surface, no other means of generating the required energy is available: "*The magnetic energy stored in the corona is the only plausible source for the energy released during large solar flares. During the last 20 years most theoretical work has concentrated on models which store magnetic energy in the corona in the form of electrical currents, and a major goal of present day research is to understand how these currents are created, and then dissipated during a flare*" [50]. In such a scenario, the corona provides the driving force for expelling atoms from the Sun.

Solar flares are well known to produce helium abundance enhancements (HEA) and have been suggested as the cause of significant ^{3}He HEAs [45]. In an impulsive flare, the ^{3}He/^{4}He ratio can be assumed to approach 1 [51] and thousand-fold enhancements of the ratio have been reported [52] . Solar energetic particle events can result in 100–10,000 fold enhancements of heavy element to oxygen ratios relative to the quiet corona [52]. Solar atmospheric ratios of Mg/O, Si/O, Fe/O and Ne/O can all be substantially elevated with flare activity [51]. In active coronal regions, significant (3–4 fold) elemental enhancements of elements with a first ionization potential (FIP) less than 10 eV can be observed with respect to the quiet photosphere [53, 54]. Within bright active regions, a further twofold elemental enhancement can be detected [55]. The absolute abundance of potassium and calcium are greater in flare plasma than in the photosphere [54].

Magnetic reconnection [49, 50], the physical mechanism invoked to drive solar flares in the gaseous models, cannot easily account for the variable elemental abundances associated with flares and coronal mass ejections [56, 57]. As a parallel, models of quiescent coronal loops result in a 10 fold excess of helium to hydrogen when a 10% helium abundance is assumed for the chromosphere [58]. Such tremendous excesses of helium call for much lower chromospheric helium abundances, but these are incompatible with levels required to account for helium in the solar winds [58]. In addition, in order to explain O and Ne abundances in the fast solar winds, a coronal He abundance of 20–40% is required [59]. The model assumes gravitational settling in the corona [59], which is highly unlikely to take place. As such, the gaseous models are struggling to coherently resolve elemental abundances in the solar winds as a result of the interaction between coronal loops, the chromosphere, and the corona. The situation relative to understanding elemental abundances in flares and coronal mass ejections is equally tenuous.

Long ago, Friedrich Zöllner recognized that solar flares required regions of increased pressure in the solar interior [60]. He placed a liquid layer within his gaseous Sun: "*we must therefore conclude that the layer of division consists of an incandescent liquid*" [60]. The need to generate pressure was justified, but could not easily survive within a fully gaseous solar model.

In the liquid metallic hydrogen model of the Sun, solar flares, coronal mass ejections, and prominences can be explained by the process of intercalation and exfoliation, as described above by Martin and Broklehurst [44]. The pressure anticipated by Zöllner [60] is produced when the intercalate atoms increasingly populate the region between two adjacent hydrogen layers. A rapid increase in temperature in this region, presumably due to localized nuclear reactions (see section 5), generates a gaseous phase whose elevated pressures manifest as solar activity. Therefore, solar flares, coronal mass ejections, and prominences share a common mechanism of formation. Their subtle differences result only from the depth of formation. Magnetic fields are not required to produce these phenomena. They are merely altered by their presence.

5.3 The Eleven Year Solar Cycle

The existence of the eleven year solar cycle remains incompletely understood [61–66]. Nonetheless, increased solar activity is associated with changes in the solar dynamo which characterize the 11 year cycle [61, 64]. Cycle periods as great as 2,400 years have been postulated [66]. Solar inertial motion (SIM), wherein the location of the center of the Sun's mass in the solar system drifts due to interaction with the giant planets [61–66], has been postulated as a possible cause of increased activity. Still, as Cionco and Compgnucci highlight: "*at present there is no clear physical mechanism relating these phenomena*" [64]. How can planetary rotations and the associated *SIM* trigger solar activity? Perhaps the Sun is already predisposed to increased surface turbulence and requires only a simple disturbance to initiate activity. In this regard, insight can be gained from the condensed model of the Sun [2, 3].

In the context of a liquid metallic hydrogen model [2, 3], non-hydrogen elements reside in the layers between hydrogen hexagonal planes forming an intercalate arrangement (see Fig. 2). With solar nuclear activity (see section 5), these interplanar regions become increasingly populated and possible intercalate lattice points occupied. Eventually, localized saturation of a given intercalate layer takes place. The maximal concentration of intercalating atoms has been reached. When this occurs, only slight disturbances, such as found through solar inertial motion, could trigger solar activity and cause the intercalate atoms to be ejected from interior layers. Solar activity then becomes linked to the need to eject saturating levels of non-hydrogen elements from the solar body. As the rate of nuclear activity must remain rather constant over the time frames involved, the Sun is constantly building elements in its interior (see section 5), degassing, and repeating the entire process. The driving force for degassing becomes lattice exclusion, but the trigger to release the instability may, or may not, remain linked to solar inertial motion.

5.4 Planet, Red Giant, and Supernova Formation

The formation of planets around a star presents unique challenges to astronomy. Many ideas have surfaced and are taught in introductory astronomy courses [67, p. 285–290]. With time, Laplace's Nebular Hypothesis [68, 69], initially proposed by Emanuel Swedenborg [70, p. 240–272], evolved into the Solar Nebular Disk Model (*SNDM*) [71]. The latter continues to be the most widely accepted theory for the formation of the solar system [71]. Yet, the problem of planet and satellite formation is far from resolved (e.g. [72–74]). In part, this is because the planets cannot be currently conceived as ejected from a young active gaseous solar mass. The prob-

lem is removed when the Sun becomes condensed matter and exfoliative forces can be harnessed to promote planet formation, especially for the solid planets of the inner solar system. The central requirement appears to be that interlayer elemental abundance must be permitted to increase dramatically in one region of the solar interior, followed by ejection from the hydrogen lattice. Over time, the Sun could thus transfer some of its angular momentum to the planets. A similar approach could be utilized to help explain satellite formation around the giant planets, as they are also rich in hydrogen [75–77].

On a tangential note, exfoliation might well account for the very low density and great dimensions of the red giants, as the experiments of Martin and Broklehurst suggest [44]. A red giant would remain condensed matter in that it was formed through a process of exfoliation from a star which had permitted a nearly uniform stage index to develop in its interior. A trigger finally turned the intercalate rapidly into the gaseous phase resulting in a red giant. In the final expanded star the dimensions would be enormous and the density greatly reduced, despite the preservation of condensed matter for the metallic hydrogen framework. Interlayer gas pressure between the layers of the expanded star would help to maintain its structural integrity. Supernova could be envisioned as produced in a similar manner, but with non-uniform staging in the interior. For instance, a band or core of intercalate material in the precursor star rapidly enters the gas phase and explodes its liquid metallic hydrogen envelope, while compressing its hydrogen core. In the end, the advantages of adopting a liquid metallic hydrogen model for the Sun are numerous and its consequences extend much beyond the solar system.

6 Evolution and Nuclear Reactions in Gaseous Stars

With the publication of the *Origin of Species* [78] Charles Darwin would send shock waves not only throughout the biological sciences, but also in areas seemingly as far removed as astronomy. The great American father of solar astronomy, George Ellery Hale, commented as follows in the first line of his text devoted to stellar evolution and experimental astronomy: "*It is not too much to say that the attitude of scientific investigators towards research has undergone a radical change since the publication of the Origin of Species*" [79]. Hale expanded on this concept throughout his first chapter, as he elegantly intertwined biological evolution and astronomy. Hale also highlighted the conflict which Herbert Spencer [21], the prominent evolutionist, had with the astronomers: "*convinced that the principle of evolution must operate universally, and that the stars must have their origin in the still unformed masses of the nebulae, [Spencer] ventured to question the conclusion that the resolution of nebulae into stars was only a question of resolving power. He had not long to wait . . .*" [79, p. 47].

Given Hale's fame as an observer for first reporting the presence of magnetic fields on the Sun [80], his leadership in constructing four record setting telescopes (at Yerkes (1), Mount Wilson (2), and Palomar (1) [81]), and his role in establishing the *Astrophysical Journal* [82], it is not surprising that *The Study of Stellar Evolution* [79] has profoundly affected the course of modern astrophysics. George Ellery Hale's interest in stellar evolution [28, 83–87] was certain to ascend to a preeminent position in modern astronomy. At the same time, since prolonged biological evolution was also associated with increased functional abilities, astronomers quickly adopted the same concepts relative to the stellar evolution. As stars aged their core temperatures increased and gradually acquired the ability to make heavier elements. Astronomers began to see the stars not only as progressing through a life cycle, but also, as endowed with different synthetic abilities. Older stars possessed hotter cores, and hence, could sustain nuclear processes thought to require higher temperatures – the synthesis of heavier and heavier elements. On the surface at least, the theory was elegant with the exception of one very serious consideration: the gaseous Sun was deprived of the ability to directly synthesize the elements.

Early on, the fathers of stellar nucleosynthesis, such as Gamow [88, 89], Bethe [90–92], von Weizsäcker [93], and Hoyle [94, 95] would advance the idea that helium could be built from hydrogen within the stars. From the onset, nucleosynthesis was linked to stellar evolution [88, 89]. Gamow believed that "*different rates of energy liberation must be due to different physical conditions inside the stars and chiefly to differences in their central temperature*" [83, p. 116]. The p–p reaction [90], which assembled helium directly from proton combinations while relying on positron and neutrino emission, was believed to be active only in low weight main sequence stars [83, p. 118]. However, for stars larger than the Sun much of the synthesis of ^{4}He came from the carbon-nitrogen-oxygen (CNO) cycle which had been independently proposed by Bethe and von Weizsäcker [91–93]. Interestingly, while the cycle required three elements of intermediate weight, Hans Bethe insisted that: "*no element heavier than ^{4}He can be built up in ordinary stars*" [92]. He argued, "*The heavier elements found in stars must therefore have existed already when the star was formed*" [92]. With those words, most of the stars were deprived of their ability to make any element beyond helium, despite the fact that mankind would eventually synthesize much heavier elements.

Bethe, of course, based his ideas on the probability of nuclear reactions in the gas phase [92, p. 435]. This was appropriate for gaseous solar models. Reaction energies were derived using accelerators and nucleosynthesis in the stars became strictly dependent on our understanding of reactions in gases. The idea that many particles could be combined simultaneously within a condensed lattice would have greatly lowered the energy required to synthesize the heavier elements. Such a concept was never applied to the Sun. Soon a detailed work by Burbidge et. al [96] organized the entire field into an

elaborate theory of nucleosynthesis which covered all of the elements. This work would continue to influence nucleosynthesis in the stars until the present day [97]. Nonetheless, the Sun itself had been crippled. All of the elements in the solar system, other than helium, had been produced by early generation stars which no longer existed.

7 Nucleosynthesis and Condensed Matter

Perhaps the greatest advantage of the liquid metallic hydrogen model of the Sun rests in the fact that atomic positions become restricted to lattice points and subject to the forces associated both with solar pressures and lattice vibrations. Hydrogen is confined to its hexagonal planes and all other elements to the intercalate positions between the hydrogen planes. The synthesis of helium would be driven by the need to relieve the strains of stellar pressures on the underlying lattice. Two protons combine to form a deuteron, with positron and neutrino emission as in the p–p reaction [98]. Upon formation, the deuteron could immediately combine with another in-plane proton resulting in the formation of ^{3}He, which would be ejected from the lattice plane into the intercalate layer. As p–p reactions continue, the population of ^{3}He would expand, and soon continue to react producing ^{4}He, as expected from branch 1 of the p–p chain [98]. With time, the intercalate region would become the birthplace of all the elements. Pressure and lattice vibrations alone can be viewed as controlling the reactions with protons readily available from the hexagonal plane. All stars gain the ability to synthesize every element [19]. Multiple elements could react simultaneously in the intercalate layer because of lattice vibrations. This greatly lowers the energy requirements on a given species for nuclear reaction. Eventually, as elemental concentrations build, the stresses against the hexagonal hydrogen planes would increase. These could then break and the intercalate region expand beyond the confines of strict lattice points. Intercalation now abandoned in this region, thick layers of non-hydrogen elements could arise. These would continue to act as nuclear furnaces. During periods of increased solar activity, localized changes in temperature could vaporize these areas and release newly synthesized elements to the stellar atmosphere beyond the solar surface. During planet formation, such regions could simply be expelled, with (or perhaps without) vaporization, from the interior of the Sun.

8 Conclusions

Much speculation has been offered in this work and the end result was deliberate. In order to consider the condensed models of the Sun, scientists must ponder upon the ability to explain the highest amount of observable phenomena in a manner consistent with known physics. The great solar physicist John Bahcall once commented: "*Science progresses as a result of the clash between theory and experiment, between speculation and measurement*" [99]. In earlier work, considerable focus was placed on establishing what was known about the Sun and the evidence it displayed with respect to its phase and composition [2–20]. Ample proof supports the idea that the Sun exists in the condensed state and Occam's razor would slice in its favor.

Given the elevated levels of hydrogen in the universe [100], a liquid metallic hydrogen framework appears not only reasonable but, in light of its thermal emission, necessary [2, 3]. The unique link between graphite and the layered form of metallic hydrogen, as first proposed by Wigner and Huntington [23], presents enormous potential to refine our concept of the stars. In this regard, graphite intercalation compounds bring a wealth of behavioral and structural information crucial to understanding the heavens [39–44]. The layered nature of liquid metallic hydrogen [23] would not only support the Sun from collapse, but would also severely limit any gravitational settling. Furthermore, exfoliation in graphite intercalate compounds [44] has profound consequences, regarding stellar structure and behavior. Solar winds and solar activity (flares, coronal mass ejections, prominences) become inherently linked to preserving the hydrogen nature of the Sun [3]. The conversion of intercalated atoms from the liquid to the gas phase, as proposed by Martin and Broklehurst [44], has profound implications towards driving solar activity which will forever remain unavailable to gaseous models. The hypothesis that the solar cycle originates from the degassing of non-hydrogen elements and their expulsion from the interior is unique to the liquid metallic hydrogen model. For the first time, a reasonable thesis is being advanced to explain both solar activity and cycles. A mechanism thereby becomes available to those who believe that solar inertial motion might trigger solar activity [61–66]. In addition, the idea that a layered metallic hydrogen lattice will choose to exclude non-hydrogen elements and sequester them within the Sun could add much needed insight relative to the formation of the planets. Exfoliation of a metallic hydrogen lattice of uniform stage might well account for both the size and density of the red giants. Most importantly, this model enables elemental synthesis in the stars. Hexagonal hydrogen planes harbor the p–p reactions, while the interlayers between proton planes become furnaces of more advanced nuclear synthesis.

There is a great deal to be gained by considering a liquid metallic hydrogen model of the Sun. Yet, in this approach, the solar lattice appears to possess long range order on par with solids, despite its liquid state [18]. Given the dimensions involved on the solar surface, even solids might appear to act as liquids. But nonetheless, the model claims the liquid state as more in keeping with observation. In this respect, the authors emphasize that long range lattice order seems to be preserved in the liquid metallic hydrogen framework of the photosphere and solar body. The Sun is fully behaving as condensed matter. As such, this thesis has been built on observation, in keeping with the philosophy of Cecilia Payne:

"*The future of a subject is the product of its past, and the hopes of astrophysics should be implicit in what the science has already achieved. Astrophysics is a young science, however, and is still, to some extent, in a position of choosing its route; it is very much to be desired that present effort should be so directed that the chosen path may lead in a permanently productive direction. The direction in which progress lies will depend on the material available, on the development of theory, and on the trend of thought . . . The future progress of theory is a harder subject for prediction, than the future progress of observation. But one thing is certain: observation must make the way for theory, and only if it does can the science have its greatest productivity . . . There is hope that the high promise of astrophysics may be brought to fruition.*"

Cecilia Payne-Gaposchkin [1, p. 199–201]

Acknowledgment

Luc Robitaille is acknowledged for the preparation of figures.

Dedication

This work is dedicated to Lindsey Marie Robitaille.

Submitted on: January 6, 2013 / Accepted on: January 10, 2013
First published in online on: February 2, 2013

References

1. Haramundanis K. Cecilia Payne-Gaposchkin: An autobiography and other recollections (2nd Edition), Cambridge University Press, Cambridge, U.K., 1996.
2. Robitaille P.M. Liquid metallic hydrogen: A building block for the liquid Sun. *Progr. Phys.*, 2011, v. 3, 60–74.
3. Robitaille P.M. Liquid Metallic Hydrogen II: A critical assessment of current and primordial helium levels in Sun. *Progr. Phys.*, 2013, v. 2, 35–47.
4. Robitaille P.M. The collapse of the Big Bang and the gaseous Sun. *New York Times*, March 17, 2002, p. A10 (available online: http://thermalphysics.org/pdf/times.pdf).
5. Robitaille P.M. Evidence for a liquid plasma model of the Sun. *Am. Phys. Soc. Meeting — April*, 2004, S280002.
6. Robitaille P.M. The Sun as a hot liquid plasma: additional evidence. *Am. Phys. Soc. Meeting — Ohio Spring*, 2004, S50002.
7. Robitaille P.M. The photosphere as condensed matter. *Am. Phys. Soc. Meeting — Ohio Fall*, 2004, S60005.
8. Robitaille P.M. The Sun as a hot liquid plasma: more evidence. *Am. Phys. Soc. Meeting — NE Fall*, 2004, S10004.
9. Robitaille P.M. The Sun as a high energy/high density liquid metallic hydrogen plasma. *The 33rd IEEE International Conference on Plasma Science*, June 4-8, 2006, Traverse City, Michigan, p. 461, DOI:10.1109/PLASMA.2006.1707334.
10. Robitaille P.M. The solar photosphere: Evidence for condensed matter. *Progr. Phys.*, 2006, v. 2, 17–21 (also found in slightly modified form within *Research Disclosure*, 2006, v. 501, 31–34; title #501019).
11. Robitaille P.M. A high temperature liquid plasma model of the Sun. *Progr. Phys.*, 2007, v. 1, 70–81 (also in arXiv: astro-ph/0410075).
12. Robitaille P.M. A radically different point of view on the CMB. In: *Questions of Modern Cosmology — Galileo's Legacy*, ed. by M. D'Onofrio and C. Burigana, Springer, New York, 2009.
13. Robitaille P.M. Liquid metallic hydrogen: Building block of a liquid Sun. *Am. Phys. Soc. Meeting — Ohio Spring*, 2011, D4.00005.
14. Robitaille P.M. On the Presence of a Distinct Solar Surface: A Reply to Hervé Faye. *Progr. Phys.*, 2011, v. 3, 75–78.
15. Robitaille P.M. On Solar Granulations, Limb Darkening, and Sunspots: Brief Insights in Remembrance of Father Angelo Secchi. *Progr. Phys.*, 2011, v. 3, 79–88.
16. Robitaille P.M. On the Temperature of the Photosphere: Energy Partition in the Sun. *Progr. Phys.*, 2011, v. 3, 89–92.
17. Robitaille P.M. Stellar opacity: The Achilles heel of the gaseous Sun. *Progr. Phys.*, 2011, v. 3, 93–99.
18. Robitaille P.M. Lessons from the Sun. *Progr. Phys.*, 2011, v. 3, 100–102.
19. Robitaille P.M. Nucleosynthesis of the elements and the liquid metallic hydrogen model of the Sun. *Am. Phys. Soc. Meeting — Four Corners Annual*, 2012, D1.00026.
20. Robitaille P.M. Magnetic Fields and Directional Spectral Emissivity in Sunspots and Faculae: Complimentary Evidence of Metallic Behavior on the Surface of the Sun. *Progr. Phys.*, 2013, v. 1, 19–24.
21. Robitaille P.M. A thermodynamic history of the solar constitution — I: The journey to a gaseous Sun. *Progr. Phys.*, 2011, v. 3, 3–25.
22. Robitaille P.M. A thermodynamic history of the solar constitution — II: The theory of a gaseous Sun and Jeans' failed liquid alternative. *Progr. Phys.*, 2011, v. 3, 41–59
23. Wigner E. and Huntington H.B. On the possibility of a metallic modification of hydrogen. *J. Chem. Phys.*, 1935, v. 3, 764–70.
24. Robitaille P.M. Blackbody radiation and the carbon particle. *Progr. Phys.*, 2008, v. 3, 36–55.
25. Robitaille P.M. Kirchhoff's Law of Thermal Emission: 150 years. *Progr. Phys.*, 2009, v. 4, 3–13.
26. Eddington A.S. On the radiative equilibrium of the stars. *Mon. Not. Roy. Astron. Soc.*, 1916, v. 77(1), 16–35 (Also found in Lang K.R. and Gingerich O.: A Source Book in Astronomy and Astrophysics, 1900–1975. Harvard University Press, Cambridge, MA, 1979, p. 225–235).
27. Kippenhahn R. and Weigert A. Stellar structure and evolution. Springer-Verlag, Berlin, 1990.
28. Clayton D.D. Principles of stellar evolution and nucleosynthesis. MgGraw-Hill, New York, 1968.
29. Eddington A.S. The internal constitution of the stars. Cambridge University Press, Cambridge, U.K., 1926.
30. Fowler R.H. On dense matter. *Mon. Not. Roy. Astron. Soc.*, 1926, v. 87, 114–122.
31. Wilson A. Observations on the solar spots. *Phil. Trans. Roy. Soc.*, 1774, v. 64, 1–30.
32. Bahcall J.N. and Pinsonneault M.H. Standard solar models, with and without helium diffusion, and the solar neutrino problem. *Rev. Mod. Phys.*, 1992, v. 64, no.4, 885–926.
33. Bachall J.N., Pinsonneault M.H. and Wasserburg G.J. Solar models with helium and heavy-element diffusion. *Rev. Mod. Phys.*, 1995, v. 67, no. 4, 781–808.
34. Greenstein G.S., Truran J.W. and Cameron A.G.W. Helium deficiency in old halo B type stars. *Nature*, 1967, v. 213, 871–873.
35. Russell H.N. On the composition of the Sun's atmosphere. *Astrophys. J.*, 1929, v. 70, 11–82.
36. Kelly B.T. Physics of graphite. Applied Science Publishers, London, U.K., 1981, p. 34–61.
37. Delhaès P. World of carbon — vol. 1: Graphite and precursors. Gordon and Breach Science Publishers, Amsterdam, The Netherlands, 2001.
38. Pierson H.O. Handbook of carbon, graphite, diamond and fullerenes: Properties, processing and applications. Noyes Publications, Park Ridge, N.J., 1993.

39. Dresselhaus M.S. and Dresselhaus G. Intercalation compounds of graphite. *Adv. Phys.*, 2002, v. 1, no. 1, 1–186 (reprinted from *Adv. Phys.*, 1981, v. 30(2), 139–326).
40. Pietronero L. and Tosatti E. Physics of intercalation compounds. Springer-Verlag, Berlin, 1981.
41. Zabel H. and Solin S.A. Graphite intercalation compounds I: Structure and dynamics. Springer-Verlag, Berlin, 1990.
42. Dresselhaus M.S. and Kalish R. Ion implantation in diamond, graphite and related materials. Springer-Verlag, Berlin, 1992.
43. Enoki T., Suzuki M. and Endo M. Graphite intercalation compounds and applications. Oxford University Press, Oxford, U.K., 2003.
44. Martin W.H. and Brocklehurst J.E. The thermal expansion behavior of pyrolytic graphite-bromine residue compounds. *Carbon*, 1964, v. 1, no. 2, 133–141.
45. Kahler S.W. Solar flares and coronal mass ejections. *Ann. Rev. Astron. Astrophys.*, 1992, v. 30, 113–141.
46. Priest E.R. Solar flare theory and the status of flare understanding. In *High Energy Solar Physics: Anticipating HESSI. ASP Conf. Ser.*, 2000, v. 206, 13–26.
47. Priest E.R. and Forbes T.G. The magnetic nature of solar flares. *Astron. Astrophys. Rev.*, 2002, v. 10, 313–377.
48. Hudson H.S. Global properties of solar flares. *Space Sci. Rev.*, 2011, v. 158, 5–41.
49. Holman G.D. The mysterious origin of solar flares. *Sci. Am.*, 2006, v. 294, no. 4, 38–45.
50. Forbes T.G. Magnetic reconnection in solar flares. *Geophys. Astrophys. Fluid Dynam.*, 1991, v. 62, 15–36.
51. Ramaty R., Mandzhavidze N., Kozlovsky B. and Murphy R.J. Solar atmospheric abundances and energy content in flare-accelerated ions from gamma-ray spectroscopy. *Astrophys. J.*, 1995, v. 455, L193–L196.
52. Reames D.V. and Ng C.K. Heavy-element abundances in solar energetic particle events. *Astrophys. J.*, 2004, v. 610, 510–522.
53. Laming J.M. Non-WKB modles of the first ionization potential effect: Implications for solar coronal heating and the coronal helium and neon abundances. *Astrophys. J.*, 2009, v. 695, 954–969.
54. Doschek G.A., Feldman U. and Seely J.F. Elemental abundances from solar flare spectra. *Mon. Not. Roy. Astron. Soc.*, 1985, v. 217, 317–326.
55. Ciaravella A., Raymond J.C., Li J., Reiser P., Gardner L.D., Ko Y.K. and Fineschi S. Elemental abundances and post-coronal mass ejection current sheet in a very hot active region. *Astrophys. J.*, 2002, v. 575, 1116–1130.
56. Feldman U., Landi E. and Laming J.M. Helium Abundance in High-Temperature Solar Flare Plasmas. *Astrophys. J.*, 2005, v. 619, no.2, 1142–1152.
57. Andretta V., Mauas P.J.D., Falchi A. and Teriaca L. Helium Line Formation and Abundance during a C-Class Flare. *Astrophys. J.*, 2008, v. 681, no. 1, 650–663.
58. Killie M.A., Lie-Svendsen Ø. and Leer E. The helium abundance in quiescent coronal loops. *Astrophys. J. Let.*, v. 632, no. 2, L155–L158.
59. Byhring H.S., Esser R. and Lie-Svendsen Ø. O and Ne in H-He fast solar wind. *Astrophys. J.*, 2011, v. 743, no. 2, 205(11p).
60. Zöllner F. On the temperature and physical constitution of the Sun. *Phil. Mag. 4th Series*, 1870, v. 40, 313–327 (essentially reprinted in: Zöllner F. On the Sun's temperature and physical constitution. *Nature*, 1870, v. 2(52), 522–526).
61. Hathaway D.H. The solar cycle. *Living Rev. Solar Phys.*, 2010, v. 7, 1–66.
62. Schwentek H. and Elling W. A possible relationship between spectral bands in sunspot number and the space-time organization of our planetary system. *Solar Phys.*, 1984, v. 93, no. 2, 403–413.
63. Grandpierre A. On the origin of solar cycle periodicity. *Astrophys. Space Sci.*, 1996, v. 243, no. 2, 393–400.
64. Cioncoa R.G. and Compagnucci R.H. Dynamical characterization of the last prolonged solar minima. *Adv. Space Res.*, 2012, v. 50, no. 10, 1434–1444.
65. Tan B. Multi-timescale solar cycles and the possible implications. *Astrophys. Space Sci.*, 2011, v. 332, no. 1, 65–72.
66. Charvátová I. Can origin of the 2400-year cycle of solar activity be caused by solar inertial motion. *Ann. Geophysicae*, 2000, v. 18, 399–405.
67. Payne-Gaposhchkin C. and Haramundanis K. Introduction to astronomy (2nd Edition), Prentice-Hall Inc., Englewood Cliffs, N.J., 1970.
68. Laplace P.S. Exposition du système du monde. Imprimerie du Cercle-Social, Paris, 1796 (available online: http://dx.doi.org/10.3931/e-rara-497; Also available in English: Pond J. The system of the world, London, 1809).
69. Numbers R.L. Creation by Natural Law: Laplace's Nebular Hypothesis in American Thought. Seattle, 1977, p. 124-132.
70. Swedenborg E. The Principia; or the first principles of natural things, being new attempts towards a philosophical explanation of the elementary world. Translated by: Augustus Clissold, W. Newbery, London, 1846.
71. Woolson M.M. Solar system — Its origin and evolution. *Quarterly J. Roy. Astron. Soc.*, 1993, v. 34, 1–20.
72. Montmerle T., Augerneau J.C., Chaussidon M., Gounell M., Marty B. and Morbidelli A. 3. Solar system formation and early evolution: The first 100 million years. *Earth, Moon, and Planets*, 2006, v. 98, 39–95.
73. Thommes E.W., Duncan M.J. and Levison H.F. The formation of Uranus and Neptune among Jupiter and Saturn. *Astrophys. J.*, 2002, v. 123, 2862–2883.
74. Stevenson D.J. Origin of the moon — The collision hypothesis. *Ann. Rev. Earth Planet Sci.*, 1987, v. , 271–315.
75. Nellis W.J., Ross M. and Holmes N.C. Temperature measurements of shock-compressed hydrogen: Implications for the interior of Jupiter. *Science*, 1995, v. 269, no. 5228, 1249–1252.
76. Nellis W.J., Weir S.T. and Mitchell A.C. Metallization and electrical conductivity of hydrogen in Jupiter. *Science*, 1996, v. 73, no. 5277, 936–938.
77. Vorberger J., Tamblyn I., Militzer B. and Bonev S.A. Hydrogen helium mixtures in the interior of giant planets. *Phys. Rev. B*, 2007, v. 75, 024206(1–11).
78. Darwin C. On the origin of species by means of natural selection, or the preservation of favoured races in the struggle for life. John Murray, London, U.K. 1859.
79. Hale G.E. The study of stellar evolution: An account of some recent methods of astrophysical research, The decennial publications of the University of Chicago — Second Series, Vol. X. University of Chicago Press, Chicago, I.L., 1908.
80. Hale G. E. On the probable existence of a magnetic field in sun-spots. *Astrophys. J.*, 1908, v. 28, 315–343.
81. Mason T. and Mason R. The journey to Palomar, PBS, DVD released on November 18, 2008 (90 minutes).
82. Newall H. F. George Ellery Hale. 1868-1938. *Obituary Not. Fell. Roy. Soc.*, 1939, v. 2(7), 522–526.
83. Gamow G. The birth and death of the sun: A lucid explanation of stellar evolution and atomic energy. New American Library, New York, N.Y., 1952.
84. Struve O. Stellar evolution: An exploration from the laboratory. Princeton University Press, Princeton, N.J., 1950.
85. Meadows A.J. Stellar evolution (2nd Edition), Pergamon Press, Oxford, U.K., 1972.

86. Arnett D. Supernovae and nucleosynthesis: An investigation of the history of matter, from the Big Bang to the present. Princeton University Press, Princeton, N.J., 1996.
87. Pagel B. E. J. Nucleosythesis and the chemical evolution of galaxies (2nd Edition), Cambridge University Press, Cambridge, U.K., 2009.
88. Gamow G. Nuclear energy sources and stellar evolution. *Phys. Rev.*, 1938, v. 53, 595–604.
89. Gamow G. Nuclear reactions in stellar evolution. *Nature*, 1939, v. 144, 620–622.
90. Bethe H.A. and Critchfield C.L. The Formation of Deuterons by Proton Combination. *Phys. Rev.*, 1938, v. 54, no. 4, 248–254.
91. Bethe H. A. Energy Production in Stars. *Phys. Rev.*, 1939, v. 55, no. 1, 103.
92. Bethe H.A. Energy Production in Stars. *Phys. Rev.*, 1939, v. 55, no. 5, 434–456.
93. von Weizsäcker C. F. Über Elementumwandlungen in Innern der Sterne II. *Physikalische Zeitschrift*, 1938, v. 39, 633–646.
94. Hoyle F. The synthesis of the elements from hydrogen. *Mon. Not. Roy. Astron. Soc.*, 1946, v. 106, 343–383.
95. Hoyle F. On nuclear reactions occurring in very hot stars. I. The synthesis of elements from carbon to nickel. *Astrophys. J. Suppl. Ser.*, 1954, v. 1, 121–146.
96. Burbidge M., Burbidge G.R., Fowler W.A. and Hoyle F. Synthesis of the elements in stars. *Rev. Mod. Phys.*, 1957, v. 29, no. 4, 547–654.
97. Wallerstein G., Iben I., Parker P., Boesgaard A.M., Hale G.M., Champagne A.E., Barnes C.A., Käppeler F., Smith V.V., Hoffman R.D., Timmes F.X., Sneden C., Boyd R.N., Meyer B.S. and Lambert D.L. Synthesis of the elements in stars: Forty years of progress. *Rev. Mod. Phys.*, 1997, v. 9, no. 4, 995–1084.
98. Bahcall J.N. Neutrinos from the Sun. *Sci. Am.*, 1969, v. 221, no. 1, 28–37.
99. Bahcall J.N. How the Sun shines. www.nobelprize.org/nobel_prizes/physics/articles/fusion/index.html?print=1
100. Payne C.H. The relative abundances of the elements. Stellar Atmospheres. Harvard Observatory Monograph no. 1 (Harlow Shapley, Editor), Harvard University Press, Cambridge, MA, 1925 (reprinted in part in Lang K.R. and Gingerich O. A source book in astronomy and astrophysics, 1900–1975, Harvard University Press, Cambridge, MA, 1979, p. 245–248).

Structure Shape Evolution in Lanthanide and Actinide Nuclei

Khalaf A.M.* and Ismail A.M.†

*Physics Department, Faculty of Science, Al-Azhar University, Cairo, Egypt. E-mail: ali_khalaf43@hotmail.com
†Hot Laboratories Center, Atomic Energy Authority, Egypt, P.No. 13759, Cairo, Egypt. E-mail: ahmedismailph@yahoo.com

To give the characteristics of the evolution of the collectivity in even-even nuclei, we studied the behavior of the energy ratios R(4/2) and R(6/4). All chains of lanthanides begins as vibrational with R(4/2) near 2.0 and move towards rotational (R(4/2) $\longrightarrow$ 3.33) as neutron number increases. A rabid jump in R(4/2) near N=90 was seen. The plot of R(4/2) against Z shows not only the existence of a shape transitions but also the change in curvature in the data for N=88 and 90, concave to convex. For intermediate structure the slopes in E-GOS (E_γ over spin) plots range between the vibrator and rotor extremes. The abnormal behavior of the two-neutron separation energies of our lanthanide nuclei as a function of neutron number around neutron number 90 is calculated. Nonlinear behavior is observed which indicate that shape phase transition is occurred in this region. The calculated reduced B(E2) transition probabilities of the low states of the ground state band in the nuclei ^{150}Nd/^{152}Sm/^{154}Gd/^{156}Dy are analyzed and compared to the prediction of vibrational U(5) and rotational SU(3) limits of interacting boson model calculations.

1 Introduction

The interacting boson model (IBM) [1, 2] and the geometric collective model (GCM) [3–5] represent two major phenomenological approaches that successfully describe nuclear collectivity. While the IBM model is purely algebraic, based on a bosonized form of the many-body problem with even numbers of fermions, the GCM model follows from a geometric description of nuclei using the Bohr-Mottelson (BM) Hamiltonian [6].

Quantum phase transitions are of great interest in many areas of physics, and their manifestations vary significantly in different systems. For nuclear systems, the IBM reveals rich features of their shape phase transitions [7–16]. Three dynamical symmetries in the IBM were shown to correspond to three typical shape phase of nuclei, known as the spherical U(5) symmetry, axially deformed SU(3) symmetry and γ-soft deformed O(6) symmetry shapes. It is also known that phase transitions coincide with transitions between dynamical symmetries, with a first order phase transition taking place in the U(5)-SU(3) transition, and a second order phase transition happening in the U(5)-O(6).

A new class of symmetries that applies to systems localized at the critical points was proposed. In particular the critical symmetry E(5) [17] has been suggested to describe critical points in the phase transition from spherical vibrator U(5) to γ-unstable rotor O(6) shapes, while X(5) [18] is designed to describe systems lying at the critical point in the transition from spherical to axially deformed systems. These are based originally on particular solutions of the Bohr-Mottelson differential equations, but are usually applied in the context of the IBM [1], since the IBM provides a simple but detailed framework in which first and second order phase transitions can be studied. In the IBM language, the symmetry E(5) corresponds to the critical point between U(5) and O(6) symmetry limits, while X(5) symmetry should describe the phase transition region between the U(5) and the SU(3) dynamical symmetries.

The purpose of this paper is to disuse the main concepts of the rapid changes in structure of lanthanide and actinide nuclei by using some good indicators like energy ratios, two-neutron separation energies and reduced electric quadruple transition probabilities.

2 Energy Ratios and Nuclear Shape Transition

Nuclear shape phases are the manifestation of the collective motion modes of nuclei. One of the best signatures of shape transition is the behavior of the ratio between the energies of the first 4^+ and 2^+ states

$$R(4/2) = \frac{E(4_1^+)}{E(2_1^+)} \tag{1}$$

along the isotopic chain. The members of vibrational nuclei have excitation energies

$$E(I) = C(I), \tag{2}$$

where C is the vibrational constant. So that the energy ratios are

$$R((I+2)/I)_{vib} = \frac{I+2}{I}. \tag{3}$$

The yrast energies of the harmonic vibrator can be written as

$$E(I) = nE(2_1^+), \tag{4}$$

where n is the phonon number. The γ-ray energies within the yrast band are given by

$$\begin{aligned} E_\gamma(I) &= E(I) - E(I-2) \\ &= E(2_1^+). \end{aligned} \tag{5}$$

It is interesting to discuss the energy levels by plotting the ratio of E_γ(I) to spin I (E-Gamma Over Spin) (E-GOS) [19] against spin I. This is not helpful to identify the structure of the nucleus, but also to discern changes as a function of spin. Therefore, the E-GOS for vibrational nuclei can be written as

$$(E_\gamma/I)_{vib} = E(2_1^+)/I \tag{6}$$

which decreases hyperbolically from $E(2_1^+)/2$ to zero. In the rigid rotor, the energies of the yrast states are:

$$E(I) = AI(I+1), \tag{7}$$

where A is the rotational parameter ($A = \hbar^2/2J$, where J represents the moment of inertia), so that the energy ratios are

$$R((I+2/I))_{rot} = \frac{(I+2)(I+3)}{I(I+1)}. \tag{8}$$

Then The γ-ray energies within the yrast band are given by

$$E_\gamma(I) = A(4I-2) \tag{9}$$

and so the E-GOS is

$$\begin{aligned}(E_\gamma/I)_{rot} &= A\left(4-\frac{2}{I}\right)\\ &= \frac{E(2_1^+)}{3}\left(2-\frac{1}{I}\right).\end{aligned} \tag{10}$$

In units of A, this evolves from 3 for I=2 up to 4 for high I, and so gradually increasing and asymptotic function of I. Also E-GOS for γ-unstable nuclei is given by

$$(E_\gamma/I)_{\gamma-soft} = \frac{E(2_1^+)}{4}\left(1+\frac{2}{I}\right). \tag{11}$$

The R(4/2) varies from the value which correspond to vibrations around a spherical shape of vibrational nuclide R(4/2)=2 to the characteristic value for excitations of well-deformed rotor R(4/2)=3.33. That is, the energy ratio R(4/2) exhibits sharp change in rapid transitional region. Even-even nuclei can be classified roughly according to ratios R(4/2) as:

$1.0 < R(4/2) < 2.0$	for magic nuclei,
$2.0 < R(4/2) < 2.4$	for vibrational nuclei,
$2.4 < R(4/2) < 2.7$	for γ-unstable nuclei,
$2.7 < R(4/2) < 3.0$	for transitional nuclei,
$3.00 < R(4/2) < 3.33$	for rotational nuclei.

To give the characteristics of the evolution of the collectivity in even-even nuclei, we study the behavior of the energy ratios R(4/2) and R(6/4). For the nuclei included in our study, all chains of lanthanides begins as vibrational with R(4/2) near 2.0 and move towards rotational (R(4/2)$\longrightarrow$3.33) as neutron number increases. For intermediate structure the slopes in E-GOS plots range between the vibrator and rotor extremes. One particular case of interest is R(4/2)=3.0 which traditionally marks the boundary where axial rotation begins to set in. A very general phenomenological model is that of the an harmonic vibrator (AHV) [20]. In this model the yrast energies are given by

$$E(I=2n) = nE(2_1^+)\frac{n(n-1)}{2}\epsilon_4, \tag{12}$$

where

$$\epsilon_4 = E(4_1^+) - 2E(2_1^+) \tag{13}$$

is the an harmonically of the 4^+ state, that is, its deviation in energy from twice the 2^+ energy, and n = I/2, n is the phonon number in a vibrational nucleus. For $\epsilon_4 = 0$ equation (12) gives the harmonic vibrator

$$E(I) = \frac{1}{2}E(2_1^+)I \quad (R(4/2) = 2). \tag{14}$$

For $\epsilon_4 = (4/3)E(2_1^+)$, it gives the rigid rotor expression

$$E(I) = \frac{1}{6}E(2_1^+)I(I+1) \quad (R(4/2) = 10/3). \tag{15}$$

For $\epsilon_4 = E(2_1^+)$, it gives

$$E(I) = \frac{1}{8}E(2_1^+)I(I+2) \quad (R(4/2) = 3.0). \tag{16}$$

E(I)/I is constant and that the E-GOS plots is flat. So, interestingly the phase transition point (R(4/2) 3.0) roughly serves to section E-GOS plots into two classes of increasing and decreasing with I, so that nuclei on the vibrator side of the phase transition are down-sloping while these to the rotor side are up-sloping.

The systematics of energy ratios of successive levels of collective bands in medium and heavy mass even-even nuclei were studied [21]. A measure of their deviation from the vibrational and rotational limiting value was found to have different magnitude and spin dependence in vibrational, rotational and γ-unstable nuclei. For a given band for each spin I, the following ratios were constructed to define the symmetry for the excited band of even-even nuclei

$$\begin{aligned}r((I+2)/I) &= \frac{R((I+2)/I)_{exp} - R((I+2)/I)_{vib}}{R((I+2)/I)_{rot} - R((I+2)/I)_{vib}}\\ &= \frac{R((I+2)/I)_{exp} - (I+2)/I}{\dfrac{2(I+2)}{I(I+1)}},\end{aligned} \tag{17}$$

where $R((I+2)/I)_{exp}$ is the experimental value of the ratio. In equation (17), the value of energy ratios, r have changed between 0.1 and 1 for yrast bands of even-even nuclei. The ratio r should be close to one for a rotational nucleus and close to zero for a vibrational nucleus, while it should have intermediate values for γ-unstable nuclei:

$0.10 \le r \le 0.35$	for vibrational nuclei,
$0.4 \le r \le 0.6$	for transitional nuclei,
$0.6 \le r \le 1.0$	for rotational nuclei.

3 Electromagnetic Transition Strengths

When the nucleus is deformed it acquires an electric-multiple moment. Consequently as it oscillates, in $\lambda\mu$ mode, it emits electric $\lambda\mu$ radiation. Now to calculate the radiative transition rates between vibrational states, we need the nuclear electric multiple operator $\hat{\mathcal{M}}$. This is given by

$$\hat{\mathcal{M}}(E\lambda,\mu) = \int_{\tau} d\tau \rho_c(r) r^{\lambda} Y_{\lambda\mu}(\theta,\phi), \tag{18}$$

$\rho_c(r)$ is the charge density of the nucleus. The electric multipole moment is defined by $\hat{Q}_\lambda$

$$\hat{Q}_\lambda = \left(\frac{16\pi}{2\lambda+1}\right)^{1/2} \mathcal{M}(E\lambda,0). \tag{19}$$

We now discuss the electric quadruple moment ($\lambda = 2$) in more detail because the electric quadruple moment Q_2 of a nucleus is a measure of the deviation of the charge distribution from spherical symmetry. We define the reduced transition probability as:

$$\begin{aligned} B(E2, I_i \longrightarrow I_f) &= \textstyle\sum_{Mf} |\langle I_i M_i | Q_2 | I_f M_f\rangle|^2 \\ &= \tfrac{1}{2I_i+1} |\langle I_i \| Q_2 \| I_f\rangle|^2, \end{aligned} \tag{20}$$

where $|\langle I_i \| Q_2 \| I_f\rangle|$ is a reduced matrix element defined by the Wigner-Eckart theorem

$$\langle I_i M_i | \mathcal{M}(E\lambda,\mu) | I_f M_f\rangle| = \langle I_i M_i \lambda\mu | I_f M_f\rangle \frac{|\langle I_i \| \mathcal{M}(E\lambda) \| I_f\rangle|}{(2I_i+1)^{1/2}}.$$

The reduced transition probability $B(E2, I_i K \longrightarrow I_f K)$ for an electric quadruple transition between two members of same rotational band with quantum number K is:

$$B(E2, I_i K \longrightarrow I_f K) = \frac{5}{16\pi} e^2 Q_0^2 \langle I_i K 20 | I_f K\rangle^2, \tag{21}$$

where Q_0 is the transition intrinsic quadruple moment and we have used

$$\sum_{m_1 m_2, m} |\langle I_1 m_1 I_2 m_2 | I m\rangle|^2 = 2I + 1. \tag{22}$$

For even-even nuclei, $K = 0$ and when $I_i = I$ and $I_f = I-2$, we get the familiar relations between $B(E2, I \longrightarrow I-2)$ and the intrinsic quadruple moment Q_0 are:

$$B(E2, I \longrightarrow I-2) = \frac{5}{16\pi} e^2 Q_0^2 \frac{3}{2} \frac{I(I-1)}{2(2I-1)(2I+1)}. \tag{23}$$

As a special case for the transition $2^+ \longrightarrow 0^+$, yields

$$B(E2, 2^+ \longrightarrow 0^+) = \frac{5}{16\pi} e^2 Q_0^2. \tag{24}$$

For the transition $I_i = I$ and $I_f = I+2$, yields

$$B(E2, I \longrightarrow I+2) = \frac{5}{16\pi} e^2 Q_0^2 \frac{3}{2} \frac{(I+2)(I+1)}{2(2I+1)(2I+2)} \tag{25}$$

and for special case for the transition $0^+ \longrightarrow 2^+$, yields

$$B(E2, 0^+ \longrightarrow 2^+) = \frac{5}{16\pi} e^2 Q_0^2. \tag{26}$$

That is

$$B(E2, 2^+ \longrightarrow 0^+) = 0.2\, B(E2, 0^+ \longrightarrow 2^+). \tag{27}$$

From equation (21), the intrinsic quadruple moment Q_0 for a $K = 0$ band of an axially symmetric rotor is extracted. For the special transition $0^+ \longrightarrow 2^+$, we get

$$eQ_0 = \left[\frac{16\pi}{5} B(E2, 0^+ \longrightarrow 2^+)\right]^{1/2} \tag{28}$$

in units of 10^{-24} cm^2.

The electric reduced transition probability $B(E\lambda)$ can be obtained from the transition probability per unit time for emission of photon of energy $\hbar\omega$, angular momentum λ and of electric type with the nucleus going from a state i to a state f defined by

$$T(E\lambda) = \frac{8\pi(\lambda+1)}{\lambda[(2\lambda+1)!!]^2} \frac{1}{\hbar} \left(\frac{E_\gamma}{\hbar c}\right)^{(2\lambda+1)}. \tag{29}$$

$T(E\lambda)$ for electric quadruple has the from

$$T(E2) = \frac{4\pi}{75} \frac{1}{\hbar} \left(\frac{E_\gamma}{\hbar c}\right)^5 B(E2). \tag{30}$$

For the quadruple transition $T(E2)$ can be derived experimentally from the relation

$$T(E2, 2^+ \longrightarrow 0^+) = \frac{ln2}{(1+\alpha)\tau_{1/2}}, \tag{31}$$

where α is the total conversion coefficient taken from the tabulated values given by Rose [22] and $\tau_{1/2}$ is the half life time. From equations (30) and (31), one can find $B(E2)$:

$$\begin{aligned} B(E2, 2^+ \longrightarrow 0^+) &= \frac{75\hbar}{4\pi} \left(\frac{\hbar c}{E_{2^+}}\right)^5 \frac{ln2}{(1+\alpha)\tau_{1/2}} \\ &= 0.565502 \left(\frac{100}{E_{2^+}}\right)^5 \frac{1}{(1+\alpha)\tau_{1/2}}, \end{aligned} \tag{32}$$

where $B(E2)$ is in units of e^2b^2 when E_{2^+} is in units of MeV and $\tau_{1/2}$ in units of nanosecond.

4 The two–neutron Separation Energies

The energy required to remove a neutron from a nucleus with Z proton and N neutron is called separation energy and is defined as:

$$S_n(Z,N) = [M(Z,N-1) + M_n - M(Z,N)]C^2. \tag{33}$$

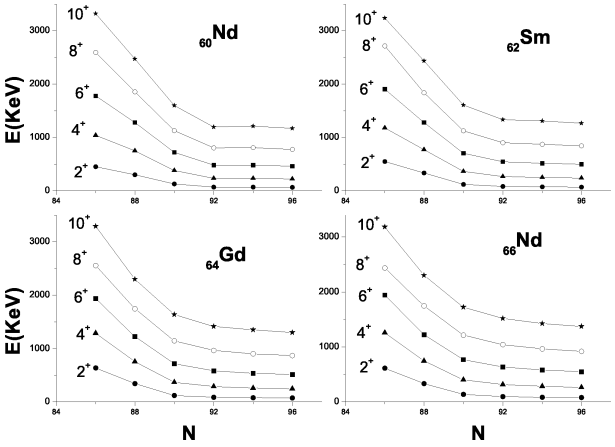

Fig. 1: Systematics of low-lying yrast level energies in even-even lanthanides Nd/Sm/Gd/Dy isotopes. The 2^+, 4^+, ..., 10^+ level energies are plotted. The states are labeled by I^π.

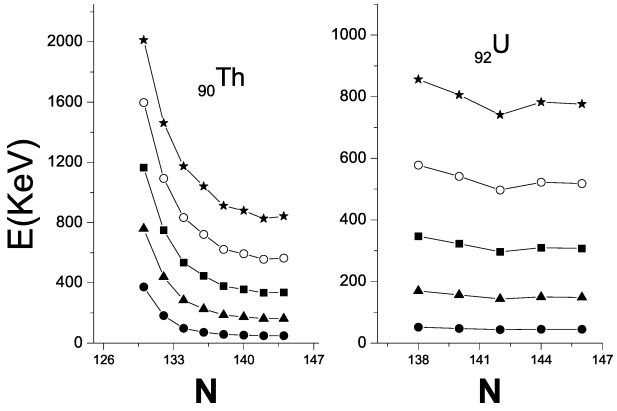

Fig. 2: The same as Fig. (1) but for actinides Th/U isotopes.

This expression can be rewritten in the form of binding energy as:

$$S_n(Z,N) = B(Z,N) - B(Z,N-1). \quad (34)$$

The definition of the two-neutron separation energies is the following:

$$S_{2n} = B(N) - B(N-1), \quad (35)$$

where N denotes the number of valence nucleon pairs and it is assumed that we are treating nuclei belonging to the first half of the neutron shell (50 - 82) filling up with increasing mass number.

5 Numerical Calculations and Discussions

The systematics of the excitation energies of the low-lying states as a function of neutron number changing from 84 to 100 in the even-even lanthanides Nd/Sm/Gd/Dy isotopes in the mass region 144–166 and the actinide Th/U isotopes in the mass region 224–238 are presented in Figures (1,2). Only the yrast state of positive parity and spin $I^\pi = 2^+, 4^+, 6^+, 8^+$ and 10^+ has been included.

The trend of increasing excitation energy of 2^+ state with decreasing neutron number, implying a corresponding fall in deformation as the N = 82 shell closure is approached. The energies of the 4^+ and 6^+ states also display the same trend. For lanthanides isotopes we can see that the energy values for each spin I states change almost linearly for $N \leq 88$ and become quite flat for $N \geq 90$. This is consistent with the onset of the Z = 64 sub-shell effect. Furthermore, the linear falling of the energy value for each I state as N goes from 86 to 88 seems to justify the linear variation of the effective proton-boson number in each isotope series.

As an example Figure (1) shows that the limits (spherical shape and well deformed rotor) are fulfilled in the Neodymium ^{144}Nd and $^{152-156}$Nd isotopes respectively, and also that there is a smooth transition between them. The ^{148}Nd isotopes could be considered as a transitional nucleus in the calculations. A rapid rise in R(4/2) between N = 88 and 90 is shown, where it increases from values of ≃2.3 typical of actual vibrational nuclei to 3.0, the traditional borderline value separating spherical from deformed nuclei to ≃3.3 the limiting value of the axial rotor model. As a matter of fact, if we compare the X(5) results (first order phase transition from a spherical vibrator to an axially deformed rotor is called X(5)) with the energy levels in ^{148}Nd, we find striking similarities, it suggested that the nucleus ^{148}Nd display the X(5) symmetry.

The nature of the low-lying states in our lanthanides and actinides chains of isotopes can be illustrated in Figures (3,4) by examining the ratios of the excitation energies R(4/2) and R(6/4) as a function of neutron number. The limiting values for R(4/2) and R(6/4) for harmonic vibrator are 2.0 and 1.5 and for rigid symmetric rotor are 0.33 and 2.1 respectively.

In lanthanides the calculated values increases gradually from vibrational value to transitional value near N=90 to rotor

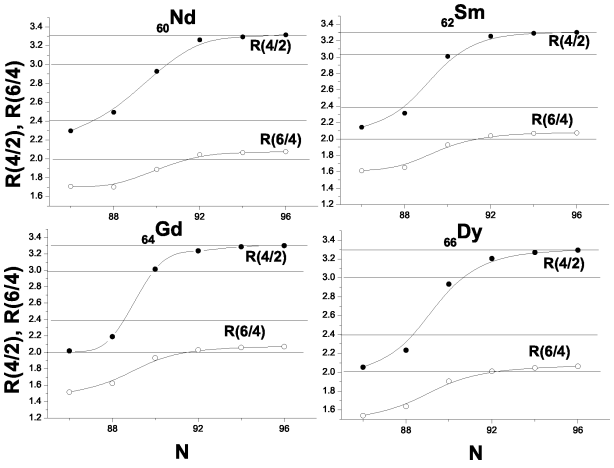

Fig. 3: Evolution of energy ratios R(4/2) and R(6/4) for lanthanides Nd/Sm/Gd/Dy isotopes as function of increasing neutron number.

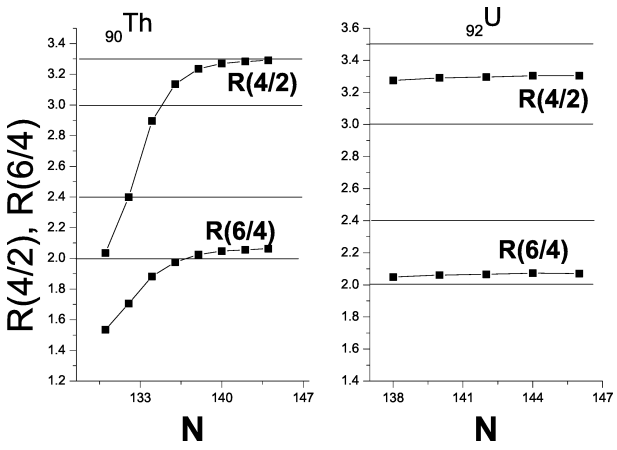

Fig. 4: The same as Fig. (3) but for actinides Th/U isotopes.

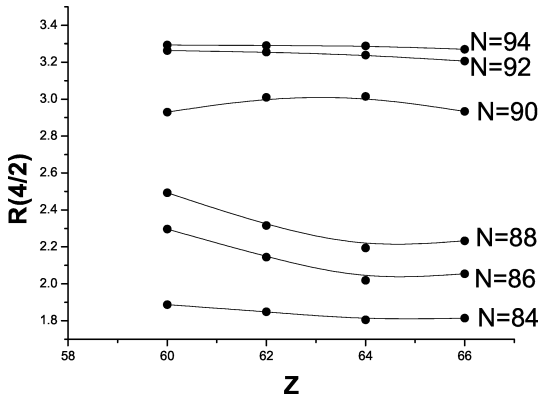

Fig. 5: The plot of R(4/2) values in the Nd/Sm/Gd/Dy region against Z. We see change in curvature in the data for N=88 and N=90 concave to convex.

value in the heavier isotopes. The energy ratios R(4/2) and R(6/4) for even A, N=88 isotopes are essentially constant for Sm, Gd and Dy.

The same data for lanthanides is plotted between R(4/2) against Z instead of N, see Figure (5). We see a rapid jump in R(4/2) near N=90. Here, the plot of R(4/2) against Z shows not only the existence of a shape transitions but also the change in curvature in the data for N=88 and 90, concave to convex. For Gd nuclei for N≤88 the behavior is typically closed shell, while for $N \geq 90$ the behavior appears to be near mid shell.

The nuclei of lanthanides region would therefore be candidates for a shape transition from vibrator to axially rotator and the N = 90 isotopes ^{150}Nd, ^{152}Sm, ^{154}Gd and ^{156}Dy are ideal candidates for X(5). Historically, sensitive studies [23] of the ^{152}Sm level scheme led to a suggestion that this nucleus gave evidence for a first order phase transition [24], its R(4/2) value is intermediate between vibrator and rotor [25]. Additional X(5) candidate in the lanthanides region have subsequently been identified in ^{150}Nd [26], ^{154}Gd [27], ^{156}Dy [28] and ^{162}Yb [29]. Fig. (6) shows R(I/2) and E-GOS plots for a vibrator, a rotor and R(4/2)=3 modes.

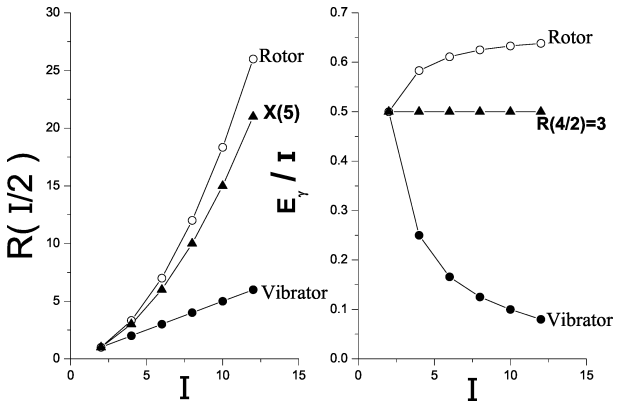

Fig. 6: Comparison of R(I/2) and E-GOS plots for three kinds of collective modes vibrator, rotor and R(4/2)=3 modes.

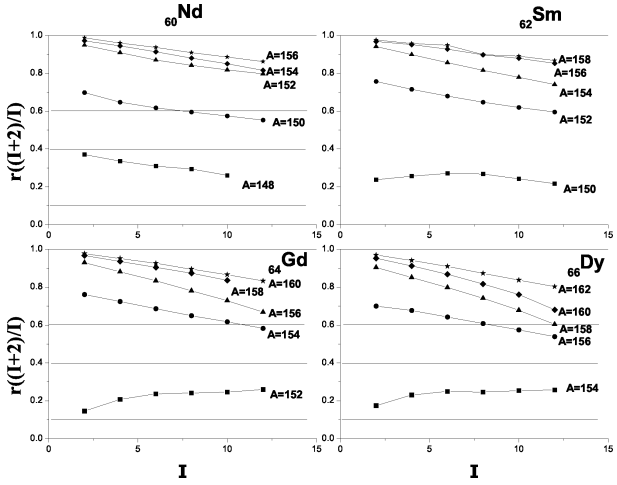

Fig. 7: The $r((I+2)/I)$ energy ratios for the ground state bands of even-even Lanthanides Nd/Sm/Gd/Dy isotopes as a function of spin I.

To investigate the dependence of energy ratios on the angular momentum, the useful criterion r((I + 2)/I) are examined for distinguishing between different kinds of collective behavior. In Figures (7,8) we show the results of our calculations for the ground state bands of the selected lanthanides and actinides isotopes. The study supports the interpretation of ^{150}Nd and ^{152}Sm as a critical point nucleus. Hence, the isotopes ^{150}Nd and ^{152}Sm are associated to X(5) symmetry. For the vibrational nuclei ^{152}Gd and ^{154}Dy, the ratios r((I + 2)/I) start with a small value and then increases with I, more rapidly in the beginning and slower at higher I's. On the other hand for rotational nucleus ^{162}Dy the ratios r((I + 2)/I) start with a value very close to one and then constantly decrease.

As an example, the abnormal behavior of the two-neutron

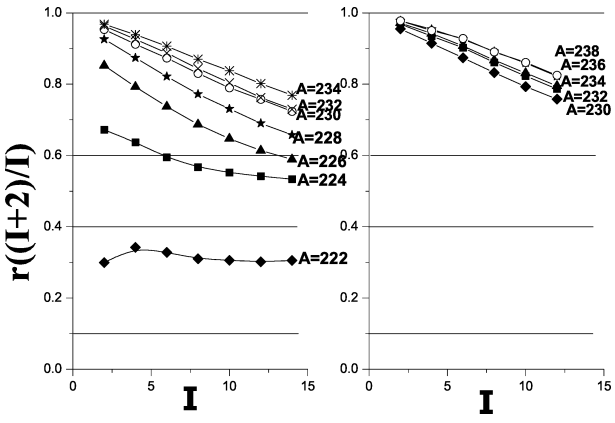

Fig. 8: The same as Fig. (7) but for Actinides Th/U isotopes.

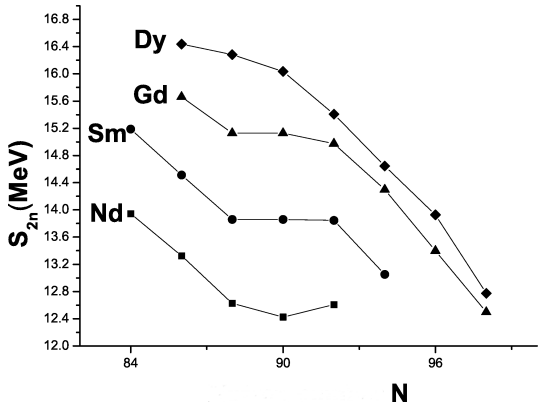

Fig. 9: Two-neutron separation energies S_{2n} for the chains Nd/Sm/Gd/Dy isotopes as a function of the number of neutrons.

separation energies S_{2n} of nuclei Nd/Sm/Gd/Dy as a function of neutron number around neutron number 90 is illustrated in Fig. (9), the nonlinear behavior of S_{2n} indicates that shape phase transition may occur in this region. It is commonly assumed that the ratio of the B(E2) reduced transition probabilities between the levels of the ground state band takes the values between vibrational and rotational limits. In the interacting boson model IBM [1] both these limits are corrected because the number of the quadruple bosons cannot exceed some maximum value N.

In the U(5) vibrational limit of IBM,

$$\frac{B(E2, I+2 \to I)}{B(E2, 2^+ \to 0^+)} = \frac{1}{2}(I+2)\left(1-\frac{1}{2N}\right)$$

and in the SU(3) rotational limit of IBM,

$$\frac{B(E2, I{+}2 \to I)}{B(E2, 2^+ \to 0^+)} = \frac{15}{2}\left(1{-}\frac{1}{2N}\right)\left(1{-}\frac{1}{2N{+}3}\right)\frac{(I{+}2)(I{+}1)}{(2I{+}3)(2I{+}5)}.$$

Our GCM calculated values of these ratios are put between these limits, *i.e.*, the IBM calculations can reproduce the E2 transition probabilities.

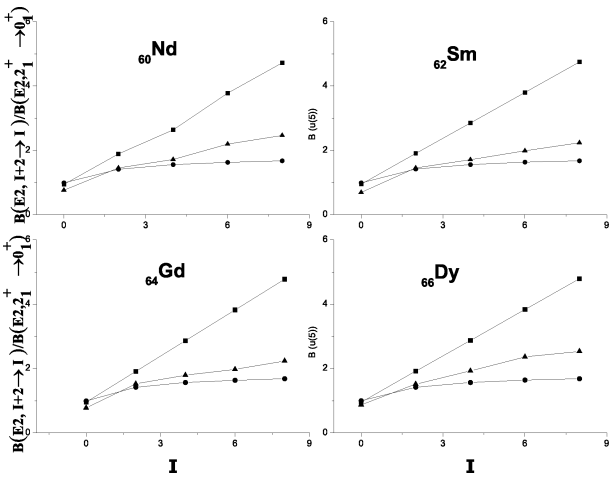

Fig. 10: The ratio $\frac{dB(E2,I+2\longrightarrow I)}{B(E2,2^+\longrightarrow 0^+}$ of reduced transition probabilities between the levels of the ground state band of ^{150}Nd, ^{152}Sm, ^{154}Gd and ^{156}Dy as compared to the U(5) and SU(3) of IBM calculations (• for U(5), ∘ for SU(3) and x for present calculation).

Table 1: The GCM parameters as derived in fitting procedure used in the calculation.

Nucleus	I	U(5) Vibrator	SU(3) Rotor	Present calculations
^{150}Nd (N=9)	0	0.94444	0.98941	0.75812
	2	1.88888	1.41345	1.45375
	4	2.63333	1.55677	1.71683
	6	3.77777	1.62962	2.19186
	8	4.72222	1.67381	2.46675
^{152}Sm (N=10)	0	0.95	0.99130	0.68900
	2	1.90	1.41614	1.45137
	4	2.85	1.55973	1.71262
	6	3.80	1.63272	1.98838
	8	4.75	1.67700	2.23512
^{154}Gd (N=11)	0	0.95454	0.99272	0.77300
	2	1.90909	1.41818	1.52393
	4	2.86363	1.56197	1.79560
	6	3.81818	1.63507	1.97412
	8	4.77272	1.67941	2.23803
^{156}Dy (N=12)	0	0.95833	0.99382	0.87381
	2	1.91666	1.41975	1.51345
	4	2.87500	1.56370	1.92725
	6	3.83333	1.63688	2.35673
	8	4.79166	1.68127	2.53512

The calculated $B(E2, I+2 \longrightarrow I)/B(E2, 2^+ \longrightarrow 0^+)$ ratios using GCM for the ground state bands of the low-lying state are presented in Table (1) and Fig. (10) together with

the results for the vibrator and rotor limits of IBM for ^{150}Nd, ^{152}Sm, ^{154}Gd and ^{156}Dy.

Submitted on January 15, 2013 / Accepted on January 21, 2013

References

1. Iachello F. and Arima A. The Interacting Boson Model. Cambridge University Press, Cambridge, England, 1987.
2. Frank A. and VanIsacker P. Algebraic Methods in Molecular and Nuclear Structure Physics. Wiley, New York, 1994.
3. Eisenberg J. and Greiner W. Nuclear Theory, Vol. I, Nuclear Models: Collective and Single-Particle Phenomena. North-Holland, Amsterdam, 1987.
4. Troltenier D., Hess P.O. and Maruhn J. Computational Nuclear Physics, Vol. I, Nuclear Structure. Springer, Berlin, Heidelberg, New York, 1991.
5. Troltenier D. Das Generalisierte Kollektivmodell. Frankfurt am Main, Germany, Report No. GSI-92-15, 1992.
6. Bohr A. and Mottelson. Nuclear Structure v. II. Benjamin, New York, 1975.
7. Jolie J. et al. Two-Level Interacting Boson Models Beyond The Mean Field. *Physical Reveiw*, 2007, v. C75, 014301R–014310R.
8. Iachello F. and Zamfir N.V. Quantum Phase Transitions in Mesoscopic Systems. *Physical Review Letters*, 2004, v. 92(3), 212501–212504.
9. Cejnar P., Heinze S. and Dobes J. Thermodynamic Analogy for Quantum Phase Transitions at Zero Temperature. *Physical Review*, 2005, v. C71, 011304R–011309R.
10. Rowe D.J. Quasi Dynamical Symmetry in an Interacting Boson Model Phase Transition. *Physical Review Letters*, 2004, v. 93, 122502–122505.
11. Liu Y.X., Mu L.Z. and Wei H. Approach to The Rotation Driven Vibrational to Axially Rotational Shape Phase Transition Along The Yrast Line of a Nucleus. *Physics Letters*, 2006, v. B633, 49–53.
12. Zhang Y., Hau Z. and Liu Y.X. Distinguishing a First Order From a Second Order Nuclear Shape Phase Transition in The Interacting Boson Model. *Physical Review*, 2007, v. C76, 011305R–011308R.
13. Arios J.M., Dukelsky J. and Garcia-Ramos J.E. Quantum Phase Transitions in the Interacting Boson Model: Integrability, Level Repulsion and Level Crossing. *Physical Review Letters*, 2003, v. 91, 162502–162504.
14. Garcia-Ramos J.E. et al. Two-Neutron Separation Energies, Binding Energies and Phase Transitions in The Interacting Boson Model. *Nuclear Physics*, 2001, v. A688, 735–754.
15. Liu M.L. Nuclear Shape-Phase Diagrams. *Physical Review*, 2007, v. C76, 054304–054307.
16. Heyde K. et al. Phase Transitions Versus Shape Coexistence. *Physical Review*, 2004, v. C69, 054304–054309.
17. Iachello F. Dynamic Symmetrcies at The Critical Point. *Physical Review Letters*, 2000, v. 85, 3580–3583.
18. Iachello F. Analytic Prescription of Critical Point Nuclei in a Spherical Axially Deformed Shape Phase Transtion. *Physical Review Letters*, 2001, v. 87, 052502–052506.
19. Regan P.H. et al. Signature for Vibrational to Rotational Evolution Along the Yrast Line. *Physical Review Letters*, 2003, v. 90, 152502–152505.
20. Zamfir N.V. et al. Study of Low-Spin States in ^{122}Cd. *Physical Review*, 1995, v. C51, 98–102.
21. Bonatsos D. and Skoures L.D. Successive Energy Ratios in Medium- and Heavy-Mass Nuclei as Indicators of Different Kinds of Collectivity. *Physical Review*, 1991, v. C43, 952R–956R.
22. Rose M.E. Internal Conversion Coefficients. Amsterdam, North Holland . North-Holland, Publishing Company 1958.
23. Casten R.F. The First Excited 0^+ State in ^{152}Sm. *Physical Review*, 1998, v. C57, 1553R–1557R.
24. Casten R.F. Kusnezov D. and Zamfir N.V. Phase Transitions in Finite Nuclei and The Integer Nucleon Number Problem. *Physical Review Letters*, 1999, v. 82, 5000–5003.
25. Clark R.M. et al. Searching For X(5) Behavior in Nuclei. *Physical Review*, 2003, v. C68, 037301–037304.
26. Krücken R. et al. B(E2) Values in ^{150}Nd and The Critical Point Symmetry X(5). *Physical Review Letters*, 2002, v. 88, 232501–232501.
27. Tonev D. et al. Transition Probabilities in ^{154}Gd: Evidence for X(5) Critical Point Symmetry. *Physical Review*, 2004, v. C69, 034334–034339.
28. Caprio M.A. et al. Low-Spin Structure of 156Dy Through γ-ray Spectroscopy. *Physical Review*, 2002, v. C66, 054310–054328.
29. McCutchan E.A. et al. Low Spin States in ^{162}Yb and The X(5) Critical Point Symmetry. *Physical Review*, 2004, v. C69, 024308–024317.

Double Surface and Fine Structure

Janez Špringer

Cankarjeva cesta 2, 9250 Gornja Radgona, Slovenia, EU. E-mail: janez_springer@t-2.net

Previously [1], one concluded that the atomic world should be elliptic and therefore the present universe which on the macro level looks like Euclidean is obviously to be heterogeneous. In this paper, one tries to solve the enigma proposing the double elliptic-hyperbolic surface. As a result of the effort, a new candidate for the exact inverse fine structure constant is given: $\alpha^{-1} = 137\left(2 - 1/\sqrt{1+\pi^2/137^2}\right) = 137.0360062543\ldots$.

1 Theoretical background

Let us consider our experience of the world is not what that world in reality is but rather how it is observed and measured. The distinction between to observe and to measure is made in this paper. The former means to count the units in the image, denoted as the average $\overline{x}$. The latter means to count the units in the inverse image, denoted as the average $\overline{x^{-1}}$. For the different values of x_i we have to deal with the next inequality:

$$\overline{x} \times \overline{x^{-1}} \neq 1. \tag{1}$$

Then the surface we live on is not, for instance, the Euclidean plane or the sphere very close to it [1], but could be, instead of it, the double elliptic-hyperbolic surface which is observed as the Euclidean plane. The average sphere is not proposed to be the triple elliptic-Euclidean-hyperbolic surface unless the Euclidean plane is not assigned to have its own identity. Let us propose that this leaves a footprint in the inverse fine structure constant α^{-1} which is in some way observed. Actually in the observation we count the number of the length units λ which are correlated with the inverse fine structure α^{-1}:

$$\alpha^{-1}_{observed} = \alpha^{-1}_{euclidean} = \frac{\alpha^{-1}_{elliptic} + \alpha^{-1}_{hyperbolic}}{2}. \tag{2}$$

And the measured elliptic fine structure constant on the atom level does not reflect exclusively the elliptic sphere, since it is the mirror of the hyperbolic sphere, too. Let us propose that this leaves a footprint in the fine structure constant α which is in some way measured. Actually in the measurement we count the number of the inverse length units $\lambda^{-1} = mv/h$ which are correlated with the fine structure α:

$$\alpha_{measured} = \frac{\alpha_{elliptic} + \alpha_{hyperbolic}}{2}. \tag{3}$$

Consequently the different inverse fine structure constants are explicitly expressed as

$$\alpha^{-1}_{measured} = \alpha^{-1}_{elliptic}\left(2 - \frac{\alpha^{-1}_{elliptic}}{\alpha^{-1}_{euclidean}}\right), \tag{4a}$$

$$\alpha^{-1}_{elliptic} = \alpha^{-1}_{euclidean} - \sqrt{\alpha^{-1}_{euclidean}\left(\alpha^{-1}_{euclidean} - \alpha^{-1}_{measured}\right)}, \tag{4b}$$

$$\alpha^{-1}_{hyperbolic} = \alpha^{-1}_{euclidean} + \sqrt{\alpha^{-1}_{euclidean}\left(\alpha^{-1}_{euclidean} - \alpha^{-1}_{measured}\right)}, \tag{4c}$$

$$\alpha^{-1}_{sphere} = \alpha^{-1}_{euclidean} \mp \sqrt{\alpha^{-1}_{euclidean}\left(\alpha^{-1}_{euclidean} - \alpha^{-1}_{measured}\right)}. \tag{4d}$$

It is easily seen that if the measured inverse fine structure constant equals the observed Euclidean one, the elliptic and hyperbolic inverse fine structure constant are identical and no average makes sense. Only in that case what is observed and measured is also real.

Let us also recall the value of the hypothetical Euclidean inverse fine structure constant [1]:

$$\alpha^{-1}_{euclidean} = \sqrt{\pi^2 + 137^2}. \tag{5}$$

2 The fine structure constant and the Hydrogen atom

The elliptic sphere of the radius of about 3679 Compton wavelengths of the electron was proposed in the Hydrogen atom previously [1], based on the assumption that only one type of the sphere is possible. If the elliptic and hyperbolic sphere coexists, the fine structure constant is a mirror of their average geometry, and what results is a different sphere picture. Without going into the details of how it looks like, some calculations can be made.

2.1 Calculation of the sphere paths

Taking into account the equation (5) and inserting in the equations (4b) and (4c), the CODATA 2012 recommended $\alpha^{-1} = 137.035999074$ for the $\alpha_{measured}$, the elliptic and hyperbolic path s in the Hydrogen atom are given in units of Compton wavelengths of the electron as:

$$\begin{aligned} s_{elliptic}(\alpha^{-1}_{elliptic}) &= 136.988254898\cdots < n = 137 \\ s_{hyperbolic}(\alpha^{-1}_{hyperbolic}) &= 137.083776540\cdots \end{aligned} \tag{6}$$

The path on the elliptic sphere being smaller than the translation component n is not plausible and leads one to the conclusion that the recommended empirical value of α^{-1} should be of a little greater size.

2.2 Calculation of the inverse fine structure constants

The translation component $n = 137$ Compton wavelengths of the electron equals the elliptic circular path s and the latter

expresses the elliptic inverse fine structure constant [1]

$$\alpha^{-1}_{elliptic} = 137, \text{ since:}$$
$$n = s = 137 \text{ Compton wavelengths of the electron.} \tag{7}$$

The theoretical inverse fine structure constant deduced from the average path on the double elliptic-hyperbolic surface is given with the equations (4a) and (5):

$$\begin{aligned} \alpha^{-1}_{theoretical} &= 137\left(2 - 1/\sqrt{1+\pi^2/137^2}\right) \\ &= 137.0360062543\cdots < \alpha^{-1}_{euclidean} \end{aligned} \tag{8}$$

The calculated constant is a little greater than the recommended CODATA 2012 α^{-1} but smaller than the hypothetical Euclidean one given by (5). The hyperbolic inverse fine structure is given by (4c):

$$\alpha^{-1}_{hyperbolic} = 137.0720314399\cdots \tag{9}$$

3 Conclusion

According to the proposed model, the electron in the Hydrogen atom moves on the elliptic-hyperbolic double surface, since the measured inverse fine structure constant is smaller than the hypothetical Euclidean one. And we live in the apparent Euclidean macro-world, since the observed inverse fine structure constant does not seem to differ from the hypothetical Euclidean one. The difference between what is observed on the macro level and what is measured in the atom world implies that neither what is observed nor what is measured is real. If the elliptic and hyperbolic sphere can coexist in the present world, a new candidate for the exact inverse fine structure constant is given by

$$\alpha^{-1}_{theoretical} = 137\left(2 - 1/\sqrt{1+\pi^2/137^2}\right) = 137.0360062543\cdots$$

Dedication

This fragment is dedicated to my granddaughters Urša and Špela.

Submitted on January 28, 2013 / Accepted on February 7, 2013

References

1. Špringer J. Fine Structure Constant as a Mirror of Sphere Geometry. *Progress in Physics*, 2013, v. 1, 12–14.

LETTERS TO PROGRESS IN PHYSICS

Commentary Relative to the Distribution of Gamma-Ray Flares on the Sun: Further Evidence for a Distinct Solar Surface

Pierre-Marie Robitaille

Department of Radiology, The Ohio State University, 395 W. 12th Ave, Columbus, Ohio 43210, USA.
robitaille.1@osu.edu

High energy gamma-ray flares are almost always observed near the limb of the Sun and are seldom, if ever, visualized in the central region of the solar disc. As such, they exhibit a powerful anisotropy best explained by invoking a true photospheric surface. In this regard, the anisotropic nature of the gamma-ray emissions from high-energy flares constitute the eighteenth line of evidence that the Sun is condensed matter.

Every body has a surface.

St. Thomas Aquinas [1]

In the middle ages, as St. Thomas Aquinas was reflecting upon *The Infinity of God*, he was confronted with this objection relative to objects and their surfaces [1]. Thomas would answer that: "*It is one thing to be infinite in essence, and another to be infinite in magnitude*" [1]. Though nearly a millennium has passed since the Dominican Friar contemplated *The Infinity of God*, the fact remains that, in the physical world, one is primarily considering magnitude, not essence: on a macroscopic scale, every physical body does indeed have a surface. Failure to meet this criterion results in an assembly of many bodies.

These ideas have consequences for astronomy. Within the context of accepted solar models, the Sun must be viewed as an assembly of bodies, since it has long ago been deprived of a real surface by gaseous constructs [2].

Conversely, the author has argued that the Sun does indeed possess a real surface [3] and he has recently assembled a wide variety of proofs that highlight its condensed state of matter (see e.g. [4] and references therein). In this brief work, an 18^{th} line of evidence is provided.

In 1989, Erich Rieger published a paper in *Solar Physics* entitled "*Solar Flares: High Energy Radiation and Particles*" [5]. In this report, Rieger provided strong evidence that flares with emissions >10 MeV are visible only near the solar limb (see Fig. 1). Rieger's findings would be highlighted by R. Ramaty and G. M. Simnett in their review on accelerated particles in solar flares: "*Gamma-ray emitting flares are observed from sites located predominantly near the limb of the Sun (see, e.g. Rieger 1989). This effect was observed for flares detected at energies >0.3 MeV, but it is at energies >10 MeV that the effect is particularly pronounced ... Since in both of these cases the bulk of the emission is bremsstrahlung from primary electrons, these results imply that the radiating electrons are anisotropic*" [6, p. 237]. It was then postulated that: "*... the anisotropy could result from the mirroring of the charged particles in the convergent chromospheric magnetic fields*" [6, p. 237] based on a theoretical analysis by Miller and Ramaty [7]. These authors comment that the emissions are "*... strongly anisotropic, with more emission in the directions tangential to the photosphere than in directions away from the Sun*" [7]. In order to account for the anisotropy of the gamma-ray emission from high energy solar flares, they invoke electron transport in the coronal region and magnetic mirroring of converging magnetic flux tubes beneath the transition region [7]. As the gaseous models of the Sun cannot support the existence of a real surface, then another mechanism must be created to "act as a surface".

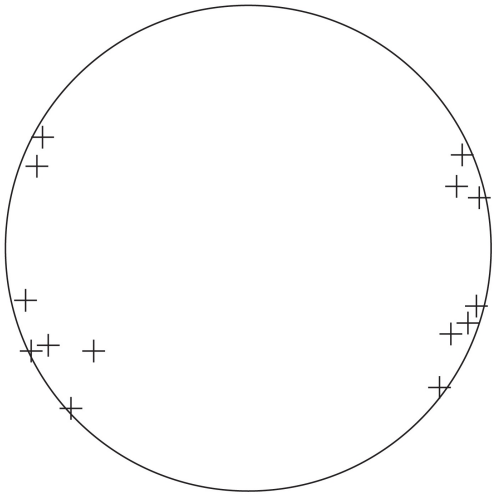

Fig. 1: Schematic representation of the relative position of flares with >10 MeV of energy on the solar disk displaying their predominance near the limb. This figure is meant only for illustrative purposes and is an adaptation based on Fig. 9 in [5] which should be examined for exact flare locations.

Within the gaseous models, the photosphere merely represents a region of increasing opacity, best regarded as an "optical illusion" [3]. The gaseous Sun possesses no sudden change in density which could allow tangential emission to its surface. In fact, modern solar models assume a density of only 10^{-7} g/cm^3 for the photosphere [8, p. 32], a density

lower than some of our earthly vacuums. Hence the use of magnetic mirroring and the convergence of field lines in order to generate surface effects in the absence of condensed matter.

In the end, the simplest way to account for the strongly anisotropic nature of high energy solar flares is to recognize the existence of a discrete surface on the Sun. This most elegantly explains why the emissions are *tangential to the photosphere*. As flares rise from the solar interior [4] they eventually arrive at the photospheric layer. High energy gamma rays are emitted tangentially to this boundary, as a real physical surface, not to an illusion [3], has been encountered.

Acknowledgment

Luc Robitaille is recognized for the preparation of Figure 1.

Dedication

Dedicated to Dominican Friars of the Province of St. Joseph.

Submitted on: January 17, 2013 / Accepted on: January 18, 2013
First published in online on: January 28, 2013

References

1. Aquinas, Thomas. ST I,7,iii: Cosimo Inc., New York, 2007.
2. Robitaille P.M. A thermodynamic history of the solar constitution — I: The journey to a gaseous Sun. *Progr. Phys.*, 2011, v. 3, 3–25.
3. Robitaille P.M. On the Presence of a Distinct Solar Surface: A Reply to Hervé Faye. *Progr. Phys.*, 2011, v. 3, 75–78.
4. Robitaille J.C. and Robitaille P.M. Liquid Metallic Hydrogen III: Intercalation and lattice exclusion versus gravitational settling and their consequences relative to internal structure, surface activity, and solar winds in the Sun. *Progr. Phys.*, 2013, v. 2, in press.
5. Rieger E. Solar flares: High-energy radiation and particles. *Solar Phys.*, 1989, v. 121, 323–345.
6. Ramata R. and Simnett G.M. Accelerated particles in solar flares. In: *The Sun in Time* (C.P. Sonett, M.S. Giampapa and M.S. Matthews, Eds.), The University of Arizona Press, Tuscon, AZ, 1991, p. 232–259.
7. Miller J.A. and Ramaty R. Relativistic electron transport and Bremsstrahlung production in solar flares. *Astrophys. J.*, 1989, v. 344, 973–990.
8. Bhatnagar A. Instrumentation and observational techniques in solar astronomy. In: *Lectures on Solar Physics* (H.M. Antia, A. Bhatnagar and R. Ulmschneider, Eds.), Springer, Berlin, 2003, p. 27–79.

LETTERS TO PROGRESS IN PHYSICS

Commentary Relative to the Seismic Structure of the Sun: Internal Rotation, Oblateness, and Solar Shape

Pierre-Marie Robitaille

Department of Radiology, The Ohio State University, 395 W. 12th Ave, Columbus, Ohio 43210, USA.
robitaille.1@osu.edu

Helioseismological studies have the ability to yield tremendous insight with respect to the internal structure and shape of the solar body. Such observations indicate that while the convection zone displays differential rotation, the core rotates as a rigid body. The latter is located below the tachocline layer, where powerful shear stresses are believed to occur. Beyond simple oblateness, seismological studies indicate that the Sun displays significant higher order shape terms (quadrupole, hexadecapole) which may, or may not, vary with the solar cycle. In this work, such seismological findings are briefly discussed with the intent of highlighting that 1) the differential rotation of the convection zone, 2) the rigid body rotation of the core, 3) the presence of the tachocline layer and 4) the appearance of higher order shape terms, all lend support to the idea that the solar body is composed of material in the condensed state. In this regard, the existence of the tachocline layer in the solar interior and the solid body rotation of the core constitute the nineteenth and twentieth lines of evidence that the Sun is condensed matter.

> *In brief, every rotating body conducts itself either as if it is it were purely liquid, or as if it were purely gaseous; there are no intermediate possibilities. Observational astronomy leaves no room for doubt that a great number of stars, perhaps even all stars . . . behave like liquids rather than gases.*
>
> Sir James Hopwood Jeans, 1929 [1]

For much of his life, James Jeans believed that stars were rotating liquids [1, 2]. On the basis of the tremendous abundance of binary systems [2], he had claimed that there could be no doubt of their condensed nature. Yet, in the paragraph which followed that quoted above, Jeans also argued: *"we are totally unable to check our theoretical results by observation"* [1, p. 219]. This apparent contradiction was previously highlighted by Alan B. Whiting [3, p. 209]. Eventually, Jeans lost sight of the observational evidence which had so convinced him. By 1944, he had abandoned liquid stars [2,4] and so did astrophysics; although in the 1960s, Subrahmanyan Chandrashekar would devote nine years of his life to the study of rotating liquid bodies [4,5]. With time however, astronomy would add to the arsenal of evidence that the Sun was liquid (see [6–8] and references therein).

Seismology, the study of low frequency waves within condensed matter, would also contribute to our understanding [9, 10]. Indeed, the mere application of seismology to the Sun has been heralded as a proof for condensed matter (see proof 5 in [8]). It is not reasonable to claim that the solar photosphere, with a density of only 10^{-7} g/cm^3 [11], can act as a mere optical illusion relative to the presence of a distinct surface [12], while at the same time forming the confines of a resonant cavity for seismological studies [13]. The author has already argued that it is not possible to conduct seismological observations on a surface whose density remains inferior to some of the best vacuums on Earth [8], despite the apparent agreement with the gaseous solar models [14, 15]. Seismology has been, and always will remain, linked to the study of condensed matter.

In this regard, seismology has brought some interesting insight into the internal structure of the Sun. The fact that the convection zone undergoes differential rotation appears well established, as is the presence of a prolate tachocline layer [9,10]. The tachocline region acts as a shear layer which separates the differential rotation in the convection zone from the solid body rotation observed in the solar core. Shear forces imply area and surface. As such, the presence of the tachocline layer in the solar interior is now advanced as the nineteenth line of evidence that the Sun is condensed matter. Furthermore, the solar core is rotating as a solid body (e.g. [10]) and this remains impossible for a gaseous object. Solid body rotation involves strong internal cohesive forces which gases cannot possess. Consequently, the solid body rotation of the solar core is now invoked as the twentieth line of evidence that the Sun is condensed matter.

Finally, it is well established that the Sun is not perfectly spherical but oblate (see [15, 16] and references therein). Indeed, the presence of solar oblateness could be related to Jean's arguments for liquid stars [2]. Since the creation of an oblate object requires internal cohesive forces which can only characterize a liquid or solid rotating sphere, solar oblateness has already been invoked as the eighth line of evidence that the Sun is condensed matter [8]. Yet, the solar shape is even more complex, characterized by quadrupolar and hex-

adecapolar terms [16], the latter of which appears dependent on the solar cycle. These additional features on the solar sphere served to complement the eighth line of evidence (solar shape [8]) that the Sun is condensed matter.

Dedication

This work is dedicated to Bernadine Healy†, Reed Fraley, Joan Patton, Bradford Stokes, and Kamilla Sigafoos for their administrative leadership in helping to create the world's first Ultra High Field MRI system at The Ohio State University.

Submitted on: January 25, 2013 / Accepted on: January 25, 2013
First published in online on: January 28, 2013

References

1. Jeans J. The universe around us. Cambridge University Press, 1929, p. 211.
2. Jeans J. Astronomy and Cosmogony. Cambridge University Press, 1928.
3. Whiting A.B. Hindsight and popular astronomy. World Scientific, New Jersey, 2011.
4. Robitaille P.M. A thermodynamic history of the solar constitution–II: The theory of the gaseous Sun and Jeans' failed liquid alternative. *Progr. Phys.*, 2011, v. 3, 3–25.
5. Chandrasekhar S. Ellipsoidal Figures of Equilibrium. Yale Unversity Press, New Haven, 1969.
6. Robitaille J.C. and Robitaille P.M. Liquid Metallic Hydrogen III: Intercalation and lattice exclusion versus gravitational settling and their consequences relative to internal structure, surface activity, and solar winds in the Sun. *Progr. Phys.*, 2013, v. 2, in press.
7. Robitaille P.M. Commentary relative to the distribution of gamma-ray flares on the Sun: Further evidence for a distinct solar surface. *Progr. Phys.*, 2013, v. 2, L1-L2.
8. Robitaille P.M. The solar photosphere: Evidence for condensed matter. *Progr. Phys.*, 2006, v. 2, 17–21 (also found in slightly modified form within *Research Disclosure*, 2006, v. 501, 31–34; title #501019).
9. Gough D.O. Seismology of the Sun and the distant stars. D. Reidel Publishing Company, Dordrecht, 1986.
10. Antia H.M. Solar interior and seismology. In: *Lectures on Solar Physics* (H.M. Antia, A. Bhatnagar and R. Ulmschneider, Eds.), Springer, Berlin, 2003, p. 80–126.
11. Bhatnagar A. Instrumentation and observational techniques in solar astronomy. In: *Lectures on Solar Physics* (H.M. Antia, A. Bhatnagar and R. Ulmschneider, Eds.), Springer, Berlin, 2003, p. 27–79.
12. Robitaille P.M. On the Presence of a Distinct Solar Surface: A Reply to Hervé Faye. *Progr. Phys.*, 2011, v. 3, 75–78.
13. Robitaille P.M. Stellar opacity: The Achilles heel of a gaseous Sun. *Progr. Phys.*, 2011, v. 3, 93–99.
14. Gough D.O., Kosovichev A.G., Toomre J., Anderson E., Antia H.M., Basu S., Chaboyer B., Chitre S.M., Christensen-Dalsgaard J., Dziembowski W.A., Eff-Darwich A., Elliott J.R., Giles P.M., Goode P.R., Guzik J.A., Harvey J.W., Hill F., Leibacher J.W., Monteiro M.J.P.F.G., Richard O., Sekii T., Shibahashi H., Takata M., Thompson M.J., Vauclair S., Vorontsov S.V. The seismic structure of the Sun. *Science*, v. 272, no. 5266, 1296–1300.
15. Godier S. and Rozelot J.P. The solar oblateness and its relationship with the structure of the tachocline and the Sun's subsurface. *Astron. Astrophys.*, 2000, v. 355, 365–374
16. Kuhn J.R., Bush R.I, Scheick X. and Scherrer P. The Sun's shape and brightness. *Nature*, 1998, v. 392, no. 6672, 155–157.

LETTERS TO PROGRESS IN PHYSICS

Commentary on the Radius of the Sun: Optical Illusion or Manifestation of a Real Surface?

Pierre-Marie Robitaille

Department of Radiology, The Ohio State University, 395 W. 12th Ave, Columbus, Ohio 43210, USA.
robitaille.1@osu.edu

In modern solar theory, the photospheric surface merely acts as an optical illusion. Gases cannot support the existence of such a boundary. Conversely, the liquid metallic hydrogen model supports the idea that the Sun has a distinct surface. Observational astronomy continues to report increasingly precise measures of solar radius and diameter. Even the smallest temporal variations in these parameters would have profound implications relative to modeling the Sun and understanding climate fluctuations on Earth. A review of the literature convincingly demonstrates that the solar body does indeed possess a measurable radius which provides, along with previous discussions (Robitaille P.M. On the Presence of a Distinct Solar Surface: A Reply to Hervé Faye. *Progr. Phys.*, 2011, v. 3, 75–78.), the twenty-first line of evidence that the Sun is comprised of condensed-matter.

> *But however difficult it may be for present theories to account for the tenuity of the solar atmosphere immediately above the photosphere, and however readily the same fact may be accounted for by the theory of Schmidt, it is certain that the observer who has studied the structure of the Sun's surface, and particularly the aspect of the spots and other markings as they approach the limb, must feel convinced that these forms actually occur at practically the same level, that is, that the photosphere is an actual and not an optical surface. Hence it is, no doubt, that the theory is apt to be more favorably regarded by mathematicians than by observers.*
>
> James Edward Keeler, 1895 [1]

James Edward Keeler was a distinguished observational astronomer [2]. Along with George Ellery Hale, he had established *The Astrophysical Journal* in 1895 [2]. In the first volume of this journal, Keeler objected to Schmidt's model of a fully gaseous Sun whose surface merely represented an optical illusion (see [3] for a full discussion). Hale echoed Keeler's objections stating, *"As a theoretical discussion the theory is interesting and valuable, but few observers of the Sun will consider it capable of accounting for the varying phenomena encountered in their investigations"* [4]. Thus, two of the greatest observational astronomers of the nineteenth century expressed serious reservations relative to the idea that the solar surface was illusionary.

Today, much effort continues to be focused on establishing a proper value for the solar radius ([5–12] and references therein). Such reports constitute a clear sign that observational astronomers recognize, at least in practice, the existence of a distinct solar surface. In fact, the measurement of the solar radius not only occupies amateur astronomers, as they map the transits of Mercury and Venus [11, 12], but also attracts the attention of our helioseismologists [5–10]. This is not solely because of the obvious implications for climate change [9]. For theoretical solar physicists, any variation in the dimensions of the Sun would have severe consequences with respect to the gaseous models [5–10]. The latter would be hard-pressed to account for fluctuations in radius. This helps to account for the reassurance experienced when the solar radius is perceived as constant [5–7].

Nonetheless, the solar radius has not definitively been established as fixed. Values obtained in the past thirty years range from $958''.54 \pm 0''.12$ to $960''.62 \pm 0''.02$ (see [10] for a complete table). In 1980, Irwin Shapiro argued that the solar radius had not decreased over time [13]. Currently, these issues cause little debate, though cyclical variations continue to be gently questioned (see [10–13] and references therein).

Perhaps the most interesting aspect of solar radius determinations remains the increased precision of the measurements over the years. Emilio et al. estimate the solar radius at $960''.12 \pm 0''.09$ [10]. This corresponds to 65 km for a radius of more than half a million kilometers (696,342 km) – an error of better than 1 part in 10,000. Others report errors on the order of $0''.02$ [10], a relatively tiny distance of less than 15 km – an error of only 2 parts in 100,000. This precision argues strongly for a distinct solar surface and the existence of a condensed solar body. It is inconceivable that a gaseous Sun would be able to create such a defined "optical illusion". The gaseous solar models argue for smoothly varying density changes, even in the region of the photosphere. As a result, the extreme precision of the solar radius determinations in the visible range, along with previous arguments for a distinct solar surface [3], constitute the twenty-first line of evidence that the Sun is condensed matter.

Additional Note

Chapman et al. [14] have recently reported variability in the Sun's diameter in association with the solar cycle. As previously mentioned, this is a topic of interest to many, though it is only quietly pursued [15]. Variations in the solar diameter with the activity cycle could produce changes in total solar irradiance, beyond the effects produced by sunspots and faculae [16, 17]. While the question of varying solar radius has not been resolved, such phenomena could be accounted for by invoking exfoliative forces within the liquid metallic hydrogen model of the Sun [18]. Exfoliation would be characterized by the production of gases within the condensed solar structure, potential resulting in an expansion of the solar radius. In sharp contrast, changes in radius remain essentially insurmountable within the context of the gaseous models.

Dedication

This work is dedicated to my eldest son, Jacob.

Submitted on: January 25, 2013 / Accepted on: January 25, 2013
First published in online on: January 28, 2013
Additional note on: February 5, 2013

References

1. Keeler J.E. Schmidt's theory of the Sun. *Astrophys. J.*, 1895, v. 1, 178–179.
2. Campbell W.W. James Edward Keeler. *Astrophys. J.*, 1900, v. 12, no. 4, 239–253.
3. Robitaille P.M. On the Presence of a Distinct Solar Surface: A Reply to Hervé Faye. *Progr. Phys.*, 2011, v. 3, 75–78.
4. Hale G.E. Notes on Schmidt's theory of the Sun. *Astrophys. J.*, 1895, v. 2, 69–74.
5. Emilio M., Kuhn J.R., Bush R.I. and Scherrer P. On the constancy of the solar diameter. *Astrophys. J.*, 2000, v. 543, 1007–1010.
6. Kuhn J.R., Bush R.I, Emilio M. and Scherrer P.H. On the constancy of the solar diameter — II. *Astrophys. J.*, 2004, v. 613, 1241–1252.
7. Bush R.I, Emilio M., and Kuhn J.R. On the constancy of the solar diameter — III. *Astrophys. J.*, 2010, v. 716, 1381–1385.
8. Lefebvre S., Bertello L., Ulrich R.K., Boyden J.E., and Rozelot J.P. Solar Radius Measurements at Mount Wilson Observatory. *Astrophys. J.*, 2006, v. 649, 444–451.
9. Raponi A., Sigismondi C., Guhl K, Nugent R. and Tegtmeier A. The measurement of solar diameter and limb darkening function with eclipse observations. *Solar Phys.*, 2012, v. 278, 269–283.
10. Emilio M., Kuhn J.R., Bush R.I, and Scholl I.F. Measuring the solar radius from space during the 2003 and 2006 Mercury transits. *Astrophys. J.*, 2012, v. 750, 135(8 pages).
11. Xie W., Sigismondi C., Wang X. and Tanga P. Venus transit, aureole and solar diameter. In: *"Solar Astrophysical Dynamos and Magnetic Activity", Proc. IAU Symp.*, No. 294, 2013.
12. Sigismondi C. Solar diameter, eclipses and transits: The importance of ground based observations. *Mem. S. A. It.*, 2013, v. 86, 100–103.
13. Shapiro I.I. Is the Sun Shrinking? *Science*, 1980, v. 208, no. 4439, 51–53.
14. Chapman G.A., Dobias J.J. and Walton S.R. On the variability of the apparent solar radius. *Astrophys. J.*, 2008, v. 681, no. 2, 1698–1702.
15. Rozelot J.P. and Damiani C. Rights and wrongs of the temporal solar radius variability. *Eur. Physical J. H*, 2012, v. 37, no. 5, 709–743.
16. de Toma G., White O.R., Chapman G.A., Walton S.R., Preminger D.G., Cookson A.M., Harvey K.L. Differences in the Sun's radiative output in cycles 22 and 23. *Astrophys. J. Letters*, 2001, v. 549, no. 1, L131–L134.
17. Walton S.R., Preminger D.G. and Chapman G.A. The contribution of faculae and network to long-term changes in the total solar irradiance. *Astrophys. J.*, 2003, v. 590, no. 2, 1088–1094.
18. Robitaille J.C. and Robitaille P.M. Liquid Metallic Hydrogen III. Intercalation and lattice exclusion versus gravitational settling and their consequences relative to internal structure, surface activity, and solar winds in the Sun. *Progr. Phys*., 2013, v. 2, 87–97.

LETTERS TO PROGRESS IN PHYSICS

Commentary on the Liquid Metallic Hydrogen Model of the Sun: Insight Relative to Coronal Holes, Sunspots, and Solar Activity

Pierre-Marie Robitaille

Department of Radiology, The Ohio State University, 395 W. 12th Ave, Columbus, Ohio 43210, USA.
robitaille.1@osu.edu

While mankind will always remain unable to sample the interior of the Sun, the presence of sunspots and coronal holes can provide clues as to its subsurface structure. Insight relative to the solar body can also be gained by recognizing that the Sun must exist in the condensed state and support a discrete lattice structure, as required for the production of its continuous spectrum. In this regard, the layered liquid metallic hydrogen lattice advanced as a condensed model of the Sun (Robitaille P.M. Liquid Metallic Hydrogen: A Building Block for the Liquid Sun. *Progr. Phys.*, 2011, v. 3, 60–74; Robitaille P.M. Liquid Metallic Hydrogen II: A Critical Assessment of Current and Primordial Helium Levels in Sun. *Progr. Phys.*, 2013, v. 2, 35–47; Robitaille J.C. and Robitaille P.M. Liquid Metallic Hydrogen III. Intercalation and Lattice Exclusion Versus Gravitational Settling and Their Consequences Relative to Internal Structure, Surface Activity, and Solar Winds in the Sun. *Progr. Phys.*, 2013, v. 2, in press) provides the ability to add structure to the solar interior. This constitutes a significant advantage over the gaseous solar models. In fact, a layered liquid metallic hydrogen lattice and the associated intercalation of non-hydrogen elements can help to account for the position of sunspots and coronal holes. At the same time, this model provides a greater understanding of the mechanisms which drive solar winds and activity.

As the laws of a liquid are different from those of a gas, a liquid star will behave differently from a gaseous star, and before we can predict the behaviour of a star we must know the state of the matter composing it.

James Hopwood Jeans, 1928 [1]

Coronal holes are strange entities, in part due to their sparse nature [2, 3]. At first glance, they seem to offer little of value with respect to our understanding of the Sun. What can be gained from "looking into a hole"? Within the context of the liquid hydrogen model of the Sun (see [4–10] and references therein), there is a great deal to be learned.

In the broadest terms, coronal holes can be described as follows: *"Coronal holes are regions of low-density plasma on the Sun that have magnetic fields that open freely into interplanetary space. During times of low activity, coronal holes cover the north and south polar caps of the Sun. During more active periods, coronal holes can exist at all solar latitudes, but they may only persist for several solar rotations before evolving into a different magnetic configuration. Ionized atoms and electrons flow along the open magnetic fields in coronal holes to form the high speed component of the solar wind"* [2]. When the Sun is quiet, coronal holes appear to be *"anchored"* onto the polar regions of solar surface (see Fig. 1): *"coronal holes, in fact, appear to display rigid rotation as if they are attached to the solar body"* [11, p. 24].

The anchoring of coronal holes to the solar surface can be viewed as the twenty-second line of evidence that the Sun is comprised of condensed matter. The other lines of evidence have already been published (see [4–10] and references therein). Rigid rotation and anchoring cannot be easily explained using the gaseous solar models. As a result, the anchoring of coronal holes is best understood in the context of a condensed solar model.

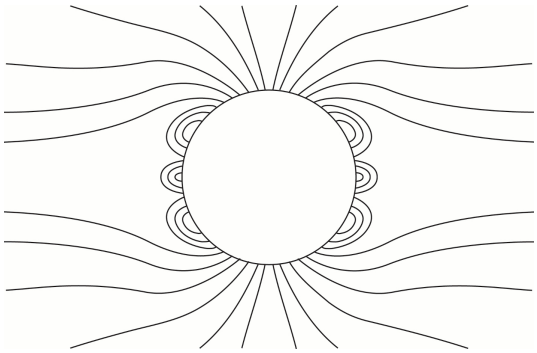

Fig. 1: Schematic representation of coronal holes over the polar caps of a quiet Sun. This figure is an adaptation based on Fig. 2 in [2].

In order to comprehend why the Sun possesses coronal holes, it is best to turn to the lattice configuration of the solar material. Robitaille and Robitaille [7] have recently advanced the hypothesis that the Sun is comprised of liquid metallic hydrogen, wherein protons are arranged in layered hexagonal planes and all other atoms exist in intercalate layers located between the hydrogen planes. Such a structure has been based

on the need to properly explain the thermal emission of the Sun [5], while at the same time, taking into account the structural tendencies of layered materials such as graphite [7].

Within the intercalation compounds of graphite, elemental diffusion orthogonal to the hexagonal carbon planes is hindered, while rapid diffusion can occur in the intercalate regions between the planes (see Fig. 2 in [7]). The same tendencies have been inferred to exist within the liquid metallic hydrogen lattice of the Sun: elemental diffusion is restricted in the direction orthogonal to the hexagonal proton planes and is greatly facilitated within each intercalate layer [7].

Hence, in order to explain the existence of coronal holes, the hexagonal liquid metallic hydrogen lattice of the Sun must be placed in a direction which is orthogonal to the solar surface at the poles. This would explain why the expulsion of ions and electrons from the Sun is facilitated. The subsurface orthogonal placement of the liquid metallic hydrogen hexagonal planes thus accounts for the origin of fast solar winds in these regions. During the quiet periods of the solar cycle, the relative orientation of the hydrogen lattice at the poles forms conduits to drive non-hydrogen elements out of the solar body. As a result, the travel time from the solar core to the surface may well be extremely brief. Given a solar radius of ∼696,342 km (see [10] and references therein) and a fast solar wind of 800 km/s [2], an atom could conceivably leave the solid core of the Sun and escape at the level of the photosphere on the poles in only fifteen minutes.

Nonetheless, during the quiet period of the solar cycle, the equatorial regions of the Sun are unable to sustain fast solar winds. This is likely to occur because the hexagonal layers of liquid metallic hydrogen are parallel to the solar surface in this region. Such an arrangement would restrict the free diffusion of elements from the solar body near the equator, resulting in the absence of fast solar winds. Only the slow component of the solar wind would be observed, precisely because of restricted diffusion of the elements across the hexagonal hydrogen planes [7]. As a result, the concentrations of non-hydrogen elements in the equatorial region of the interior would increase. Eventually, the Sun would become active in order to finally expel these elements from the hydrogen lattice, as was previously stated [7].

Sunspots would be created as hexagonal hydrogen layers are propelled through the solar surface by the force of underlying non-hydrogen elements which have now entered the gaseous phase [7]. This has been illustrated in Fig. 2. Note how the "buckling" of metallic hydrogen could result in the simultaneous formation of two sunspots of opposite polarity (Fig 2, as is usually observed), or of a single sunspot (Fig. 3, as is sometimes observed). Such as scenario also explains why the Sun has relatively "erratic" field lines. These constitute simple extensions of a metallic hydrogen lattice whose internal orientation can be highly variable.

The existence of coronal holes has implications relative to the density of the solar atmosphere. Currently, the gaseous

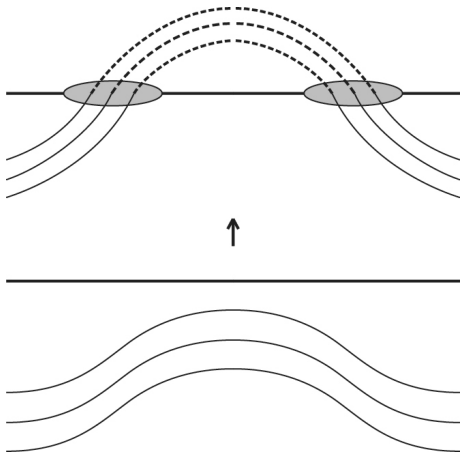

Fig. 2: Schematic representation of the appearance of a pair of sunspots on an active solar surface. The horizontal thick line illustrates the location of the photosphere, the thin lines the layers of metallic hydrogen, and the dashed lines the magnetic field. The two shaded circles outline the position of sunspots. In the lower portion of the figure, the layers of metallic hydrogen are below the level of the photosphere, but are being pushed up by intercalate elements which have entered the gas phase [7]. In the upper portion of the figure, the layers of metallic hydrogen have now broken through the photospheric level. The two sunspots are being linked solely by magnetic field lines, as the metallic hydrogen which once contained them has vaporized into the solar atmosphere. This figure is an adaptation based on Fig. 22 in [12].

solar models are used to assign photospheric and chromospheric densities on the order of 10^{-7} g/cm^3 and 10^{-12} g/cm^3, respectively [12]. In contrast, within the context of the liquid metallic hydrogen model, a photospheric density of ∼1 g/cm^3 is invoked [4–10].

At the same time, the presence of coronal holes directly suggests that chromospheric and coronal densities cannot be spherically uniform. When the Sun is quiet, coronal and chromospheric densities should be lower at the poles and possibly much higher at the equator. Fast solar winds do not typically exist in the equatorial region of the quiet Sun. In fact, it appears that the presence of magnetic field lines restrict the outward movement of ions and electrons away from the solar surface under such conditions. Such realities, when combined with the enormous mass of the Sun, suggest that, contrary to the gaseous solar models, the density of the chromosphere, in the equatorial regions of the quiet Sun, may be many orders of magnitude higher than currently believed. It would be reasonable to suggest that atmospheric densities just above the photospheric layer might far surpass those currently associated with the density of the Earth's atmosphere at sea level. This highlights the problems with extracting densities from regions of the solar atmosphere which are clearly not in local thermal equilibrium, as previously discussed [6].

The liquid metallic hydrogen model [5–7] provides an ex-

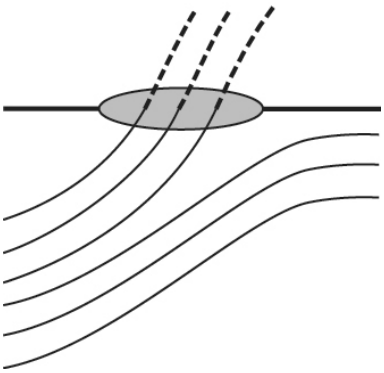

Fig. 3: Schematic representation of a single sunspot on a quiet Sun as in Fig. 2. In this figure, the layers of metallic hydrogen are below the level of the photosphere, but are being pushed up by an adjacent layer of metallic hydrogen which in turn has been displaced by intercalate elements which have entered the gas phase [7]. The sunspot is characterized by strong open magnetic field lines, as the metallic hydrogen which once contained them has vaporized into the solar atmosphere.

cellent framework through which solar activity can be understood. Over the course of the solar cycle, the Sun is alternatively degassing the poles and then the equator. It does so through the orientation of its liquid metallic hydrogen lattice. When the Sun is quiet, much of its interior is constantly being degassed through the action of the fast solar winds exiting at the poles. During this time, degassing is restricted over equatorial regions. Eventually, the Sun becomes active. This change in state is directly associated with degassing the solar interior in the regions of the equator. This helps to explain why sunspots and high energy flares are always restricted to the lower latitudes. They occur in order to degas the equatorial regions of the solar interior. Such a problem does not occur at the poles, since, during the quiet solar period, those internal regions are constantly being degassed by the fast solar winds.

In the end, how the liquid metallic hydrogen layers are oriented within the solar interior reveals a great deal with respect to the formation of sunspots, coronal holes, and measures of solar activity. The magnetic field lines that are observed above the photosphere are a direct consequence of this orientation. Conversely, in the gaseous models of the Sun, the origin of magnetic field lines, coronal holes, sunspots, flares, coronal mass ejections, prominences, and fast or slow solar winds remain areas of profound mystery. This is precisely because these models can offer no structural support for the existence of these phenomena. In order to begin to understand the Sun, structure is required. The continuous solar spectrum requires a lattice for formation. The ideal lattice would resemble the layered one adopted by graphite, as dictated by the needs of thermal emission. Wigner and Huntington have already proposed that metallic hydrogen could adopt a similar lattice [13], creating an ideal structural foundation for the Sun. Furthermore, layered materials, which mimic graphite in their structure, should be prone to forming intercalate regions, as a consequence of lattice exclusion forces [7]. In this regard, the author believes that lattice exclusion, as first postulated by Joseph Christophe Robitaille, along with the formation of intercalate regions within layered metallic hydrogen [7], constitutes the central thesis for understanding solar structure and activity.

Acknowledgment

Luc Robitaille is acknowledged for the preparation of figures.

Dedication

Dedicated to Dmitri Rabounski and Larissa Borissova in fond memory of many scientific discussions on the Sun.

Submitted on: January 25, 2013 / Accepted on: January 25, 2013
First published in online on: January 28, 2013

References

1. Jeans J.H. Astronomy and cosmogony. Cambridge University Press, Cambridge, U.K., 1928, p. 2.
2. Cranmer S.R. Coronal holes. In: *Encyclopedia of Astronomy and Astrophysics*, (Paul Murdin, Ed.), Institute of Physics Publishing, Bristol, 2001, v. 1, p. 496–501.
3. Cranmer S.R. Coronal holes. *Living Rev. Solar Phys.*, 2009, v. 6, 3–66.
4. Robitaille P.M. A high temperature liquid plasma model of the Sun. *Progr. Phys.*, 2007, v. 1, 70–81 (also in arXiv: astro-ph/0410075).
5. Robitaille P.M. Liquid Metallic Hydrogen: A Building Block for the Liquid Sun. *Progr. Phys*., 2011, v. 3, 60–74.
6. Robitaille P.M. Liquid Metallic Hydrogen II: A Critical Assessment of Current and Primordial Helium Levels in Sun. *Progr. Phys.*, 2013, v. 2, 35–47.
7. Robitaille J.C. and Robitaille P.M. Liquid Metallic Hydrogen III. Intercalation and Lattice Exclusion Versus Gravitational Settling and Their Consequences Relative to Internal Structure, Surface Activity, and Solar Winds in the Sun. *Progr. Phys*., 2013, v. 2, in press.
8. Robitaille P.M. Commentary relative to the distribution of gamma-ray flares on the Sun: Further evidence for a distinct solar surface. *Progr. Phys.*, 2013, v. 2, L1-L2.
9. Robitaille P.M. Commentary Relative to the Seismic Structure of the Sun:
Internal Rotation, Oblateness, and Solar Shape. *Progr. Phys.*, 2013, v. 2, L3-L4.
10. Robitaille P.M. Commentary on the Radius of the Sun:
Optical Illusion or Manifestation of a Real Surface? *Progr. Phys.*, 2013, v. 2, L5-L6.
11. Chitre S.M. Overview of solar physics. In: *Lectures on Solar Physics* (H.M. Antia, A. Bhatnagar and R. Ulmschneider, Eds.), Springer, Berlin, 2003, p. 1–26.
12. Bhatnagar A. Instrumentation and observational techniques in solar astronomy. In: *Lectures on Solar Physics* (H.M. Antia, A. Bhatnagar and R. Ulmschneider, Eds.), Springer, Berlin, 2003, p. 27–79.
13. Wigner E. and Huntington H.B. On the possibility of a metallic modification of hydrogen. *J. Chem. Phys.*, 1935, v. 3, 764–70.

LETTERS TO PROGRESS IN PHYSICS

Commentary on the Liquid Metallic Hydrogen Model of the Sun II. Insight Relative to Coronal Rain and Splashdown Events

Pierre-Marie Robitaille

Department of Radiology, The Ohio State University, 395 W. 12th Ave, Columbus, Ohio 43210, USA.
robitaille.1@osu.edu

Coronal rain represents blobs of solar material with a width of ~300 km and a length of ~700 km which are falling from the active region of the corona towards the solar surface along loop-like paths. Conversely, coronal showers are comprised of much larger bulks of matter, or clumps of solar rain. Beyond coronal rain and showers, the expulsion of solar matter from the surface, whether through flares, prominences, or coronal mass ejections, can result in massive disruptions which have been observed to rise far into the corona, return towards the Sun, and splashdown onto the photosphere. The existence of coronal rain and the splashdown of mass ejections onto the solar surface constitute the twenty-third and twenty-fourth lines of evidence that the Sun is condensed matter.

As the laws of a liquid are different from those of a gas, a liquid star will behave differently from a gaseous star, and before we can predict the behaviour of a star we must know the state of the matter composing it.

James Hopwood Jeans, 1928 [1]

The presence of coronal rain within the active atmosphere of the Sun has been recognized for less than a decade [2–5]. Coronal rain corresponds to *"cool and dense matter and not waves"* [5]. It appears to be *"ubiquitous"* and *"composed of a myriad of small blobs, with sizes that are, on average 300 km in width and 700 km in length"* [5]. When it aggregates, coronal rain can lead to larger clumps called *"showers"* [5]. Their rate of descent towards the solar surface can approach 120 km s^{-1}. However, such rates of descent are inferior to those inferred from the Sun's gravitational field, suggesting that they are restricted in their downward motion by gas pressure in the underlying solar atmosphere [5]. These findings are incongruent with the idea that the density of the chromosphere is in the 10^{-12} g/cm^3 range, as currently advanced by the gaseous solar models [6]. Such densities would be associated with very good vacuums on Earth. As such, it does not seem reasonable, based on these findings, that the chromospheric densities associated with the gaseous models can be correct [7]. At the same time, theoretical models relative to coronal rain now rely on *"heating and condensation cycles"* [4, 5], despite the fact that the gaseous models of the Sun preclude all material condensation. In the end, it remains more plausible to account for the behavior of coronal rain by invoking true condensation, as seen in the liquid metallic model of the Sun [7]. This constitutes the twenty-third line of evidence that the Sun is comprised of condensed matter (see [7] and references therein for the others).

In addition to coronal rain, the mass ejection event, witnessed on June 7, 2011, was particularly instructive relative to the nature of the Sun [8, 9]. On that day, a tremendous disruption occurred on the solar surface which projected material well into the corona, prior to its subsequent descent back onto the Sun. Upon striking the solar body, the multiple points of impact immediately brightened – revealing clear and distinct surface behavior on the photosphere [9]. Such visualizations highlight that the solar surface is not an optical illusion, but, indeed, acts as a real surface. Such "splashdowns" constitute the twenty-fourth line of evidence that the solar body is comprised of condensed matter. In addition, they provide complementary evidence that flares, prominences, and coronal mass ejections are also characterized by the existence, at least in part, of condensed matter.

Impressive disruptions of the solar surface have also been associated with comets, although intial analysis apparently revealed that such events were not associated with the impact of such objects onto the photosphere [10]. In the end, additional study may well reveal that comets have the ability to disrupt the solar surface, either directly through impact or indirectly by disrupting magnetic field lines above the surface.

Such visualizations highlight that the solar surface is not an optical illusion. It appears and behaves as a true liquid surface. In addition, coronal rains and mass ejection splashdowns indicate that the outer atmosphere of the Sun can support localized regions of condensed matter.

Acknowledgment

The May 10–11, 2011 solar event [10] was first brought to the author's attention by Patrice Robitaille.

Dedication

This work is dedicated to my brother, Patrice, in profound gratitude for many years of support and encouragement.

Submitted on: January 31, 2013 / Accepted on: January 31, 2013
First published in online on: February 2, 2013

References

1. Jeans J.H. Astronomy and cosmogony. Cambridge University Press, Cambridge, U.K., 1928, p. 2.
2. De Groof A., Berghmans D., van Driel-Gesztelyi L. and Poedts S. Intensity variations in EIT shutterless mode: Waves or Flows? *Astron. Astrophys.*, 2004, v. 415, no. 3, 1141–1151.
3. De Groof A., Bastiaensen C., Müller D.A.N., Berghmans D., and Poedts S. Detailed comparison of downflows seen both in EIT 30.4 nm and Big Bear Hα movies. *Astron. Astrophys.*, 2005, v. 443, no. 1, 319–328.
4. Müller D.A.N., De Groof A., Hansteen V.H. and Peter H. High-speed coronal rain. *Astron. Astrophys.*, 2005, v. 436, no. 3, 1067–1074.
5. Antolin R., Vissers G. and van der Voort L.R. On-Disk coronal rain. *Solar Phys.*, 2012, v. 280, no. 2, 457–474.
6. Bhatnagar A. Instrumentation and observational techniques in solar astronomy. In: *Lectures on Solar Physics* (H.M. Antia, A. Bhatnagar and R. Ulmschneider, Eds.), Springer, Berlin, 2003, p. 27–79.
7. Robitaille P.M. Commentary on the liquid metallic hydrogen model of the Sun: Insight relative to coronal holes, sunspots, and solar activity. *Progr. Phys.*, 2013, v. 2, L7–L9.
8. Moskowitz C. Gargantuan Sun explosion rocks astronomers. *SPACE.com* (created June 9, 2011 at 12:34 PM ET – accessed online on January 29, 2011).
9. NASA/SDO/Helioviewer.org [2011/06/07 04:00:00 to 11:00:00 UTC]. Observed well using 5 min frames SDO AIA 304. These events have been captured in video format and posted numerous times online: e.g.Newsflash *Skywatch Media* youtube.com/watch?v=aQICN0BV1Aw; Phil Plait *Bad Astronomy Blog* youtube.com/watch?v=Hyi4hjG6kDM; youtube.com/watch?v=Cjd6TQiTRAM; youtube.com/watch?v=6h1EJtmUTeM. (Accessed online on January 29, 2013).
10. SOHO NASA/ESA [2011/05/10 20:00:00 to 2011/05/11 08:00:00 UTC]. These events have been captured in video format and displayed online: e.g. youtube.com/watch?v=igeBrSGk5FA; *Russia Today* youtube.com/watch?NR=1&v=Mat4dWpszoQ&feature=fvwp. (Accessed online on January 29, 2013).

LETTERS TO PROGRESS IN PHYSICS

Commentary on the Liquid Metallic Hydrogen Model of the Sun III. Insight into Solar Lithium Abundances

Pierre-Marie Robitaille

Department of Radiology, The Ohio State University, 395 W. 12th Ave, Columbus, Ohio 43210, USA.
robitaille.1@osu.edu

The apparent depletion of lithium represents one of the greatest challenges to modern gaseous solar models. As a result, lithium has been hypothesized to undergo nuclear burning deep within the Sun. Conversely, extremely low lithium abundances can be easily accounted for within the liquid metallic hydrogen model, as lithium has been hypothesized to greatly stabilize the formation of metallic hydrogen (E. Zurek et al. A little bit of lithium does a lot for hydrogen. *Proc. Nat. Acad. Sci. USA*, 2009, v. 106, no. 42, 17640–17643). Hence, the abundances of lithium on the solar surface can be explained, not by requiring the nuclear burning of this element, but rather, by suggesting that the Sun is retaining lithium within the solar body in order to help stabilize its liquid metallic hydrogen lattice. Unlike lithium, many of the other elements synthesized within the Sun should experience powerful lattice exclusionary forces as they are driven out of the intercalate regions between the layered liquid metallic hydrogen hexagonal planes (Robitaille J.C. and Robitaille P.M. Liquid Metallic Hydrogen III. Intercalation and Lattice Exclusion Versus Gravitational Settling and Their Consequences Relative to Internal Structure, Surface Activity, and Solar Winds in the Sun. *Progr. Phys*., 2013, v. 2, in press). As for lithium, its stabilizing role within the solar interior helps to account for the lack of this element on the surface of the Sun.

As the laws of a liquid are different from those of a gas, a liquid star will behave differently from a gaseous star, and before we can predict the behaviour of a star we must know the state of the matter composing it.

James Hopwood Jeans, 1928 [1]

Solar lithium abundance [2], as determined at the photospheric level, are reduced ~140 fold when compared to meteorites [3]. Such a paucity of lithium has presented a challenge for the gaseous models of the stars, as they attempt to account for the relative absence of this element on the solar surface [2,3]. Consequently, solar scientists hypothesized that lithium is being burned deep within the convection zone [2,3]. Lithium is thought to be easily destroyed [^{7}Li(p,α)^{4}He] at temperatures above 2.6 x 10^6 K [4]. Mild mixing of lithium also helps to account for the surface depletion [4–6]. In this regard, it has been postulated that *"stars that host planets experience more mixing in their internal environment"* [7]. As a result, those who adhere to the gaseous models have proposed that greater lithium depletion occurs in stars that have orbiting planets [8], although such claims have been refuted [9]. Nonetheless, such works [7, 9] highlight the significance of the solar lithium abundance problem in astrophysics. In this regard, solar lithium abundances might be better understood within the context of the liquid metallic hydrogen model of the Sun [10–13].

Along with Neil Ashcroft, Eva Zurek and her coworkers recently advanced [14] that lithium could greatly stabilize the formation of metallic hydrogen [15, 16]. This finding has tremendous implication relative to understanding the fate of lithium within the Sun, if indeed, the solar matrix is comprised of liquid metallic hydrogen [10–13].

When the Sun was hypothesized to be built from liquid metallic hydrogen, it was important that the resulting lattice adopt a layered structure similar to graphite in order to properly account for thermal emission [11]. Thus, it was fortunate that Wigner and Huntington [15] had said that metallic hydrogen could exist in a layered lattice resembling graphite. At the same time, since graphite was known to form intercalation compounds, the extension of such chemistry to the layered form of metallic hydrogen proved natural [13]. Therefore, it was thought that the Sun would maintain the integrity of its layered hexagonal hydrogen lattice and associated conduction bands, by permitting non-hydrogen elements to reside within intercalation zones [13]. In addition, since the intercalation compounds of graphite are known to undergo exfoliative processes wherein intercalate atoms are driven out of the graphitic structure, the same mechanism was applied to the Sun [13]. Solar activity became linked to lattice exclusion and the associated expulsion of non-hydrogen atoms from the solar interior [13]. Nonetheless, it was already recognized [11] that lithium should stabilize the metallic hydrogen lattice. As a result, unlike the case for most elements, the Sun should not be working to expel lithium. Such a scenario elegantly accounts for the significant reductions in lithium abundances observed on the surface of the Sun while, at the same time,

permitting elevated lithium levels in meteorites, or other objects, which have been first synthesized within the stars. Conversely, the idea that lithium is being burned preferentially within the stars, as proposed by the gaseous models, makes it difficult to account for elevated lithium levels elsewhere in the astrophysical world. Herein lies the merit of sequestering lithium within the solar body and permitting it to participate in nuclear reactions, without preferential burning, in the context of the liquid metallic hydrogen model [10–13].

Dedication

This work is dedicated to my youngest son, Luc.

Submitted on: January 31, 2013 / Accepted on: January 31, 2013
First published in online on: February 2, 2013

References

1. Jeans J.H. Astronomy and cosmogony. Cambridge University Press, Cambridge, U.K., 1928, p. 2.
2. Grevesse N. Solar abundances of lithium, beryllium, and boron. *Solar Phys.*, 1968, v. 5, 159–180.
3. Wiens R.C., Bochsler P., Burnett D.S. and Wimmer-Schweingruber R.F. Solar and solar-wind isotopic compositions. *Earth Plan. Sci. Let.*, 2004, v. 222, 697–712.
4. Uitenbroek H. The effect of photospheric granulation on the determination of the lithium abundance in solar-type stars. *Astrophys. J.*, 1998, v. 498, 427–440.
5. Schatzman E. Turbulent transport and lithium destruction in main sequence stars. *Astron. Astrophys.*, 1977, v. 56, 211–218.
6. Pinsonneault M.H. Rotational mixing and lithium depletion. In: *Light Elements in the Universe: Proc. IAU Symposium*, 2009, v. 268, 375-380.
7. Pinsonneault M.H. A fossil record for exoplanets. *Nature*, 2009, v. 462, no. 7270, 168–169.
8. Israelian G., Delgado Mena E., Santos N.C., Sousa S.G., Mayor M., Udry S., Dominguez Cerdena C., Rebolo R. and Randich S. Enhanced lithium depletion in Sun-like stars with orbiting planets. *Nature*, 2009, v. 462, no. 7270, 189–191.
9. Baumann P., Ramirez I., Melendez J., Aslund M. and Lind K. Lithium depletion in solar-like stars: no planet connection. *Astron. Astrophys.*, 2010, v. 519, A87(11 pages).
10. Robitaille P.M. A high temperature liquid plasma model of the Sun. *Progr. Phys.*, 2007, v. 1, 70–81 (also in arXiv: astro-ph/0410075).
11. Robitaille P.M. Liquid Metallic Hydrogen: A Building Block for the Liquid Sun. *Progr. Phys.*, 2011, v. 3, 60–74.
12. Robitaille P.M. Liquid Metallic Hydrogen II: A Critical Assessment of Current and Primordial Helium Levels in Sun. *Progr. Phys.*, 2013, v. 2, 35–47.
13. Robitaille J.C. and Robitaille P.M. Liquid Metallic Hydrogen III. Intercalation and Lattice Exclusion Versus Gravitational Settling and Their Consequences Relative to Internal Structure, Surface Activity, and Solar Winds in the Sun. *Progr. Phys.*, 2013, v. 2, in press.
14. Zurek E., Hoffmann R., Ashcroft N.W., Oganov A.R., Lyakhov A.O. A little bit of lithium does a lot for hydrogen. *Proc. Nat. Acad. Sci. USA* USA, 2009, v. 106, no. 42, 17640—17643.
15. Wigner E. and Huntington H.B. On the possibility of a metallic modification of hydrogen. *J. Chem. Phys.*, 1935, v. 3, 764–70.
16. McMahon J.M., Morales M.A., Pierleoni C. and Ceperley D.M. The properties of hydrogen and helium under extreme conditions. *Rev. Mod. Phys.*, 2012, v. 84, 1607–1653.

Progress in Physics is an American scientific journal on advanced studies in physics, registered with the Library of Congress (DC, USA): ISSN 1555-5534 (print version) and ISSN 1555-5615 (online version). The journal is peer reviewed and listed in the abstracting and indexing coverage of: Mathematical Reviews of the AMS (USA), DOAJ of Lund University (Sweden), Zentralblatt MATH (Germany), Scientific Commons of the University of St.Gallen (Switzerland), Open-J-Gate (India), Referential Journal of VINITI (Russia), etc. Progress in Physics is an open-access journal published and distributed in accordance with the Budapest Open Initiative: this means that the electronic copies of both full-size version of the journal and the individual papers published therein will always be acessed for reading, download, and copying for any user free of charge. The journal is issued quarterly (four volumes per year).

Electronic version of this journal: http://www.ptep-online.com

Postal address:
Department of Mathematics and Science,
University of New Mexico, 705 Gurley Avenue, Gallup, NM 87301, USA

Printed in the United States of America